# Pathobiology of Parkinson's disease associated genes

**Giselle Sagredo**

A thesis submitted to fulfill the requirements for the degree of
Doctor of Philosophy

School of Medical Sciences
Faculty of Medicine and Health
The University of Sydney
NSW, Australia

2025

# Scholarships

This research reported in this thesis was supported in part by the award of an Aligning Science Across Parkinson's postgraduate research scholarship on genetic forms of Parkinson's Disease and of a Research Training Program scholarship to the PhD Candidate.

# Statement of Originality

This is to certify that to the best of my knowledge, the content of this thesis is my own work. This thesis has not been submitted for any degree or other purposes.

I certify that the intellectual content of this thesis is the product of my own work and that all the assistance received in preparing this thesis and sources have been acknowledged.

Signature: _____

Name: Giselle Sagredo

# Authorship Attribution Statement

The following publications are featured in this thesis:

1. **Sagredo GT**, Tanglay O, Shahdadpuri S, Fu Y, Halliday GM. α-Synuclein levels in Parkinson's disease - Cell types and forms that contribute to pathogenesis. Exp Neurol. 2024;379:114887
    - I co-wrote the manuscipt. This publication featured in chapter 1 of this thesis.

2. Lam I, Ndayisaba A, Lewis AJ, Fu Y, **Sagredo GT**, Kuzkina A, et al. Rapid iPSC inclusionopathy models shed light on formation, consequence, and molecular subtype of α-synuclein inclusions. Neuron. 2024;112(17):2886-909.e16.
    - I performed the quantitative analyses in the cortex. I co-performed the imaging and statistical analyses and co-prepared the figures. This publication featured in chapter 2 of this thesis.

In addition to the statements above, in cases where I am not the corresponding author of a published item, permission to include the published material has been granted by the corresponding author.

Giselle Sagredo, _____ , 20•12•2024

As supervisor for the candidature upon which this thesis is based, I can confirm that the authorship attribution statements above are correct.

Prof. Glenda Halliday, _____ , 20•12•2024

# Acknowledgements

I would like to thank my primary supervisor Prof. Glenda Halliday for her guidance and support throughout my candidature. Her expertise has been invaluable, and I am immensely grateful to have had her as my supervisor throughout this challenging and rewarding experience. I would also like to extend a thanks to my co-supervisor Dr. YuHong Fu.

I would like to acknowledge everyone in the Halliday team for their help and technical support, particularly Dr. Hongyun Li and Ping Wu. I would also like to thank Dr. Wen Li for her support, guidance and patience. A big thank you to the staff at Sydney Microscopy and Microanalysis, particularly Dr. Pamela Young and Dr. Michael Kuligowski for their support and kindness.

I would like to acknowledge the brain donors and their families. Tissues were supplied by the Sydney Brain Bank, which is supported by Neuroscience Research Australia and a special gift in memory of Jim Raftos from the Shaw family. I would like to thank the E46K patients and the Basque Biobank Integrated in the Platform ISCIII Biobanks and Biomodels for their collaboration.

Thank you to my family and friends for giving me the strength to persevere, I am infinitely grateful to you all.

# Table of Contents

*Scholarships* ..... *ii*

*Statement of Originality* ..... *ii*

*Authorship Attribution Statement* ..... *iii*

*Acknowledgements* ..... *iv*

*List of Figures* ..... *viii*

*List of Tables* ..... *xii*

*List of Abbreviations* ..... *xiii*

*ABSTRACT* ..... *xvi*

*CHAPTER 1: Literature Review* ..... *1*

**1.1 Introduction** ..... **1**

1.1.1 Epidemiology ..... 1

1.1.2 Clinical presentation and manifestation ..... 1

**1.2 Neuropathology** ..... **2**

1.2.1 Neuronal loss ..... 3

1.2.2 Lewy pathologies ..... 4

1.2.3 Pathophysiology ..... 6

**1.3 Genetic Aetiology** ..... **7**

1.3.1 Autosomal dominant PD genes ..... 8

1.3.1.1 SNCA ..... 8

1.3.1.2 LRRK2 ..... 14

1.3.2 Autosomal recessive PD genes ..... 22

1.3.2.1 PRKN ..... 22

1.3.2.2 PINK1 ..... 29

**1.4 Comparison of cellular changes between genetic and sporadic PD** ..... **31**

**1.5 Gaps in Knowledge** ..... **33**

**1.6 Aims and Hypotheses** ..... **34**

1.6.1 Aims ..... 34

1.6.2 Global hypotheses ..... 34

*CHAPTER 2: Definition and sequence of Lewy body formation in sporadic and SNCA mutation forms of Parkinson's disease* ..... *35*

**2.1 Abstract** ..... **35**

**2.2 Background** ..... **35**

**2.3 Methods** ..... **40**

2.3.1 Cases and tissue processing ..... 40

2.3.2 Immunofluorescence ..... 41

2.3.3 Imaging and analyses ..... 43

**2.4 Results** ..... **46**

2.4.1 Distribution and morphology of α-synuclein (α-syn) pathology in sporadic PD ..... 46

2.4.2 Distribution and morphology of α-synuclein (α-syn) pathology in *SNCA* mutation cases ..... 49

2.4.3 Quantitation of α-synuclein (α-syn) puncta in sporadic PD and PD cases with *SNCA* mutations ..... 51

2.4.4 Quantitation of stages of Lewy body (LB) types in sporadic PD and PD with *SNCA* mutations ..... 52

2.4.5 Analysis of different proteins at different Lewy body (LB) stages in sporadic PD and PD cases with *SNCA* mutations ..... 58

**2.5 Discussion** ..... **65**

*CHAPTER 3: Comparisons of protein pathologies in a chimeric mouse model with transplants of human dopamine neurons from SNCA, LRRK2 and PRKN induced pluripotent stem cells* ..... *72*

**3.1 Abstract** ..... **72**

**3.2 Introduction** ..... **73**

**3.3 Methods** ..... **75**

3.3.1 Generation of the chimeric model for analysis (performed at The Florey, The University of Melbourne) ..... 75

3.3.2 Tissue processing and immunofluorescence staining ..... 76

3.3.3 Identification of protein pathologies ..... 77

3.3.4 Imaging and analyses ..... 79

**3.4 Results** ..... **81**

3.4.1 Characterization of transplanted human iPSC-derived dopaminergic neurons by genotype ..... 81

3.4.2 Characterization of the expression and phosphorylation of α-syn and tau in transplanted human iPSC-derived dopaminergic neurons by genotype ..... 84

3.4.3 Characterization of protein pathologies in transplanted human iPSC-derived dopaminergic neurons by genotype ..... 86

**3.5 Discussion** ..... **90**

*CHAPTER 4: Brain pathology in a mature animal model with PRKN deletion .....94*

**4.1 Abstract .....94**

**4.2 Introduction .....95**

**4.3 Methods .....97**

4.3.1 Mice and tissue processing .....97

4.3.2 Proteins to be analysed .....98

4.3.3 Protein extraction and Western blot analyses .....99

4.3.4 Immunofluorescence staining, imaging and analyses .....101

4.3.5 Statistical analyses .....103

**4.4 Results .....104**

4.4.1 Core neuronal and genetic markers in the *PRKN* KO model .....104

4.4.2 α-Synuclein (α-syn) expression levels in *PRKN* KO mice .....104

4.4.3 Mitochondrial protein expression levels in *PRKN* KO mice .....105

4.4.4 Mitochondrial GRP75 immunofluorescence in cortical and nigral neurons in *PRKN* KO mice .....107

4.4.5 Glial protein levels in *PRKN* KO mice .....109

4.4.6 Mitochondrial GRP75 expression in cortical and nigral microglia .....110

**4.5 Discussion .....114**

*CHAPTER 5: General discussion and conclusions .....120*

5.1 General discussion .....120

5.2 Concluding remarks and future directions .....123

*CHAPTER 6: References .....125*

# List of Figures

**Figure 1.1** Substantia nigra (SN) dopaminergic cell loss and Lewy pathology (LP) in Parkinson's disease (PD) patients ..... 3
**Figure 1.2** Lewy pathologies (LP) and their hypothesised progression in the Parkinson's disease (PD) brain. ..... 6
**Figure 1.3** The direct pathway of the motor circuit dysregulated in Parkinson's disease (PD). ..... 7
**Figure 1.4** Structural features of the α-synuclein (α-syn) monomer. ..... 8
**Figure 1.5** Diagram illustrating the key pathogenic mechanisms of *SNCA* mutations. ..... 14
**Figure 1.6** Domain structure of the LRRK2 protein with the positions of PD-associated mutations indicated. ..... 15
**Figure 1.7** Diagram illustrating the key pathogenic mechanisms of *LRRK2* mutations. ..... 19
**Figure 1.8** Domain structure of the parkin protein with well-studied PD-associated missense mutations indicated. ..... 23
**Figure 1.9** Diagram illustrating the key pathogenic mechanisms of *PRKN* genetic mutations. ..... 26
**Figure 1.10** Domain structure of the PINK1 protein with PD-related mutations, mitochondrial processing peptidase (MPP) and presenilin-associated rhomboid-like (PARL) cleavage sites and autophosphorylation sites (S228, T257 and S402) indicated. ..... 29
**Figure 2.1** Pictorial display of cross-sectional studies (30, 64, 65, 354, 355) analysing soma-located α-syn morphology in the substantia nigra (SN) and cortex (Cx) in patients with PD and dementia with Lewy bodies (DLB). ..... 37
**Figure 2.2** Pictorial display of a live cell study (359) analysing the morphology of soma-located α-syn to determine the progressive stages in LB formation. ..... 38
**Figure 2.3** Neuronal nuclei and neuronal α-syn Lewy pathologies in the cortex. ..... 44
**Figure 2.4** Scoring of Lewy pathology (LP) in the cortex. ..... 45
**Figure 2.5** Morphological types of α-syn pathological inclusions in the cingulate cortex and substantia nigra of sporadic PD patients. ..... 48
**Figure 2.6** Mean score (± SEM) of Lewy body (LB) severity in the cingulate cortex of sporadic PD (sPD) and PD with *SNCA* mutations (gPD) ..... 49
**Figure 2.7** Morphological types of α-syn pathological inclusions in the cingulate cortex and substantia nigra (SN) of PD patients with *SNCA* mutations. ..... 50

**Figure 2.8** Mean proportion (± SEM) of cortical neurons with pS129 α-syn puncta in sporadic PD (sPD) and PD patients with *SNCA* mutations (gPD)..... 51
**Figure 2.9** Co-labelling of α-syn puncta in the cortex of sporadic PD and PD patients with *SNCA* mutations. ..... 52
**Figure 2.10** Mean proportion (± SEM) of cortical neurons with Lewy bodies (LB) in sporadic PD (sPD) and PD patients with *SNCA* mutations (gPD). ..... 53
**Figure 2.11** Ubiquitin (Ub) co-labelling in cortical Lewy bodies (LBs) in sporadic PD and PD patients with *SNCA* mutations ..... 54
**Figure 2.12** p62 co-labelling in cortical Lewy bodies (LB) in sporadic PD and PD patients with *SNCA* mutations. ..... 55
**Figure 2.13** Mean proportion (± SEM) of Lewy bodies (LB) co-labelled with ubiquitin (Ub) or p62 and the type of α-syn+ cortical LB with p62 co-labelling in sporadic PD and PD patients with *SNCA* mutations. ..... 56
**Figure 2.14** P62 and ubiquitin (Ub) co-labelling of cortical Lewy bodies (LB) in sporadic PD and PD patients with *SNCA* mutations ..... 57
**Figure 2.15** The proportion of cortical Lewy bodies (LBs) co-labelling both ubiquitin (Ub) and p62, or only ubiquitin or only p62 in sporadic and mutation PD patients. ..... 57
**Figure 2.16** Ras Homolog Family Member A (RhoA) co-labelling of cortical Lewy bodies (LB) in sporadic PD and PD patients with *SNCA* mutations ..... 58
**Figure 2.17** Mean proportion (± SEM) of Ras Homolog Family Member A (RhoA) or Ras-related protein Rab-8 (Rab8) p62+ cortical Lewy bodies (LB) and the type of RhoA+p62+ cortical LBs in sporadic PD and PD patients with *SNCA* mutations ..... 59
**Figure 2.18** Ras-related protein Rab-8 (Rab8) co-labelling of cortical Lewy bodies (LB) in sporadic PD and PD patients with *SNCA* mutations ..... 60
**Figure 2.19** Phospho-tau (AT8) co-labelling in cortical pathologies in sporadic and *SNCA* mutation PD patients ..... 63
**Figure 2.20** Ubiquitin (Ub), p62 and phospho-tau (AT8) co-labelling in Lewy body (LBs) in the cortex and substantia nigra (SN) of sporadic and *SNCA* mutation PD patients ..... 64
**Figure 2.21** Potential sequences of Lewy body (LB) formation in sporadic and *SNCA*-mutant PD based on the prevalence of the Lewy pathologies (LPs) ..... 70
**Figure 3.1** Phospho-α-syn at S129 (pS129) aggregate-like structures apparent in TH+ neurons in control (CT) and *SNCA*, *LRRK2* and *PRKN* mutation iPSC-derived VM graft transplants ..... 78

**Figure 3.2** Phospho-tau (AT8) aggregate-like structures apparent in TH+ neurons in control (CT) and *SNCA*, *LRRK2* and *PRKN* mutation iPSC-derived VM graft transplants ..... 79
**Figure 3.3** The distribution, density and morphological features of TH+ neurons in control (CT) and *SNCA*, *LRRK2* and *PRKN* mutation iPSC-derived VM graft transplants ..... 83
**Figure 3.4** Quantitation of TH+ neuronal cells, projections and cell size in control (CT) and *SNCA*, *LRRK2* and *PRKN* mutation iPSC-derived VM graft transplants..... 83
**Figure 3.5** α-Syn and tau expression in control (CT) and *SNCA*, *LRRK2* and *PRKN* mutation iPSC-derived TH+ neurons in VM transplants..... 84
**Figure 3.6** Quantitation of α-syn and tau mean intensities in control (CT) and *SNCA*, *LRRK2* and *PRKN* mutation iPSC-derived TH cell masks in VM transplants..... 85
**Figure 3.7** 3D deconvoluted image reconstructions of aggregate-like structures in *SNCA* and *LRRK2* mutation iPSC-derived TH+ neurons in VM transplants..... 88
**Figure 3.8** Phospho- α-syn and tau aggregate-like structures in control (CT) and *SNCA*, *LRRK2* and *PRKN* mutation iPSC-derived TH+ neurons in VM transplants ..... 89
**Figure 4.1** Western blot analyses of neuronal markers and parkin in the cortex (Cx) and midbrain (MB) of 6 and 12-month-old wild-type (WT) and *PRKN* knockout (KO) mice ...104
**Figure 4.2** Western blot analyses of α-syn in the cortex (Cx) and midbrain (MB) of 6 and 12-month-old wild-type (WT) and *PRKN* knockout (KO) mice.....105
**Figure 4.3** Western blot analyses of mitochondrial proteins in the cortex (Cx) and midbrain (MB) of 6 and 12-month-old wild-type (WT) and *PRKN* knockout (KO) mice .....106
**Figure 4.4** Mitochondrial fraction western blot analyses of mitochondrial proteins in the cortex of male (M) and female (F) wild-type (WT) and *PRKN* knockout (KO) mice at 12 months of age.....107
**Figure 4.5** Glucose-regulated protein 75 (GRP75) immunofluorescence in neurons in the cortex and substantia nigra of wild-type (WT) and *PRKN* knockout (KO) mice .....108
**Figure 4.6** Quantitation of glucose-regulated protein 75 (GRP75) mean intensity in cortical and nigral neurons of wild-type (WT) and *PRKN* knockout (KO) mice at 12 months of age .....109
**Figure 4.7** Western blot analyses of glial proteins in the cortex (Cx) and midbrain (MB) of 6 and 12-month-old wild-type (WT) and *PRKN* knockout (KO) mice. .....110
**Figure 4.8** Glucose-regulated protein 75 (GRP75) immunofluorescence in microglia in the cortex and substantia nigra of wild-type (WT) and *PRKN* knockout (KO) mice. .....112

**Figure 4.9** Quantitation of glucose-regulated protein 75 (GRP75) mean intensity in cortical and nigral IBA1+ cells of wild-type (WT) and *PRKN* knockout (KO) mice at 12 months of age .....112
**Figure 4.10** Microglial phenotypes in the cortex and substantia nigra of wild-type (WT) and *PRKN* knockout (KO) mice. .....113
**Figure 4.11** Quantitation of microglial cells and somal size in wild-type (WT) and *PRKN* knockout (KO) mice in the cortex (Cx) and substantia nigra (SN) at 12 months of age.....114

# List of Tables

**Table 1.1** Clinical and pathological features of different *SNCA* gene mutations. ..... 10
**Table 1.2** Clinical and pathological features of different pathogenic *LRRK2* gene mutations ..... 17
**Table 1.3** Comparison of pathological features and proteins in *SNCA*, *LRRK2* and *PRKN* mutations and sporadic Parkinson's Disease. ..... 32
**Table 2.1** Case demographics and diagnostic neuropathology (mean±std) ..... 41
**Table 2.2** Different protocols used for multiplexed immunofluorescence experiments ..... 42
**Table 2.3** List of antibodies and combinations used in this study ..... 43
**Table 2.4** Relative frequency and distribution of Lewy bodies (LB) in the cortex ..... 47
**Table 3.1** List of antibodies used in this study ..... 77
**Table 4.1** Comparison of *PRKN*-knockout (KO) mouse model phenotypes ..... 95
**Table 4.2** List of antibodies used in Western blot ..... 100
**Table 4.3** Free-floating immunofluorescence staining list of antibodies ..... 102

# List of Abbreviations

| | |
|---|---|
| 6-OHDA | 6-hydroxydopamine |
| α-Syn | α-synuclein |
| Aa | amino acid |
| ARJP | autosomal recessive juvenile parkinsonism |
| AT8 | phosphorylated tau at serine 202 and threonine 205 residues |
| ATP | adenosine triphosphate |
| AV | autophagic vacuole |
| Aβ | Amyloid-β |
| BNIP3 | BCL2 interacting protein 3 |
| BNIP3L | BCL2 interacting protein 3 like |
| CB | cerebellum |
| CMA | chaperone-mediated autophagy |
| COR | C-terminus of Ras-of-complex |
| CT | control |
| CTP | C-terminal domain |
| Cx | cortex |
| DA | dopamine/dopaminergic |
| DLB | dementia with Lewy bodies |
| DMV | dorsal motor nucleus of vagus |
| Drp1 | dynamin-1-like protein |
| EAE | experimental autoimmune encephalomyelitis |
| EOPD | early-onset Parkinson's disease |
| ER | endoplasmic reticulum |
| GDP | Guanosine diphosphate |
| GFAP | glial fibrillary acidic protein |
| GRP75 | glucose-regulated protein 75 |
| GS | glutamine synthetase |
| GTP | Guanosine triphosphate |
| GTPase | Guanosine triphosphatase |
| HIAR | heat-induced antigen retrieval |
| HO | Hoechst |
| HPC | hippocampus |
| HuD | human antigen D |
| HYP | hypothalamus |
| IBA1 | ionised calcium binding adaptor molecule 1 |
| IBR | in-between RING |
| IPSC | induced pluripotent stem cell |
| KO | knockout |
| LB | Lewy body |
| LC | locus coeruleus |
| LN | Lewy neurite |
| LP | Lewy pathology |
| LPS | lipopolysaccharide |
| LRRK2 | leucine rich repeat kinase 2 |
| Mab | monoclonal antibody |
| MAO-B | monoamine oxidase B |
| MARK1 | microtubule affinity-regulating kinase 1 |
| MB | midbrain |

| | |
|---|---|
| MMP | mitochondrial membrane potential |
| MTS | mitochondrial targeting sequence |
| NAC | non-amyloid component |
| NBM | nucleus basalis of Meynert |
| NeuN | neuronal nuclei antigen |
| NFT | neurofibrillary tangle |
| Nix | NIP3-like protein X |
| NMS | non-motor symptoms |
| NS | not specified |
| NST | nigrostriatal |
| NT | N-terminal regulatory domain |
| OMM | outer mitochondrial membrane |
| P62 | ubiquitin-binding protein p62 |
| Pab | polyclonal antibody |
| PARIS | parkin interacting substrate |
| PBS | phosphate buffered saline |
| PBST | phosphate buffered saline with tween |
| PCG-1α | proliferator-activated receptor gamma coactivator 1-α |
| PD | Parkinson's disease |
| PHF | paired-helical filament |
| Phospho-PINK1 | phosphorylated phosphatase and tensin homolog- induced putative kinase 1 |
| PRKN | parkin RBR E3 ubiquitin ligase |
| PTM | post-translational modification |
| Rab8 | Ras-related protein Rab-8 |
| REP | repressor element of parkin |
| RhoA | Ras homolog family member A |
| RING | really interesting new gene |
| ROC | Ras-of-complex |
| ROI | region of interest |
| ROS | reactive oxygen species |
| RT | room temperature |
| S129/pS129 | phosphorylated α-synuclein at serine 129 residue |
| Ser65 | serine residue 65 |
| SN | substantia nigra |
| SNARE | N-ethylmaleimide-sensitive factor attachment protein receptor |
| SNCA | synuclein alpha |
| SNpc | substantia nigra pars compacta |
| STING | stimulator of interferon genes |
| SVP | synaptic vesicle precursor |
| TBST | Tris-buffered saline with tween |
| TDP-43 | Tar DNA-binding protein 43 |
| TE buffer | Tris-ethylenediamine tetra-acetic acid buffer |
| TH | tyrosine hydroxylase |

| | |
|---|---|
| TM | transmembrane domain |
| TMEM173 | transmembrane protein 173 |
| TOMM20 | translocase of outer mitochondrial membrane protein complex subunit 20 |
| Ub | ubiquitin |
| UbL | ubiquitin-like |
| UPS | ubiquitin-proteasome system |
| VDAC1 | voltage-dependent anion channel 1 |
| VM | ventral midbrain |
| WT | wild-type |

# ABSTRACT

Parkinson's disease (PD) is a progressive neurodegenerative disorder pathologically defined by nigral neuron loss and the presence of neuronal Lewy pathologies (LP) including Lewy bodies (LB) and Lewy neurites (LN) enriched with aggregated α-synuclein (α-syn). The cause of PD remains unclear; however, it is considered that a combination of ageing, environmental and genetic factors are key contributors. Genes known to cause PD include *SNCA*, *LRRK2* and *PRKN* among others. Although most PD cases are idiopathic, studying genetic forms of PD has provided invaluable insights into the pathogenesis and pathobiology of the disease. However, the impact of PD-associated genetic mutations on cellular pathologies and comparisons across mutations is limited.

To better understand LB formation and progression, the types of LP were assessed and compared in post-mortem cortical tissue from sporadic and *SNCA*-mutation PD cases using multiplex immunofluorescence. Different LPs were identified including puncta, pale/mixed or mature LBs in all PD cases. More neurons were affected by LP in *SNCA* cases. Core proteins (p62 and ubiquitin) were found in both LB types and a proportion of LBs colocalised phosphorylated tau (phospho-tau) and these LBs appeared similar between sporadic and *SNCA*-mutation cases. However, there were some differences in previously identified LBs enriched proteins. Sporadic and E46K mutant cases had a similar high proportion of LBs colocalising the actin stabilizer RhoA, whereas few LBs colocalised RhoA in A53T and G51D cases. Sporadic PD had mainly mature LBs whereas *SNCA*-mutation cases had equal amounts of solid and pale/mixed LBs and more neurons with puncta. If LP types are indicative of progression, these data suggest that the progression of LB formation differs between sporadic and *SNCA*-related PD.

To determine if other PD mutations initiate similar neuronal pathologies, human induced pluripotent stem cell (iPSC)-derived dopaminergic neurons with *SNCA*, *LRRK2* and *PRKN* mutations transplanted into mice for 6 months were assessed and compared using free-floating multiplex immunofluorescence. A similar proportion and density of morphologically heterogenous dopaminergic neurons was identified in the grafts of all genotypes, although the *PRKN* mutation group had smaller neurons and projections. α-Syn and tau levels in the grafted dopaminergic neurons were similar in all mutant groups compared to control. Morphologically

diverse phospho-α-syn and phospho-tau immunoreactive aggregate-like structures (including puncta and LNs but not LBs) were seen in all genotype grafts, however most were not or only partially localised to grafted dopaminergic neurons. This suggests that the different mutations produce similar early protein expression and diverse aggregates. These structures may be related to early LN formation or other developmental aspects associated with the maturation of transplants.

While all grafts including *PRKN* exhibited aggregate-like structures, most *PRKN* (and some *LRRK2*) mutation cases do not typically have LBs which prompted further exploration of the impact of *PRKN* loss of function mutations on cellular pathologies using Western blot and free-floating multiplex immunofluorescence in a *PRKN* knockout (KO) mouse model assessed at 6 and 12 months. While α-syn levels were unchanged in the model, *PRKN* KO altered the levels of some mitochondrial proteins at both the 6- and 12-month time points without impacting neuronal or glial markers, or activating microglia. This suggests that these early mitochondrial changes with *PRKN* deletion may be insufficient to induce a degenerative or even a neuroinflammatory phenotype and emphasizes that *PRKN* deletion in adult mice produces only a mild mitochondrial phenotype.

These findings provide novel insights into the impact of different PD-associated genetic mutations on neuronal pathologies, particularly during LP initiation and progression. *PRKN* deletion at 6 months in mice did not produce LP, while in developing human dopaminergic neurons with *PRKN* mutations in a stressed mouse brain there was some α-syn and tau aggregation, suggesting that additional stressors may be required to initiate LP. Similar data was observed in developing human dopaminergic neurons with *LRRK2* and *SNCA* mutations, suggesting that stressors may be important in most PD-risk genotypes. The types of LP and their progression differed between sporadic and *SNCA*-related PD, with sporadic cases having uniform pathology. Along with the known absence of LP in some of these genetic phenotypes of PD, the data shows that a greater diversity of degenerative pathologies occurs with genetic forms of PD.

# CHAPTER 1: Literature Review

## 1.1 Introduction

Parkinson's disease (PD) is a complex progressive neurodegenerative disorder clinically characterised by motor and non-motor symptoms (NMS) (1). Pathologically, PD is defined by dopaminergic neuronal loss in the substantia nigra (SN), particularly focused in the lateral part of the ventral tier of the pars compacta (SNpc) (2), and the presence of Lewy bodies (LB) primarily consisting of aggregated α-synuclein (α-syn) (3). The cause of PD remains unknown; however, it is believed that ageing, genetic and environmental factors are key contributors to PD pathogenesis (4). The majority of PD cases are idiopathic, however genetic causes account for 5-10% of cases and 5-15% of PD cases report a family history (1, 4, 5).

### 1.1.1 Epidemiology

PD is the second most common neurodegenerative disorder (6). It is estimated that over 10 million people are currently living with PD globally (7), and due to the ageing population the prevalence of PD is projected to exceed 12 million by 2040 (8). PD is rare before 50 years of age, is estimated to occur in 1% of people over 60 years of age and the prevalence increases to more than 3% in people aged over 80 years (9, 10). Idiopathic PD has a mean age of onset of ~62 years and an average disease duration of ~13 years (11). It is estimated that the incidence of PD ranges between 5 to 35 per 100 000 individuals annually (10). The 2015 Deloitte Economic Access "Living with Parkinson's Disease" report estimates that 1 in every 340 people in Australia has PD and on average, 32 Australians are diagnosed with PD each day (12). Thus, it is vital to investigate this debilitating disease as it affects millions worldwide, heavily burdens the quality of life of those affected, economically burdens the healthcare system, and there are currently no cures.

### 1.1.2 Clinical presentation and manifestation

There are four cardinal motor symptoms of PD including rest tremor, bradykinesia or akinesia, rigidity and loss of postural reflexes (13, 14). Patients must present with bradykinesia and at least one of rest tremor or rigidity and have supportive criteria such as responding to dopaminergic therapy to meet the diagnostic criteria for PD (15). Secondary clinical motor

features include freezing of gait, micrography, hypomimia, dysphagia and dysarthria, among others (1, 13).

PD NMS are diverse and include neuropsychiatric disturbances (depression and anxiety), sensory abnormalities (olfactory deficits, pain and paraesthesia), sleep disorders, autonomic dysfunction (gastrointestinal and bladder dysfunction) and cognitive deficits (13, 16). Olfactory deficits are one of the most prevalent NMS with a large multicentre study (17) finding that 74.5% of PD patients present with olfactory loss. A systematic review (18) indicated 17% of PD patients have major depression. Furthermore, a cross-sectional study (19) revealed that PD-related chronic pain affects 39.3% of PD patients. Also, the Sydney Multicentre Study of PD (20) reported that dementia is present in 83% of PD patient survivors after 20-year follow-up. Therefore, NMS in the PD population are highly diverse and prevalent and can be as disabling as the motor features.

PD progression can be separated into preclinical, prodromal and motor clinical stages of which the latter can be further divided into early, mid and late-stage PD (21, 22). In the preclinical stage, PD pathology is assumed to initiate without causing symptoms. This stage is followed by a long prodromal phase which can last years to decades typically characterised by specific NMS and subtle motor symptoms (22). Rapid eye movement sleep behaviour disorder, the loss of smell or hyposmia and mood disturbances are considered early NMS of the prodromal phase as PD patients have reported these symptoms prior to the onset of motor deficits in retrospective studies (23, 24). In early-stage PD, when the threshold of 40-60% of dopaminergic cell loss is met, motor symptoms begin to manifest (21). Initial manifestations of bradykinesia are slowed movement and reaction times (13). As the disease progresses NMS and motor symptoms become increasingly severe and prevalent. Postural instability, gait disturbances, dysphagia and dementia typically manifest in late-stage PD (22).

## 1.2 Neuropathology

The pathological hallmarks of PD are dopaminergic neuronal loss in the SNpc and the presence of Lewy pathologies (LP) in the form of LBs in the neuronal cytoplasm and Lewy neurites (LN) in neuronal processes (25) (Fig. 1.1). Upon external examination of transverse brainstem sections, there is typically loss of pigmentation in the SN (Fig. 1.1), and locus coeruleus (LC)

which correlates with the loss of dopaminergic and noradrenergic neurons in these regions, respectively (26).

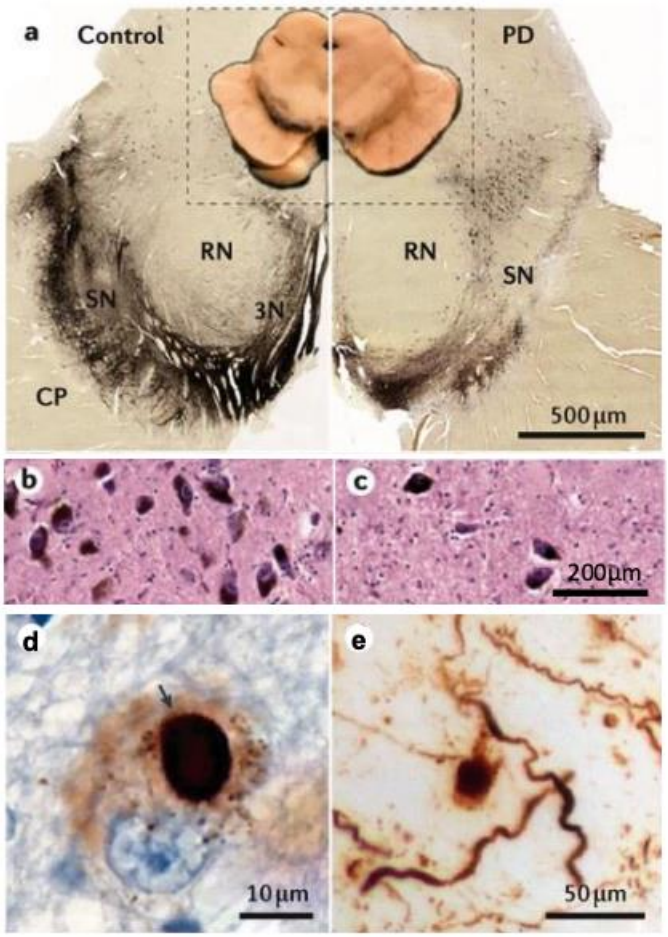


**Figure 1.1 Substantia nigra (SN) dopaminergic cell loss and Lewy pathology (LP) in Parkinson's disease (PD) patients.** Macroscopic (a, inset) and immunohistochemical (a) examination reveals pigmented dopaminergic neurons and tyrosine hydroxylase (TH) immunoreactivity in the SN of a control on the left side contrasting with a loss of pigmented dopaminergic neurons in the SN of a PD patient on the right side. Microscopic examination (b-e) reveals pigmented SN neurons in a control (b) in contrast to (c) exhibiting a loss of SN neurons in a PD patient and LPs including a Lewy body (d) and Lewy neurites (e). Figure adapted from Poewe et al., 2017 (22).

### 1.2.1 Neuronal loss

Compared with normal ageing, PD patients have a 10-fold accelerated loss of SNpc dopaminergic neurons in the first decade of the disease (2). In the early stages, dopaminergic neuronal loss is confined to the ventrolateral SN but becomes more widespread with disease progression. Cell loss also often occurs in the dorsal motor nucleus of vagus (DMV), pedunculopontine nucleus, locus coeruleus (LC) and basal forebrain, while it is rare elsewhere or in the cortex (25, 27, 28).

### 1.2.2 Lewy pathologies

Lewy pathologies encapsulate the proteinaceous inclusions LBs and LNs. It has been estimated the neurons bearing LBs die every 6 months on average in PD (29). LBs are intraneuronal eosinophilic masses consisting of ~300 molecules, primarily concentrating aggregated α-syn (3, 30, 31). α-Syn is a 140 amino acid (aa) protein composed of three domains including the N-terminal (residues 1-60), the central non-amyloid component (NAC) (residues 61-95) and the C-terminal (residues 96-140). It is abundantly expressed in the brain and particularly enriched at presynaptic nerve terminals (32, 33). There are several isoforms of α-syn which are shorter than the 140 aa sequence and are expressed at lower levels in the brain (34). While the physiological function of α-syn is incompletely understood, α-syn has been shown to have a role in regulating neurotransmitter release (35).

Native α-syn exists unfolded in solution, however the amphipathic N-terminal adopts an α-helix conformation upon binding with lipids (36, 37). The N-terminal mediates the α-syn-lipid binding interaction which is stabilised itself by the presence of lipids (37). The NAC core region of α-syn has a role in protein fibrillation and aggregation (38), and the negatively charged C-terminal region has a role in mediating interactions with other proteins (39) and the protein's chaperone activity as its deletion abolishes this activity contributing to its aggregation (40). Alternative splicing of either exon 3 or 5 produces α-syn isoforms *SNCA*126 and *SNCA*112 which have functional differences: while exon 3 deletion (*SNCA*126) disrupts the N-terminal domain which may reduce aggregation, exon 5 deletion (*SNCA*112) shortens the C-terminus which may enhance aggregation (41). Under physiological or pathological conditions, α-syn can adopt different conformations such as disordered/unfolded, ordered membrane-bound α-helical conformation, helically folded tetramers, oligomeric species and amyloid fibril structures (42).

Pathologic forms of α-syn include oligomeric and fibrillar species and post-translational modifications (PTM) of the protein which have toxic effects on different cell types and their functions as reviewed in (43). In PD pathology, soluble α-synuclein is prone to misfolding and forming toxic oligomers and protofibrils, and eventually insoluble β-sheet rich amyloid fibrils that accumulate into LBs (44). Fibrils are considered the predominant species in LBs (45, 46),

although a more recent study (47) challenged this concept suggesting that organelles, lipids and non-fibrillar forms of α-syn are the main components of LBs. α-Syn PTMs include phosphorylation, ubiquitination, acetylation, nitration, oxidation and truncations which may influence its solubility (48). The most predominant post-translationally modified α-syn species in LBs include phosphorylation at serine residue 129 (pS129), ubiquitination and truncations (49-51).

Although α-syn is phosphorylated at several sites (S87, S129, Y39, Y125, Y133 and Y136) (52), one of the most abundant forms of α-syn in LBs is pS129 often used to identify LPs (50, 52-56). However, prior to the use of α-syn or pS129, LPs were originally detected using immunolabelling for the cytoskeletal protein neurofilament and the proteolytic proteins ubiquitin and p62 which are also common LB components (57-61). LBs are defined as sizeable eosinophilic inclusions immunoreactive for α-syn and ubiquitin localised to neuronal soma with some appearing spherical with a dense core and peripheral halo morphology (30, 62). However, many different inclusion morphologies have been reported. α-Syn labels variable LPs in neurons including diffuse or punctate α-syn, aggregation centres surrounded by puncta, arch-like inclusions, cloud-like or irregularly-shaped bodies, inclusions with peripheral LBs, variably shaped and sized neurites among others (Fig. 1.2) (30, 63-66). Characterising the proteins associated with LBs together with the variable LB inclusion morphologies may provide valuable insights into LB formation and PD pathogenesis.

LBs are widely distributed throughout the central nervous system. According to the Braak staging hypothesis (Fig. 1.2), in the early stages (stage 1 and 2) corresponding to the prodromal phases of PD, LP initiates in the DMV and olfactory bulb (stage 1) and spreads through the pons (stage 2) to the SN (stage 3), basal forebrain and mesocortex (stage 4) corresponding to the symptomatic phase and then progresses to the limbic system and neocortex (stages 5 and 6 respectively) (25, 67), accounting for the wide distribution of LB pathology over time. Interestingly, neuronal loss in the SN has been reported to precede LP deposition in incidental LB disease patients classified as Braak stage 1 or 2 (68). More recently, it was similarly shown that patients with mild motor deficits had similar dopaminergic neuronal loss with or without LBs (69). These studies highlight that there may be other factors in addition to α-syn pathology contributing to dopaminergic neuronal loss in PD.

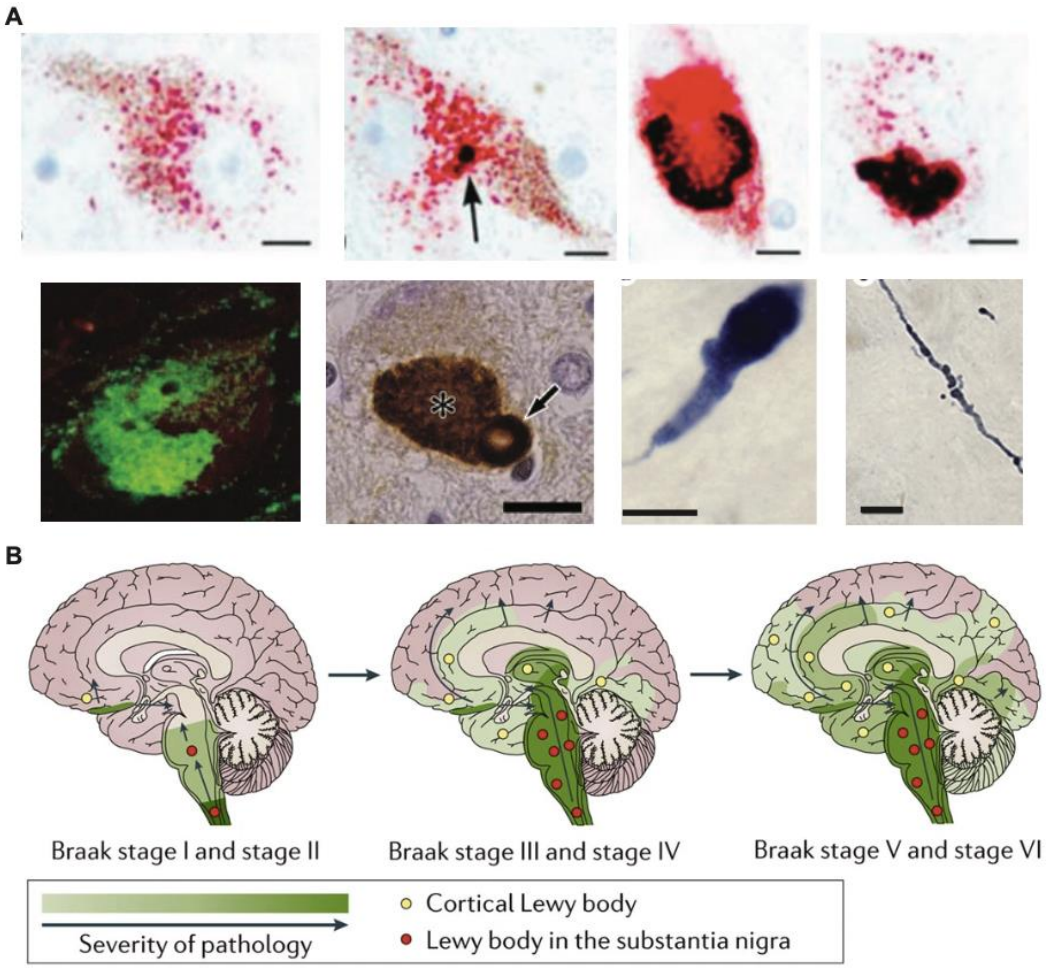


**Figure 1.2 Lewy pathologies (LP) and their hypothesised progression in the Parkinson's disease (PD) brain.** Photomicrographs reveal variable neuronal LPs (A), and the schematic diagram (B) illustrates LP progression based on the Braak staging hypothesis in the PD brain. Figure adapted from Kuusisto et al., 2003 (64), Gómez-Tortosa et al., 2000 (63), Wakabayashi et al., 2013 (30), Goedert et al., 2013 (66) and Poewe et al., 2017 (22).

### 1.2.3 Pathophysiology

PD motor signs are attributable to dopaminergic neuronal cell death in the SN which disrupts critical circuitry (direct and indirect pathways) in the brain ultimately leading to an over-inhibited thalamus and motor cortex (direct pathway shown in Fig. 1.3) (70).

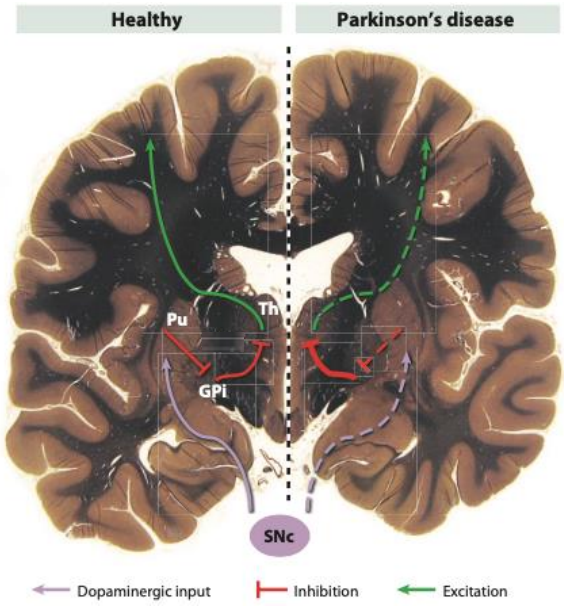


**Figure 1.3 The direct pathway of the motor circuit dysregulated in Parkinson's disease (PD).** A simplified schematic illustrating the direct pathway which becomes disrupted in PD. On the left side (healthy), the substantia nigra pars compacta (SNc) provides dopaminergic input to the putamen (Pu) which inhibits the globus pallidus interna (Gpi) subsequently inhibiting the thalamus (Th) providing an overall excitatory input to the motor cortex. On the right side (PD), due to dopaminergic cell death in the SN, the dopaminergic input is attenuated leading to increased inhibition of the excitatory thalamocortical pathway producing motor impairments. Figure from Shulman et al., 2011 (71).

## 1.3 Genetic Aetiology

Genetic forms of PD accounts for approximately 5-10% of PD cases (1, 5). There are over 200 PD-associated genes, where mutations in 24 genes have been reported to cause monogenic forms of PD in a dominant or recessive inheritance pattern (72, 73). The PD genes *SNCA*, *LRRK2*, *PRKN* and *PINK1* will be discussed in the following sections of this thesis as they are the most prevalent dominant and recessive causative genes. The identification of these genes has provided key insights into the mechanisms implicated in PD pathogenesis including α-syn aggregation, impaired proteasomal and lysosomal function, mitochondrial dysfunction and neuroinflammation leading to cell death in the SN (74).

## 1.3.1 Autosomal dominant PD genes

### 1.3.1.1 SNCA

*SNCA* – Encoding the protein α-synuclein

The *SNCA* gene encoding the α-syn protein is predominantly expressed in neurons and was the first gene associated with PD (75, 76). As seen in Fig. 1.4, the PD-associated missense mutations of the *SNCA* gene are located in the N-terminal domain of the protein (77).

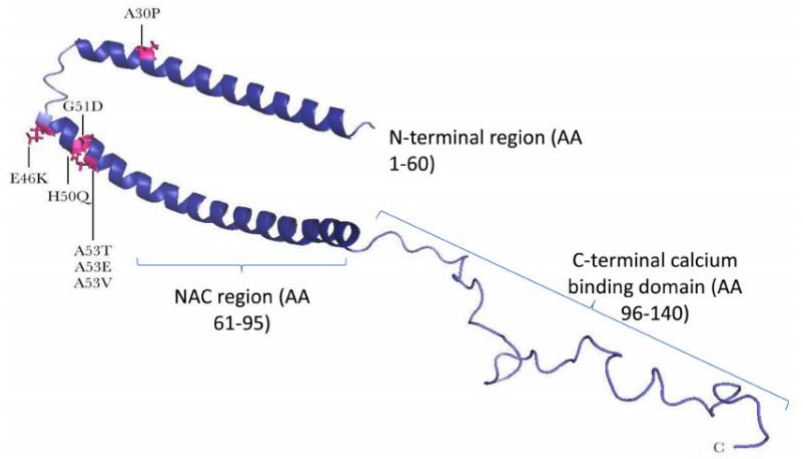


**Figure 1.4 Structural features of the α-synuclein (α-syn) monomer.** The domain structure of the α-syn protein with the positions of PD-associated missense mutations indicated. Figure from Whittaker et al., 2017 (78).

*SNCA* pathogenic mutations

The A53T mutation of the *SNCA* gene (Fig. 1.4) was the first discovered to cause autosomal dominant PD (76). Using linkage mapping Polymeropoulos *et al*. (76, 79) identified genetic markers on chromosome 4q21-q23 associated with clinical PD in a large family with dominantly inherited PD and subsequently mapped the *SNCA* gene to this chromosomal region. Based on sequence analysis, the A53T mutation was identified in the same large family and three other unrelated families with autosomal dominant PD (76). As summarised in Table 1.1, compared to sporadic PD, patients with the A53T mutation generally present with typical PD symptoms, however they have an earlier disease onset, rapid progression and prevalent cognitive and psychiatric disturbances (76, 80-84). Pathologically, A53T mutation carriers have more extensive cortical neuritic pathology compared to sporadic PD (Table 1.1). Other mutations at the A53 site of *SNCA* have been associated with familial PD, including A53E and A53V (Fig. 1.4).

Four other missense mutations in *SNCA* including A30P (85), E46K (86), H50Q (87) and G51D (88), have been identified in families with dominantly inherited PD with clinically diverse phenotypes (Fig. 1.4). Carriers of the A30P mutation present similarly to idiopathic PD cases, however, cognitive impairments are seen frequently and early in the disease progression (89). Compared to sporadic PD, an A30P patient has more glial α-syn aggregates and more aggregates in the cerebellum, precerebellar and oculomotor brainstem nuclei (90). Carriers of the E46K mutations present with more severe symptoms such as visual hallucinations and dementia and have more abundant cortical LBs (86). The H50Q and G51D mutations were identified more recently (Fig. 1.4). H50Q mutation carriers have typical PD symptoms with mild cognitive impairments and one patient had cortical LBs, plaques and neurofibrillary tangles (NFT) (87, 91, 92). The G51D mutation was identified in a family with a parkinsonian-pyramidal syndrome using whole exome sequencing (88). The G51D mutation phenotype is quite atypical and severe with an early disease onset, rapid progression, a moderate response to dopamine and characterised by pyramidal signs, psychiatric disturbances and dementia (88, 92). In contrast to sporadic PD, G51D mutation carriers have cortical neuronal loss, extensive cortical LP and glial-like inclusions in the white matter (88, 92).

Moreover, *SNCA* duplications (93) and triplications (94) account for ~1-2% of PD familial cases with autosomal dominant inheritance (95). There appears to be a relationship between *SNCA* dosage and PD phenotype severity (96, 97). Studies have shown that PD patients with *SNCA* duplication have an increased accumulation of α-syn (98) and patients with *SNCA* triplication have a doubling of α-syn mRNA and protein (97)**.** As summarised in Table 1.1, *SNCA* duplication PD patients present similarly to idiopathic PD, although some patients have more cognitive impairments or dementia and psychiatric disturbances (99). This differs from *SNCA* triplication patients who present with an earlier disease onset, faster progression and severe symptoms (100). Also, a study (98) revealed that a patient homozygous for *SNCA* duplication presented with an early disease onset at age 28 and rapid progression including early severe cognitive impairments compared to the patient's parents heterozygous for *SNCA* duplication with a much later disease onset at ages 71 and 61 years. This demonstrates the effect of *SNCA* dosage on the severity of PD even within the same family. Compared to sporadic PD, *SNCA* duplication carriers have many cortical LBs and plaques as well as some glial inclusions in different brain regions and *SNCA* triplication carriers have extensive

neuronal loss particularly in the cornu ammonis area of the hippocampus, many cortical LBs and additional glial inclusions (Table 1.1).

**Table 1.1** Clinical and pathological features of different *SNCA* gene mutations.

| Mutation (References) | Age of Onset (years) | Disease Duration (years) | Clinical Features | Pathological Features |
|---|---|---|---|---|
| A53T (76, 80-84, 101-106) | 47 ± 12 | 8 ± 4 | Levodopa-responsive parkinsonism<br>Central hypoventilation in some cases<br>Myoclonus in some cases<br>Dementia and psychiatric disturbances | Neuronal loss and LP in SN, LC, DMV, HPC and nBM<br>LNs in SN, LC, DMV, HPC, HYP, Cx<br>Some cortical neuronal loss, LBs and extensive neuritic pathology<br>Gliosis in SN, LC and HPC<br>Tau pathology in SN, LC, cingulate Cx and other brain regions |
| A30P (85, 89, 90) | 58 ± 8 | 6, 4 | Levodopa-responsive parkinsonism<br>Frequent and early cognitive impairments | Neuronal loss in SN, LC and DMV<br>Widespread LP and glial aggregates<br>More severe α-syn aggregation in CB, precerebellar and oculomotor nuclei<br>Cortical tau cytoskeletal pathology |
| E46K (86, 107, 108) | 50-65 | Age at death 64-75 | Severe levodopa-responsive parkinsonism<br>Dementia and visual hallucinations<br>Sleep disturbances, anxiety and depression | Neuronal loss in SN, LC and DMV<br>Moderate to abundant LP in SN, LC, DMV, HYP, HPC and cingulate Cx<br>Astrogliosis in SN<br>No apparent tau pathology |
| H50Q (87, 91, 92) | 60, 71 | 12 (patient with AAO of 71) | Levodopa-responsive parkinsonism<br>Cognitive decline | Neuronal loss and LP in SN and LC<br>LBs in Cx<br>Cortical plaques and NFTs in HPC and Cx |
| G51D (88, 92) | 42 ± 17 | 5-7 (except for one patient with 29 years) | Rapidly progressive parkinsonism (some patients bedridden within 5 years)<br>Mild-moderate response to levodopa<br>Pyramidal symptoms<br>Frequent psychiatric symptoms and dementia | Extensive neuronal loss in SN<br>Neuronal loss in Cx, LC, DMV and HPC<br>Widespread LP most severe in brainstem, HPC and Cx<br>Astrogliosis in SN<br>GCI-like inclusions in white matter<br>Tau pathology in HPC and entorhinal Cx |
| Duplication (93, 98, 99, 109-115) | 50 ± 11 | 13 ± 6 | Levodopa-responsive parkinsonism<br>Depression is problematic some patients<br>Psychiatric disturbances, cognitive dysfunction or dementia in some patients | Neuronal loss and LP in SN, LC, DMV, nBM and HPC<br>LBs and plaques in the Cx<br>Gliosis in SN, LC and nBM<br>NFTs in HPC<br>Some glial inclusions in SN, nBM and Cx |
| Triplication (83, 94, 97, 100, 116-118) | 40 ± 14 | 7 ± 2 | Rapidly progressive levodopa responsive parkinsonism<br>Dementia and psychiatric disturbances | Severe neuronal loss in the SN, LC, nBM and HPC<br>LP in SN, LC, HYP, HPC, nBM, Cx<br>Some glial inclusions in SN, Cx and CB white matter<br>Gliosis in HPC, nBM and Cx<br>Molecularly, there is a doubling of α-syn protein<br>Some plaques and rare NFTs in the Cx |

Values are presented as mean ± SD. AAO, age at onset; α-syn, α-synuclein; CB, cerebellum; Cx, cortex; DMV, dorsal motor nucleus of the vagus nerve; GCI, glial cytoplasmic inclusion; HPC, hippocampus; HYP, hypothalamus; LB, Lewy body; LC, locus coeruleus; LN, Lewy neurite; LP, Lewy pathology; nBM, nucleus basalis of Meynert; NFT, neurofibrillary tangle; SN, substantia nigra.

Pathogenic mechanisms of *SNCA* mutations

Based on the localisation of the A53T mutation, it was initially suggested that it may disrupt the α-helical formation and promote the β-sheet structure of the α-syn protein (76). As β-sheets are thought to play a role in the protein aggregation process, this suggested that the A53T mutation may increase the propensity for α-syn to **misfold and aggregate** to form LB inclusions (76). This was supported by an *in vitro* study (119) which demonstrated that A53T α-syn had a faster rate of fibrillation and was more prone to aggregation compared to wild-type (WT) α-syn. More recently, it was shown that the A53T mutation does not significantly disrupt the fold of α-syn, but rather alters the α-syn fibril structure causing increased aggregation and toxicity (120). A53V has similar pathogenic mechanisms to A53T, but A53E has a reduced propensity to form fibrils, but increases the load of toxic oligomers (121, 122).

An *in vitro* study (119) revealed that A30P α-syn has a greater propensity to aggregate than WT protein, although its fibrillation rate was slower than WT (see also A53E mutation). Since the A53T and A30P mutations have different mechanisms in relation to α-syn aggregation, it has been suggested that instead of increased rate of fibrillation, it is an increased rate of nonfibrillar oligomer formation which is a shared property between these α-syn mutants (123). Like the A53T mutation, E46K α-syn has a faster rate of fibrillation compared to WT protein (124). The H50Q mutation also accelerates α-syn fibrillation and oligomerisation compared to WT and additionally enhances α-syn secretion and toxicity (125). Moreover, it was shown that the G51D mutation also enhances α-syn secretion, however it attenuates α-syn aggregation (126).

Furthermore, mutations have been shown to alter the **structural dynamics** of the α-syn protein. A study (127) revealed that the A53T, E46K and A30P mutations significantly alter the site-specific structural dynamics of α-syn. Specifically, A53T and E46K mutations alter the site-specific microenvironment at the N and C termini of α-syn and all three mutations reduced solvent accessibility at the N and C termini and increased conformational rigidity at

the C terminus (127). Therefore, this may lead to the production of an aggregation-prone intermediate and contribute to the mutant's increased oligomerisation rate, and thus their propensity to aggregate (127). Furthermore, intramolecular interactions between the C- and N-termini and NAC region of α-syn have been established which is thought to inhibit α-syn oligomerisation by shielding the NAC region from adopting a β-sheet conformation (128). However, the A53T and A30P mutations disrupt this intramolecular interaction which reduces shielding of the NAC region and potentiates oligomerisation (129).

*SNCA* multiplications are associated with **increased expression and aggregation of α-syn** associated with toxic effects. A study (130) employed induced pluripotent stem cells (iPSCs) to show that iPSC-derived dopaminergic neurons with *SNCA* triplication exhibit increased α-syn accumulation and overexpression of oxidative stress markers compared to controls. More recently, a study revealed that iPSC-derived dopaminergic neurons with *SNCA* triplication had increased pS129 levels and LB-like accumulations associated with mitochondrial abnormalities (131). Furthermore, overexpression of α-syn corresponding with *SNCA* gene multiplication has been demonstrated to inhibit neurotransmitter release associated with synaptic dysfunction (132). This indicates that increased *SNCA* dosage may play a role in increasing α-syn aggregation which may enhance vulnerability to cell death. Similarly, PD A53T iPSC-derived dopaminergic neurons have revealed pan and pS129 α-syn accumulation and aggregates compared to controls (131, 133, 134). Also, A53T mice have shown neuronal α-syn accumulation, axonal swellings and pan and pS129 aggregates or LB-like inclusions associated with cell death unlike control or WT α-syn mice (135-140).

Mutant forms of α-syn have been demonstrated to disrupt various cellular functions including synaptic vesicle trafficking, mitochondrial functioning and autophagy/lysosomal functioning as well as activating neuroinflammatory phenotypes (74). α-Syn aggregation disrupts **synaptic vesicle trafficking** as indicated by large α-syn oligomers preferentially binding to synaptobrevin-2/vesicle associated membrane protein 2 (141). This binding inhibited the formation of the N-ethylmaleimide-sensitive factor attachment protein receptor (SNARE) complex preventing exocytosis, and thus dopamine release (141). Moreover, another study (142) revealed that the A30P mutant impaired SNARE-complex assembly *in vitro*. These findings (141, 142) suggest that *SNCA* mutations that promote α-syn oligomerisation may potentiate synaptic dysfunction.

**Mitochondrial dysfunction** associated with *SNCA* mutations is also implicated in PD pathogenesis. In cultured dopaminergic neurons A53T mutant α-syn accumulated in mitochondria and reduced complex I activity, increasing reactive oxygen species (ROS) at an earlier time point compared to WT α-syn (143). Recently, it was shown that iPSC-derived cortical neurons with the A53T mutation have increased levels of oligomers and mitochondrial impairments including inhibited complex I activity and increased ROS production (144). In line with this, iPSC-derived dopaminergic neurons with A53T mutation exhibit LB-like accumulations associated with increased aberrant mitochondrial morphology (131). Similarly, *in vivo* studies (145-147) have shown that A53T α-syn in neurons inhibits mitochondrial complex I function, increases mitophagy and produces mitochondrial abnormalities which can lead to increased ROS, cellular stress and cell loss. Also, both the H50Q and G51D α-syn mutants enhance mitochondrial fragmentation compared to WT α-syn likely due to their enhanced secretion of α-syn (125, 126), which could increase mitochondrial dysfunction and cellular stress.

Additionally, α-syn degradation occurs via the **autophagy-lysosomal pathway and ubiquitin-proteasome system (UPS)**, and dysfunction of these pathways contributes to α-syn accumulation (148). The A30P and A53T α-syn mutants have been reported to impair the chaperone-mediated autophagy (CMA) system by binding to the lysosomal membrane receptor lysosome-associated membrane protein 2, blocking lysosomal uptake and degradation of the mutants and of other substrate proteins (149). Further, a more recent *in vivo* study (150) showed that A53T α-syn impaired proteasome activity leading to UPS dysfunction. These studies highlight that mutant forms of α-syn block these protein degradation systems which may promote α-syn aggregation and cellular stress.

**Neuroinflammation** is also activated by *SNCA* mutations, as a recent study (151) showed that human iPSC-derived microglia harbouring the A53T mutation transplanted into mice, had increased activation compared to controls under proinflammatory conditions. Furthermore, other *in vitro* studies (152, 153) have shown that A53T and A30P (but not E46K) α-syn enhance microglial activation, ROS production and proinflammatory gene expression compared to WT α-syn or control. H50Q, G51D and A53T (but not E46K) α-syn preformed synuclein fibrils injected into the rat SN significantly increased microglial activation and

inflammatory cytokine levels compared to WT (154). While the E46K mutation does not appear to induce inflammation, another cell culture study (155) reported that the A30P and E46K mutants induced greater pro-inflammatory cytokine and chemokine release in microglia than WT. These findings support that *SNCA* mutations cause neuroinflammatory phenotypes which may contribute to cell death. The key mechanisms of *SNCA* mutations are summarised in Fig. 1.5.

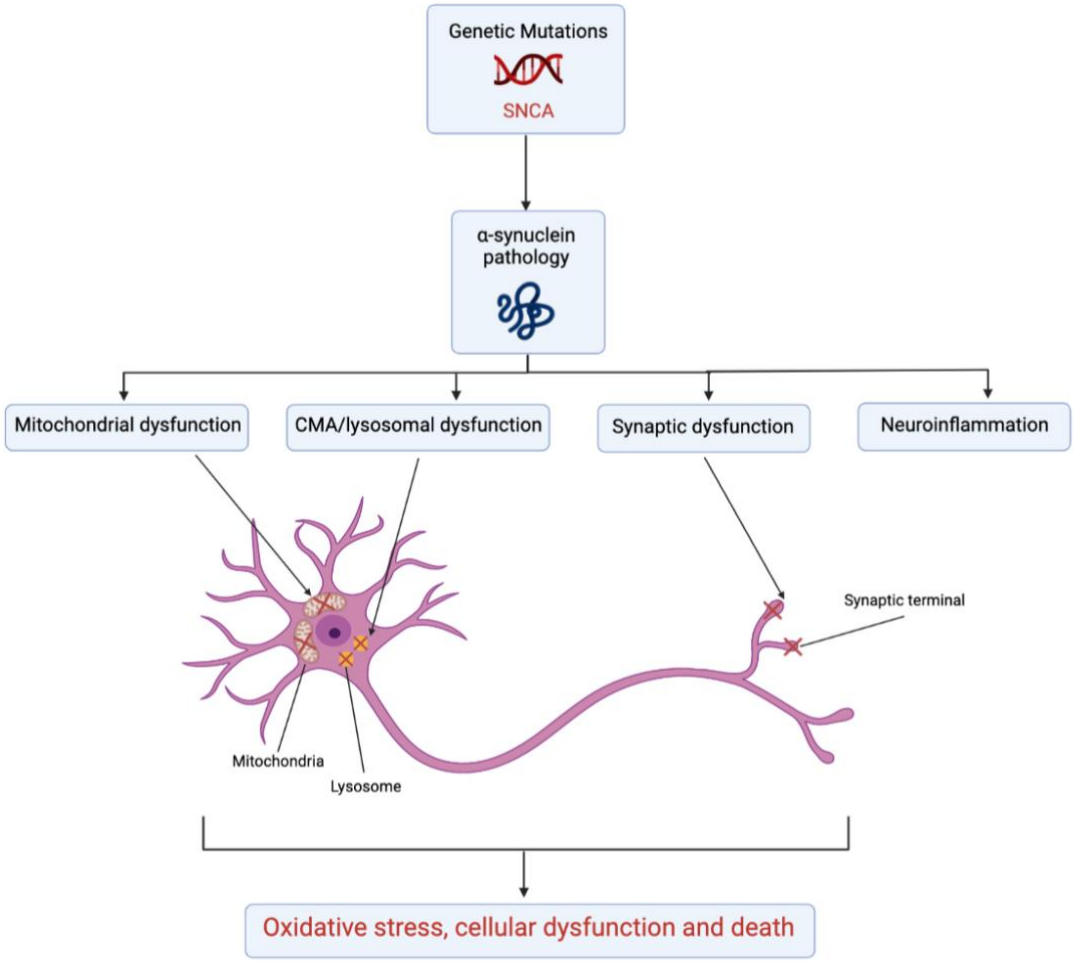


**Figure 1.5 Diagram illustrating the key pathogenic mechanisms of *SNCA* mutations.** *SNCA* gene mutations promote α-synuclein pathology including oligomerisation and aggregation which disrupts mitochondrial functioning, chaperone-mediated autophagy (CMA) and synaptic vesicle trafficking and alters neuroinflammatory responses. These toxic effects lead to oxidative stress and cellular dysfunction, rendering cells vulnerable to death. Original image created with BioRender.com.

### 1.3.1.2 LRRK2

*LRRK2*- encoding the protein LRRK2

Mutations in the leucine-rich repeat kinase 2 (*LRRK2)* gene are also associated with autosomal dominant PD (156). *LRRK2* encodes the large multifunctional LRRK2 protein consisting of

2527 aa (157). The *LRRK2* gene is predominantly expressed in microglia compared to other cell types (75). LRRK2 protein is expressed in neurons and more weakly in other glia, localised throughout cell bodies and processes associated with vesicular and membranous structures (158, 159). LRRK2 has several diverse functions including regulating vesicular trafficking, cytoskeletal dynamics, autophagy and lysosomal degradation, synaptogenesis and neurotransmission, mitochondrial function and neuroinflammatory responses (156).

LRRK2 belongs to the Ras of complex (Roc) and C-terminal of ROC protein family and consists of multiple domains with different functional properties including protein-protein interaction domains and an enzymatic core composed of Roc guanosine triphosphatase (Roc GTPase), C-terminus of ROC (COR) and protein kinase domains (Fig. 1.6). The enzymatic core enables GTPase and serine-threonine kinase enzymatic activities and dimerization of LRRK2 (157, 160). The Roc-COR tandem domain exists as a dimer and the COR domain mediates this dimerization regulating the GTPase activity (161). Dimerization of LRRK2 also appears to enhance kinase activity (162, 163). Native LRRK2 predominantly exists as a dimer that self-interacts and autophosphorylates requiring an intact C-terminus but not N-terminus to regulate its kinase activity (162). The C-terminus WD40 domain is critical for LRRK2 self-interaction and autophosphorylation activity (162).

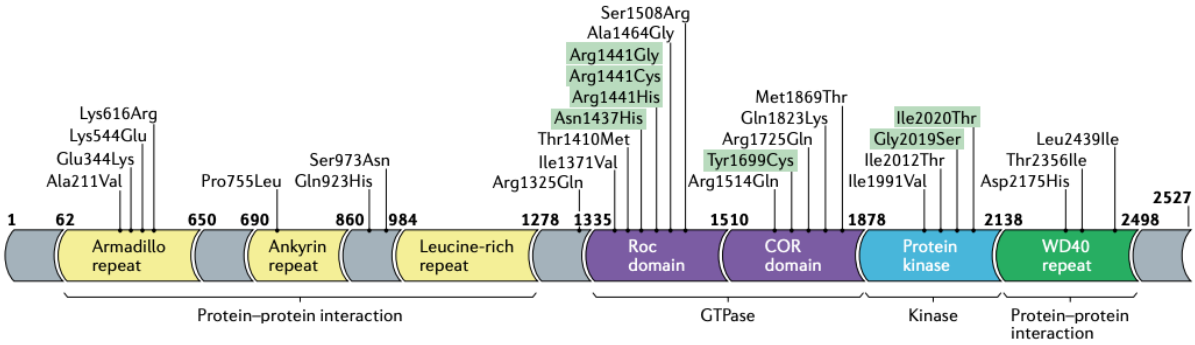


**<u>Figure 1.6</u> Domain structure of the LRRK2 protein with the positions of PD-associated mutations indicated.** The pathogenic mutations are highlighted in light green. Domains are labelled and differentiated by colour to distinguish functional properties. Figure from Tolosa et al., 2020 (160).

The GTPase domain functions as a molecular switch to regulate kinase activity cycling between guanosine diphosphate (GDP)-bound inactive state and guanosine triphosphate (GTP)-bound active state of which the active state can bind and activate downstream effectors and initiate signalling cascades (164). Both GTP binding and hydrolysis regulate and activate LRRK2 kinase activity (165). There is also evidence that the kinase domain may have a role in regulating GTPase activity, as studies (166-168) show that LRRK2 autophosphorylates the

Roc GTPase domain which influences LRRK2 GTPase activity. The protein-protein interaction domains of LRRK2 consist of structural repeat motifs including the armadillo, ankyrin and leucine-rich repeats at the N-terminus and the WD40 repeat at the C-terminus (169). It is predicted that the N-terminal armadillo, ankyrin and leucine-rich domains form an extended structure which binds to membrane and cytoskeletal structures and the WD40 domain adopts a β-sheet closed propeller structure which functions to form protein complexes (169).

Pathogenic *LRRK2* mutations

Using genome-wide linkage analysis, a locus on chromosome 12p11.2-q13.1 was identified in a family with autosomal dominant parkinsonism and named *PARK8* (170). Later studies (171, 172) identified missense and splice-site mutations in the *LRRK2* gene in families with autosomal dominant parkinsonism previously linked to the *PARK8* locus. To date, a large number of mutations in the *LRRK2* gene are associated with dominantly inherited-PD, however studies have confirmed only 8 pathogenic mutations (173), which are located in the Roc-COR tandem and kinase domain of LRRK2 (Fig. 1.6). These *LRRK2* mutations include I1371V, N1437H, R1441G, R1441C, R1441H, Y1699C, G2019S and I2020T of which the G2019S mutation is the most common (173).

The clinical and pathological features of *LRRK2* pathogenic mutations are summarised in Table 1.2. The G2019S phenotype has been reported to be clinically similar, possibly indistinguishable from idiopathic PD and it may be milder (174). Compared to sporadic PD, G2019S mutation carriers present with tremor-predominant parkinsonism with a lower risk of cognitive impairment and olfactory dysfunction and an increased risk of dystonia (174). G2019S mutation carriers have additional tau pathologies including NFTs and the presence of LP is variable compared to sporadic PD (175, 176). Similarly to G2019S mutation carriers, a recent study (177) reported that R1441G mutation carriers present with tremor-predominant parkinsonism with less frequent cognitive impairment compared to idiopathic PD. Compared to sporadic PD, R1441G/H mutation carriers have nigral neuronal loss in the absence of LP (177-179).

**Table 1.2** Clinical and pathological features of different pathogenic *LRRK2* gene mutations

| Mutation (References) | Disease Age of Onset (years) | Disease Duration (years) | Clinical Features | Pathological Features |
|---|---|---|---|---|
| Roc domain mutations<br>I1371V<br>N1437H<br>R1441C/G/H<br>(171, 172, 177-187) | 63 (highly variable for R1441 mutations and younger for I1371V/ N1437H) | 15 (longer for I1371V/ N1437H) | Levodopa-responsive PD<br>Some have asymmetric tremor-predominant parkinsonism<br>Less frequent cognitive impairment and dementia | R1441C/G/H- Typically, neuronal loss in SN in the absence of LP and some tau inclusions, gliosis in SN<br>1 case reported for N1437H/I1371V- Neuronal loss and LP in SN and LC, some LP in Cx, some Ub inclusions, gliosis in SN |
| COR domain mutations<br>Y1669C<br>(172, 188, 189) | 53 | 13 | Levodopa-responsive parkinsonism<br>Prominent initial asymmetric tremor<br>Behavioural disorder in several cases (anxiety episodes, depression, paranoia, suicidality) | Neuronal loss in SN and LC with limited/no LP<br>Few LBs in Cx (1 case)<br>Gliosis in SN<br>NFTs in HPC and EC<br>Ub inclusions in some cases |
| Protein kinase domain mutations<br>G2019S<br>I2020T<br>(174-176, 180, 190-202) | 59 ± 11 | 12 ± 9 (typically long for I2020T) | Milder than typical PD<br>Levodopa-responsive asymmetric tremor-predominant parkinsonism<br>Lower risk of cognitive impairment and hyposmia<br>Frequent dystonia<br>Psychosis in some patients | Neuronal loss in SN and LC with/without LP (generally no LP and minimal neuronal loss in LC in I2020T patients)<br>LBs in HPC and Cx (G2019S)<br>Gliosis in SN (I2020T)<br>Widespread tau inclusions including NFTs |

Values are presented as mean ± SD. Cx, cortex; EC, entorhinal cortex; HPC, hippocampus; LB, Lewy body; LC, locus coeruleus; LP, Lewy pathology; NFT, neurofibrillary tangle; SN, substantia nigra; Ub, ubiquitin.

*LRRK2* mutations affect the function of three domains

Pathogenic *LRRK2* mutations affect three of the protein's functional domains, Roc domain, COR domain and protein kinase domain (see above). These mutations have different effects on the protein function leading to PD pathology. However, the pathogenic mechanisms of *LRRK2* mutations remain to be completely understood.

**Mutations in the Roc domain of LRRK2** including R1441C and R1441G have been reported to decrease GTPase activity (203-205). *In vitro* studies (203-205) demonstrated that the R1441C/G mutants could bind to GTP, however the rate of GTP hydrolysis was decreased compared to WT LRRK2 indicating a lowered GTPase activity. Consistently, another study (206) demonstrated that compared to WT LRRK2, the R1441H mutant doubled the GTP-binding affinity of the Roc GTPase domain and similarly to the R1441C/G mutants, decreased GTPase activity. These findings (203-206) show that the R1441C/G/H mutants prolong the

binding to GTP remaining in an active GTP-bound state compromising GTP hydrolysis. However, the R1441H mutant increases the GTP-binding affinity while the R1441C/G mutants do not, therefore the mechanism by which they decrease GTPase activity is less understood. In contrast, another study (207) suggested that the R1441C/G mutants increase GTPase activity as these mutants increased GTP binding compared to WT LRRK2. However, GTP hydrolysis was not investigated and the differences in GTP binding between the mutants and WT were small. More recently, an *in vitro* study (208) demonstrated that the LRRK2 Roc domain exists as a dynamic dimer-monomer structure mediated by GDP and GTP binding, and these conformational dynamics are altered by the R1441G/C/H mutations to favour an active GTP-bound monomeric conformation. These findings (208) provide insight into the mechanism by which these mutants have decreased GTPase activity compared to WT, which this study also revealed to be four times lower than that of WT LRRK2.

A study (161) which investigated the Roc-COR tandem domain in a bacterium demonstrated that the COR domain Y1699C mutation equivalent in the prokaryotic homologue reduced GTPase activity by eightfold compared to WT LRRK2. Consistently, another study (209) reported that the Y1699C mutation reduced GTPase activity compared to WT LRRK2 in a yeast model. Although, it has been suggested to increase GTPase activity as it upregulates GTP-binding in another study (207). There is general consensus that LRRK2 Roc domain mutations cause decreased GTPase activity, and it **appears that the COR domain mutation has the same effect**, however the effect of *LRRK2* mutations on kinase activity remains contentious.

In some studies (210, 211), the Y1699C mutation had no effect on kinase activity whereas another study (207) revealed a considerable increase in kinase activity relative to WT LRRK2. The effects of the Roc domain R1441C/G/H mutations on kinase activity are similarly inconsistent (173, 210, 212). **Mutations in the protein kinase domain of *LRRK2* affect its kinase activity**. The *LRRK2* G2019S mutation has been consistently reported to increase kinase activity (207, 210, 211, 213, 214). The effect of the kinase domain I2020T mutation on kinase activity appears to be inconsistent as it has been reported to increase (207, 215), have no effect on (211), and decrease LRRK2 kinase activity (214). Therefore, the effects of *LRRK2* mutations on kinase activity are highly debatable and the inconsistent evidence supports the presence of kinase-independent mechanisms of cellular toxicity. A more recent study (216) demonstrated that G2019S-induced dopaminergic neurodegeneration observed in the rodent

brain is dependent on both kinase and GTPase activities, further supporting other mechanisms of pathogenicity.

Pathogenic mechanisms of *LRRK2* mutations

Genetic studies have provided fundamental insights into the effects of *LRRK2* mutations on protein function and conformation, however it is not well understood how these effects on the protein lead to PD pathology, specifically, neurodegeneration. Animal models and cell culture studies (210, 216-218) have revealed that expression of mutant LRRK2 induces cell death. *LRRK2* mutations can lead to this cell death by influencing several cellular processes including vesicular trafficking, cytoskeletal dynamics, autophagy and lysosomal degradation, mitochondrial function and neuroinflammation as well as impacting protein pathologies (Fig. 1.7) (156, 160).

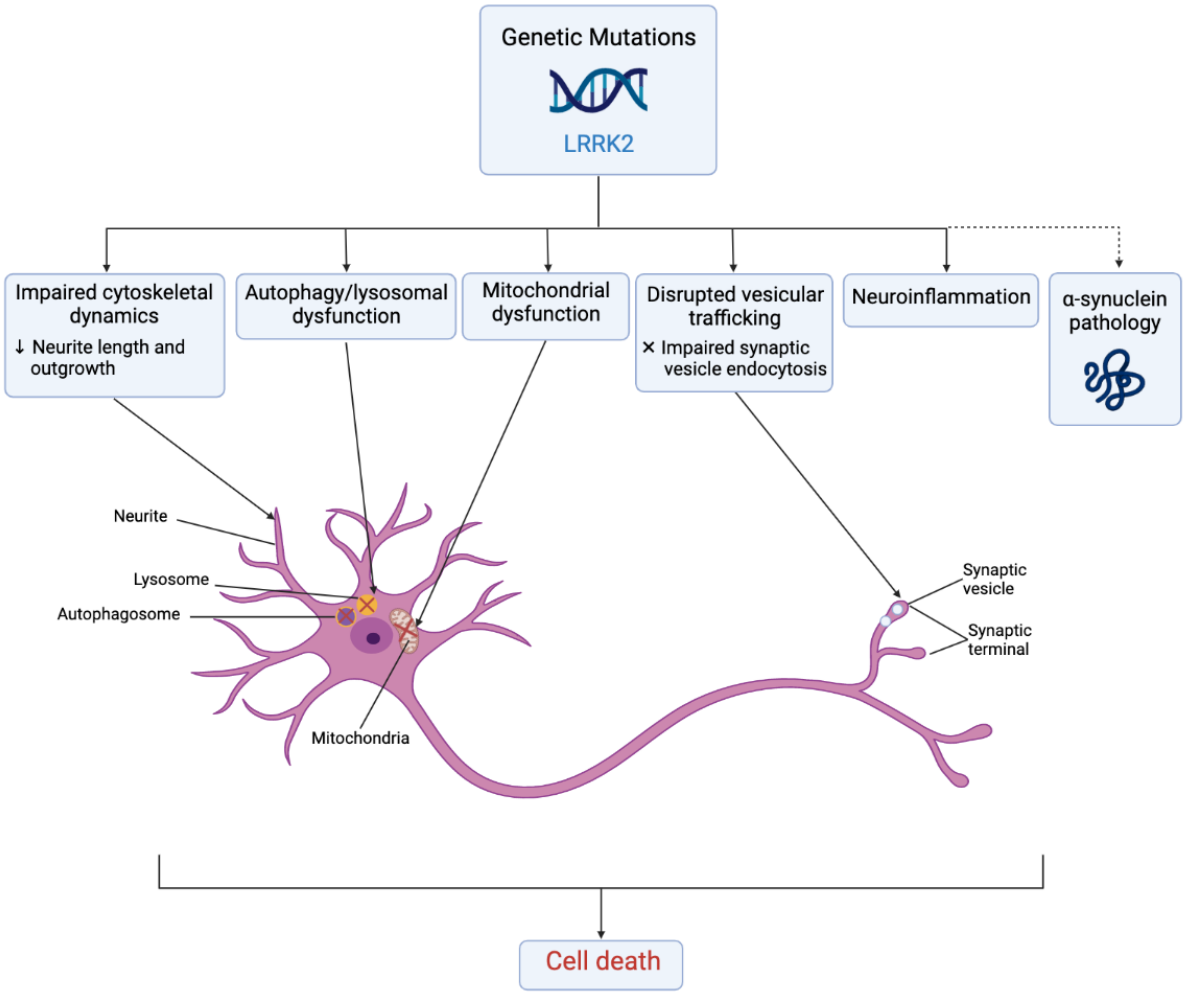


**Figure 1.7 Diagram illustrating the key pathogenic mechanisms of *LRRK2* mutations.** Mutations in the *LRRK2* gene impair cytoskeletal dynamics, autophagy and lysosomal degradation, mitochondrial functioning, vesicular trafficking and alter neuroinflammatory responses. *LRRK2* mutations also appear to influence α-

synuclein pathology and exacerbate its toxic effects. These cellular disruptions lead to oxidative stress and promote cell death. Original image created with BioRender.com.

Mutant LRRK2 influences **protein pathologies**. G20129S mutant mice have accelerated pS129 aggregation and neuronal loss in the SN and enhanced cortical tau pathology 6 months post fibril injection compared to WT mice (218, 219). Furthermore, the G2019S, R1441C and Y1699C mutants formed larger, more distinct and frequent inclusions and increased cell death (R1441C and Y1699C) compared to WT LRRK2 *in vitro* (210). Consistently, G0129S PD iPSC-derived dopaminergic neurons have shown enhanced α-syn diffuse cytoplasmic accumulations compared to control or idiopathic PD iPSC-derived neurons (220). Concurrently, these mutant neurons had morphological abnormalities associated with impaired autophagy (220). The G2019S and R1441G mutations have been shown to enhance oligomeric α-syn by impairing CMA *in vitro* and *in vivo* (221, 222). Also, G2019S PD iPSC-derived astrocytes have α-syn accumulation due to impaired CMA and macroautophagy which caused toxic effects in co-cultured control neurons (223). Recently, using PD mutant iPSC-derived neurons it was shown that the G2019S and R1441C mutations decrease the tetramer: monomer ratio of α-syn associated with increased pS129 and toxicity (224). Together, these findings highlight how LRRK2 mutants modulate α-syn pathology with further detrimental downstream effects.

LRRK2 influences **vesicular trafficking**, as a study (225) demonstrated that G2019S increased phosphorylation of a trafficking protein which impaired synaptic vesicle endocytosis. Furthermore, *in vitro* studies (226, 227) indicated that the expression of the G2019S mutation induced lysosomal enlargement, retromer-associated sorting defects and increased dopamine secretion. Also, it was recently shown that human iPSC-derived neurons expressing the R1441H mutation increased phosphorylation of a synaptic vesicle precursor (SVP) protein and impaired anterograde axonal transport of SVPs (228). *LRRK2* mutations also appear to impair **cytoskeletal dynamics** as the G2019S, I2020T and R1441G mutations reduced neurite length and branching *in vitro* (also *in vivo* for the kinase domain mutants) in an early study (229). Similarly, iPSC-derived dopaminergic neurons from G2019S PD patients, show reduced neurite length (230). In support of this, an *in vivo* study (231) revealed that the *LRRK2* G2019S mutation decreased neurogenesis, neuronal survival and neurite outgrowth in mice.

Another key mechanism of disease involving *LRRK2* mutations includes **impaired autophagy and lysosomal degradation**. An early study (232) showed that G2019S mutation shortened neurites in cell culture and increased autophagic vacuoles (AV) in somata and processes, and knockdown of essential autophagy proteins reversed these G2019S-induced effects. Another *in vitro* study (233) demonstrated that the R1441C mutation induced accumulation of multivesicular bodies and enlarged AVs with incompletely degraded material indicating autophagic dishomeostasis. Similarly, iPSC-derived dopaminergic neurons from G2019S PD patients show accumulated AVs due to their impaired clearance (220). Last year (234), it was shown that cells expressing the R1441C mutation had impaired autophagy associated with the increased kinase activity of the mutant protein. Furthermore, the expression of the G2019S, R1441C and Y1699C mutations resulted in enlarged lysosomes which were shown to be dysfunctional with inhibited degradative capacity for the G2019S mutation in mouse astrocytes (235). Similarly, another study (236) demonstrated that R1441C expressing neurons exhibited decreased autolysosome maturation and lysosomal degradation. These mutant-induced lysosomal defects have occurred both dependently and independently of kinase activity (235, 236). LRRK2 also impacts CMA as Orenstein *et al*. (222) reported that LRRK2 could be degraded via CMA, however this was compromised for the G2019S mutant in cell cultures. Additionally, overexpressed WT and G2019S LRRK2 inhibited CMA blocking lysosomal degradation, including α-syn degradation, promoting its accumulation and oligomerisation (222). Similarly, the R1441G mutation impairs CMA and causes increased oligomeric α-syn levels in the cortex and striatum of mice compared to WT (221).

*LRRK2* mutations are also implicated in **mitochondrial dysfunction**. The G2019S and R1441C mutations cause impaired mitochondrial function including reduced mitochondrial membrane potential and ATP, abnormal morphology, mitochondrial fragmentation and increased ROS levels in cell cultures (237, 238). Mitochondrial abnormalities or aggregated mitochondria indicating enhanced mitophagy have also been observed in the cortex of G2019S transgenic mice (239). In contrast, recent studies (240, 241) showed that the R1441C/G mutations cause decreased mitophagy along with impaired mitochondrial function and increased ROS production *in vitro* and in aged mice. **Neuroinflammation** also appears to be modified by *LRRK2* mutations in PD pathogenesis. A study (242) revealed that lipopolysaccharide (LPS) activated microglial cells from *LRRK2* R1441G transgenic mice secreted significantly higher proinflammatory cytokines compared to WT microglial cultures.

Additionally, conditioned medium from LPS-activated R1441G mutant microglia increased neuronal death (242). The G2019S mutation also causes increased proinflammatory cytokine levels as well as microglial activation *in vitro* and *in vivo* (243). This evidence demonstrates that *LRRK2* mutations are implicated in disrupting several cellular processes contributing to neurodegeneration in PD.

## 1.3.2 Autosomal recessive PD genes

### 1.3.2.1 PRKN

*PRKN*- encoding the protein parkin

Mutations in the parkin RBR E3 ubiquitin protein ligase *(PRKN)* gene are associated with autosomal recessive early-onset PD (EOPD) (244). The proportion of cases with *PRKN* mutations decreases with age, with 42.2% of cases under 20 years old (245). The *PRKN* gene encodes the parkin protein which is a multifunctional E3 ubiquitin ligase composed of 465 aa (246, 247). The parkin protein is expressed in neurons and weakly in glia localised to the cytosol and mitochondria (248, 249). As an E3 ubiquitin ligase, parkin carries out monoubiquitination and polyubiquitination of several substrates whereby it interacts with an E2 ubiquitin-conjugated enzyme and then transfers the ubiquitin to the lysine reside of a substrate protein to mark them for degradation (247). Parkin's activity, which is essential for the degradation of proteins by the covalent attachment of ubiquitin to the substrate proteins, mediates several cellular processes including regulating mitochondrial functioning (247, 250).

Parkin belongs the Really Interesting New Gene (RING)-between-RING family of ligases (250). Parkin is composed of several domains including an N-terminal ubiquitin-like (UbL) domain, RING0, RING1, in-between-RING (IBR), repressor element of parkin (REP) and a C-terminal RING2 domain (Fig. 1.8) (250). The domains RING0, RING1, IBR and RING2 coordinate two zinc ions each important for parkin's structural integrity, as zinc removal from parkin causes its unfolding (251). Parkin has two major functional sites in the RING1 and RING2 domains. Parkin utilises the RING1 domain as a binding site for the E2 ubiquitin-conjugated enzyme and its cysteine site in the RING2 domain to accept and transfer the ubiquitin from the E2 enzyme to the substrate protein (252).

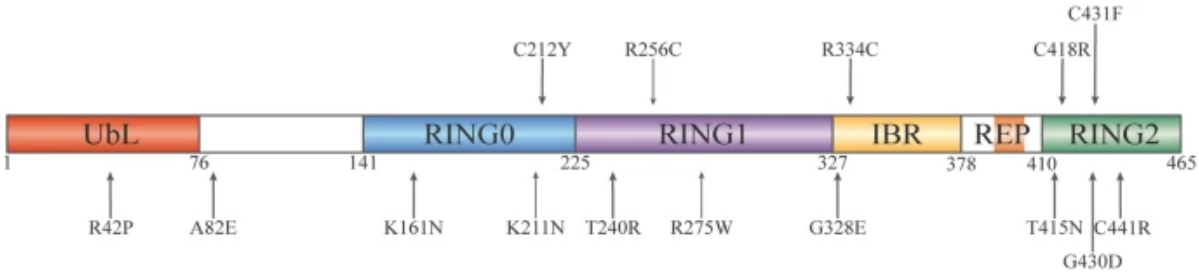


**Figure 1.8 Domain structure of the parkin protein with well-studied PD-associated missense mutations indicated.** Domains are colour-coded according to function and linker sequences are blank. Figure from Kamienieva et al., 2021 (250).

Parkin activity is regulated by several mechanisms of autoinhibition. Under basal conditions, parkin exists in an autoinhibited "closed" conformation where the binding of the E2 enzyme to the RING1 domain is blocked by the UbL and REP domains, and the cysteine catalytic site in RING2 is blocked by RING0 (253, 254). In addition to the UbL domain's autoinhibitory role (253), it is involved in proteasome association and regulating cellular parkin protein levels (255, 256). Parkin activation is dependent on the release of the interactions occluding the RING1 and RING2 domains. The phosphatase and tensin homolog-induced putative kinase 1 (*PINK1*) gene, which will be discussed in more detail below (section 1.3.2.2), plays an important role in activating parkin. Studies (257-259) have shown that *PINK1* functions upstream of *PRKN* and phosphorylates parkin at the serine 65 (Ser65) site in the UbL domain triggering opening conformations necessary for the activation of parkin. However, mutating the parkin Ser65 site does not impact parkin's ligase activity or translocation ability, suggesting the involvement of another PINK1 substrate in the activation of parkin, which was reported to be ubiquitin phosphorylated by PINK1 at its Ser65 site (260). Thus, the binding of PINK1-phosphorylated ubiquitin to parkin's RING1 domain releases the UbL domain allowing for its phosphorylation by PINK1 and subsequent binding to the RING0 domain leading to the release of RING2 and REP domains (261). This activation mechanism of parkin allows it to bind the E2 ubiquitin-conjugated enzyme and transfer ubiquitin to the cysteine site.

Pathogenic mutations of *PRKN*

The *PRKN* gene was mapped to chromosome 6q25.2-27 in families with autosomal recessive juvenile parkinsonism (ARJP) (262). Later, *PRKN* gene mutations were reported in unrelated patients with ARJP (246). The study (246) revealed that *PRKN* consists of 12 exons of which exon 4 was deleted in four ARJP patients and one patient had a five-exon deletion (exons 3-7). To date, over 130 mutations in the *PRKN* gene have been identified in PD patients comprising

exon deletions, insertions and multiplications, missense and nonsense mutations of which exon 3 deletion is the most frequent (263-265). Thirty-five of 139 *PRKN* mutations identified are classified as definitely pathogenic including R42P, K211N, C212Y, T240R, R275W, T415N, G430D, C431F and C441R, as indicated in Fig. 1.8 (250, 263).

Carriers of *PRKN* mutations have a mean age of disease onset of 32 ± 11 years and mean disease duration of 14 ± 10 years (245). Despite this earlier disease onset, the clinical syndrome associated with *PRKN* mutation carriers closely resembles that of idiopathic PD patients (244). *PRKN* mutation carriers present with levodopa-responsive parkinsonism as well as levodopa-induced dyskinesia and motor fluctuations (244, 245, 262). *PRKN* mutation carriers have more frequent dystonia and hyperreflexia compared to those without *PRKN* mutations and they also have pronounced postural instability, diurnal fluctuation and sleep benefit (244, 262, 263, 265).

Neuropathological reports (264, 266-273) have revealed that *PRKN* PD patients typically have dopaminergic neuronal loss in the SN and LC in the absence of LB pathology. Tau pathology has also been observed (270). Furthermore, a protein localisation study (248) revealed that the parkin protein was absent in all brain regions of ARJP patients whereas it was present in dopaminergic neurons of the SN, putamen and frontal lobe cortex in controls and sporadic PD patients. More recently, a study (264) reported that the neuropathology of ARJP patients with different *PRKN* mutations were largely similar, with mild to severe neuronal loss in the SN and LC occurring in all patients with LP present in 3 of the 8 cases analysed in different brain regions (264). Although LP is not typical in *PRKN* mutation carriers, it has been observed in some cases, particularly those surviving to older ages (272, 274-278).

<u>*PRKN* mutations affect the structure and function of parkin</u>

PD-related *PRKN* mutations are highly variable and have different effects on parkin. Exon deletions lead to truncation of the parkin protein and its loss of function where there is lack of parkin protein expression in mutation carriers (248, 279). Missense mutations occur across the functional domains of the protein (Fig. 1.8), and many mutations appear to induce a loss of parkin function through different mechanisms (280). These various mechanisms include aberrant solubility and an increased propensity to form intracellular aggregates decreasing normal function, reduced ubiquitination activity with decreased enzymatic activity, reduced ligase activity, and impaired binding ability reducing effective ubiquitination of substrates (280-282).

Structurally, the RING0 domain mutants K161N and K211N have been revealed to reduce parkin complex formation (283), and the T351P mutant has been reported to cause global unfolding of the IBR domain (284) promoting protein instability. Further, the UbL domain mutations R33Q, R42P, K48A and V56E caused parkin instability and rapid proteasomal degradation, accounting for the decreased full-length protein levels in the mutant cells (285). Consistently, a later study (286) demonstrated that the parkin mutants R42P, A46P and V56E induced unfolding of the UbL domain thus affecting protein stability and function. Furthermore, the C212Y, C289G and C441R parkin mutants, have reduced solubility that enhanced the propensity to form inclusions (287). Therefore, *PRKN* mutations appear to facilitate parkin dysfunction leading to PD pathobiology through different mechanisms.

Pathogenic mechanisms of mutations in *PRKN*

Parkin's role in the ubiquitination of various substrate proteins mediates several cellular processes related to mitochondrial functioning including mitochondrial fusion/fission, mitochondrial biogenesis and mitophagy (250). *PRKN* mutations can promote parkin dysfunction and contribute to PD pathogenesis by interfering with these processes and by affecting α-syn pathology as summarised in Fig. 1.9 (288).

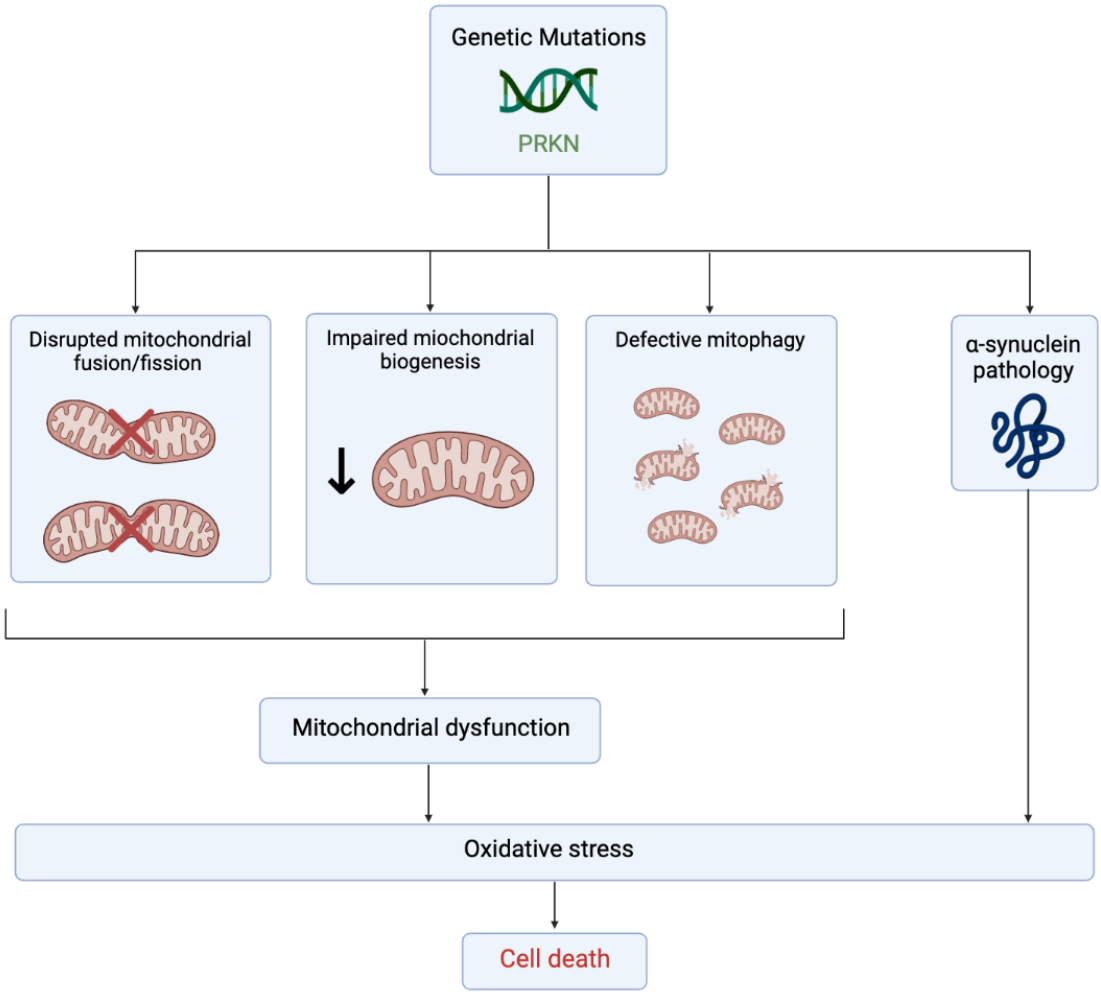


**<u>Figure 1.9</u> Diagram illustrating the key pathogenic mechanisms of *PRKN* genetic mutations.** Mutations in the *PRKN* gene impair mitochondrial fission and fusion, mitochondrial biogenesis leading to a reduced number of mitochondria and mitophagy leading to the accumulation of defective mitochondria. These impairments lead to mitochondrial dysfunction. *PRKN* genetic mutations also influence α-synuclein pathology which together with mitochondrial dysfunction, leads to oxidative stress promoting cell death. Original image created with BioRender.com.

A loss of function of parkin is implicated in the pathogenesis of PD by affecting **α-syn pathology**. In a rat model, a study (289) showed that viral expression of α-syn increased pS129 levels, inflammation and cell death and parkin co-expression reduced pS129 levels and these toxic effects indicating a protective counteracting mechanism. Similarly, in a cell model exogenous α-syn oligomers induced mitochondrial dysfunction where parkin overexpression protected against this effect (290). Nitration is another α-syn PTM which has been demonstrated to induce toxic effects in cultured neurons and loss of dopaminergic neurons in the SN of rats (291). The overexpression of monoamine oxidase B (MAO-B)

which oxidises dopamine and produces ROS in the process, has been revealed to increase nitrated α-syn nine-fold promoting its oligomerisation (292). A study (293) reported that parkin reduced the activity of MAO-B in cell culture. Later, it was revealed that loss of parkin increased MAO-B expression and thus increased dopamine-induced oxidative stress in iPSC-derived dopaminergic neurons (294). Furthermore, α-syn accumulation has been reported in iPSC-derived neurons from patients with *PRKN* mutations, although without apparent inclusions (295-297). This is in line with PD neuropathological reports (264, 266-270, 272, 273) and *PRKN* animal models (298-300). Therefore, this data highlights how *PRKN* mutations affect α-syn and may promote its oligomerisation.

**Mitochondrial fusion and fission** are critical processes to maintain mitochondrial morphology and appropriate cellular functioning, particularly in response to energy demands or cellular stress (301). Early studies (302, 303) in *Drosophila* reported defects in mitochondrial morphology relating to *PRKN* loss-of-function mutations, specifically mitochondrial swelling and disintegration of cristae suggesting disrupted mitochondrial fusion and fission. *In vitro* studies (304, 305) have shown *PRKN* silencing results in mitochondrial fragmentation. Parkin ubiquitinates the pro-fission dynamin-1-like protein (drp1) for its degradation via the proteasome-dependent pathway and parkin mutants (C431F and RING2 domain deletion) inhibit the ubiquitination of drp1 thus increasing drp1 levels (304). Parkin also ubiquitinates mitofusins (pro-fusion proteins) (306). This suggests that parkin regulates mitochondrial fission/fusion protein levels to ensure homeostasis. Overall, *PRKN* mutations appear to disturb mitochondrial fusion and fission leading to mitochondrial pathology which can disrupt cellular functions (Fig. 1.9).

**Mitochondrial biogenesis**, which is important for regulating mitochondrial quality, also appears to be disrupted by *PRKN* mutations, contributing to PD pathogenesis. Parkin ubiquitinates the parkin interacting substrate (PARIS) protein which represses peroxisome-proliferator-activated receptor gamma coactivator 1-alpha (PCG-1α) that is important for regulating mitochondrial biogenesis (307, 308). *PRKN* KO in the ventral midbrain of mice leads to reduced and smaller sized mitochondria compared to controls (309). Knockdown of PARIS mRNA in these mice reversed these effects (309), suggesting a PARIS-dependent mechanism for impaired mitochondrial biogenesis contributing to cell death. Consistent with these findings, a recent study (310) identified a reduced mitochondrial copy number, increased

PARIS levels along with decreased PGC-1α levels in *PRKN* KO human dopaminergic neuronal cultures compared to controls. Additionally, these findings (310) were replicated in iPSC-derived dopaminergic neurons from two PD patients carrying *PRKN* mutations. Thus, *PRKN* mutations contribute to PD pathogenesis by impairing mitochondrial biogenesis (Fig. 1.9) which impedes cellular functions and promotes the loss of dopaminergic neurons.

*PRKN* mutations are also implicated in disrupted **mitophagy**. PINK1 and parkin work in the same pathway to ensure efficient mitophagy. PINK1 behaves as a sensor of damaged mitochondria which leads to the activation and recruitment of parkin to these dysfunctional mitochondria to mediate mitophagy (311). There is strong evidence (310-315) to support that *PRKN* loss of function impairs mitophagy. A variety of *PRKN* mutations disrupt the recruitment of parkin to mitochondria and reduce mitophagy activity (311, 315). These defects lead to accumulated dysfunctional mitochondria (313), thus increasing cellular stress. *PRKN* mutations disturb the mitophagy process at different steps, with RING domain mutations C212Y, C289G, C418R and C441R disrupted folding and activity to prevent mitophagy, where other mutations (such as K211N, T240R and G430D) inhibit translocation to mitochondria also preventing mitophagy (312). Therefore, the evidence suggests that *PRKN* mutations disrupt the mitochondrial quality control pathway by impairing mitophagy and mitochondrial biogenesis which leads to the accumulation of defective mitochondria promoting cell death (Fig. 1.9).

While *PRKN* mutations appear to predominantly affect mitochondrial functioning and influence α-syn pathology, a relatively unexplored pathogenic pathway is neuroinflammation particularly as a downstream effect of mitochondrial dysfunction caused by parkin loss. A study (316) showed that mitochondrial stress and reduced mitophagy in *PRKN* KO mice was associated with an inflammatory phenotype. Furthermore, midbrain glia cultured from *PRKN* KO mice revealed altered glial proliferation (317). Last year, it was shown that iPSC-derived glia from *PRKN* PD patients had increased expression of cytokines and decreased expression of neurotrophic factors (318). Another study (319) revealed that activated microglia had decreased *PRKN* mRNA and parkin protein levels suggesting that *PRKN* mutations may decrease parkin levels and impair neuroinflammatory signalling. Further research is required to understand the interplay between mitochondrial dysfunction and potential neuroinflammatory pathways in a parkin context.

### 1.3.2.2 PINK1

*PINK1*- encoding the protein PINK1

Mutations in the *PINK1* gene are also associated with autosomal recessive EOPD (320, 321). The *PINK1* gene encodes the PINK1 protein which is ubiquitously expressed in the brain and localises to mitochondria and the cytosol in neurons (249, 322). PINK1 functions as a serine/threonine kinase involved in mitochondrial regulation (323). PINK1 consists of an N-terminal mitochondrial targeting sequence (MTS), a transmembrane domain (TM), an N-terminal regulatory domain (NT), a protein kinase domain and a C-terminal domain (CTD) (Fig. 1.10) (323). The MTS is important for the import of PINK1 into the mitochondrial matrix and the TM domain functions to anchor PINK1 to the mitochondrial membrane (324, 325). The NT region is also likely involved in mitochondrial import regulation and the CTD region has unknown function (326), however it may play a role in regulating PINK1 kinase activity (327). The kinase domain enables PINK1 serine/threonine kinase activity essential to the role of PINK1 in mitochondrial regulation (328).

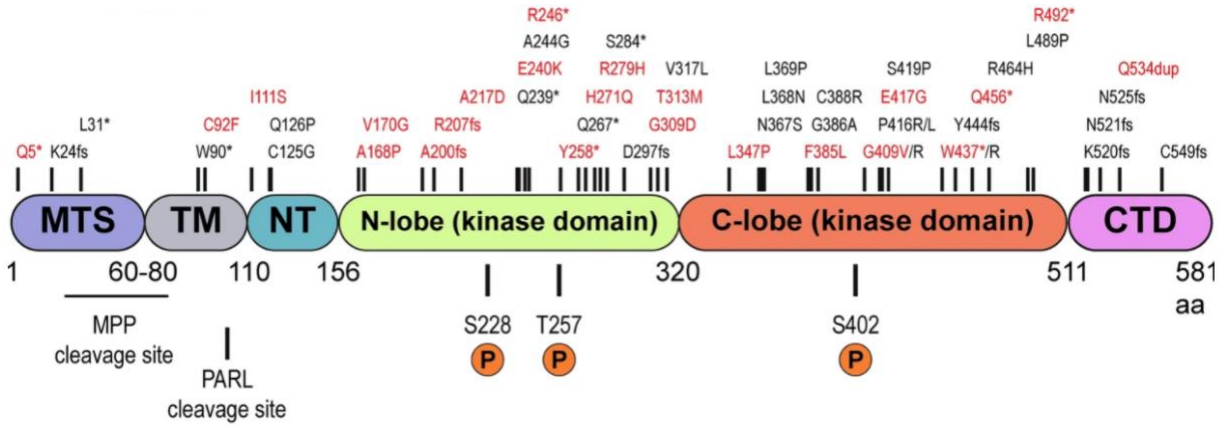


**Figure 1.10 Domain structure of the PINK1 protein with PD-related mutations, mitochondrial processing peptidase (MPP) and presenilin-associated rhomboid-like (PARL) cleavage sites and autophosphorylation sites (S228, T257 and S402) indicated.** The domains are colour-coded and mutations considered pathogenic are in red font. Figure from Quinn et al., 2020 (323).

Pathogenic mutations of *PINK1*

Linkage analysis revealed the *PINK1* gene on chromosome 1p35-36 in a large family associated with autosomal recessive EOPD (329). Over 50 mutations in the *PINK1* gene have been identified (Fig. 1.10) including missense, nonsense and structural variants (263). Out of 62 PD-related *PINK1* variants identified, 13 were classified as definitely pathogenic (Fig. 1.10) (263).

*PINK1* mutation carriers typically have levodopa-responsive early-onset parkinsonism with slow progression and levodopa-induced dyskinesia and motor fluctuations (330). Additional clinical features observed in some *PINK1* mutation carriers include dystonia and sleep benefit (320, 330), mimicking the *PRKN*-related phenotype. Also, cognitive decline and psychiatric disturbances (anxiety and depression) have been reported in *PINK1*-linked PD cases (320, 331). The neuropathological *PINK1*-related phenotype is not well characterised and appears inconsistent. Studies have reported neuronal loss and LBs in the SN sparing the LC (332), neuronal loss in the SN and LC in the absence of LB pathology (333) and neuronal loss in the SN and LC with LBs in the SN, LC and temporal cortex (334).

*PINK1* mutations in the kinase domain impair its kinase activity

PD-associated *PINK1* missense mutations occur across the domains of the PINK1 protein (Fig. 1.10) mainly accumulating in the kinase domain impairing kinase activity. An early *in vitro* study (335) using constructs lacking the mitochondrial targeting peptide and part of the C-terminus, revealed that the G309D and L347P variants (localised to the kinase domain) had significantly decreased kinase activity compared to PINK1 WT. However, another study (336) which used constructs lacking the N-terminal, revealed that the A168P and G309D missense mutants exhibited the same autophosphorylation activity as WT, suggesting that these kinase domain mutants do not affect PINK1 kinase activity. More recently, a study (337) using iPSCs derived from G411S heterozygotes revealed that neurons had reduced kinase activity compared to WT. Similar findings were obtained for kinase domain I368N mutant (338). This evidence supports that PD-associated *PINK1* kinase domain mutations reduce kinase activity promoting PD pathology.

Other pathogenic mechanisms of mutations in *PINK1*

Like parkin, PINK1 is intricately involved in mitochondrial regulation. *PINK1* mutations are implicated in the impairment of the processes relating to mitochondrial regulation contributing to PD pathology (323).

*PINK1* mutations are implicated in altering **mitochondrial dynamics** leading to impaired mitochondrial morphology. Early *Drosophila* studies (257, 339) revealed abnormal mitochondrial morphology in *PINK1* mutants compared to WT linked with dysfunction and dopaminergic neuron loss. Cell-based studies (305, 340) have also demonstrated that *PINK1*

deficiency promotes mitochondrial fragmentation and dysfunction. **Mitochondrial respiration** also appears to be disrupted by *PINK1* mutations. Studies (341, 342) have revealed that *PINK1* KO or mutations decrease Complex I activity which could increase ROS levels promoting cell death. Also, *PINK1* KO in mouse and human neurons increases mitochondrial calcium which stimulates ROS production and leads to disrupted mitochondrial respiration (343). Furthermore, it was more recently shown that older *PINK1* KO mice have impaired mitochondrial respiration associated with decreased dopamine release (344).

PINK1 recruits parkin to depolarised mitochondria to mediate **mitophagy**. *PINK1* mutant and a kinase-deficient variant do not recruit parkin to mitochondria disrupting subsequent mitophagy in mouse embryonic fibroblasts (311, 345). Both studies (311, 345) highlight the importance of the PINK1 kinase domain as the kinase activity is necessary for parkin recruitment and mitophagy. Furthermore, a study (346) revealed that parkin translocation did not occur in PD *PINK1* Q456* or V170G iPSC-derived dopaminergic neurons as opposed to WT neurons. Also, upon mitochondrial depolarisation, these *PINK1* mutant neurons exhibited increased mitochondrial DNA copy number and PGC-1α suggesting impaired mitophagy or altered biogenesis (346). Therefore, it appears that a loss of PINK1 function renders neurons vulnerable to oxidative stress and cell death by disturbing mitochondrial dynamics, respiration and mitophagy.

## 1.4 Comparison of cellular changes between genetic and sporadic PD

There are several neuropathological differences between genetic-related and sporadic PD which are summarised below in Table 1.3 for the genes which will be the focus of this thesis (*SNCA*, *LRRK2* and *PRKN*). It is also important to note the differences between mutations of each gene which are summarised in Tables 1.1 and 1.2 for *SNCA* and *LRRK2* mutations, respectively. While there are several neuropathological studies for *SNCA* and *LRRK2* mutation carriers, neuropathological reports of genetic PD overall and for *PRKN* mutation carriers are fairly limited. Also, although several pathological proteins have been examined and associated with typical mutations (Table 1.3), more colocalisation studies are needed. Furthermore, as most neuropathological reports compare one genetic mutation to control or sporadic PD, direct comparison across PD-related mutations is rare.

**Table 1.3** Comparison of pathological features and proteins in *SNCA*, *LRRK2* and *PRKN* mutations and sporadic Parkinson's Disease.

| Genotype (References) | Mutations | Mean Age of Onset (years) | Pathological features | Associated pathological proteins |
|---|---|---|---|---|
| *SNCA* (82, 86, 88, 90, 92, 97, 102-106, 112) | Missense (**A53T**, A30P, **E46K**, H50Q, **G51D**)<br>Multiplication (duplication and triplication) | 40s | Neuronal loss predominantly in SN, LC, DMV and HPC<br>Widespread LP (particularly in SN, LC, HPC and Cx)<br>Some cases have cortical neuron loss, LBs and extensive LNs<br>Glial inclusions in some cases<br>Tau pathology in some cases | α-Syn<br>Phospho-α-syn (S129/ Y125)<br>Ubiquitin<br>P62<br>Tau<br>Phospho-tau<br>Aβ<br>TDP-43 |
| *LRRK2* (172, 175-179, 182, 184, 192, 193, 197, 199, 201, 202) | Missense (I1371V, N1437H, **R1441C/G/H**, Y1669C, G2019S, I2020T) | 50s | Neuronal loss in SN and LC (some cases without neuron loss in LC)<br>Variable LP (typically absent in R1441C/G/H cases and variable in other mutations)<br>Cortical LP in some cases<br>Ubiquitin/tau inclusions in some cases | α-Syn<br>Phospho-α-syn (S129)<br>Ubiquitin<br>Tau<br>Phospho-tau<br>Aβ<br>TDP-43 |
| *PRKN* (248, 264, 266-270, 272-275, 278) | Missense (R42P, K211N, C212Y, T240R, R275W, T415N, G430D, C431F, C441R)<br>Multiplication<br>Insertion/**deletion** | 30s | Neuronal loss in SN and LC<br>Variable LP (majority of cases reported have absent LP)<br>Absence of parkin in ARJP patients<br>Tau pathology in some cases | Parkin<br>α-Syn<br>Phospho-α-syn (S129)<br>Ubiquitin<br>P62<br>Tau<br>Aβ |
| **Sporadic** (25, 27, 53, 64, 347-353) | | 60s | Moderate to severe neuronal loss in SN, LC, DMV<br>Neuronal loss may also present in other regions<br>LP in SN and widespread (dependent on Braak stage- see section 1.2.2) | α-Syn<br>Phospho-α-syn (S129)<br>Ubiquitin<br>P62<br>Tau<br>Phospho-tau<br>Aβ |

Genotype or mutations in **bold** will be the focus of this thesis. Aβ, Amyloid-β; ARJP, autosomal recessive juvenile parkinsonism; α-syn, α-synuclein; Cx, cortex; DMV, dorsal motor nucleus of the vagus nerve; HPC, hippocampus; LN, Lewy neurite; LC, locus coeruleus; LP, Lewy pathology; p62, ubiquitin-binding protein p62; phospho-, phosphorylated; S129, serine residue 129; SN, substantia nigra; TDP-43, Tar DNA-binding protein-43, Y125, tyrosine residue 125.

## 1.5 Gaps in Knowledge

While genetic forms of PD have provided abundant insights into the pathogenesis and pathobiology of the disease, the diversity of the molecular pathways involved to give a similar clinical outcome shows that significant gaps in knowledge exist.

*In terms of pathology, are the LPs in genetic forms of PD the same as those in sporadic PD?* LPs have mainly been assessed and characterised in sporadic PD cases in the brainstem to develop evidence of LB morphogenesis. While LP has been examined in mutation patients, comparisons between sporadic and genetic PD and across mutations are rare. Therefore, whether there are similarities between the progression of LPs in sporadic and genetic PD remains to be determined. Also, there is missing information as to whether there are distinct LBs associated with sporadic PD or different PD mutations which may also help to understand the pathways involved in LP progression. Studying LPs in brain regions other than the brainstem associated with less mature pathological changes may also be informative of the LP progression sequence.

*In terms of disease modelling, are the pathologies observed in the brains of genetic PD cases replicated in human mutation cell models?* There are also limited comparisons on the early changes in protein expression and initiating pathologies between genetic types of PD. Using more novel model systems may enhance our knowledge in this area.

*In terms of cases without α-syn pathology, what cellular changes occur to cause their PD pathology?* A large proportion of *LRRK2* and the majority of *PRKN* PD cases present with dopaminergic neuronal loss in the absence of LPs. To better understand the factors contributing to cell death in PD, further exploration of this relationship is needed. While *SNCA* and *LRRK2* pathogenic mechanisms have been comprehensively studied which has been instructive for understanding the pathogenesis of PD, neuroinflammatory pathways and glial changes linked to mitochondrial abnormalities in a *PRKN*-related context requires further research.

## 1.6 Aims and Hypotheses

### 1.6.1 Aims

The overarching aim of this thesis is to investigate and compare the impact of PD-associated genetic mutations on cellular pathologies in different models to further understand the pathogenesis and pathobiology of PD.

This broad aim is divided into the following sub-aims for the three genes (*SNCA*, *LRRK2* and *PRKN*) which will be the focus of this thesis:

1. To compare the types of Lewy pathology (LP) in post-mortem cortical tissue between PD patients with and without *SNCA* mutations.
2. To examine and compare protein pathology of human iPSC-derived ventral midbrain neuronal transplants carrying *SNCA*, *LRRK2* and *PRKN* mutations.
3. To investigate the effect of parkin loss on mitochondrial quality control and neuroinflammation in post-mortem *PRKN* KO mouse brain tissue.

### 1.6.2 Global hypotheses

It is hypothesised that:

1. *SNCA* mutations cause different LPs compared to sporadic PD.
2. *SNCA* mutations cause more severe LPs compared to sporadic PD.
3. PD-related mutations cause different protein pathologies in human iPSC-derived dopamine neuronal transplants.
4. Parkin loss alters mitochondrial protein expression and causes glial changes.

# CHAPTER 2: Definition and sequence of Lewy body formation in sporadic and *SNCA* mutation forms of Parkinson's disease

## 2.1 Abstract

Aim: To compare the types of Lewy pathology (LP) in post-mortem cortical tissue between Parkinson's disease (PD) cases with and without *SNCA* mutations.
Methods: Formalin-fixed paraffin-embedded post-mortem cingulate cortex from 15 sporadic, two A53T, one G51D, and two E46K *SNCA* mutation cases were assessed with multiplexed immunofluorescence labelling using Olympus slide scanners and Nikon C2 confocal imaging. The colocalisation of proteins was determined and the proportion of the neurons with LP identified. Control cases had no discernable cortical LPs.
Results: LP were identified in neurons as puncta, or mature round/solid or heterogeneous pale/mixed Lewy body (LB) deposits with all LBs colocalizing p62. In all sporadic and *SNCA* mutation PD cases, LBs were found in around 10% of neurons which concentrated in lower cortical layers. An additional 10% of cortical neurons in *SNCA* mutation but not sporadic PD cases had α-syn puncta (50% colocalized p62 and a high proportion colocalized with RhoA, a small GTPase). Sporadic PD had mainly mature round/solid LBs whereas nearly 50% of LBs in *SNCA*-related PD had mixed morphology. Some LBs colocalised phosphorylated tau protein and over 50% of LBs in sporadic and E46K-mutant PD colocalized RhoA.
Conclusion: There are significant differences in the types of cortical LPs in sporadic versus *SNCA*-related PD, with sporadic cases having a largely uniform population of mature round/solid LBs while *SNCA* mutation cases had a substantial amount of puncta and mixed LBs. These data suggest that the type and progression of cortical LB formation may differ between sporadic and *SNCA* cases.

## 2.2 Background

As discussed in the introduction (chapter 1), neuronal inclusions in the form of Lewy bodies (LB) and neurites comprised of α-synuclein (α-syn) protein, together with the loss of

dopaminergic neurons in the substantia nigra (SN) are the key neuropathological hallmarks that define Parkinson's disease (PD) (27). LBs from PD patients are composed of ~300 proteins but are particularly enriched in α-syn as well as ubiquitin and p62 (3, 30, 31). LBs are defined as sizeable mostly round or spherical soma-located inclusions that are immunoreactive to α-syn and ubiquitin/p62 some with a core and shell morphology (62). Additional α-syn aggregates occur in neurons. These include small punctate α-syn aggregations, α-syn arch-like aggregates (particularly around the nucleus), and larger irregularly-shaped heterogeneous-stained α-syn bodies considered precursors to LBs (30, 64, 65, 354, 355). LBs are found in predilection sites in the PD brain with all patients having brainstem LBs in the dorsal motor nucleus of the vagus nerve, locus coeruleus and SN, and then overtime as the disease spreads they are found in limbic and then association cortical regions. Only sensory and motor cortices are largely spared (25).

*Lewy body (LB) formation*

The process of LB formation is considered to be progressive and based on the morphological characterization of α-syn accumulation in cross-sectional cohorts of cases with LBs, it has been proposed that LB formation can be divided into several distinct formational stages (see Fig. 2.1). Most studies (30, 64, 354-356) suggest that there is an initial diffuse cytoplasmic α-syn condensation into irregular accumulations of α-syn, that transform into precursor pale bodies labelled with ubiquitin and p62 (64), that are then followed by the typical more compact LBs (see Fig. 2.1). For compaction, it is thought that p62 and ubiquitin which mark ubiquitinated proteins for degradation, are incorporated early into the precursor pale body followed overtime by LB formation (64, 357). Diffuse cytoplasmic α-syn occurs more frequently than pale bodies or LBs (358). Without more quantitative multilabel studies using these markers (α-syn, ubiquitin and p62), whether punctate α-syn is the initial pathology that will progress to a pale body or LB remains speculative. Additionally, it remains unclear how other proteins found in LBs (31) may assist with LB formation or maturation.

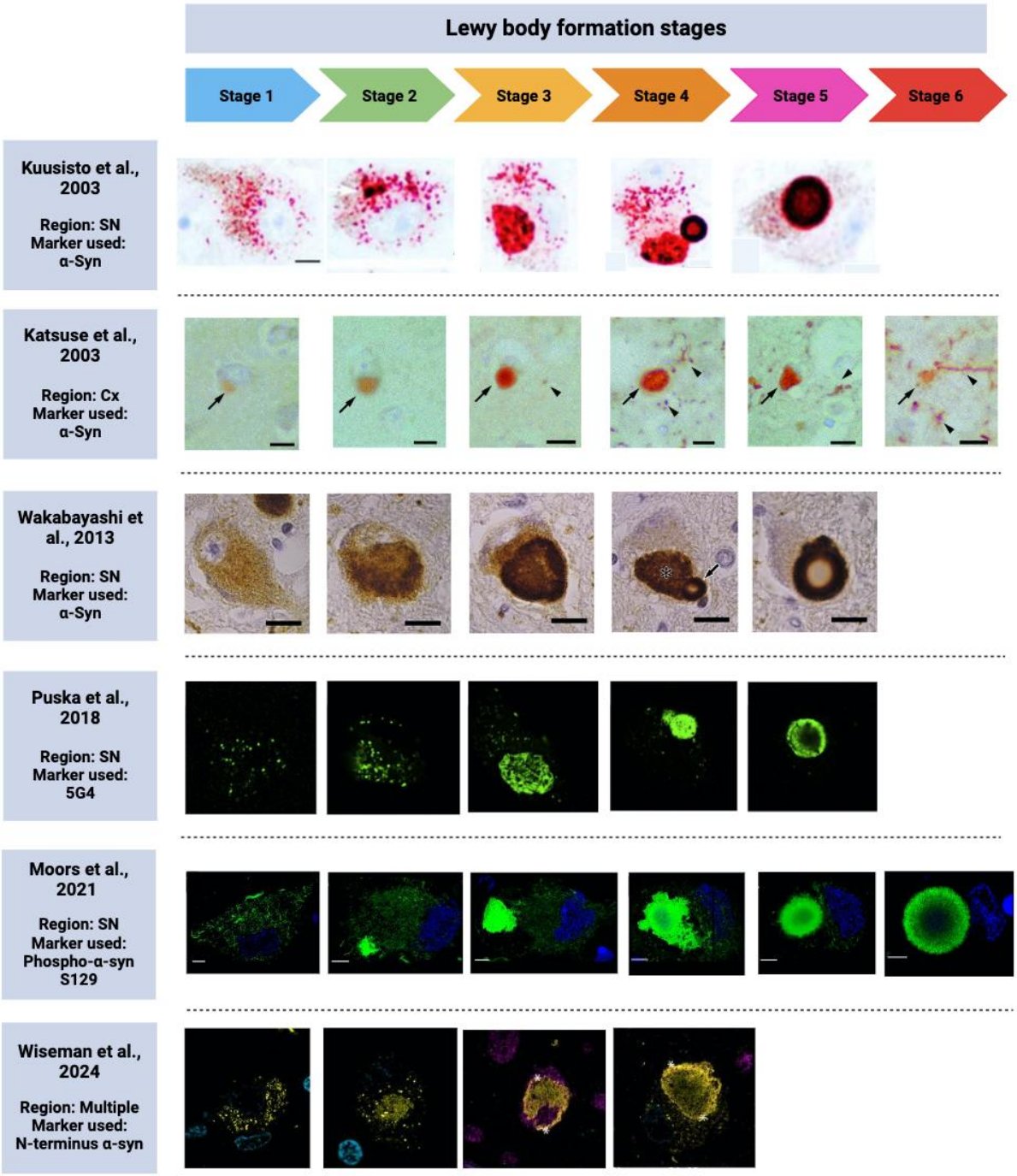


**Figure 2.1 Pictorial display of cross-sectional studies (30, 64, 65, 354, 355) analysing soma-located α-syn morphology in the substantia nigra (SN) and cortex (Cx) in patients with PD and dementia with Lewy bodies (DLB).** These studies analysed α-syn morphology using pan α-syn, S129 phosphorylated α-syn, aggregated α-syn (clone 5G4) and N-terminus α-syn antibodies to determine the progressive stages in LB formation. Note there have been no multiplexed labelled quantitation of potential stages to enhance these concepts. Created with BioRender.com.

The development of LBs has more recently been analysed in neuronal cell models using live cell imaging (359, 360). In a mouse neuronal model (359), LB formation was analysed in a

time-dependent manner where α-syn accumulation was first observed as filamentous in neuronal processes, followed by the soma that later exhibited variable morphologies of more LB-like inclusions (Fig. 2.2). More recently, using a human neuronal model (360), inclusion formation was tracked in induced pluripotent stem cell (iPSC)-derived neurons from a patient carrying the A53T *SNCA* mutation where it was found that ubiquitin+ rather than p62+ were in the most early inclusions formed that later matured to strong p62+ suggesting ubiquitin incorporation in LBs precedes p62 in their formation.

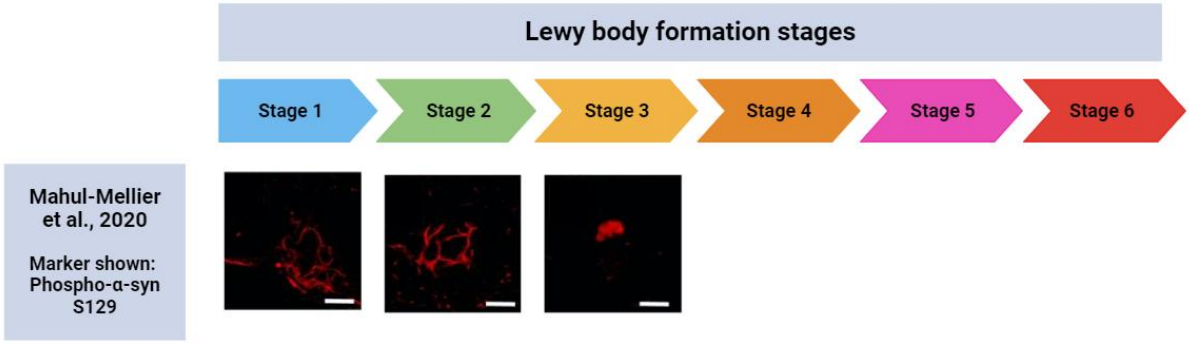


**Figure 2.2 Pictorial display of a live cell study (359) analysing the morphology of soma-located α-syn to determine the progressive stages in LB formation.** Created with BioRender.com.

*Types of α-synuclein (α-syn) found in Lewy pathologies (LP)*

There are several structurally diverse proteoforms of α-syn induced by molecular changes due to chaperoning and post-translational modifications (PTMs). Common α-syn PTMs include truncation, nitration and phosphorylation which occurs at multiple sites along the protein. The most common PTM is phosphorylation at S129 (pS129), a well-studied abundant component of LBs (50, 52-54). Other PTMs of α-syn identified in LBs include phosphorylation at S87, Y125, Y133, Y136 and Y39, nitration at Y39 and N- and C-terminally truncated (NTT and CTT) α-syn forms (50, 52, 55, 355, 361). The distribution of α-syn proteoforms within LBs can exhibit a lamellar organisation where pS129 C-terminal α-syn localize to the periphery while N-terminus, NAC-region and CTT α-syn localize in the core (355, 362). Recently, it was revealed that some of these different forms of α-syn label different inclusion types. Punctate α-syn in neurons is labelled by specific N-terminal and NAC region antibodies and occasionally nitrated Y39 (52). NAC-region, N- and C-terminal antibodies showed robust labelling of all LB types, while the other PTMs were more highly variable (52, 55). Interestingly, an intraneuronal cytoplasmic wispy network of α-syn was identified with pS129 in incidental LB disease patients prior to LB formation (355).

*Tau protein has been identified as associated with Lewy bodies (LBs)*

Although undervalued, there is increasing evidence of tau pathology in PD. Early studies (349, 363) have shown the presence of phosphorylated tau (phospho-tau) with variable morphologies in brainstem LBs from PD and DLB patients. Tau was seen on the periphery, surrounding or overlapping with α-syn in LBs (349, 363). Moreover, a recent study (69) has suggested that phospho-tau (AT8) may be the initiating seed for LP in sporadic PD and found that a proportion of LBs in the SN colocalize both AT8 tau and pS129 α-syn. They also found in PD that a greater number of SN neurons abnormally accumulate only AT8 tau and that AT8+ SN neurons occur in a proportion of people with mild motor deficits and no LBs. In those with mild motor deficits, the reduction in SN neurons was similar to those who had LBs supporting a degenerative change. This data suggests that LB formation may be preceded by AT8 tau accumulation, something that has not been evaluated in association with LB formation.

*Lewy bodies (LB) in patients with SNCA gene mutations*

Postmortem analyses of *SNCA* mutation cases are relatively rare, but in all cases similar LP types to those described for sporadic PD cases have been observed with α-syn antibody staining (82, 86, 88, 92, 102-105). Similarly, the predilection sites in the brain are similar between all *SNCA* mutation and sporadic PD cases, with all patients having brainstem LBs, followed by limbic and then neocortical LP (see above). *SNCA* mutation cases have more significant cortical LP with the types of LP varying (82, 86, 88, 92, 102-105). A53T mutation carriers have extensive neurites (82, 103-105), E46K mutation carriers have extensive LBs (86), and G51D mutation carriers have addition glial α-syn pathology (88, 92). Of note, multiplexed labelling with comparative quantitation has not been performed in cases with *SNCA* mutations. α-Syn, ubiquitin and tau have been observed in LBs, neurites and spheroids in A53T and G51D mutation cases, while no tau pathology has been observed in E46K mutation cases (82, 86, 92, 103-105). Spheroids are a pathology that is not commonly observed in sporadic PD (see details above). In the A53T cases, phospho-tau overlaps and surrounds the α-syn inclusions (103, 104). In G51D mutation patients (92), α-syn (5G4 or pS129 or pY125), ubiquitin, p62 and AT8 tau have also been assessed, with 5G4, pS129, pY125, ubiquitin and p62 identified in all LBs and neurites (although p62 labelled less neurites). AT8 tau was also observed in a proportion of α-syn inclusions in these cases (92).

This data suggests that there are subtle differences in the α-syn pathologies observed in *SNCA* mutation cases, with more inclusions overall and more cellular elements accumulating the protein.

The present study therefore aims to quantitatively evaluate LPs previously associated with different stages of LB formation (early puncta, PTM-modified pale bodies and mature LBs) using protein markers thought to be important for different stages in LB formation (pan α-syn, pS129 α-syn, ubiquitin, p62 and AT8 tau) in both sporadic and *SNCA* mutation cases with PD. To maximize the number of early and late α-syn LP evaluated, quantitation was performed on the anterior cingulate cortex, a region with limited neuronal loss even at end stage disease (27) that is a predilection site for LP in PD cases (25). The types of any LP observed were validated in remaining SN neurons in the same cases, but quantitation in the SN was not performed as neuronal loss was significant and highly variable with the potential to bias to more end-stage pathologies in this region.

## 2.3 Methods

### 2.3.1 Cases and tissue processing

Brain tissues from donors with sporadic PD (n=15), PD with *SNCA* mutations (A53T (n=2), E46K (n=2) and G51D-related PD (n=1)) and healthy age-matched controls (n=8) were obtained from the Sydney Brain Bank (www.sbb.neura.edu.au) who collects cases from regional brain donor programs and the E46K cases were from the Basque Biobank (www.biobancovsco.org) which is integrated in the Platform ISCIII Biobanks and Biomodels (National Registry of Biobanks B. B.0000140). Informed consent for banking the tissue from donors was acquired by the Sydney Brain Bank under the University of NSW HREC0937 and the Basque Biobank under PT20/00111. All cases met the diagnostic criteria for PD and no other neuropathologies (15, 25, 350, 364). This study was approved by the Human Research Ethics Committee at the University of Sydney (2020/707). There were no differences in age, gender, or postmortem delay between groups (Table 2.1).

**Table 2.1** Case demographics and diagnostic neuropathology (mean±std)

| Group | Controls | PD with *SNCA* mutations | Sporadic PD |
|---|---|---|---|
| **N (M:F)** | 8 (5:3) | 2xA53T (2:0); 2xE46K (0:2); 1xG51D (1:0) | 15 (13:2) |
| **Age at death (y)** | 90±7 | A53T 48,54; E46K 92,64; G51D 67 | 77±7 |
| **Postmortem delay (hr)** | 31±11 | A53T 27,48; E46K 25,7; G51D 21 | 20±17 |
| **Disease duration (y)** | - | A53T 7,9; E46K 6,5; G51D 5 | 17±11 |
| **Lewy body stage*** | 0 | A53T 5,4; E46K 6,5; G51D 5 | 5±1 |
| **ABC score#** | 2±1,1±1,1±1 | A53T 0,0,0; E46K 0,1/0,0; G51D 1,2,0 | 1±1,0.8±0.7,0.6±0.7 |

F=female, M=male, PD=Parkinson's disease, std=standard deviation*

* Braak et al., 2003 (25); # Hyman et al., 2012 (365)

Formalin-fixed paraffin-embedded (FFPE) anterior cingulate cortex and midbrain sections were cut at 6-8µm (one E46K mutation case was cut more thinly at 4µm) using a rotary microtome (Thermo/Microm, HM325) and mounted on Series 2 adhesive microscope slides (Trajan Scientific Medical, AU). For *SNCA* mutation cases without cingulate cortex samples, other association neocortices with samples were included.

## 2.3.2 Immunofluorescence

Experiments were performed with the most common LB relevant markers including pan α-syn, pS129 α-syn, ubiquitin and p62, new proteins identified in unbiased proteomic screening of LBs (360), and AT8 tau, which has recently been identified as a prominent marker of nigral pathology in prodromal and clinical PD (69). Multiplexed immunofluorescence experiments were performed as indicated in Table 2.2. Sections were dewaxed and rehydrated with xylene or HistoChoice and a series of graded ethanols. Heat-induced antigen retrieval was performed using the optimal buffer (see Table 2.2) for the different primary antibodies on a programmable antigen retrieval cooker (Aptum Bio Retriever 2100, Aptum Biologics Ltd, UK) for 2 hours followed by 70% formic acid treatment for 20-30 minutes. Autofluorescence quenching was performed using 0.1% sodium borohydride in phosphate-buffered saline (pH7.4, PBS) on ice for 30 minutes, followed by washes in phosphate buffered saline (PBS) and further treatments to reduce autofluorescence as listed in Table 2.2. Sections were blocked at room temperature (RT) using different reagents (see Table 2.2) and then incubated with the combination of primary antibodies (Table 2.3) in blocking buffer (containing 2% serum, 1% bovine serum albumin, 0.2% Triton X-100, 0.1% gelatin and 0.1% Tween-20 in PBS) as per Table 2.2, followed by their corresponding Alexa Fluor secondary antibodies (Table 2.3) and 4′,6-diamidino-2-phenylindole (DAPI, Sigma cat# D9542, 1 mg/mL) or bisbenzimide H 33342

trihydrochloride (Hoechst, Cat.# B2261; Sigma-Aldrich) for 2 hours at RT. Negative controls were included by omitting either the primary or secondary antibodies.

**Table 2.2** Different protocols used for multiplexed immunofluorescence experiments

| Protocol | Buffer used for HIAR | Additional autofluorescence quenching | Blocking treatments | Incubation with 1º antibodies | Mounting media & sealants |
|---|---|---|---|---|---|
| **1 using 6 laser channels for –** TH, HuD, α-syn, phospho-tau, Ub, p62 | Citrate buffer (pH6.0) | TrueBlack Lipofuscin Autofluorescence Quencher (Cat.# 23007, Biotium) in 70% ethanol for 1min prior to coverslipping | Human Fc Block (Cat.# 564220, BD Biosciences) in blocking buffer (containing 2% serum and 1% bovine serum albumin in PBS) for 30mins followed by TrueBlack IF Background Suppressor System (Cat.# 23012; Biotium) for 1h | Overnight at RT | Coverslipped with EverBrite mounting medium (Cat.# 23001, Biotium) and sealed with CoverGrip coverslip sealant (Cat.# 23005, Biotium) |
| **2 using 4 laser channels for –** Phospho-α-syn, p62, Rab8, RhoA | Citrate buffer (pH6.0) or TE buffer (pH9.0) (optimal for Rab8 and RhoA respectively) | 100mM glycine in PBS for 30min followed by 0.1% Sudan Black in 70% ethanol for another 30min prior to blocking<br><br>10mM $CuSO_4$ in 50mM ammonium acetate buffer (pH5.0) for 1h prior to coverslipping | Blocking buffer for 1h | For 48h at 4°C | Coverslipped with mounting medium (DAKO, Cat.# S3023) and sealed with nail polish |

HIAR, heat-induced antigen retrieval; HuD, Hu antigen D; Rab8, Ras-related protein Rab-8; RhoA, Ras Homolog Family Member A; TE buffer, Tris-EDTA (ethylenediamine tetra-acetic acid) buffer; TH, tyrosine hydroxylase; Ub, ubiquitin.

**Table 2.3** List of antibodies and combinations used in this study

| Primary antibodies (type, Cat.#) | Epitope (immunogen) | Dilution | Source | Fluorophore |
|---|---|---|---|---|
| Tyrosine hydroxylase (TH) (rabbit pAb, Cat.# AB152)* | Denatured TH from rat pheochromocytoma | 1.6µg/ml | Sigma Aldrich | 532 |
| HuD (rabbit mAb, Cat.# ab302514)* | aa.1-150 of human HuD | 1.6µg/ml | Abcam | 532 |
| α-Syn (goat pAb, Cat.# AF1338) | *E. coli*-derived recombinant aa.1-140 of human α-Syn | 1:200 | R&D Systems | 755 |
| Phospho-α-syn at S129 (rabbit mAb, Cat.# ab51253) | Synthetic peptide aa.100-140 of human α-Syn | 1:200 | Abcam | 647 |
| Ubiquitin (Ub) (rabbit pAb, Cat.# ab7780) | Recombinant full-length protein of human Ub | 1:100 | Abcam | 647 |
| p62 Ick ligand (mouse IgG1 mAb, Cat.# 610833) | aa.257-437 of human p62 lck ligand | 1:100 | BD Biosciences | 488 |
| Rab8 (mouse IgG2b mAb, Cat.# 610844) | aa.84-205 of human Rab8 | 1:100 | BD Biosciences | 568 |
| RhoA (mouse IgG2b mAb, Cat.# sc-166399) | aa.116-140 of human RhoA | 1:50 | Santa Cruz | 568 |
| Phospho-tau (Ser202, Thr205) (AT8) (mouse IgG1 mAb, Cat.# MN1020)* | Partially purified PHF-tau aa. 1-758 | 0.8µg/ml | ThermoFisher Scientific | 594 |
| **Secondary antibodies** | **Epitope (immunogen)** | **Dilution** | **Source** | |
| Donkey anti-goat IgG(H+L)-DyLight 755, SA5-10091 | Goat IgG Heavy and Light chains | 1:200 | ThermoFisher Scientific | |
| Donkey anti-rabbit IgG (H+L)- Alexa Fluor 647, A-31573 | Rabbit IgG Heavy and Light chains | 1:250 | ThermoFisher Scientific | |
| Goat anti-mouse IgG1-Alexa Fluor 488, A-21121 | Mouse IgG 1 | 1:250 | ThermoFisher Scientific | |
| Goat anti-mouse IgG2b-Alex Fluor 568, A-21144 | Mouse IgG 2b | 1:250 | ThermoFisher Scientific | |
| Zenon mouse IgG1 labelling kit- Alexa Fluor 594, Z25007 | Mouse IgG 1 | * | ThermoFisher Scientific | |
| Zenon rabbit labelling kit- Alexa Fluor 532, Z25303 | Rabbit IgG | * | ThermoFisher Scientific | |

* Directly conjugated. Aa, amino acid; mAb, monoclonal antibody; pAb, polyclonal antibody.

### 2.3.3 Imaging and analyses

For qualitative and quantitative analyses of pathological inclusions, images were scanned at 20x and 60x magnification on Olympus VS120 or VS200 slide scanners and the morphology and relative frequency assessed. For assessing the full range of LP, pan α-syn and pS129 α-syn immunoreactive inclusions were qualitatively and quantitively analysed in the cingulate cortex.

Neurons were identified and counted if they contained large dull nuclei (Fig. 2.3A). LBs were identified and counted if the α-syn-immunofluorescence occupied >10% of the neuronal

cytoplasm (Fig. 2.3B-G). As expected, α-syn-immunofluorescence labelled a variety of sizes and types of LP in neurons (Fig. 2.3B-G) including puncta (Fig. 2.3H, I).

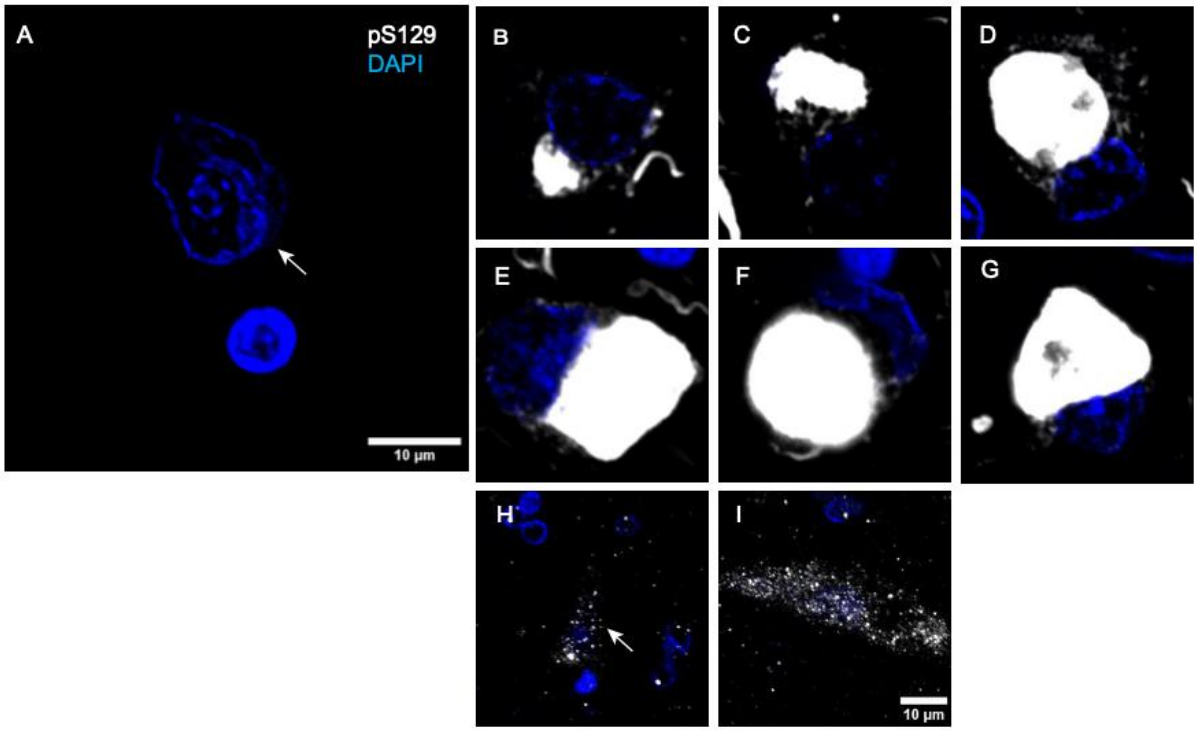


**Figure 2.3 Neuronal nuclei and neuronal α-syn Lewy pathologies in the cortex.** Confocal microscope images of the cingulate cortex from PD patients revealed neuronal nuclei as large and dull in DAPI (arrow; A) and morphologically diverse neuronal Lewy body structures of variable sizes (B-G) and puncta (arrow; H, I) based on α-syn immunofluorescence (pS129 α-syn, white; DAPI, blue). Scale in I applies to panels B-I.

The relative frequency and distribution of LP was assessed in all cases in a blinded manner and scored as none, low, moderate, or extensive as shown in Figure 2.4.

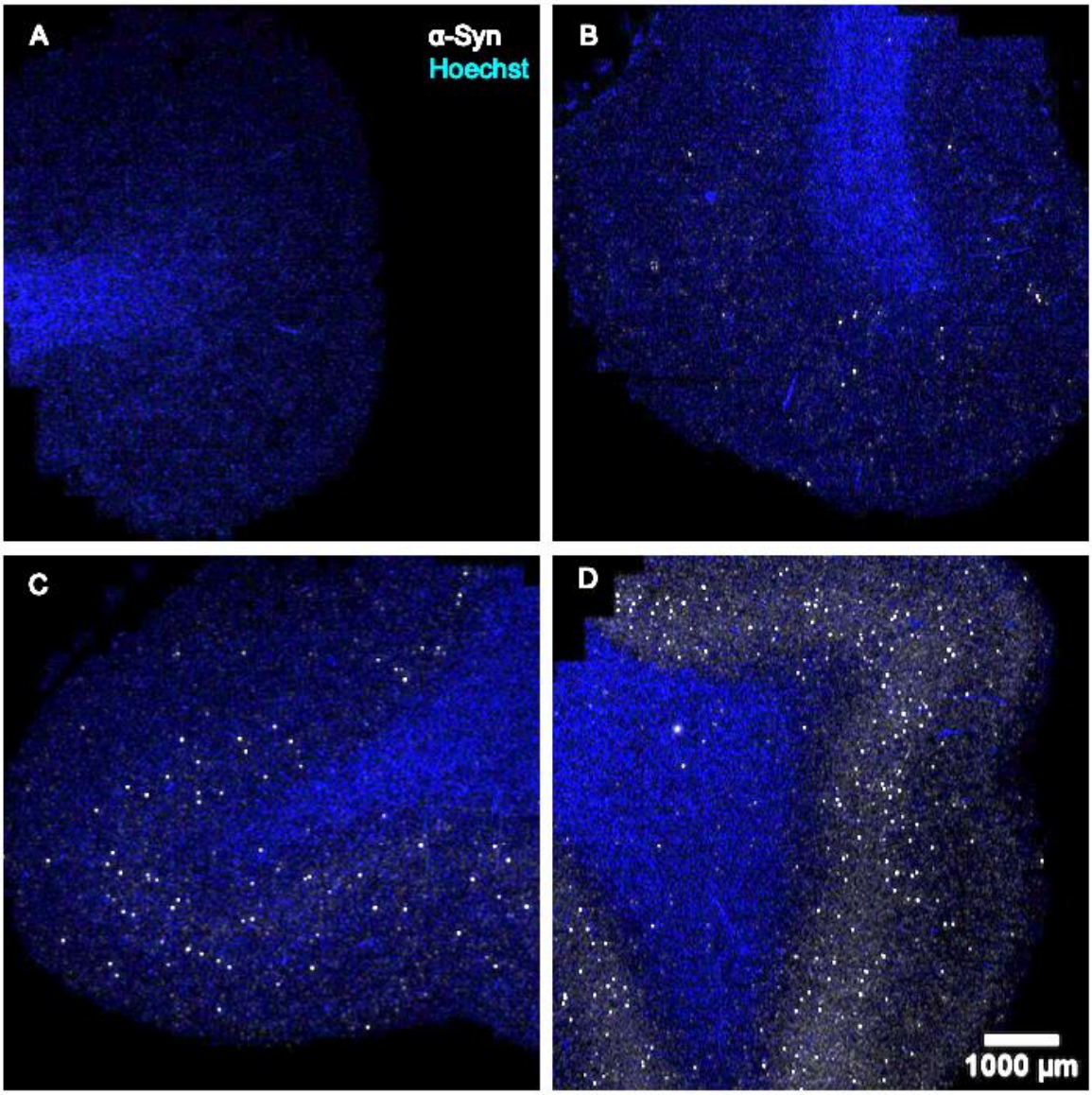


**Figure 2.4 Scoring of Lewy pathology (LP) in the cortex.** Overview scans of the cingulate cortex from control and PD patients revealed no LP (control in A), low (PD in B), moderate (PD in C) and extensive LP (PD in D) based on α-syn immunofluorescence (pan and pS129 α-syn, white; Hoechst, blue). Scale in D applies to panels A-D.

For protocol one (Table 2.2), sections were imaged using an Olympus VS200 scanner, and LP quantified using AI-assisted software (QuPath v.0.5.1) (366). Sections were scanned at 20x magnification and 2-3 90,000µm$^2$ regions of interest (ROI) in the middle to deeper layers of the cingulate cortex were annotated using the annotation tool. Neurons were either manually counted (see definition above), or for sections with HuD-immunofluorescence the positive cell detection tool and manual curation was used. Each neuron with α-syn-immunofluorescence was manually identified and this was repeated for the other proteins by toggling off each channel.

For protocol two (Table 2.2), sections were imaged using an Olympus VS120 scanner and Nikon C2 confocal microscope, and LP quantified using FIJI software (v1.53t) (367). ROIs were identified from the whole section at 20x magnification on the Olympus VS120 slide scanner and then the ROI found again at 10x magnification on the Nikon C2 confocal microscope. For quantitation, two 800x800µm large images in the deeper layers of the cingulate cortex from the ROI were captured at 40x magnification and each image split and enlarged into 9 regions with each region filling the computer screen. All neurons were identified (Class 0) using the point tools function. Each neuron with α-syn-immunofluorescence was identified with another marker (Class 1). This was repeated for the other proteins by toggling off each channel.

After identifying all α-syn-positive neurons in all sections, the percentage of these inclusions that colocalized other proteins was calculated. Non-parametric statistical tests were performed including Kruskal-Wallis, post-hoc analyses (Dunn's multiple comparisons) and Mann-Whitney U tests (Prism 10 (v.10.0.0)) to evaluate the differences in the percentage of pathological inclusions between sporadic PD and *SNCA*-mutant PD (Table 2.1) with $p < 0.05$ as the level of significance.

## 2.4 Results

### 2.4.1 Distribution and morphology of a-synuclein (α-syn) pathology in sporadic PD

As expected, α-syn labelled LBs were found in the cortex of PD cases and not controls (Table 2.4). In PD cases there was a greater concentration of LBs in middle to lower cortical layers while in controls there was an absence of LBs. This indicates that more LBs are formed in lower cortical layers with the progression of PD. A similar finding was observed in the *SNCA* mutation cases (Table 2.4).

**Table 2.4** Relative frequency and distribution of Lewy bodies (LB) in the cortex

| Group | Controls | PD with *SNCA* mutations | Sporadic PD |
|---|---|---|---|
| **LB relative frequency** | None | + - +++ | + - +++ |
| **LB distribution** | None | Mainly middle to deeper layers | Mainly middle to deeper layers |

+ = low Lewy pathology; + + = moderate Lewy pathology; + + + = extensive Lewy pathology

Both pan and pS129 α-syn immunoreactivity revealed similar diverse morphologies of LBs in the cortex and SN of sporadic PD cases, in addition to diffuse puncta in the cytoplasm (Figs. 2.3, 2.5). There were two predominant types of LBs observed in immunofluorescence which could be classed as solid/compact or mixed/intermediary (Fig. 2.5). The mixed and solid forms varied in size and shape (Fig. 2.5C-N) ranging from mostly round or spherical to more variable for the mixed form in terms of compactness and size (Fig. 2.5C-F).

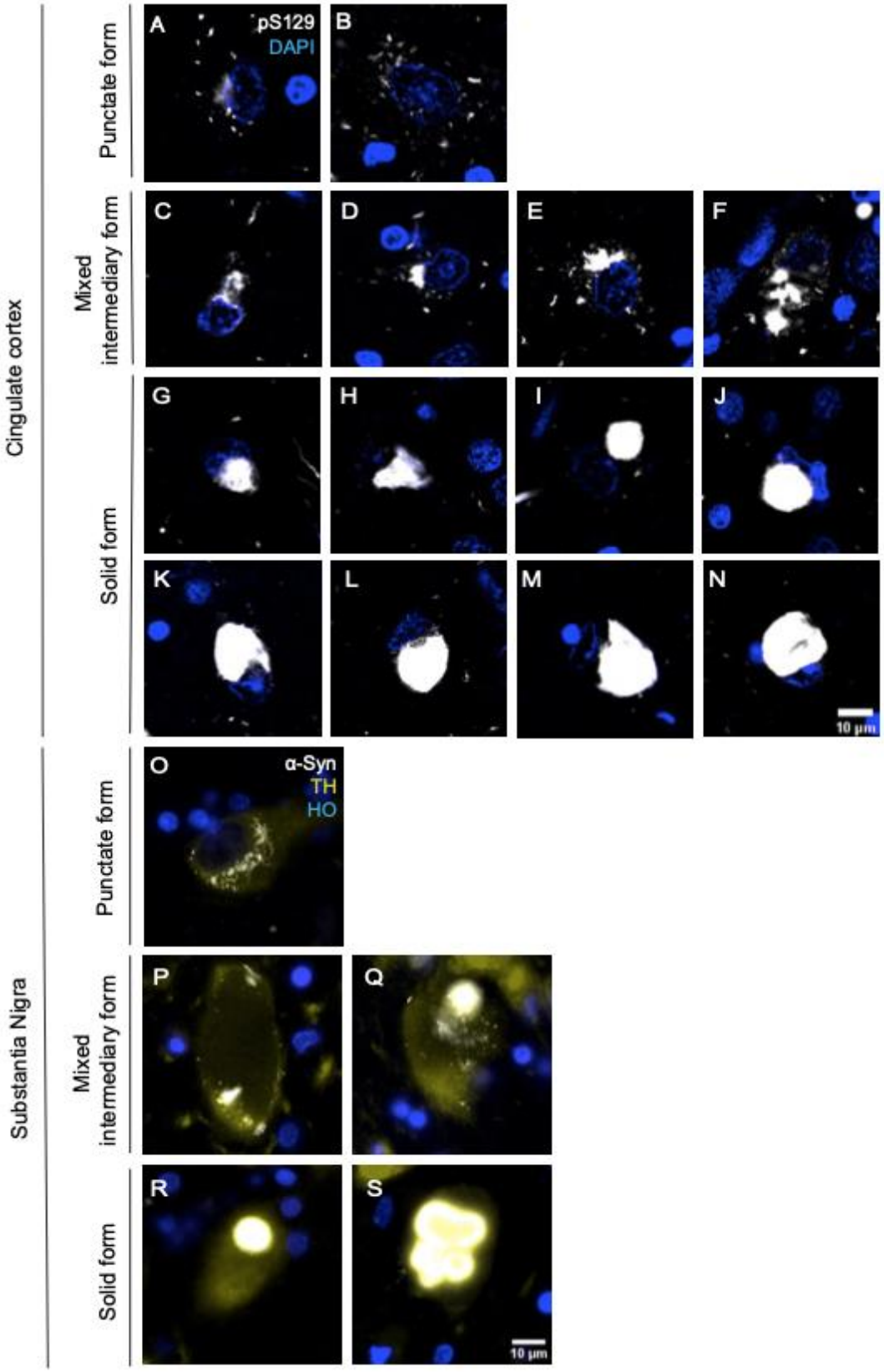


**<u>Figure 2.5</u> Morphological types of α-syn pathological inclusions in the cingulate cortex and substantia nigra of sporadic PD patients.** Photomicrographs of sections from sporadic PD patients illustrating distinct morphological types of α-syn structures in the cingulate cortex (A-N) and in the substantia nigra (O-S). In addition

to a punctate form of α-syn (A, B, O), mixed intermediary LBs varied in size, shape and compactness (C-F, P, Q) while solid LBs varied less in size and shape (G-N, R, S) based on pan and pS129 α-syn immunofluorescence (α-syn and pS129, white; tyrosine hydroxylase (TH), olive green; DAPI and Hoechst (HO), blue). Scale in N applies to panels A-N and scale in S applies to panels O-S.

### 2.4.2 Distribution and morphology of α-synuclein (α-syn) pathology in *SNCA* mutation cases

Similarly to sporadic PD cases, *SNCA* mutation cases also displayed varying degrees of puncta and LBs throughout the cortex (Fig. 2.6) with the same morphological types of inclusions seen using α-syn immunofluorescence (Fig. 2.7). There was no difference in the distribution of LBs in the cortex between *SNCA* mutation and sporadic PD cases (Table 2.4, Fig. 2.6). Similarly to sporadic PD cases, LBs were typically seen mostly in the middle to deeper cortical laminae in *SNCA* mutation cases.

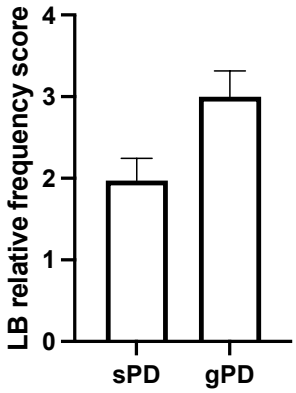


**Figure 2.6 Mean score (± SEM) of Lewy body (LB) severity in the cingulate cortex of sporadic PD (sPD) and PD with *SNCA* mutations (gPD).** Bar graph showing the relative frequency of LBs in the cortex.

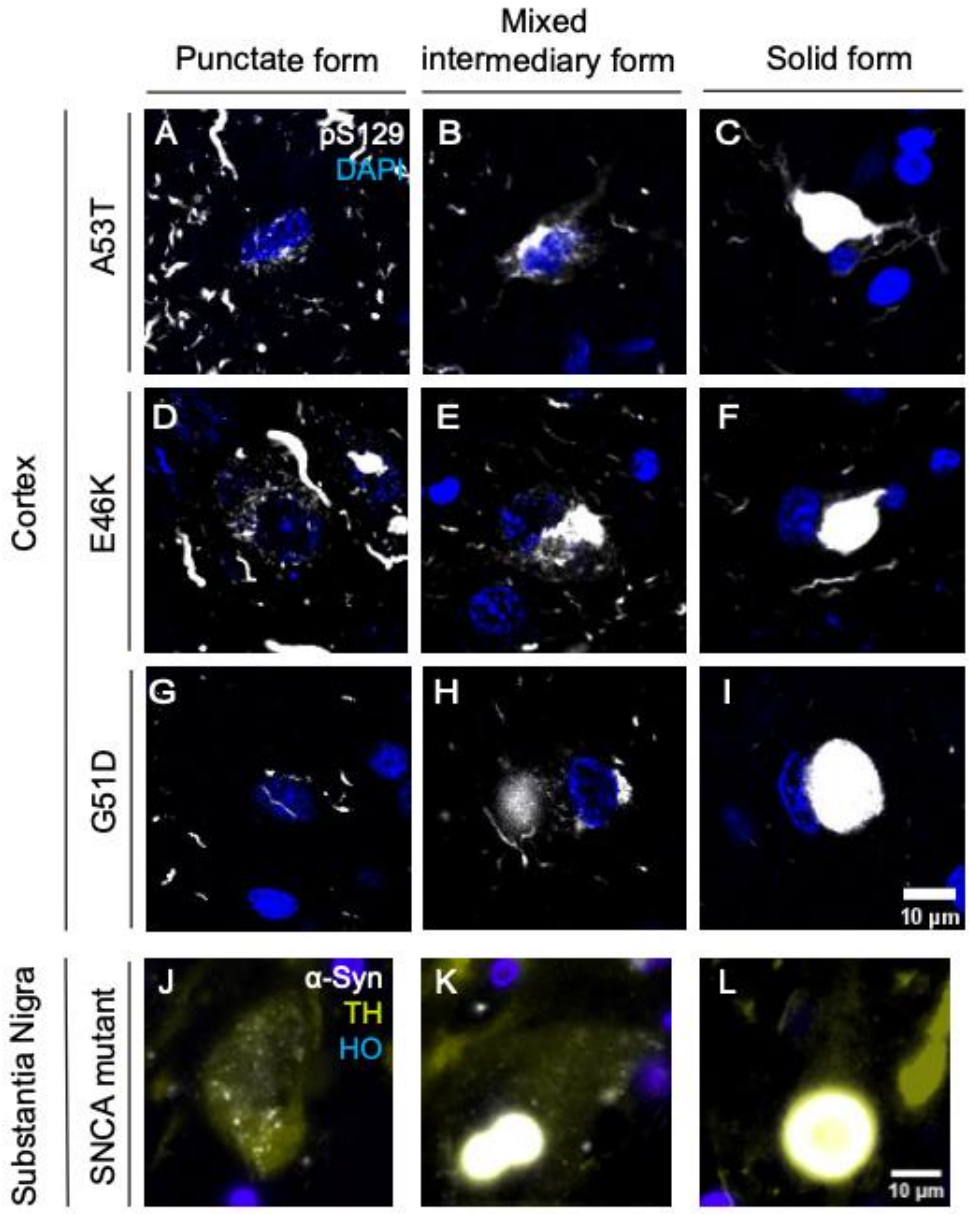


**Figure 2.7 Morphological types of α-syn pathological inclusions in the cingulate cortex and substantia nigra (SN) of PD patients with *SNCA* mutations.** Photomicrographs of sections from *SNCA* mutant patients illustrating distinct morphological types of α-syn inclusions in the cingulate cortex and/or association neocortices (A-I) and in the SN (J-L). In addition to a punctate form identified in each mutation case (first column; A, D, G and J), mixed intermediary LBs varied in size, shape and compactness (middle column; B, E, H and K) while solid LBs varied less in size and shape (last column; C, F, I and L) based on pan and pS129 α-syn immunofluorescence (α-syn and pS129, white; tyrosine hydroxylase (TH), olive green; DAPI and Hoechst (HO), blue). Scale in I applies to panels A-I and scale in L applies to panels J-L.

### 2.4.3 Quantitation of α-synuclein (α-syn) puncta in sporadic PD and PD cases with *SNCA* mutations

As discussed above, α-syn+ puncta are often considered the first stage of LB formation but have also been shown to be largely associated with lysosomes and mitochondria in PD (354-356). α-Syn was observed in fine and larger puncta (Figs. 2.3, 2.5, 2.7), but only in a relatively small proportion of cortical neurons (Fig. 2.8A). Significantly more α-syn labelled puncta were observed in *SNCA* mutation compared with sporadic PD cases (Figs. 2.8, 2.9), with just over 50% of α-syn puncta co-labelled with p62 in both sporadic and mutation PD cases (Figs. 2.8, 2.9).

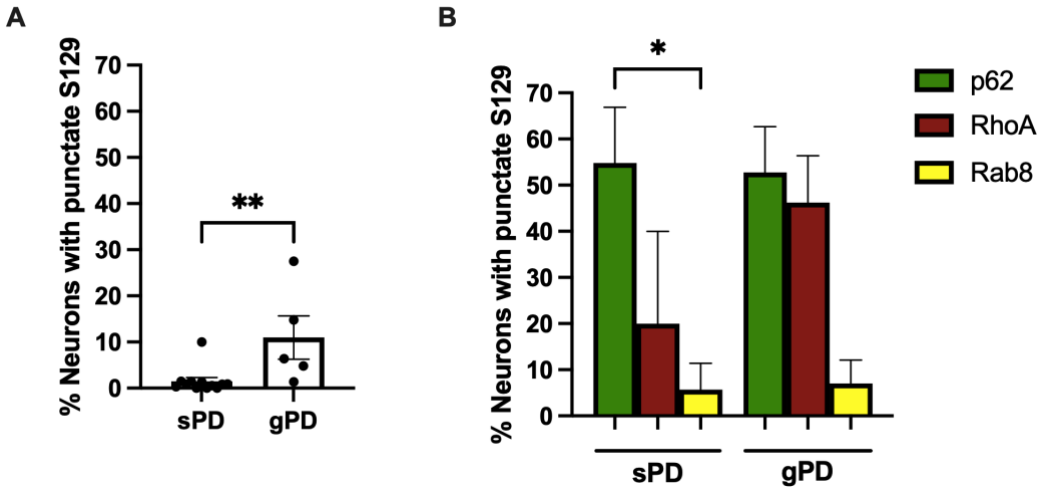


**Figure 2.8 Mean proportion (± SEM) of cortical neurons with pS129 α-syn puncta in sporadic PD (sPD) and PD patients with *SNCA* mutations (gPD).** Bar graphs showing the proportion of neurons with punctate pS129 α-syn (A) and the proportion of neurons with punctate pS129 α-syn that co-labelled with p62 (green), RhoA (dark red) or Rab8 (yellow) (B) in sporadic PD and mutation PD cases. Significance is taken at $^{**}p < 0.01$ and $^{*}p < 0.05$.

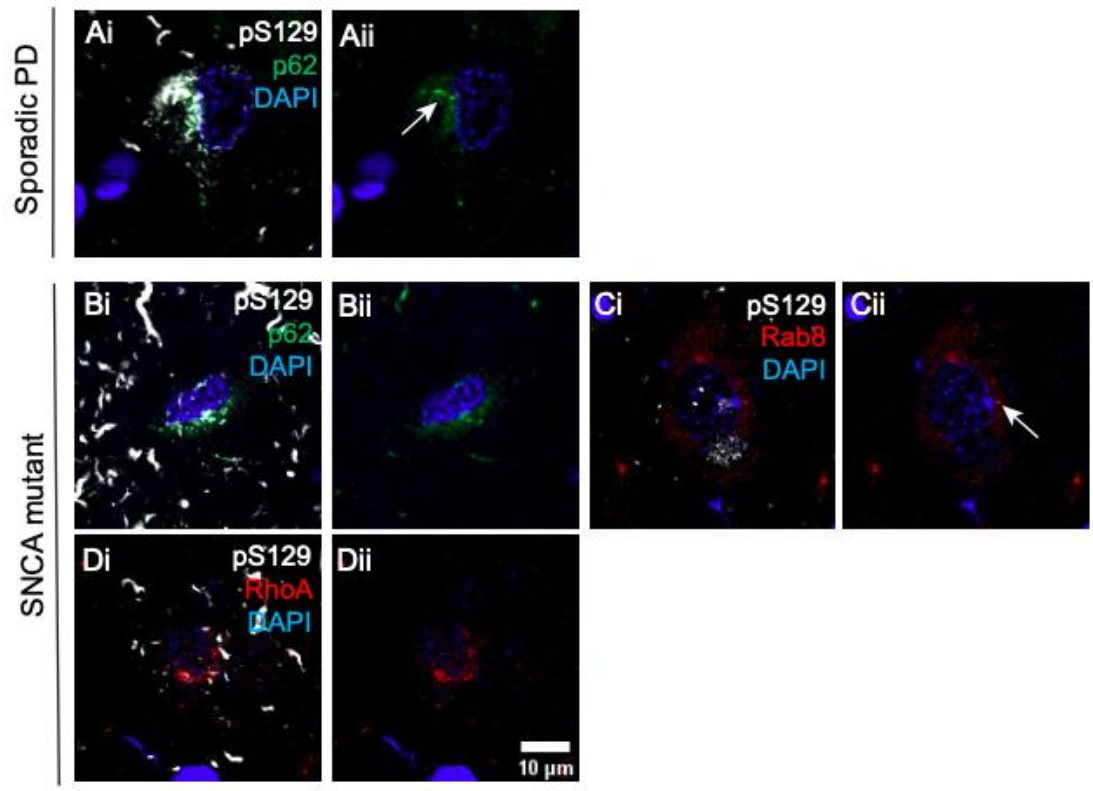


**Figure 2.9 Co-labelling of α-syn puncta in the cortex of sporadic PD and PD patients with *SNCA* mutations.** Confocal photomicrographs illustrating co-labelling of pS129 α-syn puncta (white) with p62 (green), Ras-related protein Rab-8 (Rab8) (red) and Ras Homolog Family Member A RhoA (red) (A-Di) in neurons (DAPI, blue) in the cortex of sporadic (A) and *SNCA* mutant PD patients (B-D). (i) show merged images, and (ii) shows DAPI with only p62, Rab8 or RhoA. Scale in Dii applies to panels Ai-Dii.

## 2.4.4 Quantitation of stages of Lewy body (LB) types in sporadic PD and PD with *SNCA* mutations

Similar to neurons with α-syn+ puncta, there was an increased proportion of neurons with α-syn+ LBs in PD patients with *SNCA* mutations compared to sporadic PD, particularly in E46K mutation cases (Fig. 2.10). In sporadic PD, LBs were the major α-syn+ inclusion pathology compared to significantly fewer neurons with α-syn+ puncta, whereas in *SNCA* mutation cases there were similar numbers of neurons with α-syn+ puncta only versus LBs (Figs. 2.8, 2.10). Due to variability in the mutation cases, particularly in the E46K mutation cases (Fig. 2.10), this increase was not statistically significant.

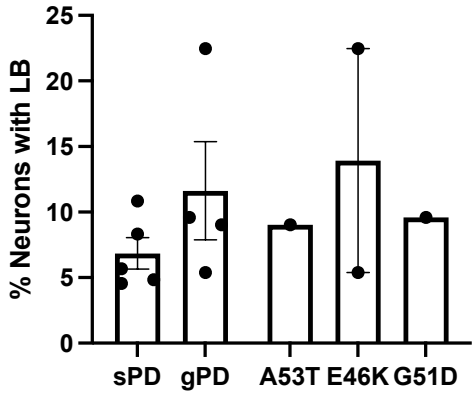


**Figure 2.10 Mean proportion (± SEM) of cortical neurons with Lewy bodies (LB) in sporadic PD (sPD) and PD patients with *SNCA* mutations (gPD).** Bar graph showing the proportion of neurons with α-syn+ LBs in sporadic and mutation PD cases, as well as in individual mutation cases.

As indicated in the background, ubiquitin and p62 tag α-syn for degradation, and are therefore considered to label similar types of LBs at their earliest stages prior to compaction. Ubiquitin labelled both solid and mixed LBs in variable intensities and morphologies in cortical neurons (Fig. 2.11). Within these solid or mixed LBs, the ubiquitin immunofluorescence appeared highly variable in both sporadic and mutation PD cases, being either granular, punctate or more solid (Fig. 2.11), suggesting the amount of α-syn that is ubiquitinated within LBs differs. Similarly to the cortex, in the SN ubiquitin also showed considerable variations within α-syn solid and mixed LBs, being punctate or more solid and varying in intensities or occasionally absent in sporadic and mutation PD (Fig. 2.20). Ubiquitin was typically negligible in SN neurons with punctate α-syn.

In contrast to ubiquitin staining, p62 labelling looked similar to the distribution of α-syn labelling in the solid and mixed LB types in both sporadic and mutation PD cases (Fig. 2.12) suggesting that most α-syn in LBs is p62 labelled. This was also seen in LBs in the SN in sporadic and mutation PD cases (Fig. 2.20). Punctate p62 was also observed with α-syn puncta in the SN of both sporadic PD and mutation cases.

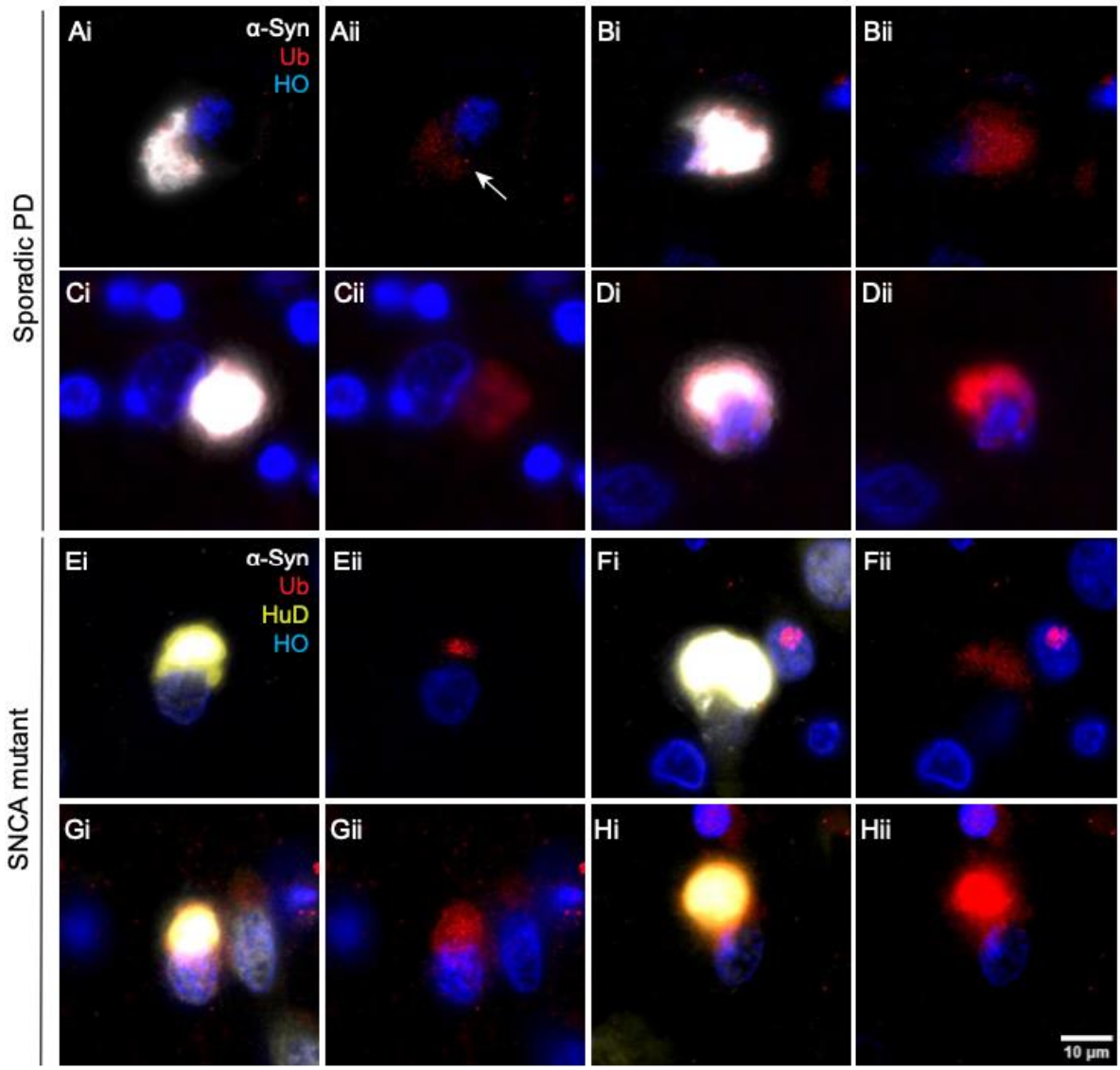


**<u>Figure 2.11</u> Ubiquitin (Ub) co-labelling in cortical Lewy bodies (LBs) in sporadic PD and PD patients with *SNCA* mutations.** Photomicrographs illustrating co-labelling of ubiquitin (red) and pan α-syn (white) (A-Hi) and the variable morphologies of ubiquitin in cortical LBs in neurons (Hu antigen D (HuD), olive green; Hoechst (HO), blue) in sporadic (A-D) and *SNCA* mutant (E-H) PD patients. In the α-syn LBs, ubiquitin appeared punctate (Ai, Aii (arrow), Ei, Eii), evenly granular (Bi-Cii, Fi-Gii) or more solid (Di, Dii, Hi, Hii). (i) are merged images, and (ii) show ubiquitin and Hoechst only. Scale in Hii applies to panels Ai-Hii.

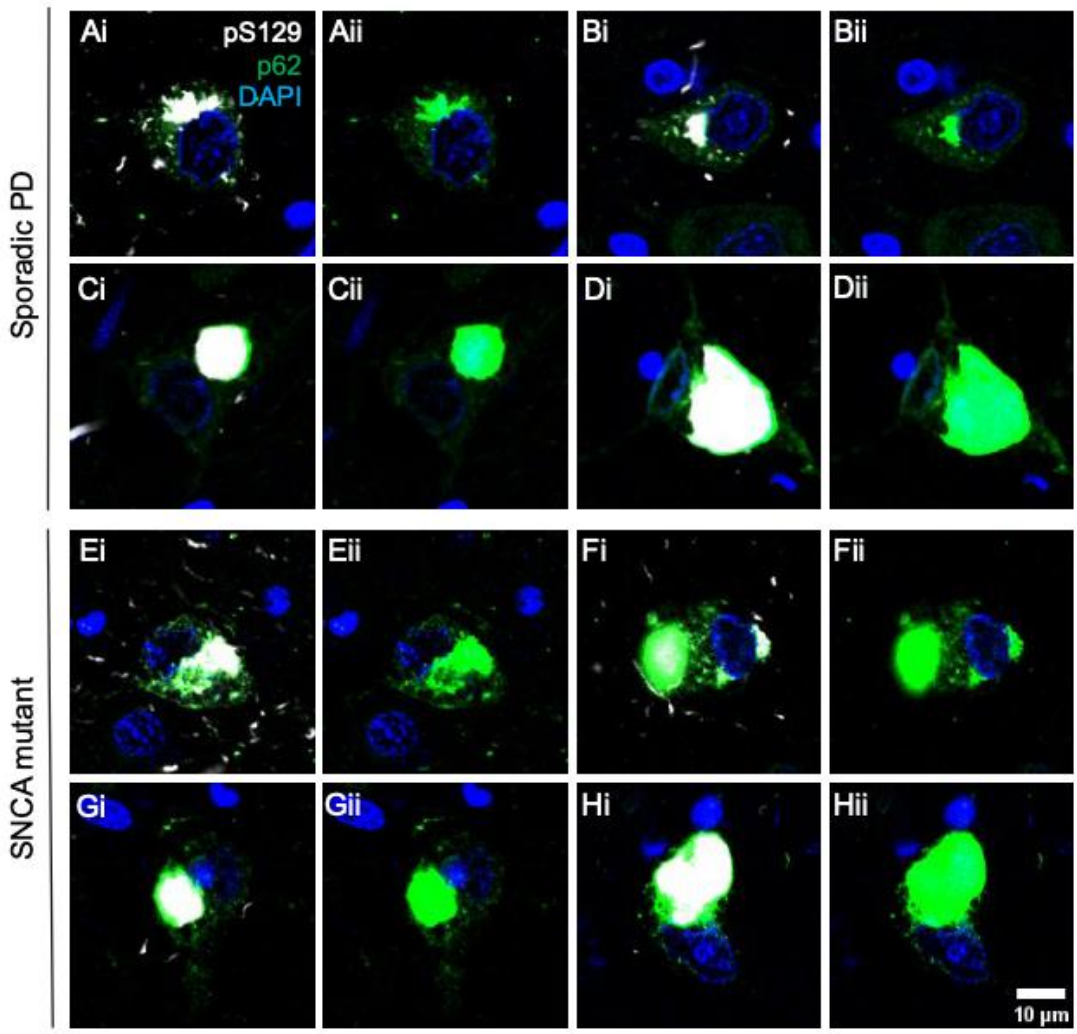


**Figure 2.12 p62 co-labelling in cortical Lewy bodies (LB) in sporadic PD and PD patients with *SNCA* mutations.** Photomicrographs illustrating co-labelling of p62 (green) and pS129 α-syn (white) (merged; A-Hi) and p62 in solid or mixed cortical LBs in neurons (DAPI, blue) in sporadic (A-D) and *SNCA* mutant PD patients (E-H). P62 resembled α-syn morphology in mixed (Ai-Bii, Ei-Fii) and in solid (Ci-Dii, Gi-Hii) LBs. (i) show merged image, and (ii) show only p62 and DAPI. Scale in Hii applies to panels Ai-Hii.

Nearly all LBs were co-labelled with ubiquitin or p62 with no difference in the proportions labelled between sporadic and mutation PD cases (Fig. 2.13A). This confirms that similar types of LBs co-label with ubiquitin and p62 in both sporadic and mutation PD (Fig. 2.14) with the majority immunoreactive for both proteins (Fig. 2.15). Of the total α-syn-labelled LBs, a small proportion were only p62+ without ubiquitin in sporadic PD, while in mutation PD a small proportion of LBs had either only ubiquitin or p62 co-labelling (Fig. 2.15). Most p62+ α-syn LBs were solid in sporadic PD whereas mutation cases had both solid and mixed types of LBs with p62+, G51D and E46K cases having the most p62+ mixed LBs (Fig. 2.13B).

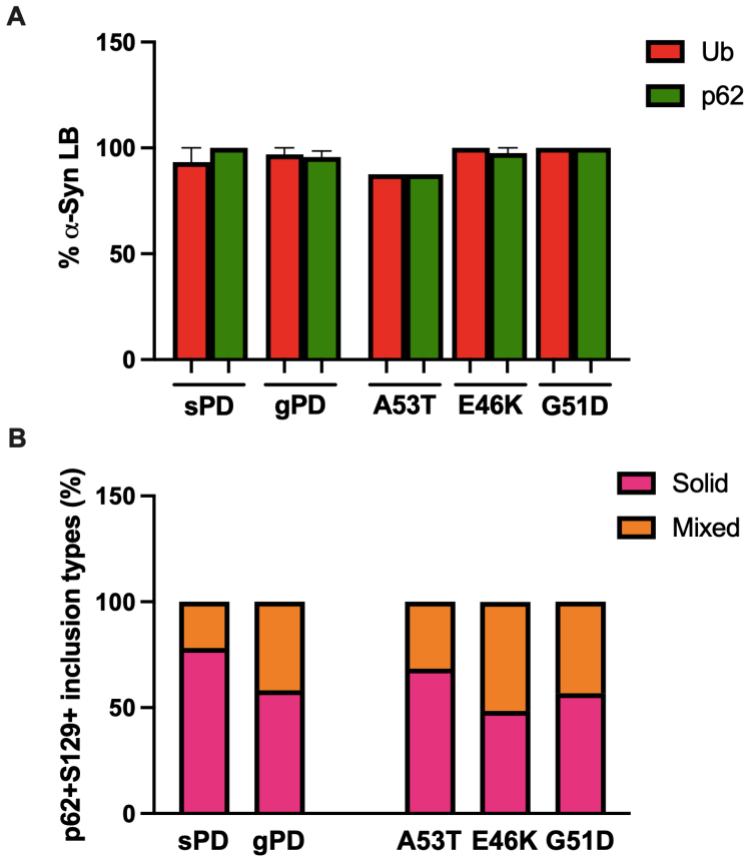


**Figure 2.13 Mean proportion (± SEM) of Lewy bodies (LB) co-labelled with ubiquitin (Ub) or p62 and the type of α-syn+ cortical LB with p62 co-labelling in sporadic PD and PD patients with *SNCA* mutations.** Bar graphs showing the proportion of the α-syn+ LB that have ubiquitin or p62+ co-labelling in sporadic and mutation PD, as well as in the individual mutation cases (A). Stacked bar graphs showing the morphological type of p62+ and pS129 α-syn+ LBs (solid, pink; mixed, orange) in sporadic and mutation PD case, as well as in individual mutation cases (B).

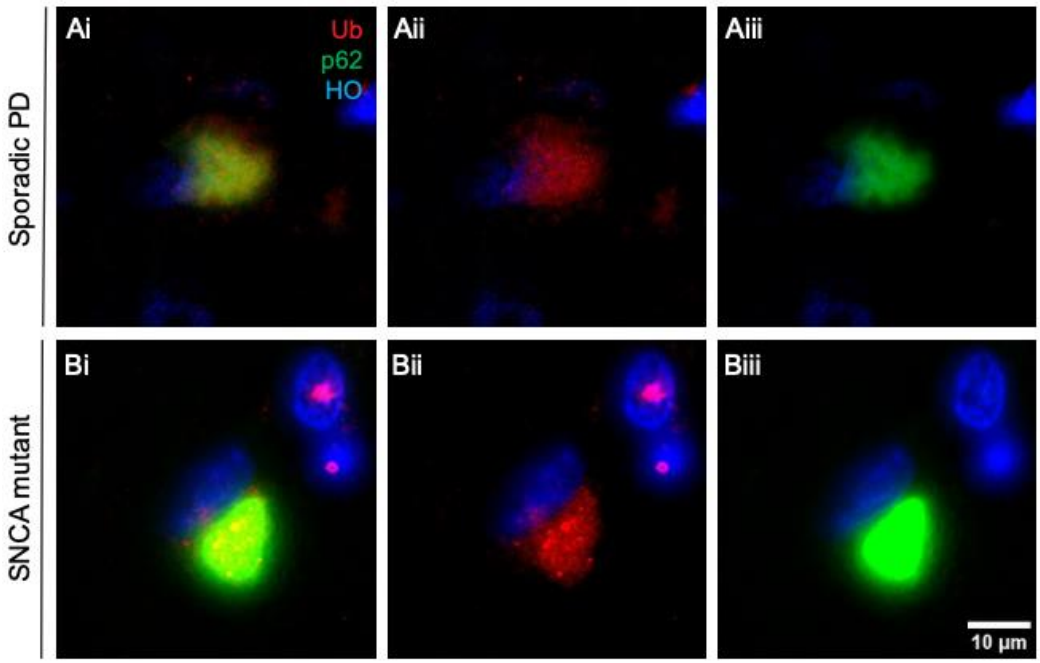


**Figure 2.14 P62 and ubiquitin (Ub) co-labelling of cortical Lewy bodies (LB) in sporadic PD and PD patients with *SNCA* mutations.** Photomicrographs illustrating co-labelling of p62 (green) or ubiquitin (red) (merged; Ai, Bi) in cortical LBs in neurons (Hoechst (HO), blue) of sporadic (A) and *SNCA* mutant patients (B). (i) show merged image, (ii) show only ubiquitin and Hoechst and (iii) show only p62 and Hoechst. Scale in Bii applies to panels Ai-Biii.

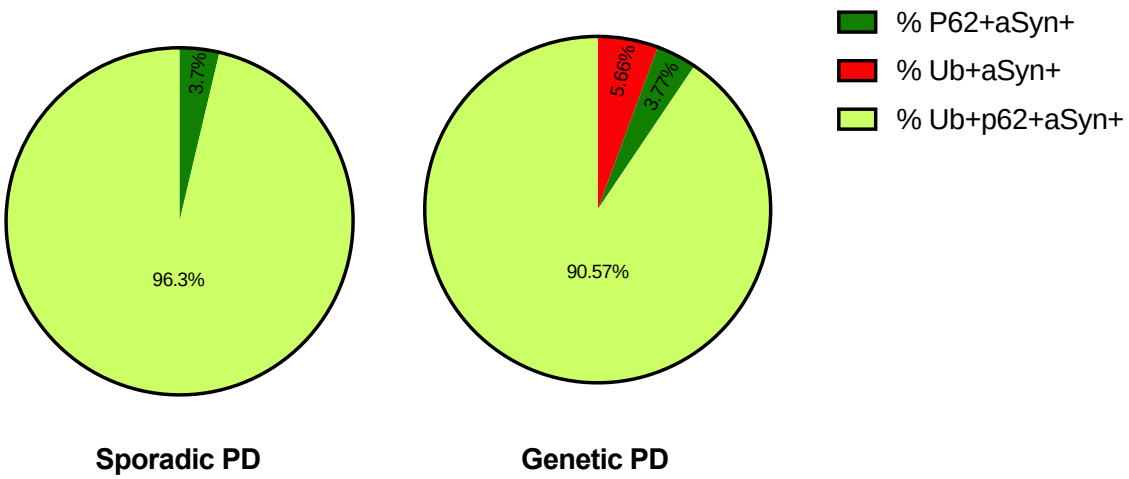


**Figure 2.15 The proportion of cortical Lewy bodies (LBs) co-labelling both ubiquitin (Ub) and p62, or only ubiquitin or only p62 in sporadic and mutation PD patients.** Pie charts showing the proportion of the α-syn+ LBs that co-label both ubiquitin and p62 (lime green), only ubiquitin (red) or only p62 (green) in sporadic and mutation PD.

### 2.4.5 Analysis of different proteins at different Lewy body (LB) stages in sporadic PD and PD cases with *SNCA* mutations

Ras homolog gene family member A (RhoA) - is a small GTPase of the Rho family that is highly expressed in the nervous system and is involved in regulating multiple signal transduction pathways that influence a diverse range of cellular functions, including cytoskeletal dynamics, cell death and autophagy among others (368, 369). RhoA has recently been identified in unbiased screens as associated with more toxic forms of LBs (360).

RhoA labelled all types of α-syn+ LP, including puncta and the different types of LBs (Figs. 2.9, 2.16). Fine and larger pS129 α-syn+ puncta co-labelled with RhoA, and in the mutation cases approximately half of the neurons with puncta had RhoA+ pS129 α-syn+ puncta (Figs. 2.8, 2.9). However, pS129 α-syn+ puncta in sporadic PD cases only rarely co-labelled with RhoA (Figs. 2.8, 2.9) suggesting differences between the α-syn+ puncta in sporadic versus mutation PD cases.

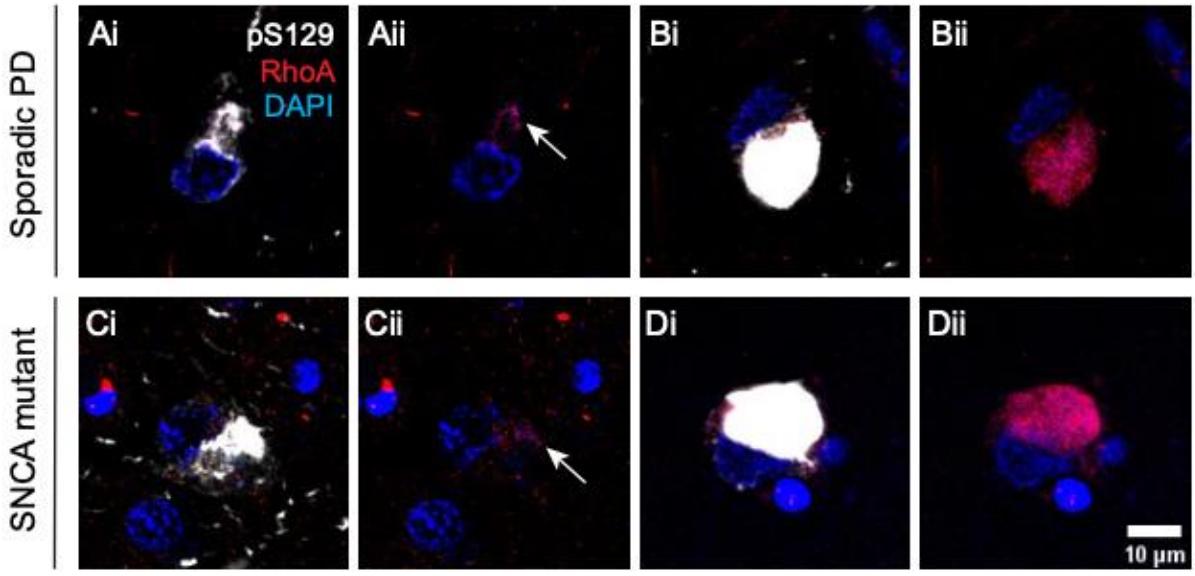


**Figure 2.16 Ras Homolog Family Member A (RhoA) co-labelling of cortical Lewy bodies (LB) in sporadic PD and PD patients with *SNCA* mutations.** Photomicrographs illustrating co-labelling of RhoA (red) and pS129 α-syn (white) in solid or mixed cortical LBs in neurons (DAPI, blue) in sporadic (A-B) and *SNCA* mutant PD patients (C-D). RhoA appeared punctate (arrow; Aii, Cii) or evenly granular (Bii, Dii) in mixed (Ai, Ci) and solid (Bi, Di) cortical LBs in sporadic and mutation PD patients. (i) show merged image, and (ii) show only RhoA and DAPI. Scale in Dii applies to panels Ai-Dii.

In solid and mixed LBs, RhoA mainly appeared as evenly granular or sometimes punctate (Fig. 2.16). There was a decreased proportion of RhoA+p62+ α-syn+ LBs in *SNCA*-mutant PD compared to sporadic PD, although the proportion of RhoA+p62+ α-syn+ LBs in E46K mutation cases was similar to sporadic cases (Fig. 2.17). These RhoA+p62+ α-syn+ LBs were predominantly solid in sporadic PD, with mainly mixed inclusions in the E46K cases (Fig. 2.17). Few p62+ α-syn+ LBs also contained RhoA in the A53T and G51D mutation cases (Fig. 2.17) with mainly solid inclusions in the A53T mutation cases as seen in sporadic PD (Fig. 2.17). This data suggest that RhoA is incorporated into LBs at a similar time as p62, and that it is largely excluded from LBs in cases with A53T and G51D *SNCA* mutations.

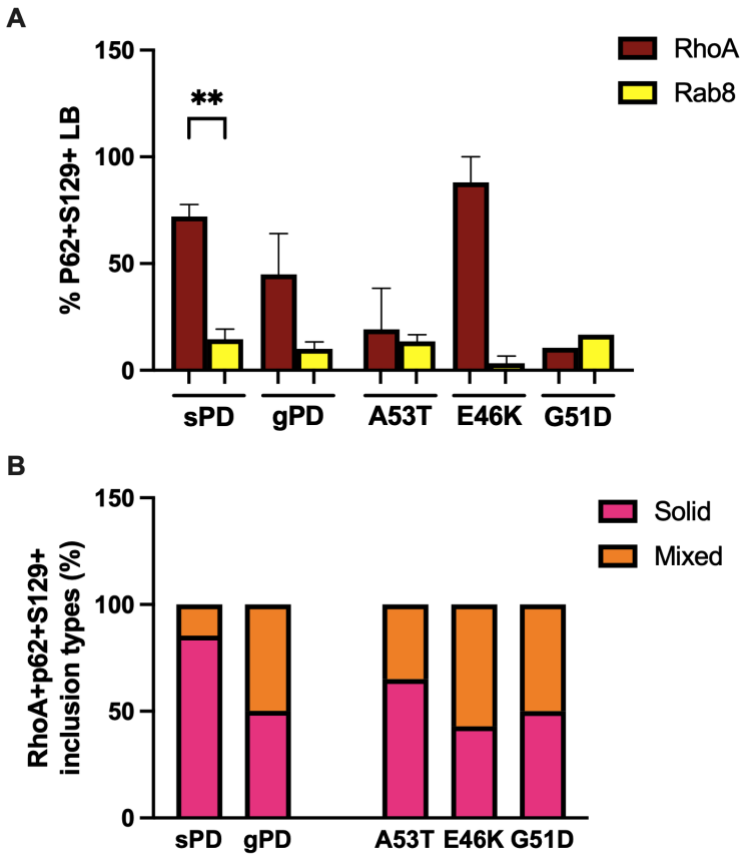


**Figure 2.17 Mean proportion (± SEM) of Ras Homolog Family Member A (RhoA) or Ras-related protein Rab-8 (Rab8) p62+ cortical Lewy bodies (LB) and the type of RhoA+p62+ cortical LBs in sporadic PD and PD patients with *SNCA* mutations.** Bar graph showing the proportion of p62+ pS129 α-syn+ LBs that were RhoA+ (dark red) and Rab8+ (yellow) in sporadic and mutation PD and in individual mutation cases (A). Stacked bar graphs showing the types of RhoA+p62+S129+ LBs (solid, pink; mixed, orange) in sporadic and mutation PD and in individual mutation cases (B). Significance is taken at **p < 0.01.

Ras-related protein Rab-8 (Rab8) - is a small GTPase of the large Rab family of proteins that are membrane organisers, coordinating consecutive stages of transport within cells (370, 371). Rab8 has been linked to PD as it is activated by phosphorylation by both PINK1 and LRRK2 (372) and was recently identified in an unbiased screen as one of the Rab proteins incorporated into lipid-rich LBs (360).

Rab8 also labelled all types of α-syn+ LP, including puncta and the different types of LBs (Figs. 2.9, 2.18). Rab8+ α-syn+ neuronal puncta were rare in both sporadic and mutation cases of PD (Fig. 2.8) suggesting that it is not significantly involved in the development of this type of inclusion.

In solid and mixed LBs, Rab8 mainly appeared as evenly granular in sporadic PD (Fig. 2.18A, B) but mainly punctate or aggregated in PD cases with *SNCA* mutations (Fig. 2.18C, D). Rab8+ LBs were rare in both sporadic and mutation PD cases, especially in the E46K mutation cases where hardly any Rab8+ LB were seen (Fig. 2.17A). This data suggest that Rab8 is rarely incorporated into LBs.

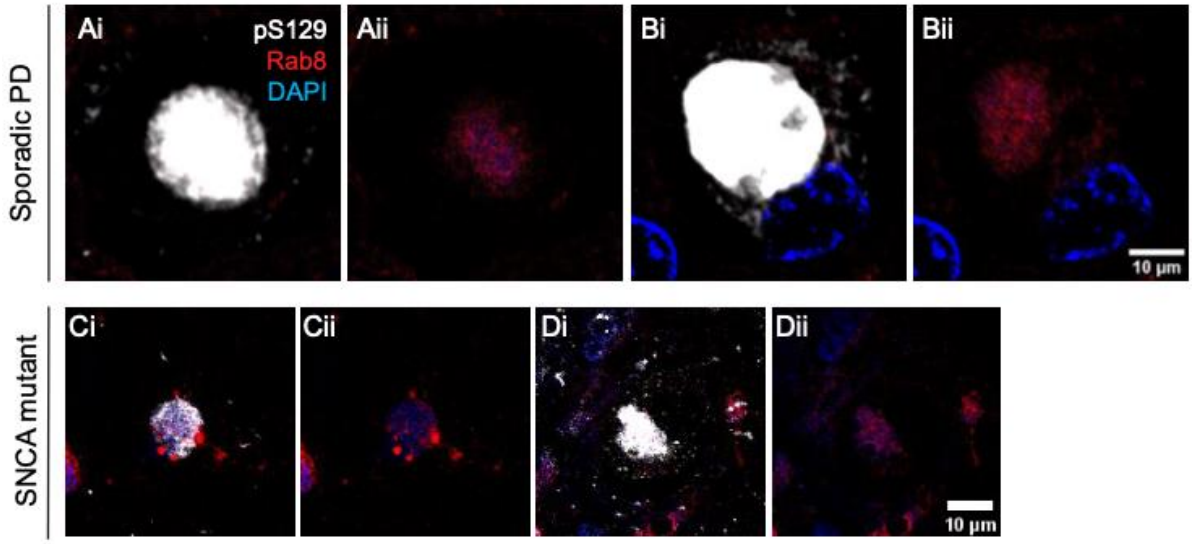


**Figure 2.18 Ras-related protein Rab-8 (Rab8) co-labelling of cortical Lewy bodies (LB) in sporadic PD and PD patients with *SNCA* mutations.** Photomicrographs illustrating co-labelling of Rab8 (red) and pS129 α-syn (white) in solid or mixed cortical LBs in neurons (DAPI, blue) of sporadic (A, B) and *SNCA* mutant PD patients (C, D). In sporadic PD patients Rab8 appeared evenly granular (Aii, Bii) in solid (A) or mixed (B) LBs. In mutation cases, Rab8 was punctate or aggregated (Cii) and evenly granular (Dii) in mixed LBs (C, D). (i) show merged image, and (ii) show only Rab8 and DAPI. Scale in Bii applies to panels Ai-Bii and scale in Dii applies to panels Ci-Dii.

Phosphorylated microtubule-associated protein tau (AT8) - becomes abnormally phosphorylated in tauopathies and forms aggregates of paired helical filaments (PHF-tau). AT8 is a PHF-tau-specific monoclonal antibody that is a commonly used marker of neuropathology because of its recognition of abnormally phosphorylated tau. As discussed above, AT8 tau accumulation has been recently associated with LBs in PD (69), although there have been no replication studies to date.

AT8 tau immunoreactivity was typically absent in neurons with punctate α-syn, indicating it is not associated with this type of α-syn pathology. In both sporadic and mutation PD cases, weak AT8 tau+ immunoreactivity was observed in cortical and SN LBs with a slightly more granular appearance (Figs. 2.19, 2.20). Of note, in the SN most mixed LBs lacked AT8 tau+.

In addition to staining LBs, AT8 tau also strongly labelled aggregates, neurites and neuronal inclusions not immunoreactive for α-syn in the cortex and SN of all case types, including controls (Figs. 2.19, 2.20). These AT8 tau+ non-LB inclusions varied in size and were occasionally co-labelled with p62 and ubiquitin. Large AT8 tau+ only neuronal inclusions that filled the soma were rarer in the SN than the cortex.

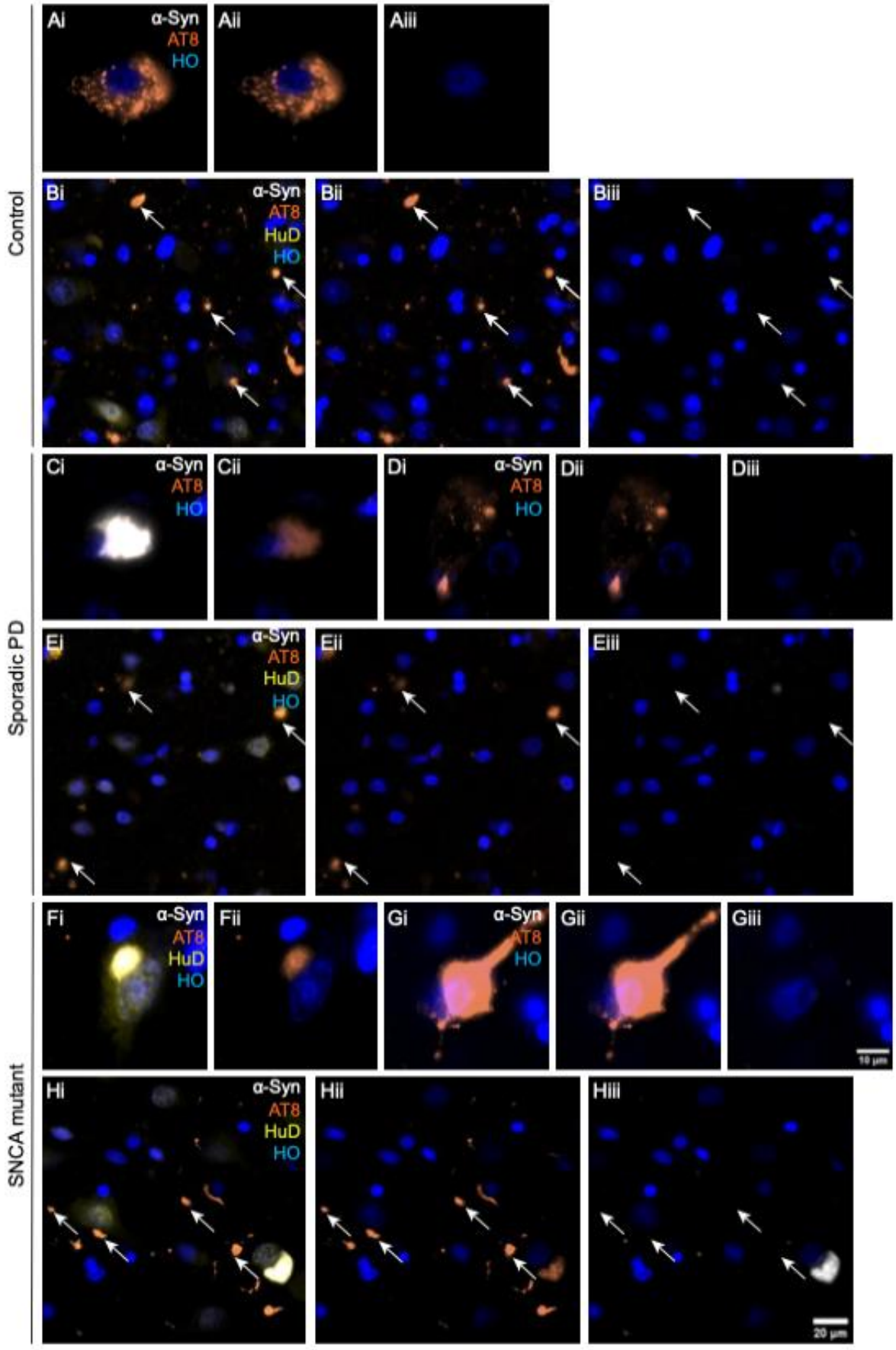
Control
Sporadic PD
SNCA mutant
Ai
α-Syn
AT8
HO
Aii
Aiii
Bi
α-Syn
AT8
HuD
HO
Bii
Biii
Ci
α-Syn
AT8
HO
Cii
Di
α-Syn
AT8
HO
Dii
Diii
Ei
α-Syn
AT8
HuD
HO
Eii
Eiii
Fi
α-Syn
AT8
HuD
HO
Fii
Gi
α-Syn
AT8
HO
Gii
Giii
10 µm
Hi
α-Syn
AT8
HuD
HO
Hii
Hiii
20 µm

**Figure 2.19 Phospho-tau (AT8) co-labelling in cortical pathologies in sporadic and *SNCA* mutation PD patients.** Photomicrographs illustrating co-labelling of AT8 tau (orange) and α-syn (white) (Ci, Cii, Fi, Fii) in cortical LBs in neurons (Hu antigen D (HuD), olive green; Hoechst (HO), blue) of sporadic PD (C-G) and *SNCA* mutant cases (F-H). In the absence of α-syn, AT8 tau aggregates accumulated in cortical neuronal soma (Ai-Aiii, Di-Diii) and in a solid form filling the whole neuron including the soma and processes (Gi-Giii) in all groups. Other AT8 tau+ aggregates and neurites not immunoreactive for α-syn (white arrows; Bi-Biii, Ei-Eiii, Hi-Hiii) were also observed in all groups. (i) are merged images, (ii) show AT8 and Hoechst only and (iii) show α-syn and Hoechst only. Scale in Gii applies to panels Ai-Aiii, Ci-Diii and Fi-Giii and scale in Hiii applies to panels Bi-Biii, Ei-Eiii and Hi-Hiii.

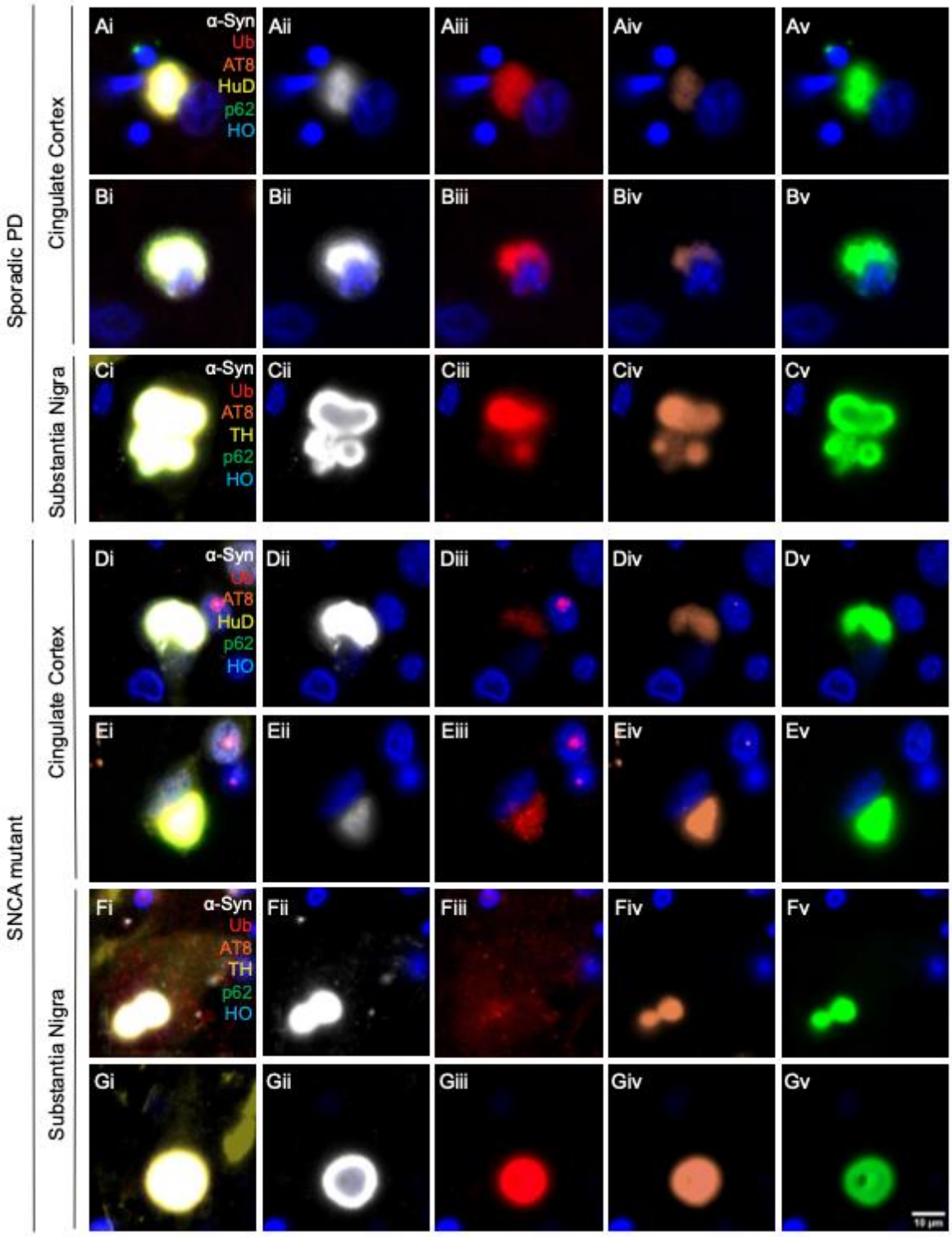


**Figure 2.20 Ubiquitin (Ub), p62 and phospho-tau (AT8) co-labelling in Lewy body (LBs) in the cortex and substantia nigra (SN) of sporadic and *SNCA* mutation PD patients.** Photomicrographs illustrating co-labelling of ubiquitin (red), AT8 tau (orange), p62 (lime green) and α-syn (white) (merged; A-Gi) in solid (A-C, E, G) or mixed (D, F) LBs in cortical neurons (Hu antigen D (HuD); Hoechst (HO), blue) and dopaminergic SN neurons (tyrosine hydroxylase (TH); Hoechst, blue) of sporadic (A-C) and *SNCA* mutant PD patients (D-G). (i) show merged image, (ii) show only α-syn and Hoechst, (iii) show only Ub and Hoechst, (iv) show only AT8 and Hoechst and (v) show only p62 and Hoechst. Scale in Gv applies to panels Ai-Gv.

## 2.5 Discussion

The present study quantitatively evaluated the proportion of cortical neurons with early puncta, PTM-modified pale/mixed LBs and mature round LBs in patients with PD using protein markers thought to be important for the progressive formation of these intracellular LPs. Importantly, the study directly compared these LPs to those in cases with different *SNCA* mutations, as most animal and cellular models evaluating LP formation use *SNCA* mutations. The main findings were that 1) both types of LBs colocalised p62 and ubiquitin, suggesting that PTMs occur very early prior to compaction in LB formation, 2) RhoA was not involved in LB formation in the A53T and G51D mutation cases, suggesting that mutations in this region impact on the binding of this protein, 3) sporadic PD had mainly solid mature LBs, while in *SNCA*-related PD up to half the LBs were of the pale/mixed type, suggesting that LB formation may differ in mutation cases, 4) the distribution of LB-containing neurons in all PD cases was similar, showing that the same neurons are vulnerable to LB formation even if different types of LBs are formed, and 5) *SNCA* mutation cases had more neurons with LBs and additional neurons with α-syn puncta (more rarely seen in sporadic PD), suggesting increased toxicity in mutation cases. These data overall show that core proteins and PTMs in LBs are similar in sporadic and *SNCA* mutation cases of PD, that more neurons are affected by pathologic α-syn in *SNCA* mutation cases compared with sporadic PD, and that LP type differs significantly between *SNCA* mutation cases and sporadic PD, possibly due to differences in associated protein binding to mutated α-syn (e.g. RhoA).

*Core proteins in Lewy pathologies (LP)*

α-Syn+ LBs mostly colocalised ubiquitin and p62 and sometimes phospho-tau, in line with previous studies (64, 69, 349, 363). As expected, most LBs contained pS129+ α-syn, ubiquitin and p62. In fact, the pS129 PTM is known as the most common form of pathologic α-syn in LBs (56) and is often used to define LPs. Studies show that most LBs also label with ubiquitin and p62 (60, 64), although these proteins have not been consistently reported in puncta in sporadic PD (64). For LB compaction, it is thought that p62 and ubiquitin are incorporated early into the precursor pale/mixed body followed overtime by LB maturation (64) and the data presented is consistent with this - pale/mixed LBs have already incorporated ubiquitin and p62. Diffuse cytoplasmic α-syn occurs more frequently than the pale/mixed or mature round LBs (358), consistent with the concept that the obvious ubiquitination of α-syn in LBs is disease specific due to overwhelming transcriptionally downregulated proteostatic machinery in

neurons containing LBs (373-376). If all LBs already have incorporated these core PTMs, when do these α-syn protein changes occur? In the present study >50% of α-syn+ puncta co-labelled with p62, suggesting that this early LP may be the precursor to LBs, as previously suggested (see Fig. 2.1). p62 is a classical marker of autophagy targeting ubiquitinated proteins for degradation in the lysosome (357). It should be noted that several studies have shown that α-syn+ puncta co-label with lysosomal markers indicating their correct targeting for degradation in PD (354, 356). But more importantly, a recent study has shown that these α-syn+ puncta contain a more soluble form of α-syn compared with the insoluble form found in LBs in sporadic PD (56, 356). This could suggest that the lysosomal pathway is still working for the 50% of α-syn+ puncta that are ubiquitinated. Indeed, the proportion of cortical neurons with α-syn+ puncta in sporadic PD was very low, consistent with their continued functioning to clear this more soluble α-syn.

This study validates the recent study emphasizing the colocalization of phospho-tau in LBs in sporadic PD (69). It is also the first to assess these different proteins in cortical neurons where LP may not be as mature as in the brainstem. Tau is classed as one of the group 2 proteins (α-syn-binding proteins) found in LBs which also include agrin, 14-3-3 protein, microtubule-associated protein 1B and synphilin-1 (30). In animal models, the loss of tau delays the progression of α-syn pathology and tau-modified α-syn fibrils enhance seeding activity (377-379) supporting the concept that tau facilitates α-syn aggregation. Electron microscopy in human LBs has shown that the α-syn and AT8 tau filaments differ in their structure with AT8 tau fibrils being longer than the α-syn fibrils but shorter than fibrils in neurofibrillary tangles (348). Importantly, the microtubule affinity-regulating kinase 1 (MARK1), which phosphorylates tau decreasing its association with microtubules, is also colocalized to α-syn+ LBs as well as to puncta in less mature α-syn+ deposits (380), suggesting the phosphorylation of tau by MARK1 is associated with α-syn pathology and occurs prior to LB formation. Tau protein binds to spectrin and actin filaments (381) and animal models have identified an α-syn dependent rearrangement that impairs these cytoskeletal elements to impact on mitochondria and neuronal viability (382-384). This may be associated with the pS129 α-syn reorganization of the neuronal cytoskeletal network to incorporate β-tubulin into the structural cage to corral LB formation (355).

Although phospho-tau has been observed in LBs previously, phospho-tau+ LBs have largely been evaluated in the brainstem with variable outcomes (69, 349, 363). Using the antibodies in the present study, a proportion of cortical LBs were observed to contain phospho-tau, and we found the same result in PD patients with *SNCA* mutations. Colocalization of α-syn and phospho-tau in different brain regions of A53T and G51D cases have been published (92, 103, 104) but limited colocalization studies have been performed overall in other types of mutations. Our data show similar colocalization of α-syn and AT8 tau in some cortical LBs in cases with *SNCA* mutations to those with sporadic PD. We also observed phospho-tau in nigral LBs. Brainstem tau pathology is usually characterized by an increase in 3-repeat tau (385), which is a marker of new axon generation (386) and of more advanced pathological lesions (387, 388), but also of isoform specific aggregation following its acetylation (389). Acetylation of α-syn has recently been shown to be important for its pathologic transmission, in addition to its phosphorylation (390). Histone deacetylase 6 inhibition acetylates both tau and α-syn (391) and colocalizes to LBs where electron microscopy shows it binds to LB filaments (392) with its inhibition protecting against α-syn toxicity in an animal model (393). Because LBs are only identified using the Campbell-Switzer silver stain (which identifies 3-repeat and not 4-repeat tau inclusions) and not the Gallyas silver stain (which identifies 4-repeat and not 3-repeat tau inclusions) (394), the isoform that may be most relevant in the LB fibrils may be 3-repeat tau, even if both tau isoforms have been identified in most nigral neurons with LBs (69).

*Significantly more neurons have Lewy pathologies (LP) in SNCA mutation cases of Parkinson's disease (PD) compared with sporadic disease*

While this study is limited by the small number of *SNCA* mutation cases and the variability in the E46K cases, this is the first study to quantitatively compare LPs in cases with different *SNCA* mutations and sporadic PD. Although one of the E46K cases showed more variability with a lower proportion of neurons with LBs and a higher proportion of neurons with puncta, which may have been influenced by the thinner section thickness (see methods), the data supports that more neurons are affected by LP in *SNCA* mutation cases. *SNCA* mutation cases had twice as many neurons with α-syn+ LBs and as many neurons again with additional α-syn+ puncta. In total, >20% of cortical neurons contained α-syn+ LPs compared with just over 5% in sporadic PD. These differences were most prominent when assessing α-syn+ puncta which were not frequently observed in sporadic PD. There is abundant evidence indicating that *SNCA* mutations enhance α-syn oligomerisation and/or fibrillation (119, 122-124, 127, 395-

397) supporting the concept that patients with these mutations would have an acceleration of LP formation. However, if α-syn+ puncta are functional lysosomes, this could suggest that *SNCA* mutation cases also have more neurons degrading mutant α-syn.

*α-Synuclein occurs in diverse Lewy pathologies (LP) in SNCA mutation cases compared with sporadic disease*

Not only could *SNCA* mutation cases be differentiated from sporadic PD by the presence of cortical neurons with α-syn+ puncta, they also had significantly more cortical neurons with mixed LPs as well and approximately the same amount with mature round LBs. This suggests that the two additional types of LP are greatly expanded in PD patients with *SNCA* mutations. Pathogenic mutations in *SNCA* have been shown to impair their lysosomal degradation, altering protein homeostasis and increasing cellular protein concentration by extending their degradation half-life (398). The increase in these additional pathologies in cases with *SNCA* mutations is likely due to this, particularly the enhanced α-syn+ puncta that are likely to align with lysosomes. Using *SNCA* mutations in cell models (360), two types of α-syn+ inclusion pathologies have been identified, a fibril-rich inclusion which is similar to mature round LBs, and a more toxic lipid-rich inclusion which dominated neurons with the E46K mutation and is similar to pale/mixed LBs. This may suggest that pale/mixed and punctate LPs are more driven by impaired lysosomal degradation of mutant α-syn, while mature round LB may sequester non-mutant α-syn and have more similarities to sporadic PD.

The majority of mature round LBs in sporadic PD cases contained RhoA, a major regulator of actin stabilization (368, 369), with inhibition of RhoA shown to reduce α-syn expression, aggregation and pathology (399-401), suggesting that RhoA also plays a role in LB formation. Compared with sporadic PD, RhoA was found in less than half of all LBs and around half of α-syn puncta in *SNCA* mutation cases. The binding of RhoA to α-syn was reduced in both A53T and G51D cases compared to E46K cases. A30P mutations in *SNCA* have also been linked to actin destabilization (402). While the data suggest variation in the binding of RhoA to different α-syn mutants, overall, the data suggest a shift in RhoA's association with α-syn to less stable α-syn forms in *SNCA* mutation cases. This is consistent with the cell models using *SNCA* mutations that revealed RhoA colocalised more with toxic lipid-rich inclusions rather than more neuroprotective fibril-rich inclusions (360).

*Conclusions and concepts for further testing*

This study has shown that 1) core proteins in LB are similar in both sporadic and *SNCA* mutation cases of PD, 2) these core proteins occur in both subtypes of LB (pale/mixed and round/mature) but not in all puncta, and 3) that there is more LP on average in cases with *SNCA* mutations than in sporadic PD. It is therefore this last point which mainly distinguishes *SNCA* mutation cases from sporadic cases of PD.

While previous concepts of LB formation have been intuitively based on a progression from smaller to larger aggregates of α-syn that then cause physical cellular disruption and degradation (see Fig. 2.1), the prevalence of these types of LP in sporadic PD may question this assumption. Of the LPs observed, neurons with only small puncta represented ~1.5% of neurons while 6.8% of neurons on average had LB (78% with the round/mature type). If the expectation is that there is a maturation of LP to a pinnacle of a larger disruptive aggregate, then it should be that the most prevalent LP in sporadic PD would be puncta, then mixed/pale LBs, with lower levels of the most mature/round disruptive LBs (see Fig. 2.1). However, the reverse occurs in sporadic PD, and this is despite the cortical region analyzed considered to contain less mature pathology than the brainstem. Also, similar small numbers of neurons in controls had α-syn immunopositive puncta (2.4%), as may be expected for normal lysosomal degradation of such aggregates. It should be noted that in cell cultures seeded with pre-formed fibrils, round LBs form by 21 days from ribbon-like structures that can be seen at 7-14 days (359), reflecting a relatively rapid formation of these LPs. By contrast, in the SN pars compacta it has been estimated that the degradation of LBs occurs over a 6–16-month period (29). As there is no significant neuronal loss in the cortical region analysed in sporadic PD (28, 403), this suggests there is a reversal of the current concept of their formation and that LBs turnover in cortical neurons, hypothetically going from a rapidly formed round/mature LBs to be broken down to a mixed LB and then to lysosomal associated α-syn puncta. This concept would fit with the prevalence of the LPs observed in sporadic PD.

Applying the same logic to *SNCA*-related PD suggests a potential different pathological sequence for LB formation. Puncta are as prevalent as LBs in cortical neurons, and the doubling of LBs observed in *SNCA*-related PD compared with sporadic PD is due to the increase in mixed/pale LBs. This prevalence data would indicate that α-syn puncta (most prevalent) form both round/mature LB and mixed/pale LBs in equal proportions. These LPs may be more

resistant to degradation than those without mutant α-syn in sporadic PD. Alternatively, if the same process described above for sporadic PD occurs in *SNCA* mutation cases, then the substantive increase in mixed/pale LBs and puncta could indicate just more difficulties overall with the degradation of LBs made with mutant α-syn. However, cell cultures using different *SNCA* mutations show the formation of two main LB types, one more prevalent in E46K mutant neurons contains more lipid (pale/mixed) and one more prevalent in A53T mutant neurons contains mainly fibrils (round/mature) (360). This supports the former concept of LB formation in *SNCA* mutation cases rather than one similar to that for sporadic PD. The difference in the formation of LPs in *SNCA* mutants versus sporadic PD is depicted in Fig. 2.21.

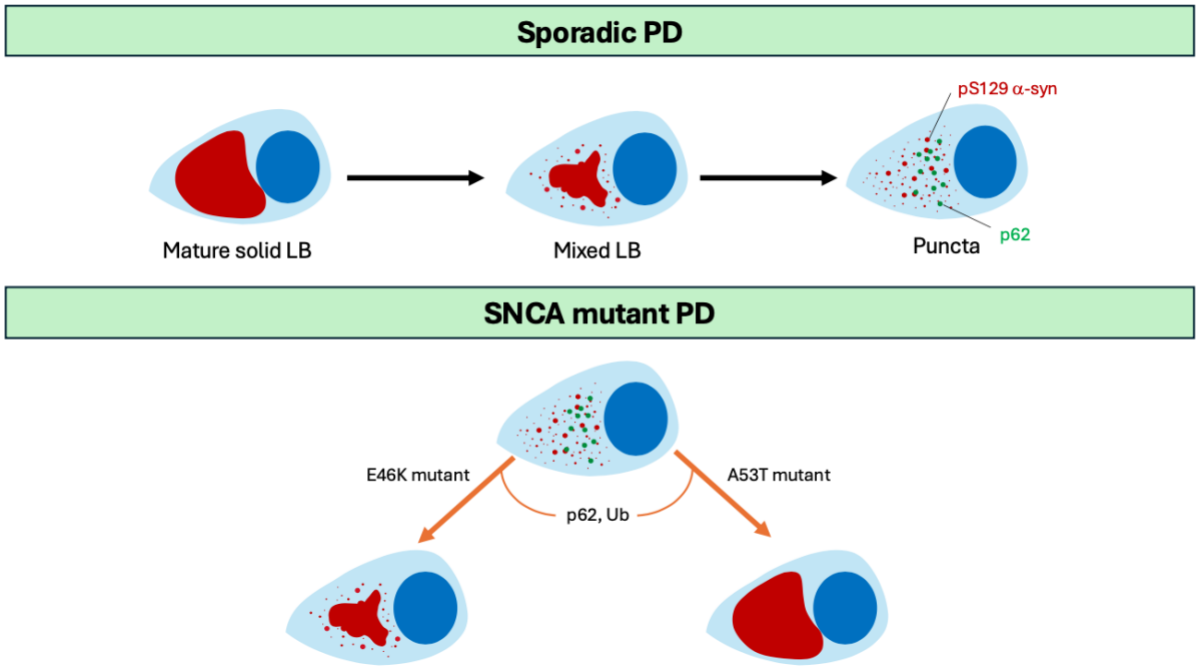


**Figure 2.21 Potential sequences of Lewy body (LB) formation in sporadic and *SNCA*-mutant PD based on the prevalence of the Lewy pathologies (LPs).** Hypothetically, in sporadic PD, rapidly formed mature solid LBs may dissociate to become mixed LBs representing an intermediary stage and then terminate as pS129 α-syn puncta likely representing the cell's attempt to degrade α-syn. In *SNCA*-mutant PD there is a different potential pathway where mixed and mature solid LBs may arise in equal proportions from puncta incorporating and aggregating additional proteins (more p62 and ubiquitin (Ub)).

Overall, more cortical neurons were affected by α-syn LPs in *SNCA*-related PD cases compared to sporadic PD and there were significant differences in the types of LPs in *SNCA* mutation cases compared to sporadic PD, with sporadic cases having a largely uniform (mature/solid)

population of LBs while *SNCA* mutation cases had both solid and mixed LBs. Differences were also observed in the colocalisation of LBs with the actin stabilizing protein RhoA, with a similar high proportion of LBs colocalising RhoA in sporadic and E46K mutant PD while few LBs colocalised RhoA in A53T or G51D cases. This suggests that additional molecular pathways are likely involved in the different types of LB formation, with E46K cases having more pale/mixed LBs with RhoA and sporadic PD having mainly mature/round LBs containing RhoA. This may suggest that RhoA is involved in the rapid formation of wild-type α-syn fibrils that form round/mature LBs, but also associates with E46K α-syn and lipids to form mixed/pale LBs. These data confirm the involvement of RhoA in the progression of LB formation, as recently proposed (360), but also suggest that the involvement of this molecular pathway that may impact developing LPs in different ways in sporadic PD versus cases with *SNCA*-mutations.

# CHAPTER 3: Comparisons of protein pathologies in a chimeric mouse model with transplants of human dopamine neurons from *SNCA*, *LRRK2* and *PRKN* induced pluripotent stem cells

## 3.1 Abstract

Aim: To examine and compare protein pathology of human induced pluripotent stem cell (iPSC)-derived ventral midbrain (VM) neuronal transplants carrying *SNCA*, *LRRK2* and *PRKN* mutations.

Methods: A chimeric mouse model with transplanted human iPSC-derived dopaminergic neurons was generated at The Florey, University of Melbourne for analysis. Multiplex free-floating α-synuclein (α-syn) and tau immunofluorescence was performed on frozen mouse brain sections from mice with transplanted cell lines from control patients (n= 3), *SNCA* (n= 3), *LRRK2* (n =3) and *PRKN* (n= 2) mutation patients to examine protein pathologies in grafted human dopaminergic neurons. Sections were scanned and all dopaminergic neurons in the grafts identified, characterised and assessed for α-syn and tau levels and for the presence of pathology. High magnification 3D confocal imaging and deconvolution were performed for further assessment of pathology in the grafted dopaminergic neurons. Non-parametric statistics were used to determine differences between groups in the quantity and size of dopaminergic neurons and in the α-syn and tau levels in grafted neurons.

Results: A similar quantity of morphologically heterogenous dopaminergic neurons were identified in the grafts of all genotypes. Although there was high variability, the *PRKN* mutation group had smaller dopaminergic neuronal cell bodies and projections compared to the other grafts. α-Syn and tau levels in the grafted dopaminergic neurons were similar in all groups. Diverse pS129 and AT8-labelled aggregate-like structures were identified in the grafts of all genotypes, however the majority were extracellular or only partially localised to the grafted dopaminergic neurons.

Conclusion: These data suggest that there are similar protein pathologies in iPSC-derived dopaminergic neuronal transplants across genotypes. Grafted dopaminergic neurons expressed similar levels of α-syn and tau across genotypes. Morphologically diverse aggregate-like

pS129 and AT8-labelled structures were identified in the grafts of all genotypes, however none were conclusively or entirely within the grafted dopaminergic neurons. Most of these structures did not recapitulate Lewy body (LB) features and may be related to developmental aspects or other Lewy pathologies.

## 3.2 Introduction

As mentioned in the previous chapter, proteinaceous α-synuclein (α-syn) inclusions termed Lewy bodies (LB) together with nigral neuron loss define Parkinson's Disease (PD) (27), however PD pathogenesis and comparisons across PD-related genes remains to be fully elucidated. Human induced pluripotent stem cell (iPSC) neuronal models expressing *SNCA* multiplications, mutant forms of α-syn or other common PD-related gene mutations such as *LRRK*2 and *PRKN* have revealed increased α-syn levels and aggregation and other cellular degenerative processes implicated in PD (404, 405). To better our understanding of PD and elaborate on the previous chapter which focused on nigral and cortical LB pathology in sporadic and *SNCA*-related PD, a similar study of human iPSC-derived neurons from PD patients with *SNCA, LRRK2* and *PRKN* mutations in the environment of a living brain will be performed in this chapter to provide unique comparative insights into the pathogenesis of these inclusions.

*iPSC PD-related mutation model pathologies*

Cell culture studies (406-409) have revealed that PD iPSC-derived neurons from patients who carried *SNCA* multiplications demonstrate α-syn aggregation, insolubility and phosphorylation that associate with higher oxidative stress levels, mitochondrial defects and neuronal death. α-Syn aggregate morphology in PD iPSC-derived cortical and dopaminergic neurons with *SNCA* triplication has been described mainly as punctate (407, 408). A study (408) which used PD iPSCs with *SNCA* triplication reported that α-syn aggregates in neuronal soma varied in size (under 1μm to 5μm) and had a punctate appearance in dopaminergic neurons and a more diffuse appearance in cholinergic neurons potentially reflecting heterogenous LB morphologies in the PD brain as discussed in the previous chapter. Also, most α-syn aggregates were under 1μm in size (408). Similarly, α-syn aggregates or accumulations and neuritic pathologies accompanied by reduced neurite outgrowth and mitochondrial defects have been observed in PD iPSC-derived neurons with the A53T mutation (131, 133, 134). Swollen

structures containing α-syn and tau in neuronal processes and LB-like accumulations of phospho-α-syn at S129 (pS129) surrounding nuclei have also been observed in A53T iPSCs (131, 133).

Human iPSC models with mutations in the *LRRK2* and *PRKN* genes have also revealed α-syn pathologies. Cell culture studies (218, 220) have reported diffuse accumulated α-syn and aggregates in the soma of human iPSC-derived neurons with *LRRK2* mutations. Similarly, α-syn accumulation has been seen in iPSC-derived neurons from patients with *PRKN* mutations (295-297) without apparent inclusions formed which concurs with post-mortem data (264, 266-273) that indicates the majority of PD patients with *PRKN* mutations do not have LB pathology.

*Human PD iPSC transplant model pathologies*

There are limited studies that have investigated pathologies in iPSC transplants from PD patients. An early study (410) revealed that idiopathic PD iPSC-derived dopaminergic neurons transplanted into the striatum of a 6-hydroxydopamine (6-OHDA) PD mouse model survived in high numbers, projected TH+ fibres towards other cells within the graft and did not contain any α-syn inclusions. However, punctate α-syn was seen in the synapses of some graft neurons and in the mouse striatum (410). Another study (411) revealed similar findings and additionally indicated that idiopathic PD iPSC-derived neurons transplanted into α-syn transgenic mice did not show α-syn inclusions or pathology 6 months post-transplantation.

Contrastingly, iPSC neuronal transplants from PD patients carrying mutations demonstrate enhanced α-syn levels or pathology (412-414). Despite the emergence of α-syn aggregates in prolonged cultures of iPSC-derived neurons from a PD patient carrying the A53T mutation, aggregates were not observed in these cells in transplants (412). PD iPSC-derived neurons with the A53T mutation transplanted into 6-OHDA mice revealed high survival and exhibited increased α-syn expression in the graft 12 weeks post-transplantation without inclusion formation, indicating a potential initial stage prior to pathology (412). Similarly, another study (413) reported that after 11 weeks PD iPSC-derived neurons with a *LRRK2* mutation transplanted into 6-OHDA mice also demonstrated enhanced α-syn expression levels without aggregates. However, aggregates have been reported in PD iPSC-derived neurons with *SNCA* triplication which survived transplantation into 6-OHDA rats and a small proportion of grafted

cells had α-syn inclusions 6 months post-transplantation which varied in size and usually appeared granular or punctate (414).

Therefore, this study aims to quantitatively and qualitatively examine and compare protein expression and pathology based on PD-related pathological protein markers (pan α-syn, pS129 α-syn, tau and phospho-tau (AT8)) of iPSC-derived VM dopaminergic neuronal transplants from controls and PD patients carrying *SNCA* (A53T), *LRRK2* (R1441G) and *PRKN* (loss of function or LoF) mutations.

## 3.3 Methods

### 3.3.1 Generation of the chimeric model for analysis (performed at The Florey, The University of Melbourne)

There are a number of steps required.

1) Making or obtaining the iPSCs – iPSC lines with *LRRK2* R1441G (n=3) and *SNCA* A53T (n=3) used in the analyses presented in this article were obtained from the Golub Capital iPSC Parkinson's Progression Markers Initiative (PPMI) Sub-study (https://www.ppmi-info.org/access-data-specimens/request-cell-lines). As such, the investigators within PPMI contributed to the design and implementation of PPMI and/or provided data and collected samples but did not participate in the analysis or writing of this report. For up-to-date information on the study, visit PPMI-info.org for mutations obtained from the Golub Capital iPSC Parkinson's Progression Marker Initiative (PPMI) sub-study (www.ppmi-info.org/cell-lines). Neurologically normal control lines (n=2) were also obtained from PPMI. Another control line (KOLF2-1J) was obtained from the Jackson Laboratory (#JIPSC1000) and has been described previously (415). *PRKN* iPSCs were made at The Florey by Dmitry Ovchinnikov (416, 417).
2) Expanding the iPSCs for differentiation was performed by Prof Clare Parish's laboratory at The Florey (418).
3) Differentiating the iPSCs into dopamine neurons was performed by Prof Clare Parish's team at The Florey (418).
4) Lesioning athymic nude mice using 6-OHDA and waiting 2 weeks was performed and overseen by Prof Lachlan Thompson's team at The Florey (419).

5) Transplanting the iPSCs into the lesioned striatum of mice (419, 420), waiting 6 months, perfuse fixing the brains with 4% paraformaldehyde, transferring the brains to a 20% sucrose solution at 4°C for a minimum of 24 hours, and cutting the brains into 30-µm thick serial coronal sections on a freezing microtome was performed and overseen by Prof Lachlan Thompson's team at The Florey.

### 3.3.2 Tissue processing and immunofluorescence staining

Tissue sections were obtained from colleagues at The Florey (2-3 cell lines per group, up to 50 sections per mouse, 10-14 mice per genotype (controls, n=10; *SNCA*, n= 14; *LRRK2*, n=12; *PRKN*, n=11) and stained free floating for immunofluorescence markers tyrosine hydroxylase (TH) and pathological markers (Table 3.1). Briefly, sections were washed for 30 minutes in phosphate buffered saline (PBS) followed by antigen retrieval which was performed by incubating the sections in 10mM sodium citrate buffer at 98°C for 22 minutes. After cooling to room temperature (RT), sections were washed in PBS. Sections were then treated with blocking buffer (containing 2% donkey serum, 1% bovine serum albumin solution, 0.2% Triton X-100, 0.1% gelatin and 0.1% Tween-20 in PBS (PBST)) for 2 hours at RT. Sections were incubated in a combination of primary antibodies in blocking buffer as per Table 3.1 for ~72 hours at 4°C, followed by 0.1% PBST washes and incubation with their corresponding Alexa Fluor secondary antibodies (Table 3.1) and bisbenzimide H 33342 trihydrochloride (Hoechst, Cat.# B2261; Sigma-Aldrich) in blocking buffer for 2 hours at RT. Sections were washed again in 0.1% PBST followed by PBS and then coverslipped using mounting medium (Cat.# S3023, DAKO) and sealed with CoverGrip coverslip sealant (Cat.# 23005, Biotium). Negative controls were included by omitting either the primary or secondary antibodies.

**Table 3.1** List of antibodies used in this study

| Primary antibodies (type, Cat.#) | Epitope (immunogen) | Dilution | Source | Fluorophore |
|---|---|---|---|---|
| Tyrosine hydroxylase (TH) (mouse IgG2b mAb, Cat.# TA506549) | Full length human recombinant protein of human TH | 1:200 | ThermoFisher Scientific | 647 |
| Pan α-Syn ((Syn204) mouse IgG2a mAb, Cat.# 838201) | Syn 204 raised using recombinant α-syn and recognises aa.1-130 of α-syn | 1:200 | Biolegend | 568 |
| Phospho-α-syn at S129 (rabbit mAb, Cat.# ab51253) | Synthetic peptide aa.100-140 of human α-Syn | 1:500 | Abcam | 488 |
| Pan tau ((SP70) rabbit mAb, Cat.# SAB5500182) | Synthetic peptide N-terminus of human tau | 1:200 | Sigma Aldrich | 568 |
| Phospho-tau (Ser202, Thr205) (AT8) (mouse IgG1 mAb, Cat.# MN1020)* | Partially purified PHF-tau aa. 1-758 | 1:200 | ThermoFisher Scientific | 488 |
| **Secondary antibodies** | **Epitope (immunogen)** | **Dilution** | **Source** | |
| Goat anti-mouse IgG2b-Alexa Fluor 647, A-21242 | Mouse IgG 2b | 1:200, 250 | ThermoFisher Scientific | |
| Goat anti-mouse IgG2a-Alexa Fluor 568, A-21134 | Mouse IgG 2a | 1:250 | ThermoFisher Scientific | |
| Donkey anti-rabbit- Alexa Fluor 488, A-21206 | Rabbit IgG | 1:200 | ThermoFisher Scientific | |
| Donkey anti-rabbit- Alex Fluor 568, A-21134 | Rabbit IgG | 1:250 | ThermoFisher Scientific | |
| Goat anti-mouse IgG1- Alexa Fluor 488, A21206 | Mouse IgG 1 | 1:250 | ThermoFisher Scientific | |

Aa, amino acid; mAb, monoclonal antibody; pAb, polyclonal antibody

### 3.3.3 Identification of protein pathologies

Dopaminergic grafted neurons were identified and manually counted based on TH immunoreactivity, usually together with a large dull nucleus in scanned images (Fig. 3.1 and 3.2). Aggregate-like structures were identified, counted and analysed in 3D image reconstructions if pS129 immunofluorescence appeared within or partially within TH+ neuronal somata in scanned images. Similarly, aggregate-like structures labelled by AT8 immunofluorescence were identified and further analysed in 3D images if they appeared within or partially within TH+ neuronal somata in scanned images (Fig. 3.2). Morphologically diverse neuronal structures were labelled with pS129 and AT8 immunofluorescence (Fig. 3.1 and 3.2).

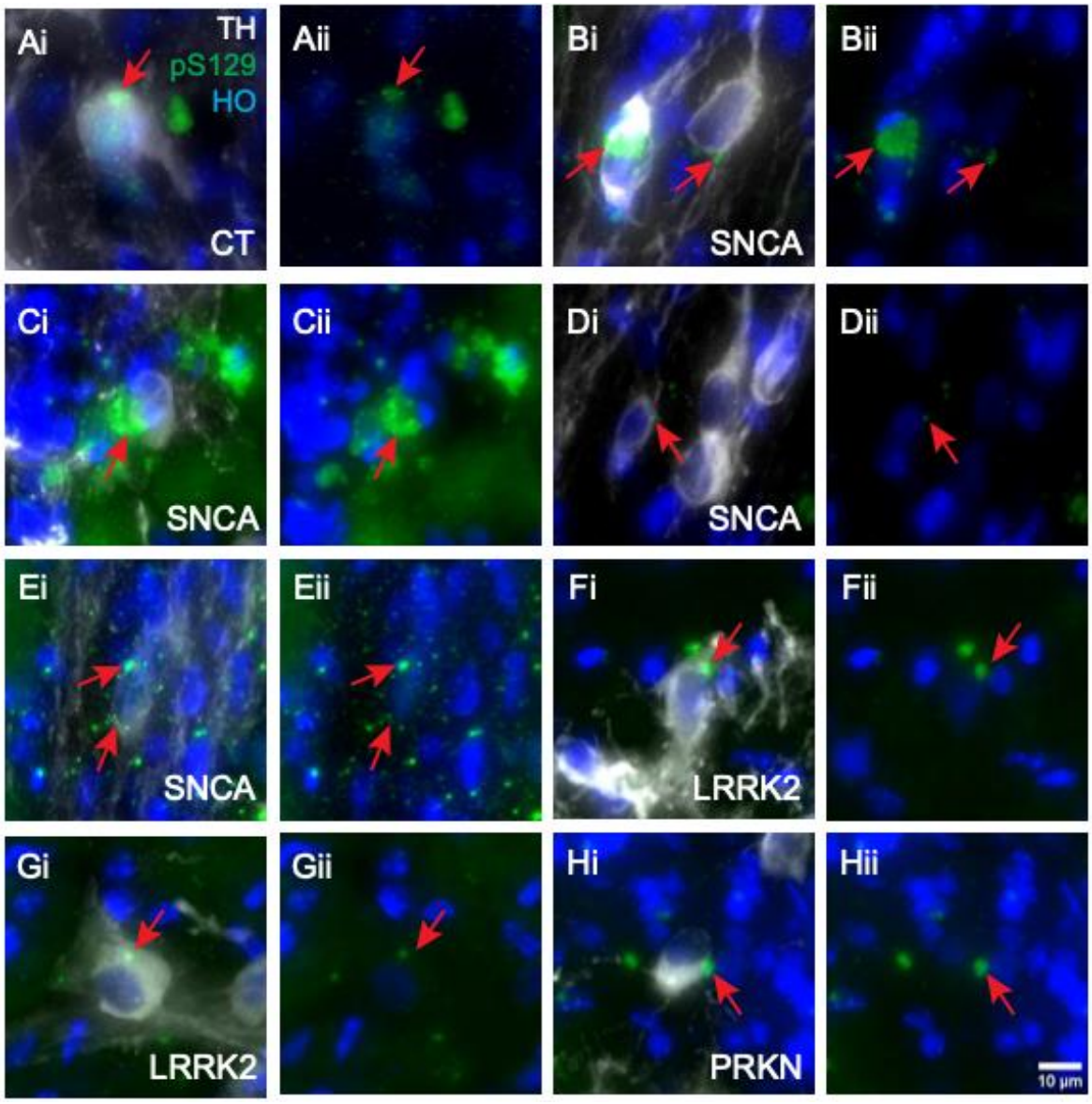


**Figure 3.1 Phospho-α-syn at S129 (pS129) aggregate-like structures apparent in TH+ neurons in control (CT) and *SNCA*, *LRRK2* and *PRKN* mutation iPSC-derived VM graft transplants.** Scanned images illustrating the various aggregate-like structures labelled by pS129 immunofluorescence (red arrows, Ai-Hii) apparent in TH+ neurons in iPSC-derived VM grafts. Immunofluorescent images revealed tyrosine hydroxylase (TH), white; pS129, green; Hoechst (HO), blue. (i) merged images. (ii) only pS129 and Hoechst images. Scale bar (10µm) in Hii applies to all panels.

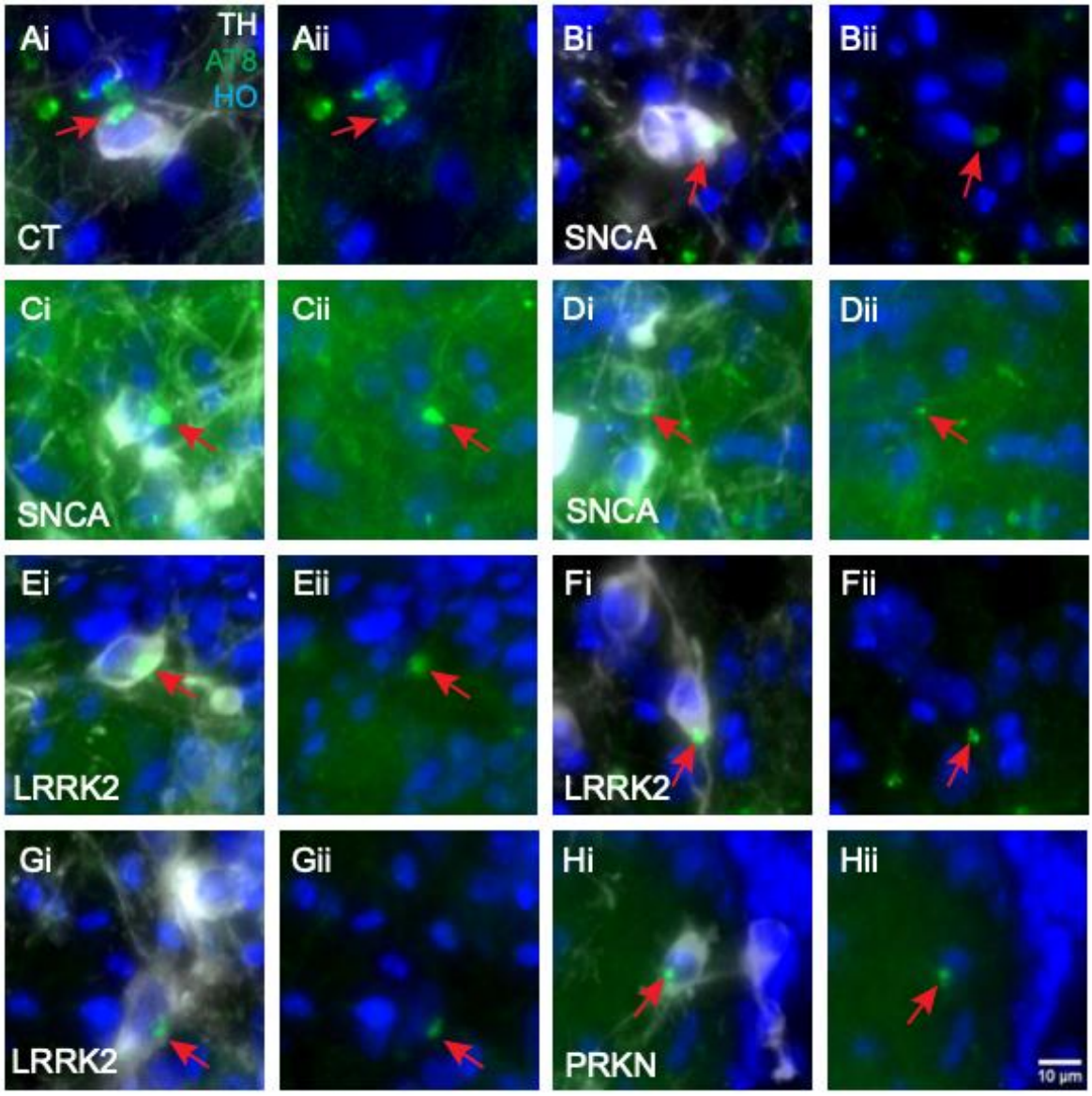


**Figure 3.2 Phospho-tau (AT8) aggregate-like structures apparent in TH+ neurons in control (CT) and *SNCA, LRRK2* and *PRKN* mutation iPSC-derived VM graft transplants.** Scanned images illustrating the various aggregate-like structures labelled by AT8 immunofluorescence (red arrows, Ai-Hii) apparent in TH+ neurons in iPSC-derived VM grafts. Immunofluorescent images revealed tyrosine hydroxylase (TH), white; AT8, green; Hoechst (HO), blue. (i) merged images. (ii) only AT8 and Hoechst images. Scale bar (10µm) in Hii applies to all panels.

### 3.3.4 Imaging and analyses

For qualitative and quantitative analyses of iPSC-derived VM neuronal transplants, images of whole brain sections and higher magnification images of graft cells were captured using the Olympus VS200 slide scanner and on the Nikon C2 confocal microscope. For qualitative analyses of iPSC-derived VM graft transplants, images were captured at multiple magnifications on the confocal microscope. A 10x overview image of the graft was captured,

followed by regions of interest (ROIs) at multiple magnifications (60x-120x) to capture cell morphology and any potential pathologies. Z-stacks at 120x (step size= 0.3µm) were also performed followed by Huygens deconvolution using Huygens Professional version 23.04 (Scientific Volume Imaging, The Netherlands, http://svi.nl) for qualitative analyses. Parameters including laser, gain and offset were selected based on single channel labelling for the graft of each section. For both qualitative and quantitative analyses of iPSC-derived VM graft transplants, images were captured at 20x magnification with a z-range and z-spacing of 12µm and 1.5µm, respectively, and at 60x at one z-plane on the slide scanner.

For image analysis, FIJI, v. 2.9.0/1.53t (367), and QuPath, v. 0.5.0 (366), software were used. For quantitation, QuPath was used. Briefly, the polygon annotation tool was used to contour the graft based on pan α-syn and pS129 staining together with the outline observed from the mobile images captured prior to staining. The graft contour provided the area ($\mu m^2$) of the graft and was then used to detect total cell number, TH+ cell number and intensity data. The cell detection tool was used to identify the total cell number using the Hoechst channel in the graft annotation created. Firstly, a small region was annotated close to the graft contour to test the accuracy of the cell detection parameters. This was performed in different areas to account for different nuclei intensities and morphologies. Once the parameters (nucleus parameters including sigma, minimum and maximum area, intensity, and cell expansion) used resulted in a count which was within 10% of a manual count, these parameters were then applied to the graft annotation for cell detection. TH+ cells were manually counted using the points tool. Pathological data was acquired in a similar manner by manually counting TH+ neurons with pS129 immunofluorescence (see definition above) by toggling off individual channels together with the counted "TH+ cells point annotation". Intensity data was extracted from the graft contour by using the "add intensity features" function or thresholds were created using different intensity parameters, to generate masks within the graft annotation. The first mask of the TH+ area fraction included all TH immunoreactivity within the graft and the second mask utilized a much higher intensity to identify mainly the TH+ cells and major processes or projections. The intensity threshold was guided by the detection measurements provided for the Cell: TH mean and standard deviation. The detection of mean intensities of other channels within the TH+ masks was determined by adding intensity features to the masks.

After identifying all TH+ neurons in the graft, the following parameters were calculated - TH+ cell proportion, density, projections and cell size. TH+ neurons with apparent pS129 immunofluorescence in the graft from scanned images were assessed at higher magnification and few were found to have intracellular pathological inclusions. Therefore, the percentage of TH+ neurons with pS129 labelling was not calculated. Non-parametric statistics were performed using Kruskal-Wallis tests and post-hoc Dunn's multiple comparisons tests (Prism 10 (v.10.0.0)) to identify any differences in the above parameters between control, *SNCA*, *LRRK2* and *PRKN* mutation groups with $p < 0.05$ as the level of significance.

## 3.4 Results

### 3.4.1 Characterization of transplanted human iPSC-derived dopaminergic neurons by genotype

To determine whether there were any differences in TH+ neuronal growth in the iPSC-derived VM grafts between mutation groups relative to controls, the TH+ neuronal cell morphology, proportion, density and the size of cell bodies and projections in the grafts was analysed.

TH+ neurons showed variable distribution patterns across genotypes, most commonly seen distributed throughout the graft or along the periphery of the graft (Fig. 3.3A). Occasionally, a dense group of TH+ neurons were seen in the core of the graft in some of the mutation graft transplants (e.g. Fig. 3.3A SNCA 1 and PRKN 2). TH+ neurons had heterogenous morphology in the grafts of the same genotype as well as across groups (Fig. 3.3B). Additionally, some TH+ neurons in mutation lines appeared ill-defined and more clustered together (e.g. Fig. 3.3B SNCA 1 and 2 and LRRK2 2).

Although TH+ neuronal morphology and distribution throughout the grafts was variable, there were no genotype differences in the proportion or density of TH+ neurons in the grafts (Fig. 3.3A, 3.4A, B). However, while all groups showed variability in cell size and the length or thickness of projections (Fig. 3.3B and C, 3.4C), TH+ neurons and projections from the *PRKN* mutation group were smaller compared to the other groups, particularly the *LRRK2* mutation group and controls (Fig. 3.4C).

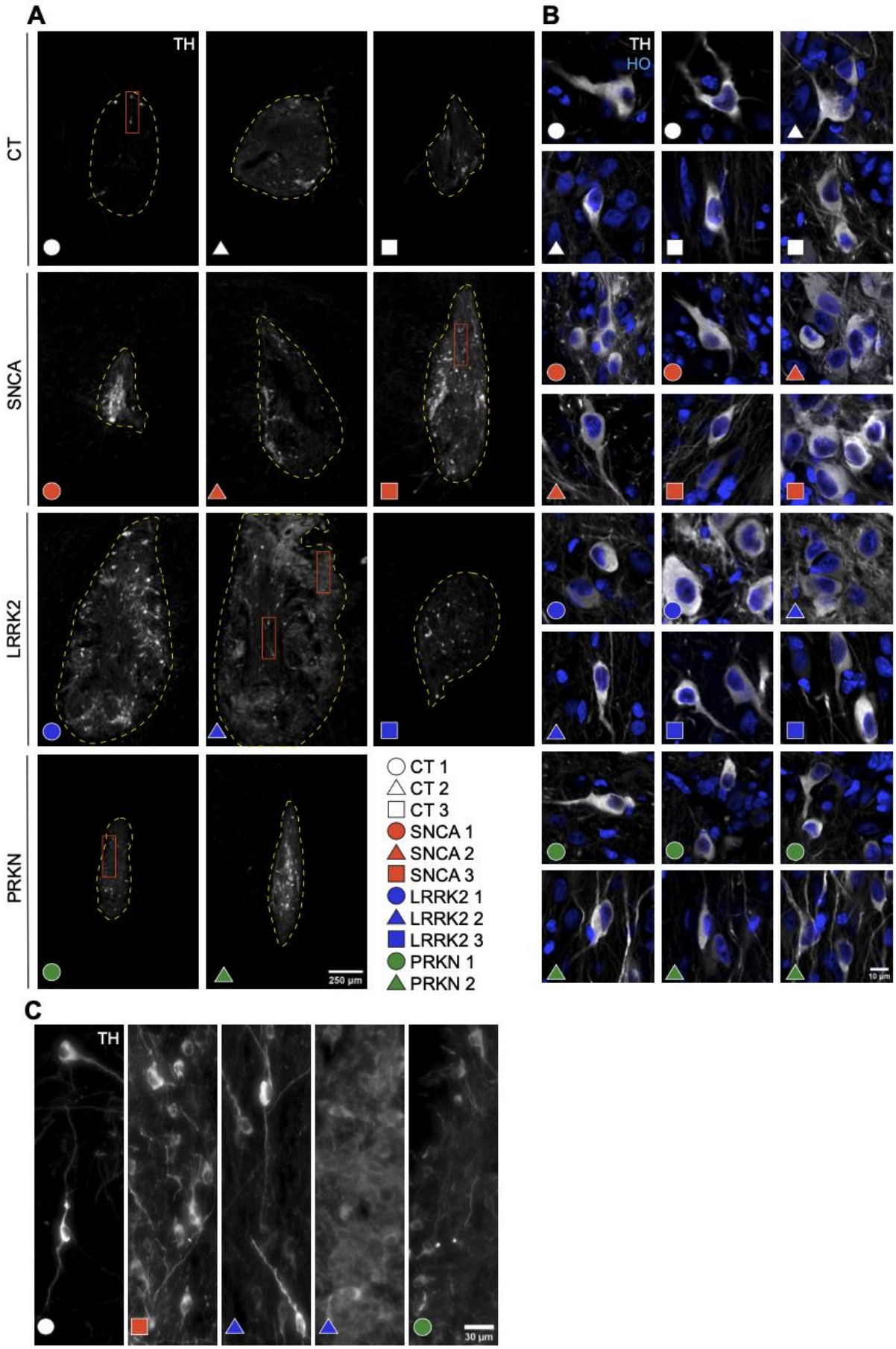
A
B
C
TH
HO
CT
SNCA
LRRK2
PRKN
CT 1
CT 2
CT 3
SNCA 1
SNCA 2
SNCA 3
LRRK2 1
LRRK2 2
LRRK2 3
PRKN 1
PRKN 2
250 µm
10 µm
30 µm

**Figure 3.3 The distribution, density and morphological features of TH+ neurons in control (CT) and *SNCA*, *LRRK2* and *PRKN* mutation iPSC-derived VM graft transplants.** Scanned images illustrating the distribution and density of TH+ neurons (A) and their projections (C; insets in A) in iPSC-derived VM grafts (outlined in dashed yellow line) from controls and mutation cell lines. Confocal images showing variable TH+ neuronal morphology and major projections (B) based on TH immunofluorescence (TH, white; Hoechst (HO), blue). Scale bar = 250µm in A, 10µm in B and 30µm in C.

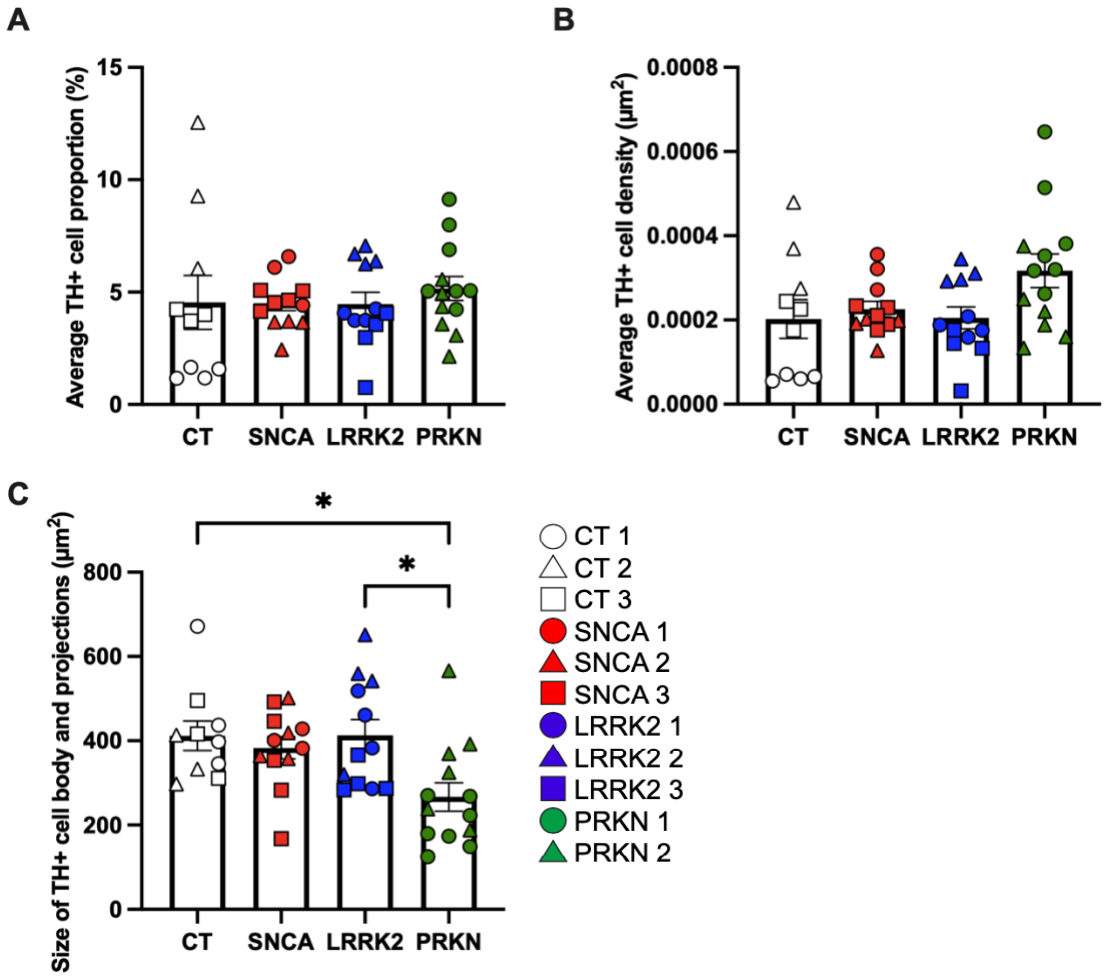


**Figure 3.4 Quantitation of TH+ neuronal cells, projections and cell size in control (CT) and *SNCA*, *LRRK2* and *PRKN* mutation iPSC-derived VM graft transplants.** Bar graphs showing the proportion (A), density (B), projections and cell size (C) of TH+ neurons in VM grafts from control and mutation cell lines. Data represent the mean ± SEM**.** Significance is taken at *p < 0.05.

### 3.4.2 Characterization of the expression and phosphorylation of α-syn and tau in transplanted human iPSC-derived dopaminergic neurons by genotype

The intensities of α-syn and tau were measured in TH+ cell masks within the grafts. Pan-α-syn expression appeared punctate throughout the graft and was either punctate or evenly distributed in TH+ cells (Fig. 3.5A-D). pS129 expression was weaker in the grafts and in TH+ cells, except for in aggregate-like structures observed within and outside of TH+ cells (Fig. 3.5A-D). Pan-tau expression was granular or fibrillar throughout the graft and evenly and more faintly expressed in TH+ neurons (Fig. 3.5E-H). Phospho-tau (AT8) appeared granular throughout the graft and in TH+ cells and was expressed more strongly in aggregate-like structures (Fig. 3.5E-H).

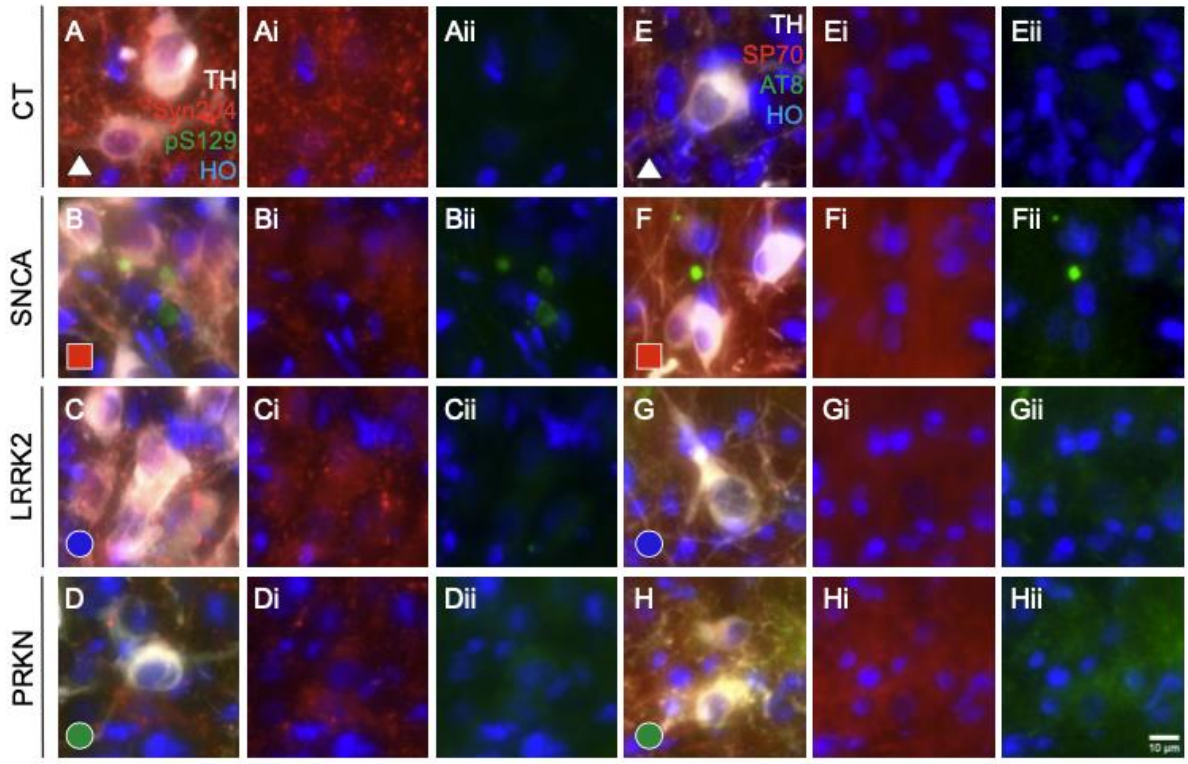


**Figure 3.5 α-Syn and tau expression in control (CT) and *SNCA, LRRK2* and *PRKN* mutation iPSC-derived TH+ neurons in VM transplants.** Scanned images illustrating the expression of pan α-syn (Syn204) (Ai-Di, second column), phospho-α-syn at S129 (pS129) (Aii-Dii, third column), pan-tau (SP70) (Ei-Hi, fifth column) and phospho-tau (AT8) (Eii-Hii, last column) in iPSC-derived VM graft TH+ cells from control and mutation cell lines. TH, white; Syn204 and SP70, red; pS129 and AT8, green; Hoechst (HO), blue. Images A-D show α -syn expression and E-H show tau expression where first column and fourth columns show merged images. (i) show only Syn204 or SP70 with Hoechst. (ii) show only pS129 or AT8 and Hoechst. Scale bar (10μm) in Hii applies to all panels. Legend used in Fig. 3.3 and 3.4 applies to Fig. 3.5.

While all groups revealed similar α-syn expression levels in the graft masked TH+ neurons (Fig. 3.5A-D and 3.6A), the *LRRK2* mutation group revealed an increase in α-syn expression compared to the other groups (Fig. 3.6A). Contrastingly, pS129 expression was reduced in masked TH+ neurons of the *LRRK2* mutation group compared to the other groups, although all groups had low pS129 levels (Fig. 3.6B). The *SNCA* mutation group showed increased pS129 expression compared to the other groups (Fig. 3.6B), although this was not statistically significant due to cell line variability. Similarly to α-syn, tau and phospho-tau (AT8) expression levels in the masked TH+ neurons were similar between groups (Fig. 3.5E-H, 3.6C and D).

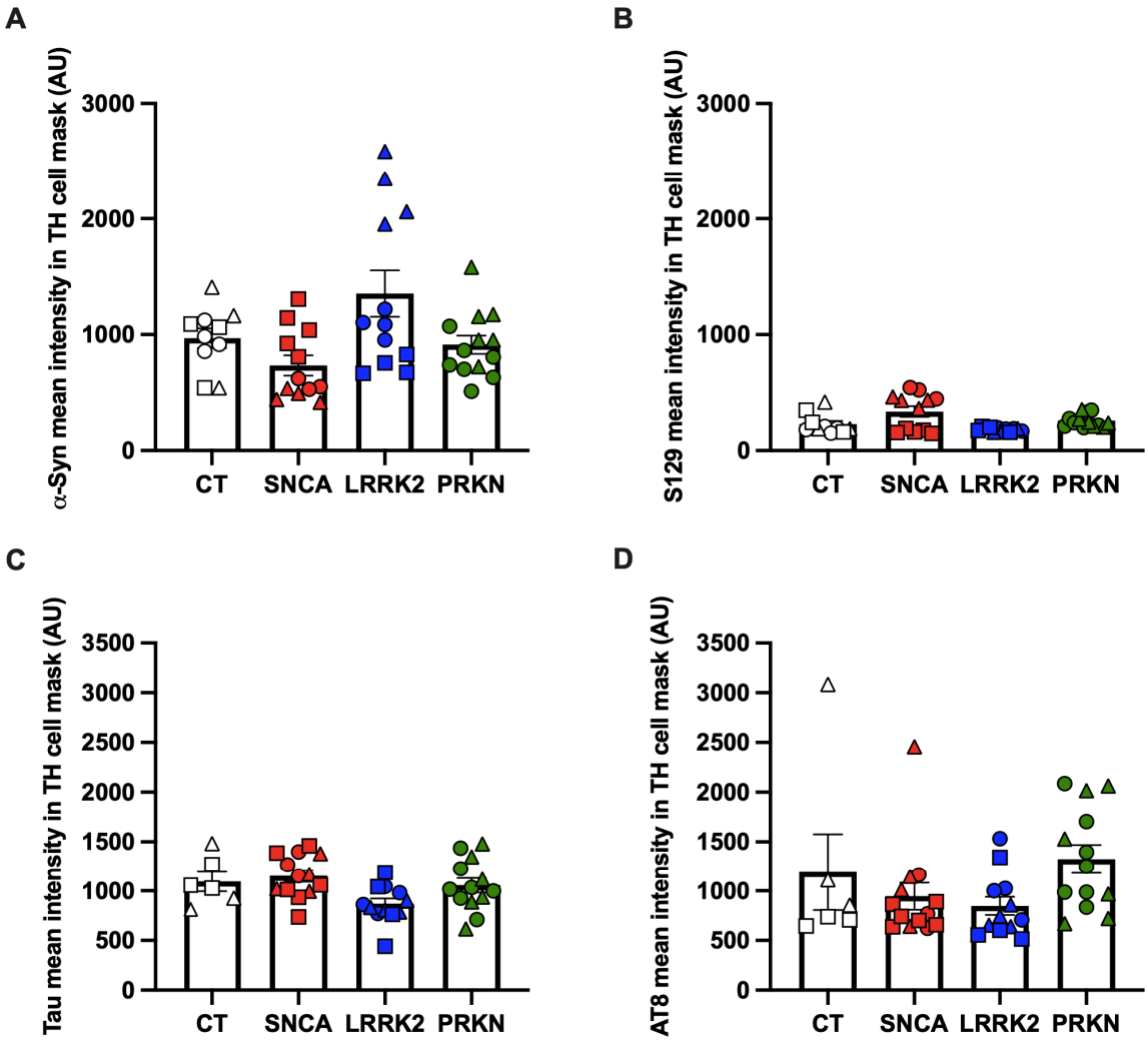


**Figure 3.6 Quantitation of α-syn and tau mean intensities in control (CT) and *SNCA, LRRK2* and *PRKN* mutation iPSC-derived TH cell masks in VM transplants.** Bar graphs showing the mean fluorescence intensities of pan α-syn (A), phospho-α-syn at S129 (S129) (B), pan tau (C) and phospho-tau (AT8) (D) in TH

cell masks in VM grafts from control and mutation cell lines. Data represent the mean ± SEM**.** Legend used in Fig. 3.3 and 3.4 applies to Fig. 3.6.

### 3.4.3 Characterization of protein pathologies in transplanted human iPSC-derived dopaminergic neurons by genotype

As discussed in the previous chapter, α-syn and AT8 identified LB structures in cortical and nigral neurons of sporadic and *SNCA* mutation PD cases. We sought to examine these pathological protein markers in grafted *SNCA*, *LRRK2* and *PRKN* mutation iPSC-derived TH+ neurons. 3D image deconvolution and reconstruction, identified both pS129 and AT8-labelled aggregate-like structures in grafts (Fig. 3.7 and 3.8). pS129-labelled structures were typically observed extracellularly surrounding or only partially inside graft TH+ neurons (Fig. 3.7A-D) suggesting an absence of LB-like pathology within the grafted TH+ neurons. While some pS129-labelled structures were more clearly outside the TH+ neurons in 3D images (Fig. 3.7A, C (red arrows) and D), others were less clear in their localization (Fig. 3.7B and C (yellow arrows)). Some pS129 aggregate-like structures appeared to be partially within or invaginated into the TH+ neurons (Fig. 3.7B and C (yellow arrows)) at sites with less TH immunopositivity. This could suggest that these inclusions displaced the normal neuronal cytoplasm, but alternatively it could indicate that these aggregate-like structures were not within the TH neuronal cytoplasm.

Similarly, AT8-labelled structures were also seen extracellularly to TH+ neurons (Fig. 3.7E) while others appeared to be partially inside the TH+ neurons (Fig. 3.7F and H) or on the edge of the cell body (Fig. 3.7G). Weak TH immunopositivity (e.g. Fig. 3.7F) appeared reduced upon deconvolution, although AT8-labelled structures were associated with the nucleus of TH+ neurons and are likely partially inside these neurons. Another AT8 aggregate-like structure in Fig. 3.7H also appeared partially inside the TH+ neurons but with little to no TH immunopositivity where the structure is localised to. This aggregate-like structure (Fig. 3.7H) appeared hollow where the weakest AT8 signal was nearest to the TH neurons (compare Fig. 3.7E-H). These structures are unlike the LBs observed in the previous chapter.

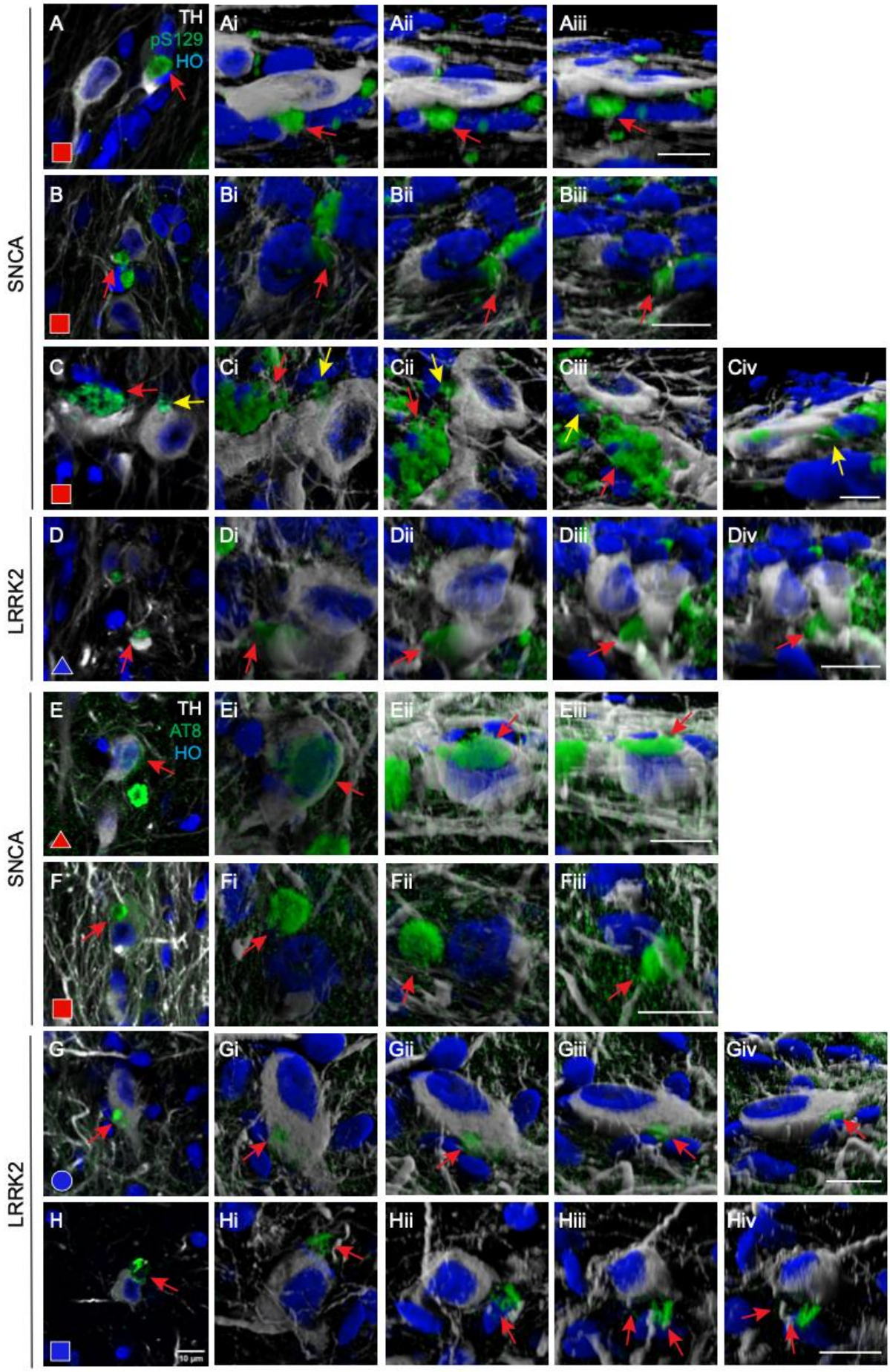
SNCA
LRRK2
SNCA
LRRK2
A
TH
pS129
HO
Ai
Aii
Aiii
B
Bi
Bii
Biii
C
Ci
Cii
Ciii
Civ
D
Di
Dii
Diii
Div
E
TH
AT8
HO
Ei
Eii
Eiii
F
Fi
Fii
Fiii
G
Gi
Gii
Giii
Giv
H
Hi
Hii
Hiii
Hiv
10 µm

**Figure 3.7 3D deconvoluted image reconstructions of aggregate-like structures in *SNCA* and *LRRK2* mutation iPSC-derived TH+ neurons in VM transplants.** 2D confocal images (first column) and their corresponding 3D deconvoluted image reconstructions (second to fourth column) illustrating the phospho-α-syn at S129 (pS129) (red and yellow arrows, A-D) and phospho-tau (AT8) (red arrows, E-H) aggregate-like structures apparent in iPSC-derived VM graft TH+ neurons from mutation cell lines. The various structures labelled by pS129 and AT8 could be viewed at different angles in the 3D reconstructions (second to fourth column). Different coloured arrows were used in C to differentiate 2 different aggregate-like structures in the 2D confocal image (first column) and in the 3D reconstruction (Ci-Civ). TH, white; pS129 and AT8, green; Hoechst (HO), blue. The scale bar (10µm) in H applies to all panels in the first column and the scale bars (10µm) in Aiii, Biii, Civ, Div, Eiii, Fiii, Giv and Hiv apply to panels Ai-Aiii, Bi-Biii, Ci-Civ, Di-Div, Ei-Eiii, Fi-Fiii, Gi-Giv and Hi-Hiv respectively. Legend used in Fig. 3 and 4 applies to Fig. 7.

As can be seen in 2D scanner and confocal images, pS129 and AT8 immunofluorescence labelled variable aggregate-like structures ranging from small granule-like aggregates (Fig. 3.8A), similar to that seen previously (414), to larger structures which appeared to be inside or on the edge of TH+ neurons in both control and mutation groups (Fig. 3.8). As both 2D scanner (Fig. 3.8A) and higher magnification confocal images (Fig. 3.8B) did not conclusively show aggregate-like structures to be localised within TH+ cell bodies, these structures were then analysed in 3D images. As mentioned above, 3D imaging provided more insights into the localisation of these structures and showed that few of these structures were definitively localised in TH+ neuronal cell bodies, suggesting an absence of LBs or potentially highlighting an earlier stage of PD pathogenesis of Lewy neurite formation, as shown with live cell imaging in cell cultures (360).

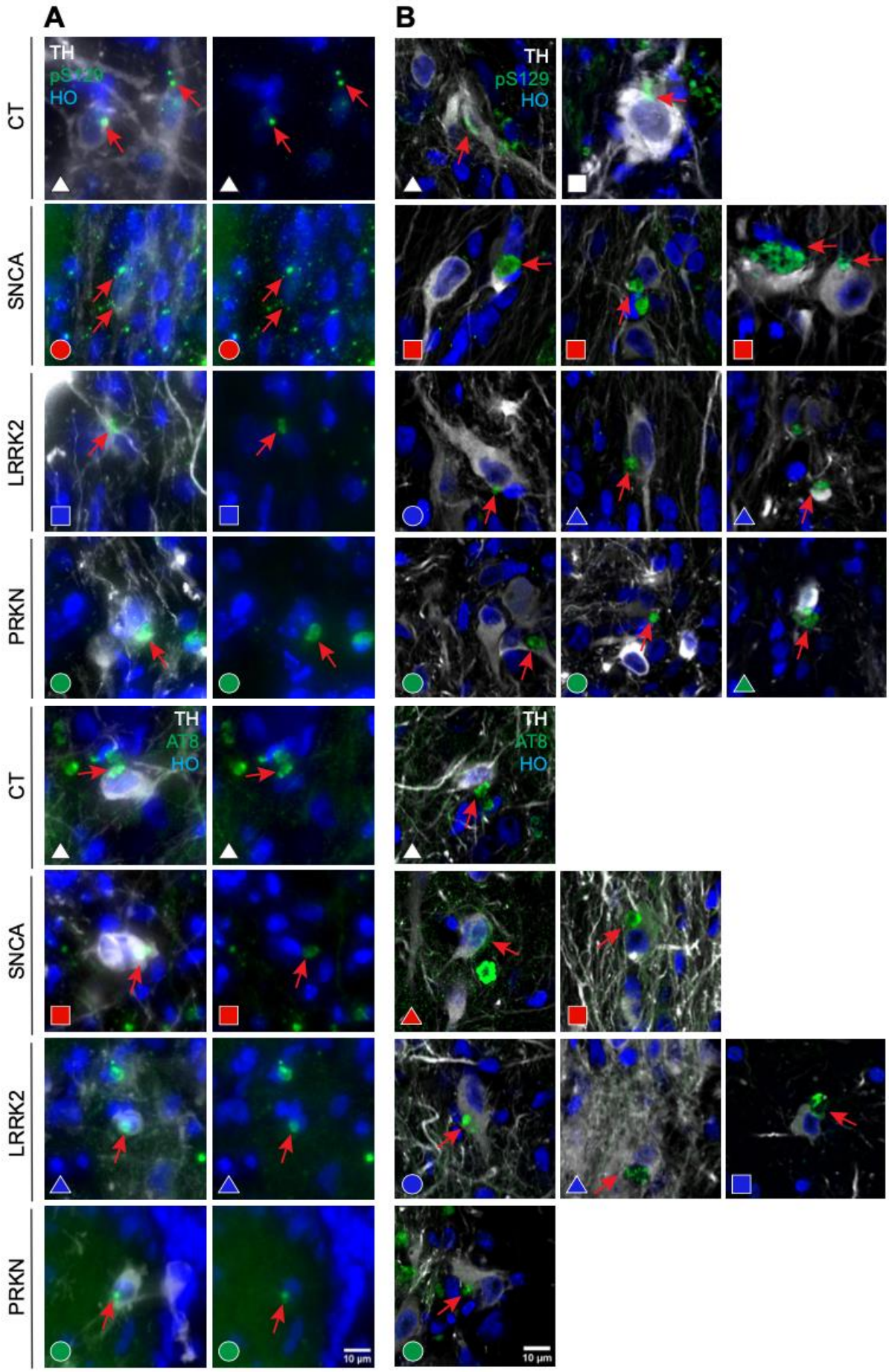


**Figure 3.8 Phospho- α-syn and tau aggregate-like structures in control (CT) and *SNCA*, *LRRK2* and *PRKN***

**mutation iPSC-derived TH+ neurons in VM transplants.** Scanned (A) and confocal (B) images illustrating the phospho-α-syn at S129 (pS129) (red arrows, A and B) and phospho-tau (AT8) (red arrows, A and B) aggregate-like structures in iPSC-derived VM graft TH+ neurons from controls and mutation cell lines. In A the first image is merged (TH, white; pS129 and AT8, green; Hoechst (HO), blue) and the second image (second column) shows only pS129/AT8 and Hoechst. Scale bar (10μm) in the last panel of A and B applies to all panels in A and B respectively. Legend used in Fig. 3.3 and 3.4 applies to Fig. 3.8.

## 3.5 Discussion

Neuropathological comparisons in patients with different causal PD genes are limited and assess mainly end-stage pathologies influenced by diverse individual environmental and aging factors (see previous chapter of *SNCA* mutation cases), rather than identifying the earliest pathological changes caused by these mutations. These limitations can be overcome by comparing early pathological changes in human neurons with different gene mutations in cell cultures, although these neurons are not fully functional and do not interact with the variety of brain cells required for full functionality. To determine early pathology in human neurons with different causal PD genes, a chimeric mouse model was used in this chapter which allowed the differentiation of human iPSC-derived midbrain neurons from PD patients with different mutations (*SNCA*, *LRRK2* and *PRKN*) to mature in the environment of a living brain. This standardized paradigm allowed direct comparisons of early pathologic changes in these cell lines, providing unique insights into PD inclusion formation. In the iPSC-derived transplants matured to 6 months for the current study, 1) morphologically heterogenous populations of TH+ neurons of similar proportions and density were identified, 2) smaller TH+ neurons occurred in the *PRKN* mutation group compared with the other groups, 3) similar levels of pan α-syn and pan tau in grafted TH+ neurons between groups were found, and 4) variable pS129 and AT8+ aggregate-like structures occurred in the grafts of all groups that only partially occurred inside the TH+ neurons.

Morphologically diverse TH+ neurons were identified within the same graft and across groups and did not differ in their proportion or density of TH+ neurons between groups. This suggests that neuronal growth is similar between the human iPSC-derived dopaminergic neurons of different genotypes and that these PD-related mutations do not impact on the development of these neurons. This is similar to studies assessing *SNCA* A53T and triplication as well as *LRRK2* G2019S iPSC-derived neurons that when transplanted into mice survived and differentiated (412-414). While similar experimental studies have not been performed for

*PRKN* mutations, the data presented suggests that human iPSC-derived dopaminergic neurons with this genotype also do not display significant developmental difficulties.

While human iPSC-derived dopaminergic neurons from all genotypes developed and matured in the mouse brain, those with *PRKN* loss of function mutations were smaller. This indicates a delayed maturation in the *PRKN* iPSC-derived dopaminergic neurons compared with other causal PD mutations. This is in line with *in vitro* studies (421, 422) that have shown that iPSC-derived dopaminergic neurons from *PRKN* mutation patients demonstrate reduced maturation, neurite length and complexity. Further, *PRKN* iPSC-derived dopaminergic neurons have smaller and less functional mitochondria and less mitochondrial contact with endoplasmic reticulum that impacts mitochondrial $Ca^{2+}$ flux compared with iPSC-derived non-dopaminergic neurons (423, 424). These differences may account for the maturation difficulty of the *PRKN* iPSC-derived dopaminergic neurons observed in the present study. Importantly, the impact of *PRKN* mutations does not seem to be confined to dopaminergic neurons as reduced astrocytes are also observed in *PRKN* iPSC-derived midbrain organoids (425) suggesting that *PRKN* mutations also impact on midbrain astrocytes which may also impede the maturation of dopaminergic neurons.

While other studies have noted enhanced pan α-syn expression in mutant PD iPSC-derived grafts (412, 413), pan tau expression has not been quantitatively evaluated. In the present study pan α-syn and pan tau expression levels in mutant PD iPSC-derived graft TH+ cell masks were similar compared to control. While a previous study found significantly more pan α-syn in *SNCA* A53T iPSC-derived grafts, this finding was a general α-syn increase which was mainly in synapses and was not masked for TH (412). Further, the *SNCA* A53T iPSC-derived grafts were found to integrate less into the host brain at 12 weeks compared with control grafts (412), suggesting that the comparative increase in synapses within the *SNCA* A53T iPSC-derived grafts may have been due to the local confinement of projections to the graft. The data presented in this thesis shows no increase in pan α-syn levels in *SNCA* A53T iPSC-derived TH+ structures within the grafts. There was also no increase in pan tau levels. Also, *LRRK2* and *PRKN* iPSC-derived TH+ neurons had no increases in pan α-syn or pan tau levels. This data suggests that these PD genes do not predispose iPSC-derived TH+ neurons matured to 6 months to develop early indications of increased substrate for inclusion formation.

Variable pS129 and AT8-labelled aggregate-like structures were observed in the grafts of all groups. In a previous study (414), pS129-labelled granular aggregates were observed in *SNCA* triplication iPSC-derived TH+ neurons 6 months post-transplantation, some of which were in weak TH+ cells consistent with TH down-regulation. A recent study assessing *SNCA* triplication and knockout iPSC-derived dopaminergic neurons also showed reduced TH neuronal expression (426), and other models (427, 428) have revealed that dopaminergic neurons with aggregated α-syn or increased α-syn expression show reduced TH immunoreactivity and gene expression. Reduced TH expression with increased α-syn expression is a known characteristic of vulnerable neurons in PD (429). In the present study, some pS129-labelled structures appeared similar to these granular aggregates (414), however they varied in size and shape significantly. Moreover, their localisation in TH+ neurons could not be ascertained in 2D images and while 3D deconvoluted images provided some clarity, some aggregate-like structures remained ambiguous in their localisation to TH+ neurons, and none were conclusively or completely intracellular. Some TH+ neurons appeared to have pS129 or AT8-labelled structures partially inside or invaginated in the cell but in these cases the TH signal of the cell was weak overall or the area where the structure was partially inside the cell had weak TH signal, as seen previously (414). Together these data suggest that TH may be down-regulated in dopaminergic neurons with these aggregate-like structures.

The localization of some of the aggregate-like structures that appear partially inside or invaginated on the edge and protruding from TH+ cells bodies may also suggest a stage of LB development consistent with an initiating neuritic pathology within cellular processes. Both human sections (430) and cell models (360) have identified neuritic pathology as often initiating early aggregations observed in neurons, and phospho-tau is increased during brain development corresponding to the period of neurite outgrowth (431, 432). This data suggests that the aggregate-like structures observed in the grafts of all genotypes may be related to the upregulation of these proteins in neuritic structures. Tau is a cytoskeletal protein belonging to the family of microtubule-associated proteins enriched in axons similar to neurofilament which it has been shown to interact with (433). Some of the AT8-labelled aggregate-like structures identified appeared hollow with AT8 mainly labelling the surface of the structure surrounding a hollow core. It has been reported that LBs and LN are composed of concentric layers where α-syn localises to the core encapsulated by neurofilament expression (430, 434) suggesting that AT8 may concentrate on the periphery of these abnormal structures. The type and location

of these structures and previous studies showing that neurites precede LB formation (25, 30, 430, 434, 435) support the concept that some of these structures represent early neuritic pathology observed in all genotypes. This may suggest that such early pathology does not predispose to full mature LB formation at this development age.

The employment of iPSC technology has become increasingly prevalent to model PD, and xenotransplantation has provided a platform to study PD-derived iPSCs *in vivo* allowing enhanced maturation of neurons compared to *in vitro*. Using a chimeric mouse model provides the opportunity to more closely model PD in a more comparable environment as opposed to maintaining cells in culture dishes. However, the microenvironment remains a limitation of the model as it does not completely represent the PD brain, particularly regarding inflammatory mechanisms. Further, as the aggregate-like structures observed in this study did not recapitulate LB features, this model remains limited by time. While challenging, longer term studies exceeding the 6-month post-transplantation timepoint are needed to clarify whether these aggregate-like structures are initiating pathologies that develop into mature LBs.

Neuropathological studies comparing different PD-related mutations remain largely elusive and such studies cannot assess the earliest pathologies that occur but rather report on end-stage pathologies of variable durations. Despite the limitations, this is the first study to compare protein pathologies across *SNCA*, *LRRK2* and *PRKN* mutations using a standardized model of human iPSC-derived dopaminergic neuronal transplants. This study showed limited pathologic protein changes in the iPSC-derived dopaminergic neuronal grafts with no differences observed across genotypes. While dopaminergic neuronal cell bodies and projections were smaller in the *PRKN* mutation group suggesting impeded maturation in this group, they grew similarly overall in grafts and expressed similar levels of α-syn and tau. Morphologically diverse aggregate-like pS129 and AT8-labelled structures were identified in the grafts of all genotypes, however none were conclusively or entirely within the grafted dopaminergic neurons, due to reduced TH expression in cells with these aggregates. Most of these structures did not recapitulate the LB features identified in chapter 2 and thus appear to be related more to developmental aspects or other earlier neuritic changes known to precede LB inclusion formation. Future studies are needed to further assess these aggregate-like structures with other LB markers such as p62 and ubiquitin and to elucidate the temporal changes of their formation.

# CHAPTER 4: Brain pathology in a mature animal model with *PRKN* deletion

## 4.1 Abstract

Aim: To investigate the effect of parkin loss on mitochondrial quality control and neuroinflammation in post-mortem *PRKN* knockout (KO) mouse brain tissue.
Methods: Cerebral cortex and midbrain tissue from 6 and 12-month-old wild-type (WT) (n=27) and *PRKN* KO (n=32) mice was assessed using Western blot analyses and multiplex free-floating immunofluorescence. Western blot analyses were performed on cortex and midbrain total proteins and cortex mitochondrial fractions to assess mitochondrial and glial protein expression. Multiplex immunofluorescence was performed on cortex and midbrain sections to compare mitochondrial expression in specific cell types using confocal imaging. Non-parametric statistics were used to determine differences in protein expression between WT and *PRKN* KO mice. Parkin was not detected in the *PRKN* KO mice.
Results: There were no differences in the expression of neuronal markers between WT and *PRKN* KO mice. α-Synuclein (pan and phosphorylated-α-syn) levels were also similar between genotypes. Parkin loss altered the expression of some mitochondrial proteins such as GRP75 which was decreased by 19.5% in the midbrain compared to the cortex and TOMM20 levels which were increased by 51.7% in cortical mitochondrial fractions in *PRKN* KO mice relative to WT. No differences were found in GRP75 protein levels between WT and *PRKN* KO neurons or microglia in the cortex or substantia nigra (SN). Microglial morphology, number and somal size were also similar between *PRKN* KO and WT mice in the cortex and SN.
Conclusion: Parkin loss alters the expression of mitochondrial proteins GRP75 and TOMM20, while there are similar neuronal, pathological and glial protein levels between WT and *PRKN* KO mice. GRP75 protein levels were similar between genotypes in cortical and nigral neurons and microglia suggesting that the altered GRP75 levels may implicate other cell types. Cortical and nigral microglial morphology, numbers and somal area were similar between WT and *PRKN* KO mice suggesting microglia are not activated. These data suggest that parkin loss alters specific mitochondrial proteins which may be insufficient to induce a neuroinflammatory phenotype.

## 4.2 Introduction

The previous chapter explored protein pathologies in induced pluripotent stem cell (iPSC)-derived dopaminergic neuronal transplants from Parkinson's disease (PD) patients carrying *SNCA*, *LRRK2* and *PRKN* mutations. All grafts exhibited aggregate-like structures in the previous study *in vivo*, but patients with *PRKN* loss of function mutations do not have significant Lewy body (LB) inclusions in their brains at autopsy, with this form of genetic PD being considered a non-synucleinopathy form of PD (264, 266-270, 272, 273). However, they do have significant dopamine cell loss and limited neuropathology in their entire brain (264, 266-270, 272, 273). The lack of inclusion formation also occurs in animal models using *PRKN* gene deletion with these animals also not showing LB inclusions (see Table 4.1). In addition, many of the *PRKN* knockout (KO) models also have limited dopamine cell loss. This suggests that compensation and/or corrective mechanisms occur following *PRKN* deletion in mice.

**Table 4.1** Comparison of *PRKN*-knockout (KO) mouse model phenotypes

| Study | Mouse Model Strain and Mutation | Age (m) | Sex (M/F; NS) | Behavioural findings | Pathological features |
|---|---|---|---|---|---|
| Goldberg et al., 2003 (298) | C57BL/6; Exon 3 deletion | 6, 12, 18, 24 | NS | No difference in general/ exploration behaviour<br>Mild motor deficits (tests sensitive to NST dysfunction) | No α-syn or ubiquitin inclusions in any brain regions<br>Normal morphology of TH+ neurons in the SN and LC<br>No difference in the number of TH+ neurons in the SN at 12-24 m<br>↑ Extracellular striatal DA<br>No difference in levels of α-syn in whole brain |
| Itier et al., 2003 (436) | 129SV and mixed 129SV, C57BL/6; Exon 3 deletion | 2-24 | M/F | No difference in general behaviour<br>↓ Exploratory behaviour | No difference in α-syn, ubiquitin staining at 24 m<br>No difference in the number of TH+ neurons in the SN<br>No difference in TH protein levels in striatum and brainstem |
| Palacino et al., 2004 (437) | Mixed C57BL/6, 129SV and 129SV; Exon 3 deletion | 3-20 | M/F | - | ↓ Levels of proteins involved in mitochondrial respiration and oxidative stress protection in the ventral MB at 8 m<br>Impaired mitochondrial function in the striatum<br>Normal mitochondrial morphology in the striatum<br>↓ Antioxidant capacity<br>↑ Oxidative damage at 18-20 m |
| von Coelln et al., 2004 (438) | C57BL/6; Exon 7 deletion | 2-24 | M/F | No difference in general behaviour<br>No difference in balance or motor function | No difference in α-syn, GFAP or ubiquitin staining in the Cx and MB<br>No difference in DA nerve terminals in the striatum at 18 m<br>No difference in DA neuron morphology in the SN at 18 m |

| | | | | | |
|---|---|---|---|---|---|
| | | | | | ↓ Number of TH+ neurons in the LC at 2, 12-18 m (no difference in the SN)<br>No difference in DA in striatum |
| Perez and Palmiter, 2005 (439) | Mixed 129S4, SvJaeSor and C57BL/6, 129S4/SvJaeSor; Exon 2 deletion | 3-24 | M | No difference in general/ exploratory behaviour<br>No motor deficits indicative of NST dysfunction | No difference in TH, α-syn or ubiquitin staining<br>No difference in the levels of DA in the striatum at 22 m<br>Intact DA neurons in SN without pathology at 22 m |
| Periquet et al., 2005 (440) | 129SV; Exon 3 deletion | 2, 12 | NS | - | 87 proteins altered by at least 45% in the Cx and striatum<br>↑ Levels of GRP75 and VDAC1 among others in the striatum at 12 months<br>↓ Levels of GS in the striatum at 2 m<br>↑ Levels of GRP75 in the Cx at 12 m |
| Sato et al., 2006 (441) | C57BL/6J; Exon 2 deletion | 3,12 | NS | No difference in general behaviour | Normal morphology of TH+ neurons<br>No difference in the number of TH+ neurons in the SN and LC at 3 m<br>↑ Levels of DA in SN at 12 m (no difference in the striatum)<br>↓ DA synthesis and release in the striatum at 12 m |
| Stichel et al., 2007 (442) | C57BL/6 and 129SVJ; Exon 3 deletion | 3, 12-14 | NS | - | No difference in the number or morphology of TH+ neurons in the SN at 12 m<br>No apparent micro- or astrogliosis in the Cx and SN at 12 m<br>↑ Number of damaged mitochondria in DA neurons in the SN at 12-14 m<br>↓ Mitochondrial respiratory rate in the SN at 14 m |
| Schmidt et al., 2011 (443) | C57BL/6 and 129SVJ; Exon 3 deletion | 3, 12-15 | NS | - | ↑ Structurally abnormal mitochondria (disintegrated/broken cristae, enlarged, protrusions) in glial cells in the SN at 3 and 12 m<br>↑ Number of damaged mitochondria in glial cells in the SN at 3 and 12-15 m<br>↑ Mitochondrial-related proteins (not GRP75) in cultured astrocytes |
| Pickrell et al., 2015 (299) | B6.129S4-Park2tmShn/J; Exon 3 deletion | 3,12 | NS | No motor deficits indicative of NST dysfunction | No α-syn pathology<br>No difference in the number of TH+ neurons in the SN and LC at 48-52 wk<br>No difference in DA levels in the striatum at 48-52 wk<br>No difference in GFAP or IBA1 staining in Cx and striatum at 3 m |
| Noda et al., 2020 (300) | C57BL/6J; Exon 2 deletion | ~27 | M | Motor behavioural deficits at 110 weeks | No Lewy pathology at 120 wk<br>↑ Small mitochondrial accumulation in TH+ neurons in the SN at 110 wk indicating mitochondrial fragmentation<br>Small, round, and fragmented mitochondria with broken matrix and cristae in DA neurons in the SN at 110 wk<br>↑ Number of fragmented mitochondria in DA neurons in the SN at 110 wk |

| | | | | | |
|---|---|---|---|---|---|
| | | | | | ↓ Number of TH+ neurons in the center of SN at 110 wk<br>↓ Striatal DA levels at 120 wk |
| Cossu et al., 2021 (444) | C57BL/6J; Exon 2 deletion (EAE model) | 2-3 | F | No motor deficits | No significant differences in the number of astrocytes (GFAP) or microglia (IBA1) in the striatum (before immunization or at disease peak) |

α-Syn, α-synuclein; Cx, cortex; DA, dopamine; EAE, experimental autoimmune encephalomyelitis; GFAP, glial fibrillary acidic protein; GRP75, glucose-regulated protein 75; GS, glutamine synthetase; IBA1, ionized calcium binding adaptor molecule 1; LC, locus coeruleus; MB, midbrain; M/F, male/female; m, months; NS, not specified; NST, nigrostriatal; SN, substantia nigra; TH, tyrosine hydroxylase; VDAC1, voltage-dependent anion channel 1; wk, week.

As reviewed in the introductory chapter, parkin encoded by the *PRKN* gene is integral to mitochondrial quality control where it ubiquitinates cytosolic and mitochondrial proteins to flag them for degradation for efficient regulation of mitochondrial fission/fusion, biogenesis and mitophagy (250, 445). While *PRKN* KO animal models do not have a significant PD phenotype, when assessed they have mitochondrial damage (see Table 4.1 for review), a feature also seen in human *PRKN* iPSC models which have increased α-synuclein (α-syn) accumulation without aggregate formation (295-297). In addition to the parkin pathway, mitochondria clearance is also mediated by other proteins including BCL2 interacting protein 3 (BNIP3) and NIP3-like protein X (Nix) serving as mitophagy receptors (446, 447). These alternate mitochondrial clearance pathways or other ubiquitin ligases could account for the mild phenotype observed in these models. Regardless, the *PRKN* KO animals can be considered a model of the very earliest mitochondrial abnormalities detected with *PRKN* deletion. To understand additional pathology associated with early mitochondrial dysfunction with *PRKN* abnormalities, this chapter investigates the severity of mitochondrial structural and functional protein changes and any associated downstream cellular effects in a *PRKN* KO mouse model.

# 4.3 Methods

## 4.3.1 Mice and tissue processing

28–30-week-old wild-type (WT) (n=27) and *PRKN* KO (exon 3 deletion) (n=32) male and female mice were obtained from Australian Bioresources (WT) and the Jackson Laboratory (*PRKN* KO). The *PRKN* KO line was maintained by crossing male KO with female KO at

Australia, Bioresources, Moss Vale, Australia. All mice were on the C57BL/6 background and were housed and maintained under specific pathogen free conditions in the animal house facility at the Brain and Mind Centre, The University of Sydney. The mice received food and water ad libitum. Animal use in this study was ethically approved by the University of Sydney's Animal Ethics Committee (2019/1506).

Mice were euthanized at 6 (WT n=7, *PRKN* KO n=6) and 12 (WT n=20, *PRKN* KO n=26) months and perfused with 1x phosphate buffered saline (PBS). Brains were surgically extracted and either:

1) dissected into different brain regions (cortical and midbrain) and frozen at -80ºC for Western blot analyses (WT n=21, *PRKN* KO n=25),
2) halved sagitally and one side dissected and frozen at -80ºC and the other side postfixed for immunofluorescent staining (WT n=7, *PRKN* KO n=8) or
3) fixed whole for immunofluorescent staining (WT n=1).

For immunofluorescent staining, whole or half brains were fixed with 4% paraformaldehyde and transferred to a 20% sucrose solution at 4°C for a minimum of 24 hours. Brains were embedded in Tissue-Tek O.C.T. compound (Cat.# 4583, Sakura) for frozen sectioning at -12°C using the CryoStar NX50 Cryostat (ThermoFisher Scientific). 40µm thick coronal serial sections were collected into 8 vials and stored at -20°C in anti-freezing solution.

### 4.3.2 Proteins to be analysed

For mitochondrial changes, several proteins were analysed including voltage-dependent anion channel 1 (VDAC1), glucose-regulated protein 75 (GRP75), translocase of outer mitochondrial membrane protein complex subunit 20 (TOMM20) and Nix. These proteins, some of which are parkin substrates (VDAC1, TOMM20 and Nix), have been shown to be crucial for mitochondrial quality control and function (445, 448-451). VDAC1 transports metabolites and ions including calcium at the OMM and plays a key role in regulating mitophagy and apoptosis (448, 452). GRP75 is a mitochondrial stress response chaperone protein mainly localised to the mitochondrial matrix where it facilitates protein import of mitochondrial matrix proteins (453). In the mitochondrial-associated membrane, GRP75 tethers the endoplasmic reticulum (ER) to mitochondria to facilitate calcium transport by linking ER-localised inositol triphosphate receptor 3 ($IP_3R$) to VDAC1 (454, 455). TOMM20 and Nix are located on the outer

mitochondrial membrane (OMM) and are involved in protein import and mediating mitophagy, respectively (456, 457).

For potentially linked cellular changes, microglia will be identified using the ionized calcium binding adaptor molecule (IBA1) and the less commonly used stimulator of interferon genes/transmembrane protein 173 (TMEM173) for subtyping.

### 4.3.3 Protein extraction and Western blot analyses

Frozen samples were bought to room temperature and homogenised with Tungsten Carbide beads (Cat.# 69997, Qiagen) in microcentrifuge tubes by shaking vigorously in the TissueLyser II system (Qiagen) for 30 seconds, twice. The resulting liquid was removed and centrifuged at 32,000 g (20 min); the supernatant was transferred into a new tubes. Total protein was extracted using RIPA buffer (Cat.# ab156034, Abcam) and mitochondrial proteins were isolated from cortical extracts using the Mitochondria Isolation Kit for Tissue (Cat.# 89801, ThermoFisher Scientific) and prepared according to the kit's instructions. Protein concentrations were then determined using a BCA assay according to the manufacturer's instructions (Cat.# 23227, ThermoFisher Scientific).

Western blotting was then used to quantify relative protein levels. Proteins (50µg for total proteins and 15µg for mitochondrial fractions) were heated at 95ºC in loading buffer (containing β-mercaptoethanol and loading dye) for 5 minutes, then loaded onto the polyacrylamide gel (Cat.# 5678023, BioRad), run at 180V for 60 min at room temperature (RT) and transferred at 90V for 90 mins at 4°C (Cat.# 1704071, BioRad). After the completion of the transfer, the membrane was rinsed with TBST (TRIS-buffered saline with 0.1% TWEEN), then blocked with 5% skim milk in TBST for one hour to prevent non-specific binding. Each protein was incubated with the primary antibody (Table 4.2) overnight at 4°C. The next day, the membranes were washed with TBST and incubated with the corresponding secondary antibodies (Table 4.2) for an hour at RT.

**Table 4.2** List of antibodies used in Western blot

| **Primary antibodies (type, Cat.#)** | **Epitope (immunogen)** | **Dilution** | **Source** |
|---|---|---|---|
| Mitochondrial Proteins | | | |
| Parkin (PRK8) (mouse IgG2b mAb, Cat.# sc-32282) | Raised using aa. 399-465 of human parkin | 1:2000 | Santa Cruz |
| VDAC1/Porin + VDAC3 (mouse IgG2b mAb, Cat.# ab14734) | Recombinant full-length protein | 1:2000 | Abcam |
| GRP75/MOT (mouse IgG3 mAb, Cat.# ab2799) | Synthetic peptide corresponding to mouse GRP75/MOT aa. 661-679 | 1:2000 | Abcam |
| TOMM20 (rabbit pAb, Cat.# ab78547) | Synthetic peptide corresponding to human TOMM20 aa 100 to the C-terminus | 1:2000 | Abcam |
| BNIP3L/NIX (rabbit mAb, Cat.# ab109414) | Synthetic peptide corresponding to human BNIP3L/NIX C-terminus | 1:2000 | Abcam |
| Neuronal Markers | | | |
| NeuN (rabbit mAb, Cat.# ab177487) | Synthetic peptide corresponding to human NeuN N-terminus | 1:2000 | Abcam |
| Tyrosine Hydroxylase (TH) (rabbit pAb, Cat.# ab152) | Denatured tyrosine hydroxylase from rat pheochromocytoma | 1:2000 | Sigma Aldrich |
| Glial Cell Markers | | | |
| Glutamine Synthetase (GS) (mouse IgG2a mAb, Cat.# MAB302) | Glutamine synthetase purified from sheep brain | 1:2000 | Sigma Aldrich |
| IBA1 (rabbit mAb, Cat.# ab178847) | Synthetic peptide corresponding to human IBA1 N-terminus | 1:2000 | Abcam |
| STING/TMEM173 (mouse IgG2b mAb, Cat.# MAB7169) | *E. coli*-derived recombinant human STING/TMEM173 aa. 215-379 | 1:2000 | R&D Systems |
| Synapse proteins | | | |
| α-Synuclein (mouse IgG1 mAb, Cat.# 610787) | Rat synuclein-1 aa. 15-123 | 1:2000 | BD Biosciences |
| Phospho-α-synuclein at S129 (rabbit mAb, Cat.# ab51253) | Synthetic peptide aa.100-140 of human α-Syn | 1:2000 | Abcam |
| **Secondary antibodies** | **Epitope (immunogen)** | **Dilution** | **Source** |
| Donkey anti-mouse IgG (H+L), HRP, 715-035-150 | Mouse IgG heavy and light chains | 1: 10 000 | Jackson Immunoresearch |
| Donkey anti-rabbit IgG (H+L), HRP, 711-035-152 | Rabbit IgG heavy and light chains | 1: 10 000 | Jackson Immunoresearch |

Aa, amino acid; BNIP3L, BCL2 interacting protein 3 like; GRP75, glucose-regulated protein 75; IBA1, ionized calcium binding adaptor molecule 1; mAb, monoclonal antibody; NeuN, neuronal nuclei antigen; Nix, NIP3-like protein X; pAb, polyclonal antibody; STING/TMEM173, stimulator of interferon genes/transmembrane protein 173; TOMM20, translocase of outer mitochondrial membrane protein complex subunit 20; VDAC1/3, voltage-dependent anion channel 1/3.

Finally, depending on the level of intensity needed, either weak (Immobilon Forte Western HRP substrate, Cat.# WBLUF0500; Merck Millipore) or strong (SuperSignal West Atto Ultimate Sensitivity Substrate, Cat.# A38556; ThermoFisher Scientific) enhanced chemiluminescent substrate was applied to the membrane according to package instructions. The BioRad ChemiDoc system was used for imaging. The image with the highest intensity that was not oversaturated was selected for further analysis. The membranes were then

stripped by immersing them in stripping buffer for 20 minutes at RT. ImageLab software (Image Lab Software (RRID:SCR_014210)) was used to quantify protein band intensities. There is strong evidence that α-syn in PD interacts with actin, a microtubule critical for cytoskeleton formation (458). Therefore, protein level standardisation was performed using total protein levels rather than beta-actin levels, as is standard.

### 4.3.4 Immunofluorescence staining, imaging and analyses

Cortical and midbrain tissue sections were stained free floating for immunofluorescence neuronal, glial and mitochondrial markers (Table 4.3). Briefly, sections were washed in PBS for 30 minutes and then incubated in 10mM sodium citrate buffer at 85°C for 30 minutes. After cooling to RT, sections were washed in PBS and quenched using 0.1% sodium borohydride in PBS for 30 minutes. Sections were then washed in PBS and blocked with blocking buffer (containing 2% donkey serum, 1% bovine serum albumin solution, 0.2% Triton X-100, 0.1% gelatin and 0.1% Tween-20 in PBS) for 1 hour at RT. Sections were then incubated in primary antibodies (Table 4.3) in blocking buffer overnight at RT, followed by PBST washes and corresponding Alexa Fluor secondary antibodies (Table 4.3) and bisbenzimide H 33342 trihydrochloride (Hoechst, Cat.# B2261; Sigma-Aldrich) in blocking buffer for 2 hours at RT. Sections were washed again in PBST followed by PBS and then coverslipped using mounting medium (Cat.# S3023, DAKO) and sealed with CoverGrip coverslip sealant (Cat.# 23005, Biotium) or nail polish. Negative controls were included by omitting either the primary or secondary antibodies.

**Table 4.3** Free-floating immunofluorescence staining list of antibodies

| Primary antibodies (type, Cat.#) | Epitope (immunogen) | Dilution | Source | Fluorophore |
|---|---|---|---|---|
| Mitochondrial Proteins | | | | |
| GRP75/MOT (mouse IgG3 mAb, Cat.# ab2799) | Synthetic peptide corresponding to mouse GRP75/MOT aa. 661-679 | 1:200 | Abcam | 488 |
| Neuronal Markers | | | | |
| NeuN (mouse IgG2b mAb, Cat.# ab104224) | Recombinant fragment corresponding to Human NeuN aa 1-100 (N terminal) | 1:500 | Abcam | 568 |
| Tyrosine Hydroxylase (TH) (rabbit mAb, Cat.# ab137869) | Synthetic peptide corresponding to human TH | 1:400 | Abcam | 647 |
| Glial Cell Markers | | | | |
| IBA1 (mouse IgG1 mAb, Cat.# SAB2702364) | Recombinant protein encompassing a sequence within the centre region of human IBA1 | 1:200 | Sigma Aldrich | 647 |
| STING/TMEM173 (rabbit pAb, Cat.# PA5-23381) | Synthetic peptide aa. 310-360 of STING protein | 1:100 | ThermoFisher Scientific | 568 |
| **Secondary antibodies** | **Epitope (immunogen)** | **Dilution** | **Source** | |
| Goat anti-mouse IgG3-Alexa Fluor 488, A-21151 | Mouse IgG 3 | 1:400 | ThermoFisher Scientific | |
| Goat anti-mouse IgG2b-Alex Fluor 568, A-21144 | Mouse IgG 2b | 1:400 | ThermoFisher Scientific | |
| Donkey anti-rabbit IgG (H+L)- Alexa Fluor 647, A-31573 | Rabbit IgG Heavy and Light chains | 1:400 | ThermoFisher Scientific | |
| Goat anti-mouse IgG1-Alexa Fluor 647, A-21240 | Mouse IgG 1 | 1:400 | ThermoFisher Scientific | |
| Donkey anti-rabbit IgG (H+L)- Alexa Fluor 568, A-10042 | Rabbit IgG Heavy and Light chains | 1:400 | ThermoFisher Scientific | |

Aa, amino acid; GRP75, glucose-regulated protein 75; IBA1, ionized calcium binding adaptor molecule 1; mAb, monoclonal antibody; NeuN, neuronal nuclei antigen; pAb, polyclonal antibody; STING/TMEM173, stimulator of interferon genes/transmembrane protein 173.

Cortical and midbrain sections were imaged using the Nikon C2 Confocal microscope. Overview brain sections were captured at 10x magnification and then regions of interest (ROIs). For the analyses of neurons, 3-4 ROI images in cortical layers and 6-11 ROI images in the substantia nigra (SN)) were identified and captured at 80x magnification (158x158µm). For the analyses of microglia, 2 large ROI images (586x586µm) in cortical layers and 6-8 ROI images (158x158µm) in the SN were identified and captured at 80x magnification.

Neurons were identified with neuronal markers (neuronal nuclei antigen (NeuN) or tyrosine hydroxylase (TH) immunofluorescence) and were contoured using the freehand selections function to measure mean GRP75 protein cellular intensity levels using FIJI software (version 1.53q) (367). Another annotation was drawn in the GRP75 channel to measure mean background to use for correction.

Microglia were identified with microglial markers (IBA1 and TMEM173 immunofluorescence). For quantitation, 6-8 images from 2 WT and 2 *PRKN* cases were selected for training images to create object classifiers and automate the detection of IBA1+ and TMEM173+ microglia using Qupath (v 0.5.0) (366). A single stitched training image was created, and cell detection tool used in an annotated rectangle to identify the total cell number in the Hoechst channel. Once the parameters (nucleus parameters including sigma, minimum and maximum area, intensity, and cell expansion) resulted in a count which was within 10% of a manual count in the rectangle, these parameters were then applied to similar annotated rectangles in the training image for the detection of all nuclei. Using the brush or wand tool, regions or cells were then annotated and classed as "Ignore" or "IBA1+". These annotations were used to train the object classifier to detect IBA+ microglia. This process was repeated for TMEM173+ microglia. Following the creation of object classifiers for microglia types, all images were then analysed. A full image annotation was created, and Hoechst+ total cell number and IBA1+ ± TMEM173+ microglia identified and counted using object classifiers together with some manual curation. The proportion and density of IBA1+, TMEM173+ and IBA1+TMEM173+ microglia were calculated. Using the wand tool, 10 IBA1+ microglial cells per large image and 1-5 IBA1+ microglial cells per smaller image were contoured and the somal area ($\mu m^2$) and GRP75 mean intensity per cell determined.

### 4.3.5 Statistical analyses

Non-parametric statistical tests were conducted using Prism (version 10.0.0) with $p < 0.05$ as the level of significance. Kruskal-Wallis, post-hoc analyses (Dunn's multiple comparisons) and Mann-Whitney U tests were performed to compare the differences in relative protein levels and the proportion or density of glia between WT and *PRKN* KO groups.

## 4.4 Results

### 4.4.1 Core neuronal and genetic markers in the *PRKN* KO model

As expected, there was no detectable parkin in *PRKN* KO mice in the cortex and midbrain relative to WT mice (Fig. 4.1A). Further, there were no significant differences in the levels of neuronal markers, NeuN and TH, between WT and *PRKN* KO mice in the cortex and midbrain (Fig. 4.1) indicating an absence of neuronal loss as observed previously (Table 4.1).

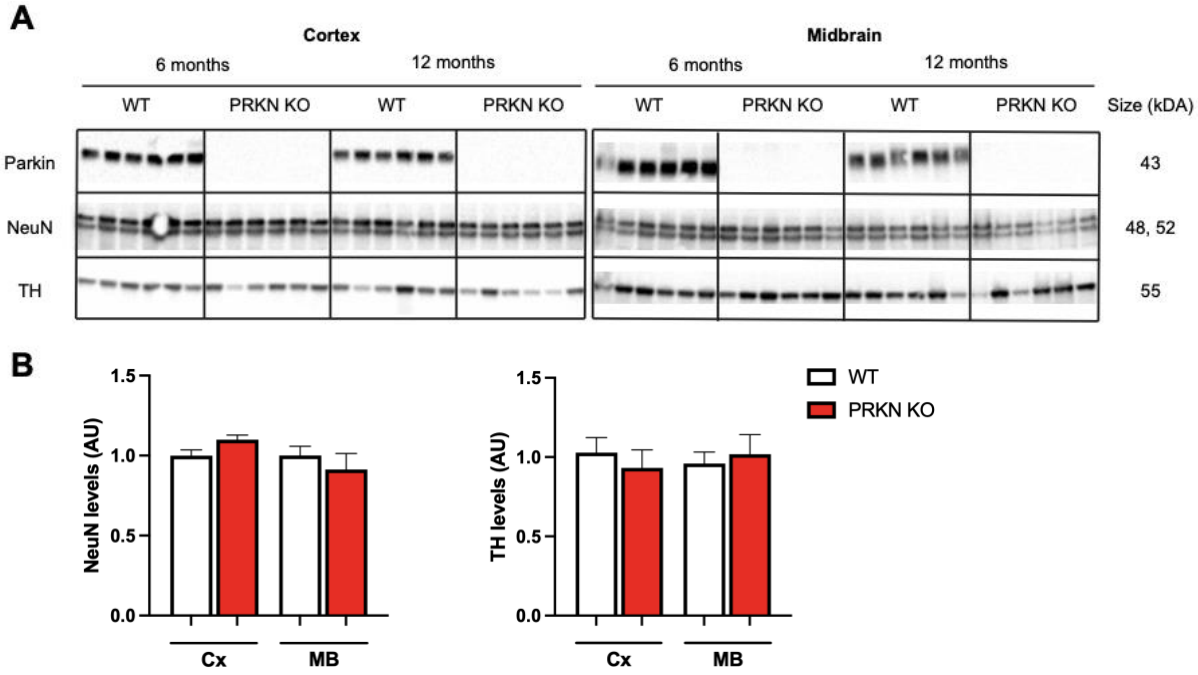


**Figure 4.1 Western blot analyses of neuronal markers and parkin in the cortex (Cx) and midbrain (MB) of 6 and 12-month-old wild-type (WT) and *PRKN* knockout (KO) mice.** Western blots illustrating the protein expression levels of parkin, neuronal nuclei antigen (NeuN) and tyrosine hydroxylase (TH) in the cortex and midbrain of WT and *PRKN* KO mice (A) quantified in (B). Data represent the mean ± SEM**.**

### 4.4.2 α-Synuclein (α-syn) expression levels in *PRKN* KO mice

There is evidence indicating parkin influences α-syn pathology as it regulates α-syn post-translational modifications and its degradation (279, 289, 290, 459). Therefore, the levels of α-syn were investigated in *PRKN* KO mice. As observed previously (298), α-syn levels were similar between *PRKN* KO and WT mice in the cortex and midbrain (Fig. 4.2). Similarly, there were no significant differences in the levels of phospho-α-syn S129 (pS129) between *PRKN* KO and WT mice (Fig. 4.2).

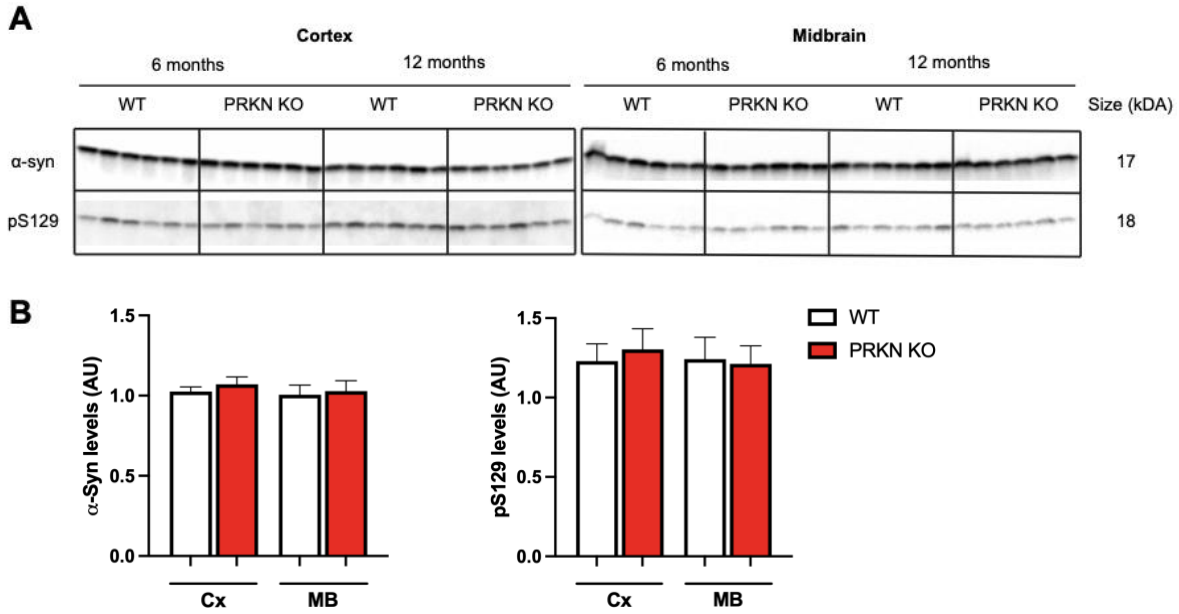


**Figure 4.2 Western blot analyses of α-syn in the cortex (Cx) and midbrain (MB) of 6 and 12-month-old wild-type (WT) and *PRKN* knockout (KO) mice.** Western blots illustrating the protein expression levels of α-syn and phospho-α-syn S129 (pS129) in the cortex and midbrain of WT and *PRKN* KO mice (A) quantified in (B). Data represent the mean ± SEM.

### 4.4.3 Mitochondrial protein expression levels in *PRKN* KO mice

While mitochondrial protein expression levels were similar between WT and *PRKN* KO mice in the cortex and midbrain (Fig. 4.3), parkin loss appeared to alter the expression of GRP75. Compared to WT mice, GRP75 levels were significantly decreased in the midbrain by 19.5% but not the cortex in *PRKN* KO mice (Fig. 4.3), while VDAC1, TOMM20 and Nix levels were similar between *PRKN* KO and WT mice in both regions (Fig. 4.3).

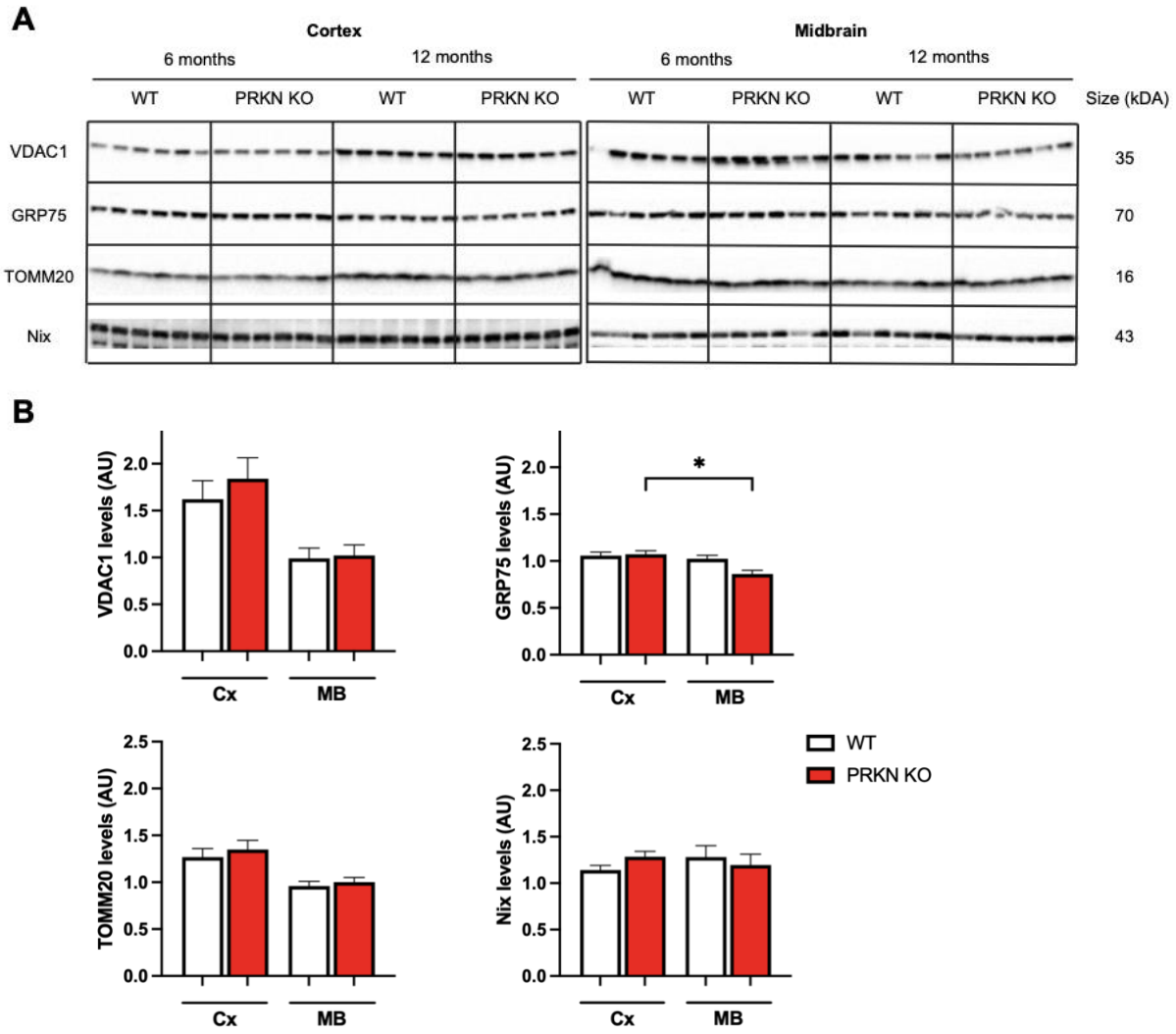


**Figure 4.3 Western blot analyses of mitochondrial proteins in the cortex (Cx) and midbrain (MB) of 6 and 12-month-old wild-type (WT) and *PRKN* knockout (KO) mice.** Western blots illustrating the protein expression levels of voltage-dependent anion channel 1 (VDAC1), glucose-regulated protein 75 (GRP75), translocase of outer mitochondrial membrane protein complex subunit 20 (TOMM20) and NIP3-like protein X (Nix) in the cortex and midbrain of WT and *PRKN* KO mice (A) quantified in (B). Data represent the mean ± SEM**.** Significance is taken at *$p < 0.05$.

Assessment of just the mitochondrial fractionation in 12-month-old mice cortex showed TOMM20 levels were significantly increased by 51.7% in *PRKN* KO mice relative to WT (Fig. 4.4), but there was no difference in the levels of VDAC1, GRP75 or Nix levels between genotypes (Fig. 4.4).

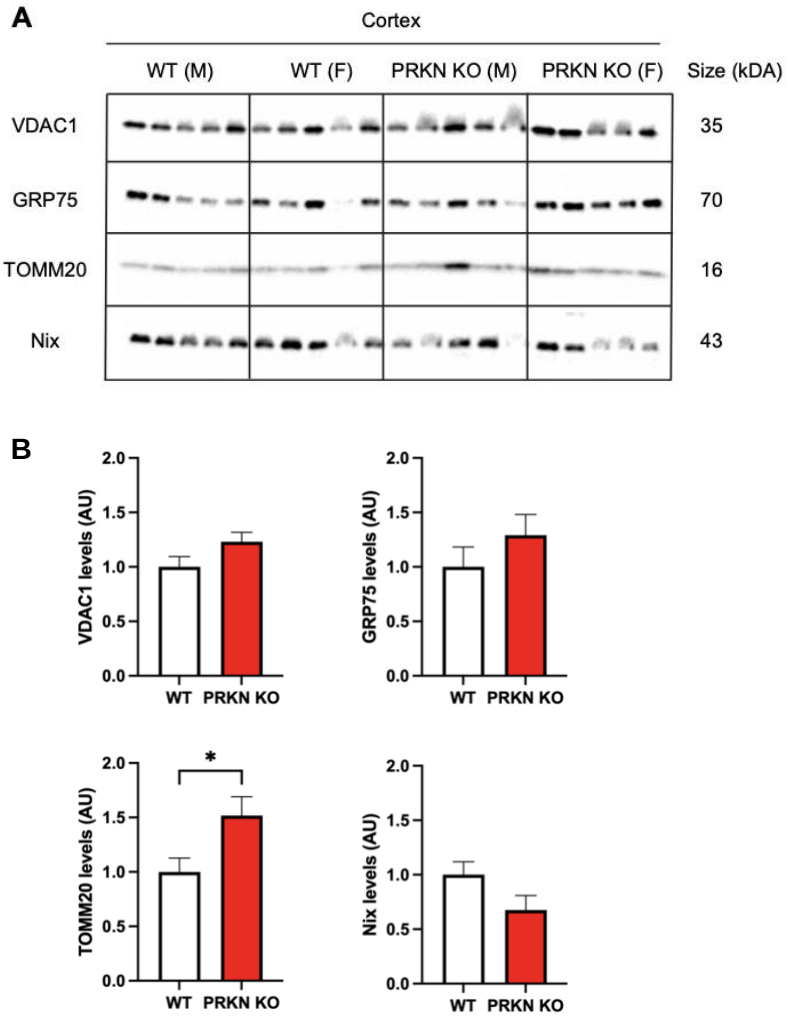


**Figure 4.4 Mitochondrial fraction western blot analyses of mitochondrial proteins in the cortex of male (M) and female (F) wild-type (WT) and *PRKN* knockout (KO) mice at 12 months of age.** Mitochondrial fraction western blots illustrating the protein expression levels of voltage-dependent anion channel 1 (VDAC1), glucose-regulated protein 75 (GRP75), translocase of outer mitochondrial membrane protein complex subunit 20 (TOMM20) and NIP3-like protein X (Nix) in the cortex of WT and *PRKN* KO mice (A) quantified in (B). Data represent the mean ± SEM**.** Significance is taken at $*p < 0.05$.

### 4.4.4 Mitochondrial GRP75 immunofluorescence in cortical and nigral neurons in *PRKN* KO mice

As the western blots showed altered GRP75 levels in the midbrain compared to the cortex specific to parkin loss, the location and levels of GRP75 protein were investigated in cortical and nigral neurons in 12-month-old mice. GRP75 immunofluorescence appeared granular in cortical and nigral neurons in WT and *PRKN* KO mice (Fig. 4.5). Although the intensity of GRP75 protein expression appeared stronger in cortical and nigral neurons of *PRKN* KO mice compared to WT (Fig. 4.5), the mean cellular intensity of GRP75 was not statistically different in cortical and nigral neurons of *PRKN* KO mice compared to WT (Fig. 4.6).

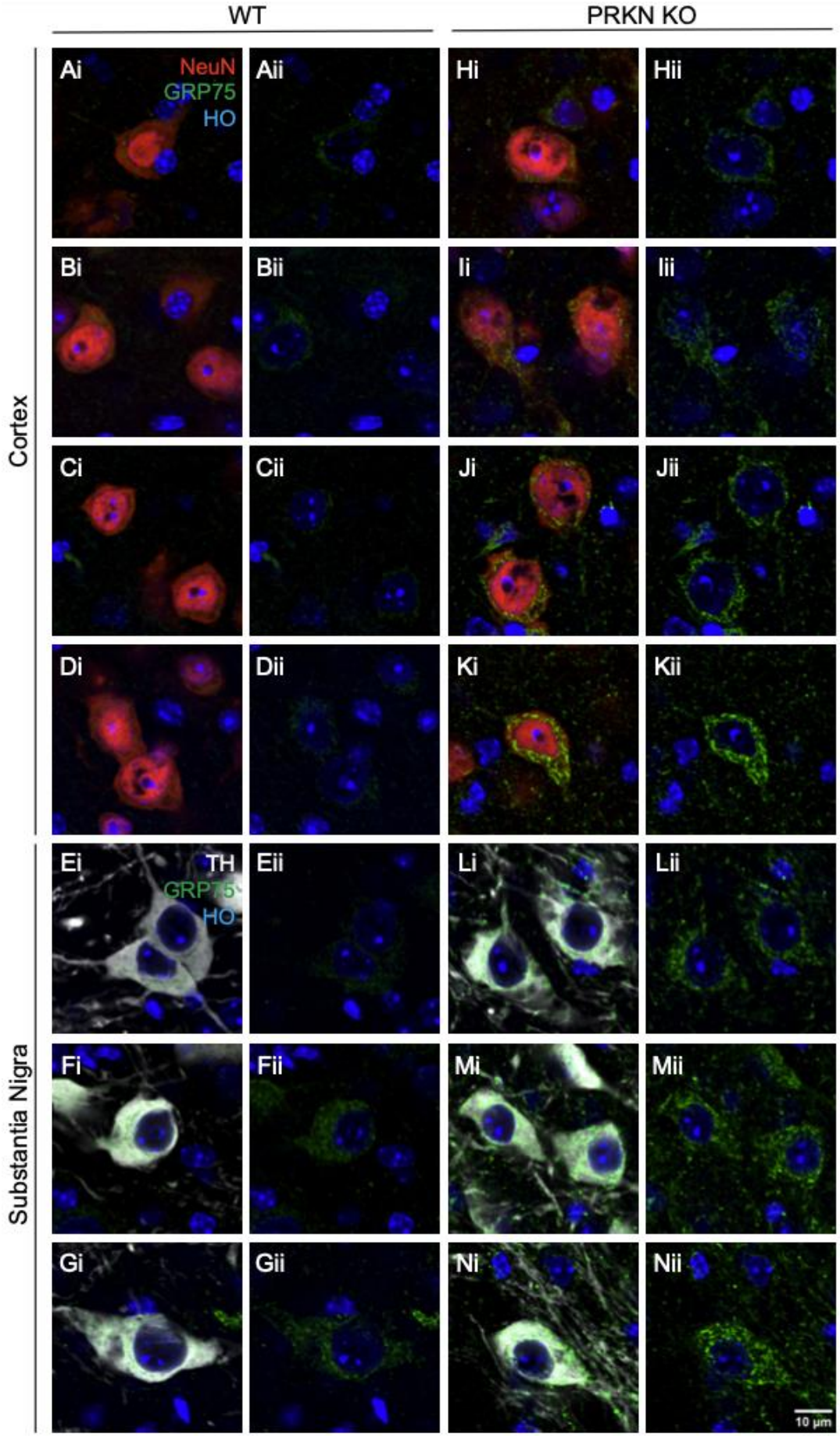


**Figure 4.5 Glucose-regulated protein 75 (GRP75) immunofluorescence in neurons in the cortex and**

**substantia nigra of wild-type (WT) and *PRKN* knockout (KO) mice.** Photomicrographs showing GRP75 (green) immunofluorescence in cortical NeuN+ and nigral TH+ neurons (neuronal nuclei antigen (NeuN), red; tyrosine hydroxylase (TH), white; Hoechst (HO), blue) in 12-month-old WT (A-G) and *PRKN* KO (H-N) mice. (i) show merged image and (ii) show GRP75 and Hoechst only. The scale bar (10µm) in Nii applies to all panels.

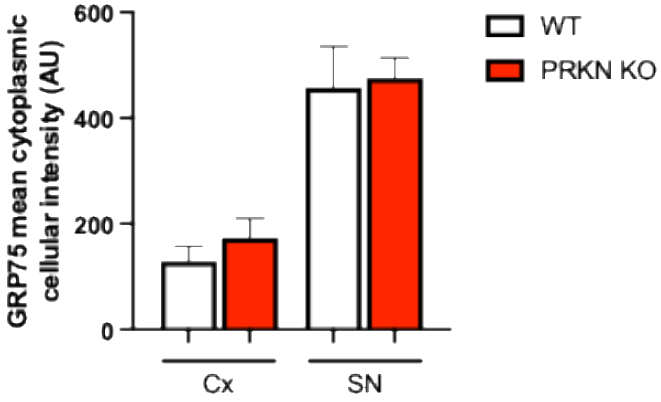


**Figure 4.6 Quantitation of glucose-regulated protein 75 (GRP75) mean intensity in cortical and nigral neurons of wild-type (WT) and *PRKN* knockout (KO) mice at 12 months of age.** Bar graph showing the mean GRP75 fluorescence intensity in neurons in the cortex (Cx) and substantia nigra (SN) of WT and *PRKN* KO mice. Data represent the mean ± SEM**.**

## 4.4.5 Glial protein levels in *PRKN* KO mice

While some studies (Table 4.1) have not observed changes in glial staining in *PRKN* KO mice, there is evidence (316, 443) of mitochondrial abnormalities in glia and inflammatory phenotypes linked to mitochondrial stress in *PRKN* KO mice, although this remains understudied. Therefore, glial protein levels in *PRKN* KO mice were investigated. IBA1, TMEM173 and glutamine synthetase (GS) levels were similar between *PRKN* KO and WT mice in the cortex and midbrain (Fig. 4.7).

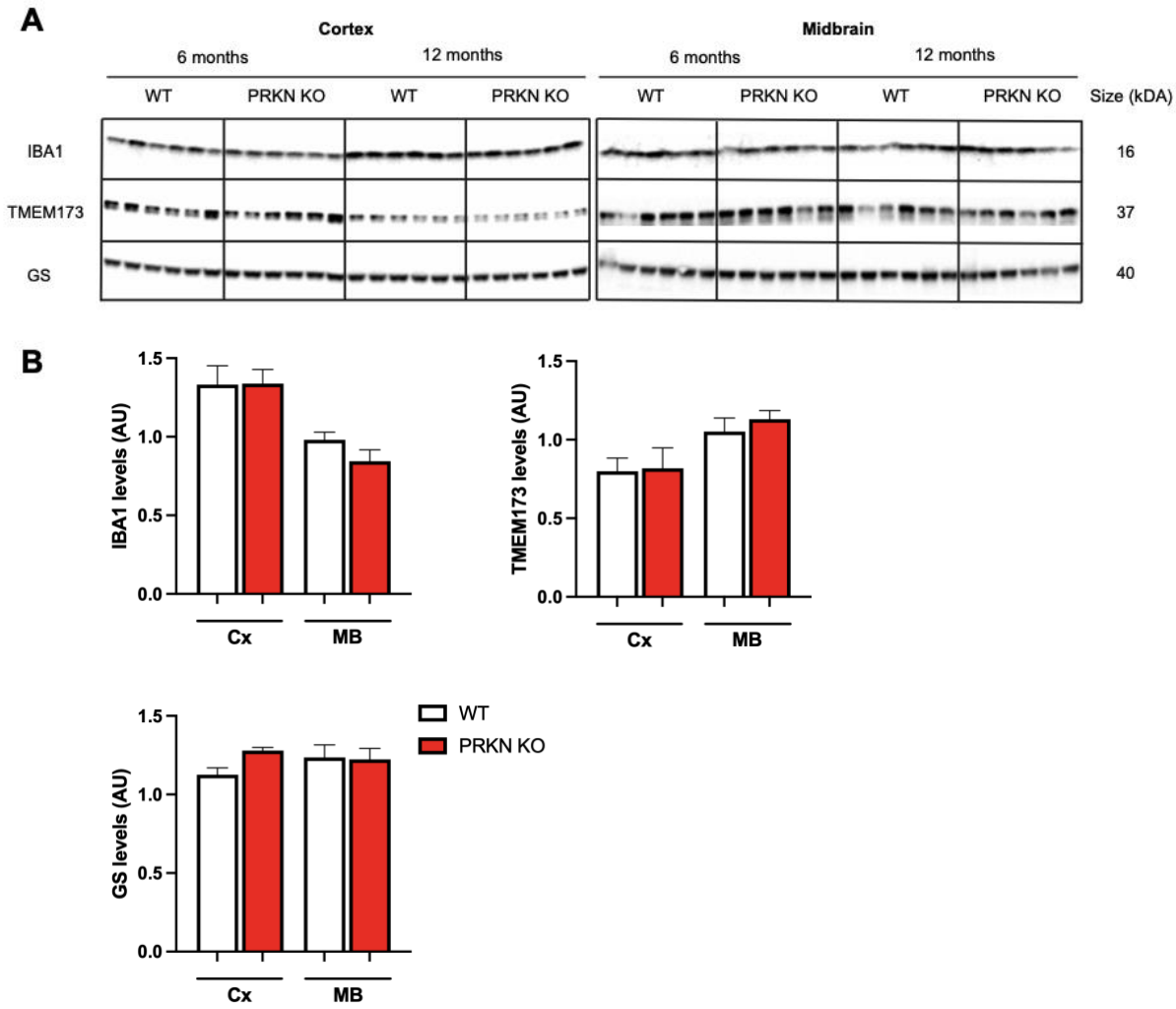


**Figure 4.7 Western blot analyses of glial proteins in the cortex (Cx) and midbrain (MB) of 6 and 12-month-old wild-type (WT) and *PRKN* knockout (KO) mice.** Western blots illustrating the protein expression levels of ionized calcium binding adaptor molecule 1 (IBA1), stimulator of interferon genes/transmembrane protein 173 (TMEM173) and glutamine synthetase (GS) in the cortex and midbrain of WT and *PRKN* KO mice (A) quantified in (B). Results are presented as mean ± SEM.

## 4.4.6 Mitochondrial GRP75 expression in cortical and nigral microglia

To determine whether there were any mitochondrial abnormalities that may be linked to potential glial changes, microglia and GRP75 protein expression in microglia were assessed. Low GRP75 protein expression was observed in microglia, which had a granular morphology without apparent differences in intensities between WT and *PRKN* KO cortical and nigral microglia (Fig. 4.8). GRP75 protein expression levels in IBA1+ microglia were similar between WT and *PRKN* KO in the cortex and SN (Fig. 4.9).

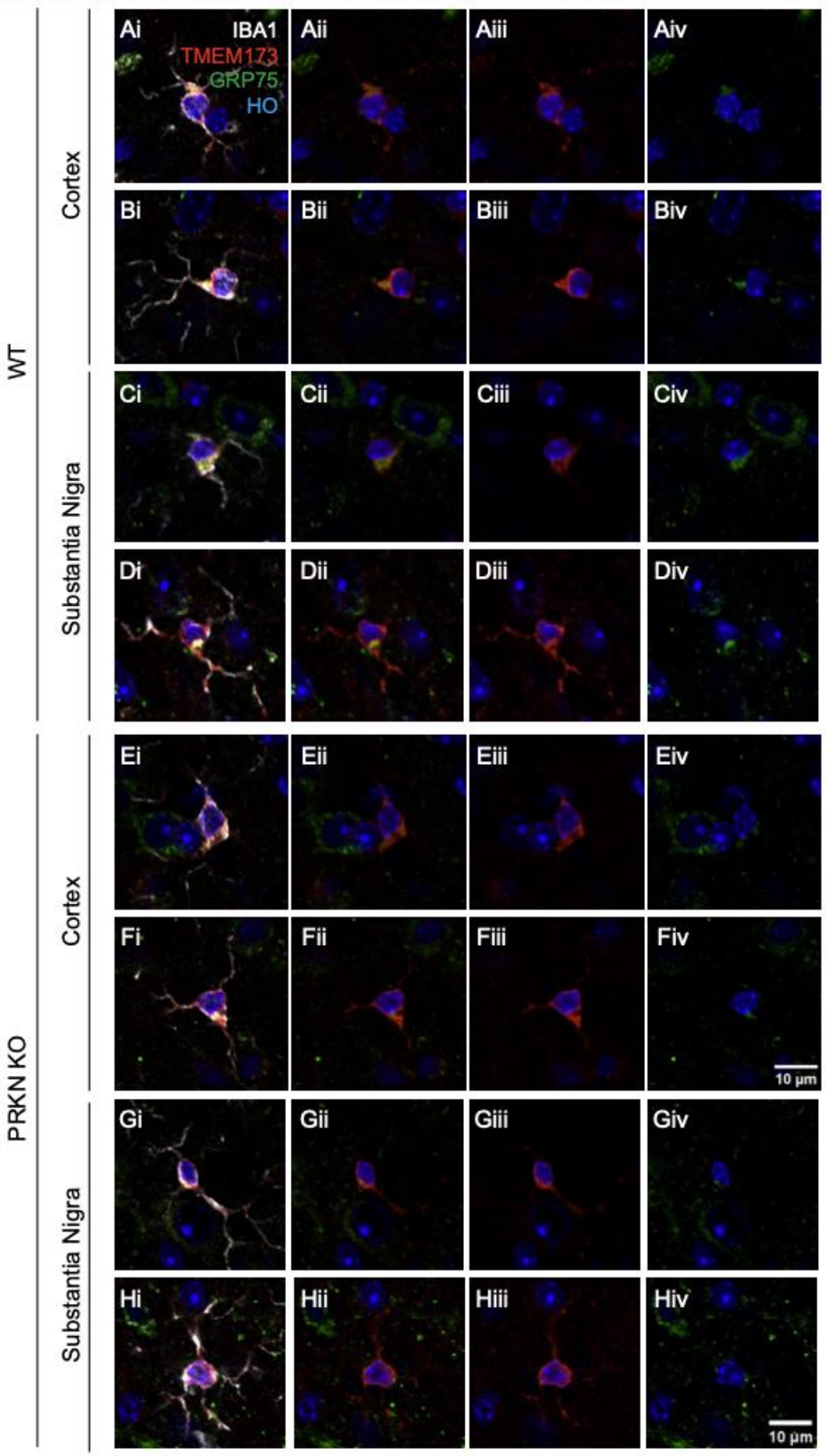
WT
PRKN KO
Cortex
Substantia Nigra
Cortex
Substantia Nigra
Ai
IBA1
TMEM173
GRP75
HO
Aii
Aiii
Aiv
Bi
Bii
Biii
Biv
Ci
Cii
Ciii
Civ
Di
Dii
Diii
Div
Ei
Eii
Eiii
Eiv
Fi
Fii
Fiii
Fiv
10 µm
Gi
Gii
Giii
Giv
Hi
Hii
Hiii
Hiv
10 µm

**Figure 4.8 Glucose-regulated protein 75 (GRP75) immunofluorescence in microglia in the cortex and substantia nigra of wild-type (WT) and *PRKN* knockout (KO) mice.** Photomicrographs showing GRP75 (green) immunofluorescence in ionized calcium binding adaptor molecule 1 (IBA1) (white) and stimulator of interferon genes/ transmembrane protein 173 (TMEM173) (red) cortical and nigral microglia (Hoechst (HO), blue) in 12-month-old WT (A-D) and *PRKN* KO (E-H) mice. (i) show merged image, (ii) show TMEM173, GRP75 and Hoechst, (iii) and (iv) show TMEM173 or GRP75 with Hoechst only respectively. The scale bar (10µm) in Fiv applies to panels A, B, E and F and the scale bar (10µm) in Hiv applies to panels C, D, G and H.

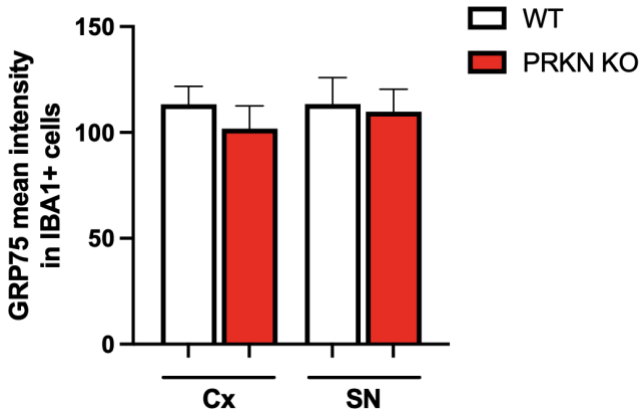


**Figure 4.9 Quantitation of glucose-regulated protein 75 (GRP75) mean intensity in cortical and nigral IBA1+ cells of wild-type (WT) and *PRKN* knockout (KO) mice at 12 months of age.** Bar graph showing the mean GRP75 fluorescence intensity in ionized calcium binding adaptor molecule 1 (IBA1) microglial cells in the cortex (Cx) and substantia nigra (SN) of WT and *PRKN* KO mice. Data represent the mean ± SEM**.**

IBA1-labelled microglia were morphologically heterogenous in WT and *PRKN* KO mice where some were ramified with variably shaped cell bodies while others had rounder cell bodies with few or no ramifications (Fig. 4.10). However, there were no differences between WT and *PRKN* KO mice in the proportion or density of microglial cells that were IBA1+, TMEM173+ or labelled by both, in either the cortex or SN (Fig. 4.11). Similarly, there were no differences in microglial somal size (based on IBA1 labelling) between WT and *PRKN* KO mice (Fig. 4.11).

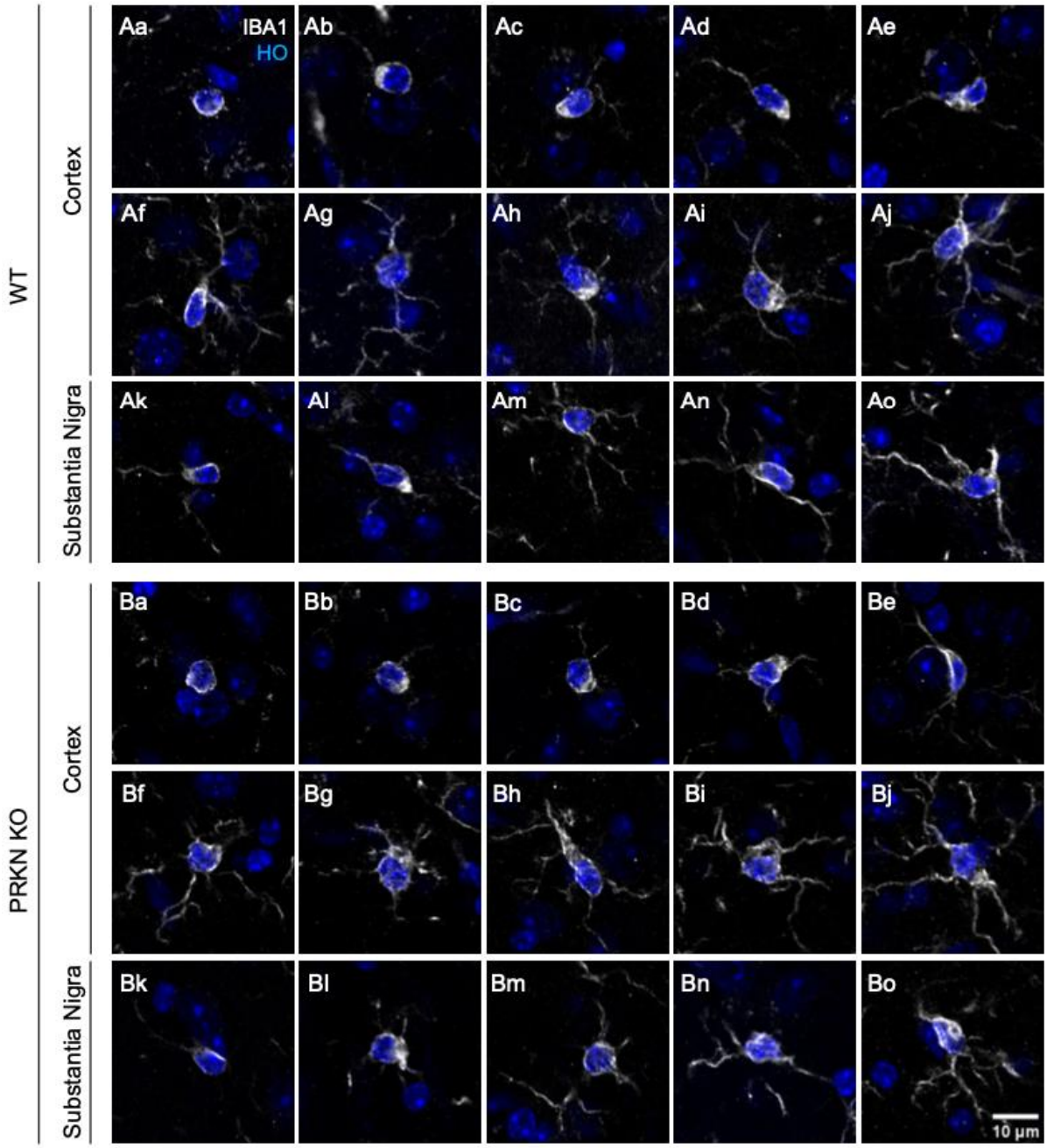


**<u>Figure 4.10</u> Microglial phenotypes in the cortex and substantia nigra of wild-type (WT) and *PRKN* knockout (KO) mice.** Photomicrographs showing various IBA1+ (IBA1, white; Hoechst (HO), blue) microglial phenotypes ranging from more rounded cell bodies with minimal processes to more ramified cells in the cortex (Aa-Aj, Ba-Bj) and substantia nigra (Ak-Ao, Bk-Bo) of WT (A) and *PRKN* KO (B) mice. The scale bar (10µm) in Bo applies to all panels.

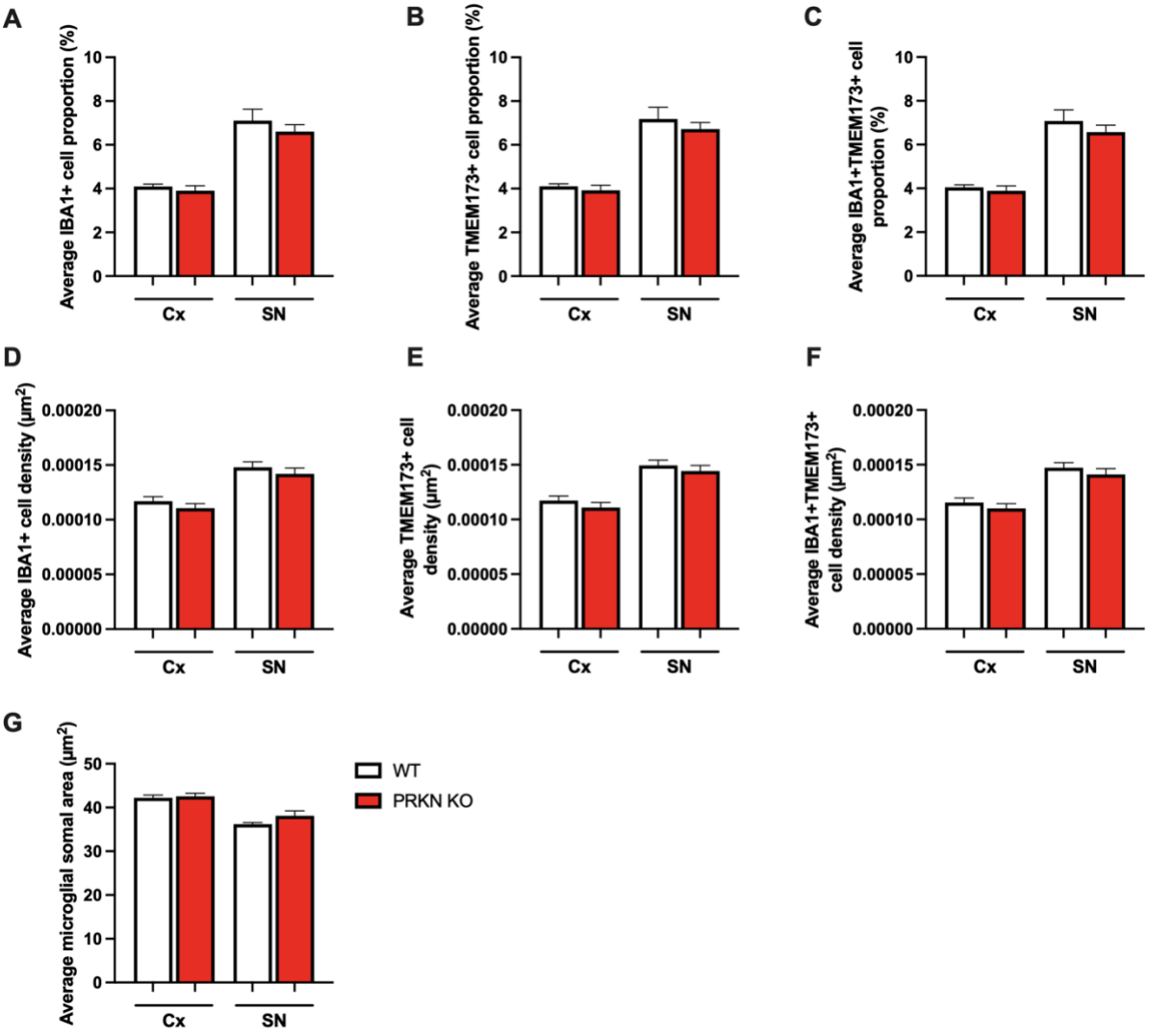


**Figure 4.11 Quantitation of microglial cells and somal size in wild-type (WT) and *PRKN* knockout (KO) mice in the cortex (Cx) and substantia nigra (SN) at 12 months of age.** Bar graphs showing the proportion (A-C), density (D-F) and somal size (G) of microglia labelled by ionized calcium binding adaptor molecule 1 (IBA1) (A, D, G), stimulator of interferon genes/ transmembrane protein 173 (TMEM173) (B, E) or both (C, F) in the cortex and substantia nigra of WT and *PRKN* KO mice. Data represent the mean ± SEM**.**

## 4.5 Discussion

The present study investigated the effect of parkin loss on mitochondrial quality control and neuroinflammation using a *PRKN* KO mouse model by quantitatively assessing the expression of mitochondrial and glial proteins in the cortex and midbrain. The main findings were that 1) the expression of TH, NeuN, pan and pS129 α-syn were similar between WT and *PRKN* KO mice suggesting an absence of neuronal loss or pathological inclusions, 2) parkin loss altered the expression of GRP75 and TOMM20 proteins, while glial protein expression was similar between WT and *PRKN* KO mice suggesting impaired mitochondrial

quality control without glial changes, 3) GRP75 protein expression levels in cortical and nigral neurons and microglia were similar between WT and *PRKN* KO mice suggesting the change in GRP75 levels is specific to other cell types, and 4) microglial morphology, number and somal size were similar between *PRKN* KO and WT mice suggesting an absence of neuroinflammatory phenotypes. Together, these findings show that some mitochondrial proteins are altered in *PRKN* KO mice while neuronal, pathological and glial proteins as well as microglial phenotypes are similar between WT and *PRKN* KO mice.

*Core neuronal and pathological markers of PRKN KO model*

The expression levels of neuronal markers TH and NeuN were similar in the cortex and midbrain between WT and *PRKN* KO mice suggesting a lack of neuronal loss in line with previous studies observing no differences in nigral TH+ neuronal expression between WT and *PRKN* KO mice (Table 4.1). Only one study (300) (Table 4.1) has reported TH+ neuronal loss in the centre of the SN in 110-week-old *PRKN* KO mice with an exon 2 deletion. This suggests that neuronal loss in *PRKN* KO mouse models may be age dependent occurring only after 24 months (300) rather than the 6 and 12 month-old mice used in this thesis and previous studies (Table 4.1). The type of mutation may also account for phenotypic differences, however this is less likely considering all other studies have used different *PRKN* mutations and not observed neuronal loss (Table 4.1).

Similarly, pan and pS129 α-syn expression levels were unaltered in *PRKN* KO mice. Parkin and α-syn have been shown to interact as parkin decreases the levels of pan and pS129 α-syn and its associated toxicity *in vivo* (289). Similarly, a study (460) in Macaque monkeys revealed that parkin overexpression led to reduced pan and pS129 α-syn accumulation in neurons. Also, glycosylated α-syn has been demonstrated as a parkin substrate (279). This suggests a loss of parkin may result in increased α-syn levels, however, our study which is the first to assess pS129 α-syn levels in *PRKN* KO mice shows that both pan and pS129 α-syn protein expression are unaltered. Consistent with this, a previous study (298) revealed that the protein levels of pan and glycosylated α-syn were similar in brain homogenates between WT and *PRKN* KO mice. Further supporting our data, studies (Table 4.1) have not observed any α-syn pathological inclusions in *PRKN* KO mice, a finding comparable to human *PRKN*-related PD patients where the majority have an absence of Lewy pathologies (264, 266-273). This could suggest that in the context of α-syn accumulation parkin acts to

reduce its levels and toxicity, though in its absence in *PRKN*-related PD there may be different functional mechanisms to degrade α-syn and regulate its levels. It should be noted that unlike the mice in this thesis and previous studies (Table 4.1), these *PRKN*-related PD patients generally have significant neuronal loss (264, 266-273), a feature that may occur only after some time as observed in mice at 110 weeks (300). Alternatively, *PRKN* KO mouse models may have compensatory mechanisms to protect against neuronal degeneration.

*The levels of the mitochondrial proteins GRP75 and TOMM20 are altered in PRKN KO mice*
Most mitochondrial proteins were similar between WT and *PRKN* KO mice, however in *PRKN* KO mice GRP75 was decreased in the midbrain by ~20% compared to the cortex and TOMM20 was significantly increased by ~50% in cortical mitochondrial fractions. As mentioned in the methods, GRP75 is a mitochondrial stress response chaperone protein and TOMM20 is a receptor protein with both involved in protein import.

A study (461) found that GRP75 was significantly decreased in SN mitochondrial fractions from PD patients compared to controls. Similarly, GRP75 was also decreased in frontal cortex cytosol-enriched fractions from PD patients (462). In a PD rat model, GRP75 striatal levels were reduced (463). However, in *PRKN* KO mice, GRP75 protein levels were increased in the cortex at 12 months of age (440) (Table 4.1). Results in this thesis show that the total levels of GRP75 were similar between WT and *PRKN* KO mice in the cortex and although not statistically significant, GRP75 was decreased in *PRKN* KO mice compared to WT in the midbrain. More importantly GRP75 levels were significantly decreased in the midbrain of *PRKN* KO mice compared to the cortex while they were similar between the cortex and midbrain in WT mice indicating parkin loss produces this regional difference. The effects of upregulated/downregulated GRP75 have proven inconsistent. Under physiological conditions, human cells overexpressing GRP75 have reduced reactive oxygen species (ROS) levels and improved mitochondrial membrane potential (MMP) while GRP75 knockdown has the opposite effects (464). Furthermore, under proteolytic stress conditions, GRP75 overexpression was protective against increased stress-induced ROS levels and impaired MMP (464) with GRP75 knockdown in human cells activating a mitochondrial stress response (465). Similarly, another study revealed that GRP75 knockdown caused mitochondrial dysfunction in human cells under oxidative stress conditions (466). Interestingly, parkin overexpression rescued the phenotypes induced by GRP75 knockdown

(465, 466). In contrast, in PD cellular models GRP75 overexpression enhanced toxicity, mitochondrial complex I inhibition, oxidative stress and proteasomal dysfunction (461). In line with this, a more recent study (455) showed that under oxidative stress conditions GRP75 silencing reduced ER-mitochondrial coupling and prevented cell death and mitochondrial dysfunction (increased mitochondrial ROS production, impaired MMP and mitochondrial respiration) while increased GRP75 expression increased cell death in a mouse cell model. Together, this suggests that the decreased GRP75 levels observed in this study in the midbrain compared to the cortex in *PRKN* KO mice may reflect impaired mitochondrial function in the midbrain affecting cell functioning and downstream targets which is exacerbated in the absence of parkin. This change may underlie the more selective vulnerability of the midbrain to PD with *PRKN* loss of function.

While VDAC1 and GRP75 were not statistically increased in the cortical mitochondrial fractions of *PRKN* KO mice, TOMM20 was statistically increased in that protein fraction. As VDAC1, TOMM20 and Nix are ubiquitinated by parkin (448-451), it was expected they would all accumulate in the absence of parkin, however this was only the case for TOMM20 in the mitochondrial fractions which has not been explored in other *PRKN* KO mouse models. The levels of both TOMM20 and a nuclear-encoded mitochondrial protein have been shown to be decreased in SN homogenates from PD patients suggesting impaired mitochondrial import (456), but this could be due to the loss of dopamine neurons in PD. Of note, TOMM20 overexpression is not protective *in vivo* in a PD complex-I-induced mouse model and instead TOMM20 overexpression worsened dopaminergic cell death, whereas in the dopaminergic neuroblastoma cell line BE(2)-M17 treated with a complex-I inhibitor, overexpression of TOMM20 protects against aspects of induced mitochondrial dysfunction such as the reduction of oxidative phosphorylation system cytochrome c oxidase subunit IV and increased ROS production and partially protected against cell death (456). Human cell culture experiments show that overexpression of TOMM20 ameliorates the inhibitory effects of α-syn on protein import and downstream effects such as impaired mitochondrial respiration (467). An increased interaction between α-syn and TOMM20 in dopamine neurons associates with decreased mitochondrial protein import in both PD patients and animal models (467) and TOMM20 overexpression in rats protects against α-syn-impaired mitochondrial protein import and α-syn-induced dopaminergic cell death, suggesting that the effects of TOMM20 upregulation appear to depend on the pathological context (468).

Therefore, in the presence of α-syn the increase in mitochondrial TOMM20 levels may represent a protective mechanism to preserve appropriate mitochondrial functioning and prevent cell death in the cortex.

*GRP75 protein levels are unaltered in cortical and nigral neurons and microglia in PRKN KO mice*

This is the first study to assess GRP75 protein levels in different cell types in *PRKN* KO mice. GRP75 protein expression appeared granular in neurons and glia and was overall low in microglia. This is consistent with immunohistochemistry performed in the SN of PD patients which revealed minimal GPR75 protein staining in glia and a granular expression in neurons (461). However, this study reported an apparent stronger GRP75 expression in the neurons from controls compared to PD patients (461), whereas in the present study GRP75 expression appeared stronger in the *PRKN* KO mouse neurons, although following quantification of the fluorescence, the levels of GRP75 in cortical and nigral neurons was similar between WT and *PRKN* KO mice. Similarly, the levels of GRP75 in cortical and nigral microglia was comparable between WT and *PRKN* KO mice. This suggests that neurons and microglia in this *PRKN* KO model may not have significant mitochondrial stress and the decreased GRP75 levels in the midbrain of *PRKN* KO mice compared to the cortex may be due to other cell types, although this requires further investigation.

*Glial protein expression levels and microglial morphology, numbers and somal size are similar between WT and PRKN KO mice*

The protein levels of microglial markers IBA1 and TMEM173 and the astrocytic marker GS were similar between WT and *PRKN* KO mice. This is supported by previous studies (Table 4.1) which have observed no differences in IBA1 or GFAP staining in *PRKN* KO mice, however a study (440) reported decreased GS levels in the striatum of 2-month-old *PRKN* KO mice (Table 4.1). This disparity to the present study may be due to the age of the mice and the region analysed.

Neuroinflammatory pathways remain understudied in the context of *PRKN*-related PD, particularly in association with impaired mitochondrial functioning. There is evidence to suggest that astrocytes and microglia are implicated in *PRKN*-related PD pathogenesis. Electron microscopy has revealed that *PRKN* KO mice have increased mitochondrial

abnormalities and damaged mitochondria in SN astrocytes and microglia (443). Furthermore, cell culture studies (469-471) have shown that *PRKN* KO mouse glia have increased cytokine release and reduced neurotrophic functions under endoplasmic reticulum stress conditions, altered growth, reduced neuroprotective function, increased IBA1 staining and proportion of hypertrophic cells (microglia) in response to proinflammatory stimuli and NLRP3 inflammasome activation. Moreover, an inflammatory phenotype has been reported in *PRKN* KO mice following mitochondrial stress, which could be rescued by the knockdown of TMEM173 (316). However, the present study observed no differences in IBA1+ microglial morphology, proportion, density, or somal area between WT and *PRKN* KO mice and similarly saw no differences in the proportion or density of TMEM173+ microglia between genotypes suggesting an absence of a neuroinflammatory phenotype in this *PRKN* KO model. Taken together with the finding that GRP75 protein levels were similar between WT and *PRKN* KO cortical and nigral neurons and microglia, the data suggest that mitochondria are not under significant stress and are not severely impacted by parkin loss to induce neuroinflammation.

*Conclusions*

Overall, this study has shown that while neuronal, pathological and glial protein levels are similar between WT and *PRKN* KO mice, parkin loss alters the expression of mitochondrial proteins GRP75 and TOMM20. GRP75 protein levels were similar between genotypes in cortical and nigral neurons and microglia suggesting that other cell types may be implicated to account for the decreased GRP75 levels in the midbrain of *PRKN* KO mice. An inflammatory phenotype was not observed in *PRKN* KO mice as cortical and nigral microglial morphology, numbers and somal area were similar between WT and *PRKN* KO mice. These data suggest that parkin loss alters specific mitochondrial proteins which may be insufficient to induce a neuroinflammatory phenotype.

# CHAPTER 5: General discussion and conclusions

## 5.1 General discussion

This thesis assessed cellular pathologies in PD genetic mutation cases and models. While most PD cases are idiopathic, there are several PD-causative genes including *SNCA*, *LRRK2* and *PRKN*, with these genes being the most common causes of autosomal dominant and recessive PD (472). Genetic forms of PD have provided abundant insights into the pathogenesis and pathobiology of PD. However, the impacts of PD-associated genetic mutations on cellular pathologies and particularly comparisons to sporadic PD and across mutations remains underexplored. Further research into this may enhance our understanding of PD pathobiology and may highlight differences between sporadic and genetic PD or between mutations to better tailor treatments. Therefore, this thesis investigated and compared the impact of *SNCA*, *LRRK2* and *PRKN* genetic mutations on cellular pathologies using *SNCA*-related PD post-mortem cortical tissue, PD mutation patient iPSC-derived dopamine neuronal transplants and a *PRKN* KO mouse model.

Several studies have provided insights into LB formation and progression, mainly using LP morphology in the brainstem of dementia with LB and sporadic PD patients (30, 64, 65, 354-356). However, comparisons of LPs between sporadic and genetic PD and across mutations remain elusive and as such it is unknown whether LP formation and progression is similar between sporadic and genetic PD. Also, as there is limited research on the characterisation of LPs in PD mutation cases, it remains to be determined whether there are distinct LBs or pathologies associated with sporadic PD or specific PD mutations which could better inform the underlying pathways of LP progression. Furthermore, studying LPs in the cortex which is associated with less mature pathology or in more novel models that allow us to better characterise early pathological changes, may enhance our understanding of the LP progression sequence. To address these gaps in knowledge, neuronal pathologies were assessed and compared in sporadic and *SNCA* mutation A53T, E46K and G51D PD post-mortem cortical tissue (chapter 2) as well as in iPSC-derived dopaminergic neurons from PD mutant patients carrying *SNCA*, *LRRK2* and *PRKN* mutations 6 months post-transplantation into athymic mice (chapter 3).

Various LPs were identified including puncta, heterogeneous pale/mixed and mature/rounder LBs in all PD cases, although more neurons had LP in *SNCA* mutation cases (chapter 2). There were significant differences in LP types between sporadic and *SNCA*-related PD, where sporadic PD had a more uniform population of mature/rounder LBs while *SNCA* cases had approximately half of each LB type and more neurons with puncta. The large proportion of neurons with puncta in *SNCA*-related PD compared with sporadic PD shows a significant difference in the intracellular accumulation of mutant α-syn. As discussed in chapter 2, a number of studies have shown that *SNCA* mutant neurons but not their isogenic controls accumulate punctate α-syn in lysosomes and multivesicular bodies, consistent with the observation of increased punctate α-syn aggregations in neurons in *SNCA* mutation cases. In addition, there were differences in the proportion of LBs colocalising the actin stabiliser RhoA which was recently shown to label more toxic lipid-rich inclusions in *SNCA* mutation cell models (360). RhoA was found in most LBs in the E46K cases but not in LBs in the other *SNCA* mutations studied. Previous studies have shown that A53T mutants lead to more mature α-syn fibrils, while E46K mutants lead to more stable but less abundant α-syn fibrils (473) associated with lipids and RhoA activation (360). This may be why the type of LBs differed between the different mutation types with less fibrils available in the E46K mutation cases leading to less mature LBs. Interestingly, sporadic and E46K mutant PD cases had a similar high proportion of LBs colocalising RhoA, while A53T and G51D cases had few LBs colocalising RhoA. This suggests that sporadic PD also has a similar proportion of less mature α-syn fibrils and more lipids in their LBs. This has been confirmed by electron microscopy (47). While the number of *SNCA* mutation cases analysed was low due to their prevalence, the data highlights that there are distinct LBs in A53T and G51D *SNCA*-related PD. Furthermore, modelling using the prevalence of the different types of LPs suggests diverse underlying pathways of LP progression. These findings provide support for the concept that sporadic and *SNCA*-related PD have different sequences of cortical LB formation and progression, enhancing our current understanding of LP progression in models that may use different mutant α-syn.

As there was a diversity of LP in different *SNCA* mutation cases (chapter 2), whether such diversity extends to other PD genetic mutations was assessed in PD mutant iPSC-derived dopamine neuronal transplants (chapter 3). Studying LP in *SNCA*, *LRRK2* and *PRKN* PD iPSC-derived dopaminergic neurons in the environment of a living brain provided unique

insights into early pathological changes compared to studying the same cells *in vitro*. There are limited studies that have explored pathologies in transplanted neurons derived from PD mutant patients (412-414) and this is the first study to compare pathologies in such transplants across different PD genetic mutations.

The expression levels of α-syn and tau and their phosphorylated forms were similar across all genotypes in grafted human dopaminergic neurons (chapter 3). Also, morphologically diverse phospho-α-syn and phospho-tau immunoreactive aggregate-like structures were seen in all genotype grafts, however most were not or only partially localised to the grafted human dopaminergic neurons. Based on their morphology and localization, these structures resembled puncta and LNs but not LBs. While there are different early LPs in sporadic and *SNCA*-related PD post-mortem cortical tissue (chapter 2), this data (chapter 3) suggests that the different PD mutations produce similar early protein expression and diverse aggregate-like structures in transplanted human dopaminergic neurons, thus potentially having similar initiating pathologies in this cell type. Such structures may relate to early LN formation or developmental aspects of maturing human grafts and it remains to be determined whether upregulation of phospho-α-syn and phospho-tau is sufficient over the longer term to induce LPs in more mature functioning dopaminergic neurons. As such, these findings are informative for future studies to mature these human dopaminergic neurons *in vivo* for longer than 6 months to determine whether this allows the transplanted neurons to more closely recapitulate the characteristic features found in later life in PD. The morphological analysis of the different mutant human dopaminergic neurons (chapter 3) determined that all grafts had a similar quantity of morphologically heterogenous dopaminergic neurons, but that the *PRKN* mutation group had significantly smaller neurons and projections compared to controls. This suggests that although the overall cell survivability and growth was similar between grafts, the maturation of cells was impeded in the *PRKN* group compared to the other mutations. This may impact on the development of LPs in *PRKN* dopaminergic neurons, a finding consistent with limited LPs in the brains of *PRKN* mutation cases (264, 266-273).

In addition to *PRKN*-linked PD patients having a loss of dopaminergic neurons with limited LP, *PRKN* KO animal models typically do not show any LP (177, 178, 264, 266-270, 272, 273, 298-300, 436, 439). This relationship between cell death and LP requires further

exploration. However, curiously all human dopaminergic grafts, even the *PRKN*-derived transplants, exhibited phospho-α-syn aggregate-like structures (chapter 3). Therefore, we further explored the impact of a *PRKN* loss of function mutation on cellular pathologies in a *PRKN* KO animal model at 6 and 12 months (chapter 4). Pan and phospho-α-syn levels as well as neuronal marker expression levels were unchanged in *PRKN* KO mice suggesting a mild phenotype without LP or cell loss. This is in line with previous studies which have shown unchanged levels of α-syn, an absence of pathology and of dopaminergic neuronal loss (298, 299, 436, 439, 441, 442), although this is the first study to show that phospho-α-syn levels are also unaltered. Therefore, *PRKN* KO mice at 6 months do not appear to have pathology, however 6 months post-transplantation *PRKN* PD-derived dopamine neuronal transplants in a stressed environment show phospho-α-syn and phospho-tau accumulations. This suggests that the initiation of degenerative LPs may be contingent on the presence of other stress factors.

While there is abundant research on *SNCA* and *LRRK2* mutation pathogenic mechanisms to better understand PD pathogenesis, there are limited studies on neuroinflammatory pathways and glial changes linked to mitochondrial abnormalities in a *PRKN*-related context. In this study (chapter 4), *PRKN* KO altered the expression levels of mitochondrial-related proteins GRP75 and TOMM20 although without changing glial marker expression levels or inducing an inflammatory phenotype in microglia. Also, GRP75 protein levels in neurons and microglia were unchanged suggesting that the total protein change is not specific to these cell types. These findings suggest that while *PRKN* KO alters the expression of some mitochondrial-related proteins, this does not produce apparent pathological, degenerative or inflammatory features. This data reinforces that *PRKN* KO animal models produce a mild PD phenotype as previously suggested and could prompt future studies to utilise *PRKN* PD-derived iPSC transplants instead as an avenue to further explore the pathogenesis of *PRKN*-related PD.

## 5.2 Concluding remarks and future directions

Overall, this thesis has provided novel insights on the impact of PD-associated genetic mutations on cellular pathologies and has highlighted key similarities and differences in their impact. The types of LP are significantly different between sporadic and *SNCA*-related PD highlighting that LB formation and progression may differ between sporadic and *SNCA*-

related PD using LP types as a model for their sequence. Also, as *SNCA* mutation cases had different proportions of LBs colocalising RhoA, this suggests molecular differences in LB composition between mutations and potentially a greater diversity of LPs between different mutations in different genes. However, developing dopaminergic neurons from *SNCA*, *LRRK2* and *PRKN* PD patient iPSCs had similar expression of α-syn, tau and their phosphorylated forms and all grafts developed aggregate-like structures 6 months post-transplantation which could indicate similar initiating pathologies across mutations. While *PRKN* grafts had aggregate-like structures at 6 months, *PRKN* loss in mice at 6 months did not show altered pan or phospho-α-syn levels and had an absence of pathology. These *PRKN* KO mice demonstrated a mild mitochondrial phenotype suggesting other factors may be required to initiate LP or degeneration *in vivo*.

Future studies should extend the neuropathological findings of chapter 2 in other PD mutation cases, particularly PD patients with mutations in different genes. Further neuropathological studies on LP using other markers may also enhance our understanding of LB formation and progression by potentially identifying other distinct pathologies specific to a genotype. Molecular studies should also explore the pathway that RhoA is involved in to differently impact developing LPs. Furthermore, future studies must also employ other markers to more comprehensively assess the aggregate-like structures in the iPSC-derived neuronal transplants. This study (chapter 3) could also be replicated at different time points or a time point exceeding 6 months, to enable clearer insights into initiating pathologies and their progression. In future, this study (chapter 3) could also employ sporadic PD-derived iPSCs for a more comprehensive comparison. Also, as the *LRRK2* and *PRKN*-derived grafts produced some aggregation that are usually absent in end-stage *LRRK2* R1411G and *PRKN* PD brains, there needs to be further research to understand the specific stress factors initiating these accumulations and the timing and mechanism of their disappearance. This may provide novel insights into other causes contributing to the high variability of neuronal cell loss and severity of LP in PD. Also, the high variability between *PRKN* models needs further exploration to understand the factors driving or protecting any α-syn pathology. The findings presented in this thesis reveal a great diversity of pathologies in genetic forms of PD.

# CHAPTER 6: References


1. Balestrino R, Schapira AHV. Parkinson disease. Eur J Neurol. 2020;27(1):27-42.
2. Fearnley JM, Lees AJ. Ageing and Parkinson's disease: substantia nigra regional selectivity. Brain. 1991;114 ( Pt 5):2283-301.
3. Spillantini MG, Schmidt ML, Lee VMY, Trojanowski JQ, Jakes R, Goedert M. α-Synuclein in Lewy bodies. Nature. 1997;388(6645):839-40.
4. Bandres-Ciga S, Diez-Fairen M, Kim JJ, Singleton AB. Genetics of Parkinson's disease: An introspection of its journey towards precision medicine. Neurobiology of Disease. 2020;137:104782.
5. Lesage S, Brice A. Parkinson's disease: from monogenic forms to genetic susceptibility factors. Human molecular genetics. 2009;18(R1):R48-R59.
6. Mhyre TR, Boyd JT, Hamill RW, Maguire-Zeiss KA. Parkinson's disease. Subcell Biochem. 2012;65:389-455.
7. Ball N, Teo WP, Chandra S, Chapman J. Parkinson's Disease and the Environment. Front Neurol. 2019;10:218.
8. Dorsey ER, Bloem BR. The Parkinson Pandemic-A Call to Action. JAMA Neurol. 2018;75(1):9-10.
9. de Lau LML, Breteler MMB. Epidemiology of Parkinson's disease. Lancet neurology. 2006;5(6):525-35.
10. Simon DK, Tanner CM, Brundin P. Parkinson Disease Epidemiology, Pathology, Genetics, and Pathophysiology. Clin Geriatr Med. 2020;36(1):1-12.
11. Hughes AJ, Daniel SE, Blankson S, Lees AJ. A clinicopathologic study of 100 cases of Parkinson's disease. Arch Neurol. 1993;50(2):140-8.
12. Deloitte AE. Living with Parkinson's Disease: An updated economic analysis 2014. 2015.
13. Jankovic J. Parkinson's disease: clinical features and diagnosis. J Neurol Neurosurg Psychiatry. 2008;79(4):368-76.
14. Varadi C. Clinical Features of Parkinson's Disease: The Evolution of Critical Symptoms. Biology (Basel). 2020;9(5).
15. Postuma RB, Berg D, Stern M, Poewe W, Olanow CW, Oertel W, et al. MDS clinical diagnostic criteria for Parkinson's disease. Mov Disord. 2015;30(12):1591-601.
16. Schapira AHV, Chaudhuri KR, Jenner P. Non-motor features of Parkinson disease. Nat Rev Neurosci. 2017;18(7):435-50.
17. Haehner A, Boesveldt S, Berendse HW, Mackay-Sim A, Fleischmann J, Silburn PA, et al. Prevalence of smell loss in Parkinson's disease – A multicenter study. Parkinsonism & related disorders. 2009;15(7):490-4.
18. Reijnders JSAM, Ehrt U, Weber WEJ, Aarsland D, Leentjens AFG. A systematic review of prevalence studies of depression in Parkinson's disease. Movement disorders. 2008;23(2):183-9.
19. Nègre-Pagès L, Regragui W, Bouhassira D, Grandjean H, Rascol O. Chronic pain in Parkinson's disease: The cross-sectional French DoPaMiP survey. Movement disorders. 2008;23(10):1361-9.

20. Hely MA, Reid WGJ, Adena MA, Halliday GM, Morris JGL. The Sydney multicenter study of Parkinson's disease: The inevitability of dementia at 20 years. Movement disorders. 2008;23(6):837-44.
21. Mahlknecht P, Seppi K, Poewe W. The Concept of Prodromal Parkinson's Disease. Journal of Parkinson's disease. 2015;5(4):681-97.
22. Poewe W, Seppi K, Tanner CM, Halliday GM, Brundin P, Volkmann J, et al. Parkinson disease. Nat Rev Dis Primers. 2017;3:17013.
23. Gaenslen A, Swid I, Liepelt-Scarfone I, Godau J, Berg D. The patients' perception of prodromal symptoms before the initial diagnosis of Parkinson's disease. Mov Disord. 2011;26(4):653-8.
24. Pont-Sunyer C, Hotter A, Gaig C, Seppi K, Compta Y, Katzenschlager R, et al. The Onset of Nonmotor Symptoms in Parkinson's disease (The ONSET PD Study). Movement Disorders. 2015;30(2):229-37.
25. Braak H, Del Tredici K, Rüb U, de Vos RA, Jansen Steur EN, Braak E. Staging of brain pathology related to sporadic Parkinson's disease. Neurobiol Aging. 2003;24(2):197-211.
26. Dickson DW. Parkinson's disease and parkinsonism: neuropathology. Cold Spring Harb Perspect Med. 2012;2(8).
27. Giguère N, Burke Nanni S, Trudeau L-E. On Cell Loss and Selective Vulnerability of Neuronal Populations in Parkinson's Disease. Frontiers in Neurology. 2018;9.
28. Pedersen KM, Marner L, Pakkenberg H, Pakkenberg B. No global loss of neocortical neurons in parkinson's disease: A quantitative stereological study. Movement Disorders. 2005;20(2):164-71.
29. Greffard S, Verny M, Bonnet AM, Seilhean D, Hauw JJ, Duyckaerts C. A stable proportion of Lewy body bearing neurons in the substantia nigra suggests a model in which the Lewy body causes neuronal death. Neurobiol Aging. 2010;31(1):99-103.
30. Wakabayashi K, Tanji K, Odagiri S, Miki Y, Mori F, Takahashi H. The Lewy Body in Parkinson's Disease and Related Neurodegenerative Disorders. Molecular neurobiology. 2013;47(2):495-508.
31. Leverenz JB, Umar I, Wang Q, Montine TJ, McMillan PJ, Tsuang DW, et al. Proteomic identification of novel proteins in cortical lewy bodies. Brain Pathol. 2007;17(2):139-45.
32. Jakes R, Spillantini MG, Goedert M. Identification of two distinct synucleins from human brain. FEBS letters. 1994;345(1):27-32.
33. Mehra S, Sahay S, Maji SK. α-Synuclein misfolding and aggregation: Implications in Parkinson's disease pathogenesis. Biochimica et biophysica acta Proteins and proteomics. 2019;1867(10):890-908.
34. Bungeroth M, Appenzeller S, Regulin A, Völker W, Lorenzen I, Grötzinger J, et al. Differential aggregation properties of alpha-synuclein isoforms. Neurobiology of aging. 2014;35(8):1913-9.
35. Calabresi P, Di Lazzaro G, Marino G, Campanelli F, Ghiglieri V. Advances in understanding the function of alpha-synuclein: implications for Parkinson's disease. Brain. 2023;146(9):3587-97.

36. Eliezer D, Kutluay E, Bussell JR, Browne G. Conformational properties of alpha-synuclein in its free and lipid-associated states. Journal of molecular biology. 2001;307(4):1061-73.
37. Davidson WS, Jonas A, Clayton DF, George JM. Stabilization of α-Synuclein Secondary Structure upon Binding to Synthetic Membranes*. Journal of Biological Chemistry. 1998;273(16):9443-9.
38. Waxman EA, Mazzulli JR, Giasson BI. Characterization of Hydrophobic Residue Requirements for α-Synuclein Fibrillization. Biochemistry (Easton). 2009;48(40):9427-36.
39. Burré J, Sharma M, Tsetsenis T, Buchman V, Etherton MR, Südhof TC. Alpha-synuclein promotes SNARE-complex assembly in vivo and in vitro. Science. 2010;329(5999):1663-7.
40. Kim TD, Paik SR, Yang CH. Structural and functional implications of C-terminal regions of α-synuclein. Biochemistry. 2002;41(46):13782-90.
41. Tseng E, Rowell WJ, Glenn O-C, Hon T, Barrera J, Kujawa S, et al. The Landscape of SNCA Transcripts Across Synucleinopathies: New Insights From Long Reads Sequencing Analysis. Frontiers in Genetics. 2019;10(584).
42. Li A, Rastegar C, Mao X. α-Synuclein Conformational Plasticity: Physiologic States, Pathologic Strains, and Biotechnological Applications. Biomolecules. 2022;12(7).
43. Sagredo GT, Tanglay O, Shahdadpuri S, Fu Y, Halliday GM. α-Synuclein levels in Parkinson's disease - Cell types and forms that contribute to pathogenesis. Exp Neurol. 2024;379:114887.
44. Bigi A, Cascella R, Cecchi C. α-Synuclein oligomers and fibrils: partners in crime in synucleinopathies. Neural Regen Res. 2023;18(11):2332-42.
45. Baba M, Nakajo S, Tu PH, Tomita T, Nakaya K, Lee VM, et al. Aggregation of alpha-synuclein in Lewy bodies of sporadic Parkinson's disease and dementia with Lewy bodies. Am J Pathol. 1998;152(4):879-84.
46. Spillantini MG, Crowther RA, Jakes R, Hasegawa M, Goedert M. α-Synuclein in filamentous inclusions of Lewy bodies from Parkinson’s disease and dementia with Lewy bodies. Proceedings of the National Academy of Sciences. 1998;95(11):6469-73.
47. Shahmoradian SH, Lewis AJ, Genoud C, Hench J, Moors TE, Navarro PP, et al. Lewy pathology in Parkinson’s disease consists of crowded organelles and lipid membranes. Nature Neuroscience. 2019;22(7):1099-109.
48. Burré J, Sharma M, Südhof TC. Cell Biology and Pathophysiology of α-Synuclein. Cold Spring Harb Perspect Med. 2018;8(3).
49. Hasegawa M, Fujiwara H, Nonaka T, Wakabayashi K, Takahashi H, Lee VM, et al. Phosphorylated alpha-synuclein is ubiquitinated in alpha-synucleinopathy lesions. J Biol Chem. 2002;277(50):49071-6.
50. Anderson JP, Walker DE, Goldstein JM, de Laat R, Banducci K, Caccavello RJ, et al. Phosphorylation of Ser-129 is the dominant pathological modification of alpha-synuclein in familial and sporadic Lewy body disease. J Biol Chem. 2006;281(40):29739-52.

51. Fares MB, Jagannath S, Lashuel HA. Reverse engineering Lewy bodies: how far have we come and how far can we go? Nature Reviews Neuroscience. 2021;22(2):111-31.
52. Altay MF, Kumar ST, Burtscher J, Jagannath S, Strand C, Miki Y, et al. Development and validation of an expanded antibody toolset that captures alpha-synuclein pathological diversity in Lewy body diseases. NPJ Parkinsons Dis. 2023;9(1):161.
53. Fujiwara H, Hasegawa M, Dohmae N, Kawashima A, Masliah E, Goldberg MS, et al. alpha-Synuclein is phosphorylated in synucleinopathy lesions. Nat Cell Biol. 2002;4(2):160-4.
54. Waxman EA, Giasson BI. Specificity and Regulation of Casein Kinase-Mediated Phosphorylation of α-Synuclein. Journal of Neuropathology & Experimental Neurology. 2008;67(5):402-16.
55. Sonustun B, Altay MF, Strand C, Ebanks K, Hondhamuni G, Warner TT, et al. Pathological Relevance of Post-Translationally Modified Alpha-Synuclein (pSer87, pSer129, nTyr39) in Idiopathic Parkinson's Disease and Multiple System Atrophy. Cells. 2022;11(5).
56. Choi SG, Tittle T, Garcia-Prada D, Kordower JH, Melki R, Killinger BA. Alpha-synuclein aggregates are phosphatase resistant. Acta Neuropathol Commun. 2024;12(1):84.
57. Goldman JE, Yen SH, Chiu FC, Peress NS. Lewy bodies of Parkinson's disease contain neurofilament antigens. Science. 1983;221(4615):1082-4.
58. Kuzuhara S, Mori H, Izumiyama N, Yoshimura M, Ihara Y. Lewy bodies are ubiquitinated. A light and electron microscopic immunocytochemical study. Acta Neuropathol. 1988;75(4):345-53.
59. Lowe J, Blanchard A, Morrell K, Lennox G, Reynolds L, Billett M, et al. Ubiquitin is a common factor in intermediate filament inclusion bodies of diverse type in man, including those of Parkinson's disease, Pick's disease, and Alzheimer's disease, as well as Rosenthal fibres in cerebellar astrocytomas, cytoplasmic bodies in muscle, and mallory bodies in alcoholic liver disease. J Pathol. 1988;155(1):9-15.
60. Kuusisto E, Salminen A, Alafuzoff I. Ubiquitin-binding protein p62 is present in neuronal and glial inclusions in human tauopathies and synucleinopathies. Neuroreport. 2001;12(10):2085-90.
61. Zatloukal K, Stumptner C, Fuchsbichler A, Heid H, Schnoelzer M, Kenner L, et al. p62 Is a common component of cytoplasmic inclusions in protein aggregation diseases. Am J Pathol. 2002;160(1):255-63.
62. Moors TE, Milovanovic D. Defining a Lewy Body: Running Up the Hill of Shifting Definitions and Evolving Concepts. J Parkinsons Dis. 2024;14(1):17-33.
63. Gómez-Tortosa E, Newell K, Irizarry MC, Sanders JL, Hyman BT. alpha-Synuclein immunoreactivity in dementia with Lewy bodies: morphological staging and comparison with ubiquitin immunostaining. Acta Neuropathol. 2000;99(4):352-7.
64. Kuusisto E, Parkkinen L, Alafuzoff I. Morphogenesis of Lewy bodies: dissimilar incorporation of alpha-synuclein, ubiquitin, and p62. J Neuropathol Exp Neurol. 2003;62(12):1241-53.

65. Katsuse O, Iseki E, Marui W, Kosaka K. Developmental stages of cortical Lewy bodies and their relation to axonal transport blockage in brains of patients with dementia with Lewy bodies. J Neurol Sci. 2003;211(1-2):29-35.
66. Goedert M, Spillantini MG, Del Tredici K, Braak H. 100 years of Lewy pathology. Nature Reviews Neurology. 2013;9(1):13-24.
67. Braak H, Ghebremedhin E, Rüb U, Bratzke H, Del Tredici K. Stages in the development of Parkinson's disease-related pathology. Cell and Tissue Research. 2004;318(1):121-34.
68. Milber JM, Noorigian JV, Morley JF, Petrovitch H, White L, Ross GW, et al. Lewy pathology is not the first sign of degeneration in vulnerable neurons in Parkinson disease. Neurology. 2012;79(24):2307-14.
69. Chu Y, Hirst WD, Federoff HJ, Harms AS, Stoessl AJ, Kordower JH. Nigrostriatal tau pathology in parkinsonism and Parkinson's disease. Brain. 2024;147(2):444-57.
70. McGregor MM, Nelson AB. Circuit Mechanisms of Parkinson's Disease. Neuron. 2019;101(6):1042-56.
71. Shulman JM, De Jager PL, Feany MB. Parkinson's disease: genetics and pathogenesis. Annu Rev Pathol. 2011;6:193-222.
72. Blauwendraat C, Nalls MA, Singleton AB. The genetic architecture of Parkinson's disease. Lancet neurology. 2020;19(2):170-8.
73. Funayama M, Nishioka K, Li Y, Hattori N. Molecular genetics of Parkinson's disease: Contributions and global trends. Journal of Human Genetics. 2023;68(3):125-30.
74. Morris HR, Spillantini MG, Sue CM, Williams-Gray CH. The pathogenesis of Parkinson's disease. The Lancet. 2024;403(10423):293-304.
75. Zhang Y, Sloan SA, Clarke LE, Caneda C, Plaza CA, Blumenthal PD, et al. Purification and Characterization of Progenitor and Mature Human Astrocytes Reveals Transcriptional and Functional Differences with Mouse. Neuron. 2016;89(1):37-53.
76. Polymeropoulos MH, Lavedan C, Stenroos ES, Chandrasekharappa S, Athanassiadou A, Papapetropoulos T, et al. Mutation in the α-synuclein gene identified in families with Parkinson's disease. Science (American Association for the Advancement of Science). 1997;276(5321):2045-7.
77. Brás J, Gibbons E, Guerreiro R. Genetics of synucleins in neurodegenerative diseases. Acta Neuropathologica. 2021;141(4):471-90.
78. Whittaker H, Qui Y, Bettencourt C, Houlden H. Multiple system atrophy: Genetic risks and alpha-synuclein mutations. F1000Research. 2017;6:2072.
79. Polymeropoulos MH, Higgins JJ, Lazzarini AM, Nussbaum RL, Duvoisin RC, Golbe LI, et al. Mapping of a Gene for Parkinson's Disease to Chromosome 4q21-q23. Science (American Association for the Advancement of Science). 1996;274(5290):1197-9.
80. Golbe LI, Lazzarini AM, Duvoisin RC, Iorio GD, Sanges G, Bonavita V, et al. Clinical genetic analysis of Parkinson's disease in the contursi kindred. Annals of neurology. 1996;40(5):767-75.

81. Bostantjopoulou S, Katsarou Z, Papadimitriou A, Veletza V, Hatzigeorgiou G, Lees A. Clinical features of parkinsonian patients with the α-synuclein (G209A) mutation. Movement disorders. 2001;16(6):1007-13.
82. Spira PJ, Sharpe DM, Halliday G, Cavanagh J, Nicholson GA. Clinical and pathological features of a parkinsonian syndrome in a family with an Ala53Thr α-synuclein mutation. Annals of neurology. 2001;49(3):313-9.
83. Kasten M, Klein C. The many faces of alpha-synuclein mutations. Movement disorders. 2013;28(6):697-701.
84. Papadimitriou D, Antonelou R, Miligkos M, Maniati M, Papagiannakis N, Bostantjopoulou S, et al. Motor and Nonmotor Features of Carriers of the p.A53T Alpha-Synuclein Mutation: A Longitudinal Study. Movement Disorders. 2016;31(8):1226-30.
85. Krüger R, Kuhn W, Müller T, Woitalla D, Graeber M, Kösel S, et al. Ala30Pro mutation in the gene encoding alpha-synuclein in Parkinson's disease. Nature genetics. 1998;18(2):106-8.
86. Zarranz JJ, Alegre J, Gómez-Esteban JC, Lezcano E, Ros R, Ampuero I, et al. The new mutation, E46K, of α-synuclein causes parkinson and Lewy body dementia. Annals of neurology. 2004;55(2):164-73.
87. Appel-Cresswell S, Vilarino-Guell C, Encarnacion M, Sherman H, Yu I, Shah B, et al. Alpha-synuclein p.H50Q, a novel pathogenic mutation for Parkinson's disease. Movement disorders. 2013;28(6):811-3.
88. Lesage S, Anheim M, Letournel F, Bousset L, Honoré A, Rozas N, et al. G51D α-synuclein mutation causes a novel parkinsonian-pyramidal syndrome. Ann Neurol. 2013;73(4):459-71.
89. Kruger R, Kuhn W, Leenders KL, Sprengelmeyer R, Muller T, Woitalla D, et al. Familial parkinsonism with synuclein pathology - Clinical and PET studies of A30P mutation carriers. Neurology. 2001;56(10):1355-62.
90. Seidel K, Schöls L, Nuber S, Petrasch-Parwez E, Gierga K, Wszolek Z, et al. First appraisal of brain pathology owing to A30P mutant alpha-synuclein. Ann Neurol. 2010;67(5):684-9.
91. Proukakis C, Dudzik CG, Brier T, MacKay DS, Cooper JM, Millhauser GL, et al. A novel α-synuclein missense mutation in Parkinson disease. Neurology. 2013;80(11):1062-4.
92. Kiely AP, Ling H, Asi YT, Kara E, Proukakis C, Schapira AH, et al. Distinct clinical and neuropathological features of G51D SNCA mutation cases compared with SNCA duplication and H50Q mutation. Molecular neurodegeneration. 2015;10:41-.
93. Ibáñez P, Bonnet AM, Débarges B, Lohmann E, Tison F, Pollak P, et al. Causal relation between alpha-synuclein gene duplication and familial Parkinson's disease. The Lancet (British edition). 2004;364(9440):1169-71.
94. Singleton AB, Farrer M, Lincoln S, Crawley A, Hanson M, Maraganore D, et al. α-Synuclein Locus Triplication Causes Parkinson's Disease. Science (American Association for the Advancement of Science). 2003;302(5646):841-.

95. Kalinderi K, Bostantjopoulou S, Fidani L. The genetic background of Parkinson's disease: current progress and future prospects. Acta neurologica Scandinavica. 2016;134(5):314-26.
96. Ross OA, Braithwaite AT, Skipper LM, Kachergus J, Hulihan MM, Middleton FA, et al. Genomic investigation of α-synuclein multiplication and parkinsonism. Annals of neurology. 2008;63(6):743-50.
97. Farrer M, Kachergus J, Forno L, Lincoln S, Wang D-S, Hulihan M, et al. Comparison of kindreds with parkinsonism and α-synuclein genomic multiplications. Annals of neurology. 2004;55(2):174-9.
98. Ikeuchi T, Kakita A, Shiga A, Kasuga K, Kaneko H, Tan CF, et al. Patients homozygous and heterozygous for SNCA duplication in a family with parkinsonism and dementia. Arch Neurol. 2008;65(4):514-9.
99. Nishioka K, Ross OA, Ishii K, Kachergus JM, Ishiwata K, Kitagawa M, et al. Expanding the clinical phenotype of SNCA duplication carriers. Mov Disord. 2009;24(12):1811-9.
100. Muenter MD, Forno LS, Hornykiewicz O, Kish SJ, Maraganore DM, Caselli RJ, et al. Hereditary form of parkinsonism—dementia. Annals of Neurology. 1998;43(6):768-81.
101. Papapetropoulos S, Paschalis C, Athanassiadou A, Papadimitriou A, Ellul J, Polymeropoulos MH, et al. Clinical phenotype in patients with alpha-synuclein Parkinson's disease living in Greece in comparison with patients with sporadic Parkinson's disease. J Neurol Neurosurg Psychiatry. 2001;70(5):662-5.
102. Golbe LI, Di Iorio G, Bonavita V, Miller DC, Duvoisin RC. A large kindred with autosomal dominant Parkinson's disease. Ann Neurol. 1990;27(3):276-82.
103. Duda JE, Giasson BI, Mabon ME, Miller DC, Golbe LI, Lee VM, et al. Concurrence of alpha-synuclein and tau brain pathology in the Contursi kindred. Acta Neuropathol. 2002;104(1):7-11.
104. Kotzbauer PT, Giasson BI, Kravitz AV, Golbe LI, Mark MH, Trojanowski JQ, et al. Fibrillization of α-synuclein and tau in familial Parkinson's disease caused by the A53T α-synuclein mutation. Experimental Neurology. 2004;187(2):279-88.
105. Markopoulou K, Dickson DW, McComb RD, Wszolek ZK, Katechalidou L, Avery L, et al. Clinical, neuropathological and genotypic variability in SNCA A53T familial Parkinson's disease. Variability in familial Parkinson's disease. Acta Neuropathol. 2008;116(1):25-35.
106. Nishioka K, Hashizume Y, Takanashi M, Daida K, Li Y, Yoshino H, et al. Pathological findings in a patient with alpha-synuclein p.A53T and familial Parkinson's disease. Parkinsonism Relat Disord. 2020;81:183-7.
107. Pimentel MMG, Rodrigues FC, Leite MAA, Campos Júnior M, Rosso AL, Nicaretta DH, et al. Parkinson disease: α-synuclein mutational screening and new clinical insight into the p.E46K mutation. Parkinsonism & Related Disorders. 2015;21(6):586-9.
108. Senkevich K, Miliukhina I, Zhuravlev A, Shumilova M, Beletskaia M, Skvortsova T, et al. Autosomal Dominant Parkinson's Disease Caused by SNCA p.E46K Mutation in a Family with Russian Ancestry. Mov Disord. 2024;39(8):1424-5.

109. Nishioka K, Hayashi S, Farrer MJ, Singleton AB, Yoshino H, Imai H, et al. Clinical heterogeneity of α-synuclein gene duplication in Parkinson's disease. Annals of Neurology. 2006;59(2):298-309.
110. Wakabayashi K, Hayashi S, Ishikawa A, Hayashi T, Okuizumi K, Tanaka H, et al. Autosomal dominant diffuse Lewy body disease. Acta Neuropathologica. 1998;96(2):207-10.
111. Chartier-Harlin M-C, Kachergus J, Roumier C, Mouroux V, Douay X, Lincoln S, et al. A-synuclein locus duplication as a cause of familial Parkinson's disease. The Lancet (British edition). 2004;364(9440):1167.
112. Obi T, Nishioka K, Ross OA, Terada T, Yamazaki K, Sugiura A, et al. Clinicopathologic study of a SNCA gene duplication patient with Parkinson disease and dementia. Neurology. 2008;70(3):238-41.
113. Uchiyama T, Ikeuchi T, Ouchi Y, Sakamoto M, Kasuga K, Shiga A, et al. Prominent psychiatric symptoms and glucose hypometabolism in a family with a SNCA duplication. Neurology. 2008;71(16):1289-91.
114. Ahn TB, Kim SY, Kim JY, Park SS, Lee DS, Min HJ, et al. alpha-Synuclein gene duplication is present in sporadic Parkinson disease. Neurology. 2008;70(1):43-9.
115. Shin CW, Kim HJ, Park SS, Kim SY, Kim JY, Jeon BS. Two Parkinson's disease patients with α-synuclein gene duplication and rapid cognitive decline. Movement Disorders. 2010;25(7):957-9.
116. Waters CH, Miller CA. Autosomal dominant Lewy body parkinsonism in a four-generation family. Annals of Neurology. 1994;35(1):59-64.
117. Gwinn-Hardy K, Mehta ND, Farrer M, Maraganore D, Muenter M, Yen SH, et al. Distinctive neuropathology revealed by alpha-synuclein antibodies in hereditary parkinsonism and dementia linked to chromosome 4p. Acta Neuropathol. 2000;99(6):663-72.
118. Sekine T, Kagaya H, Funayama M, Li Y, Yoshino H, Tomiyama H, et al. Clinical course of the first Asian family with Parkinsonism related to SNCA triplication. Movement Disorders. 2010;25(16):2871-5.
119. Li J, Uversky VN, Fink AL. Effect of Familial Parkinson's Disease Point Mutations A30P and A53T on the Structural Properties, Aggregation, and Fibrillation of Human α-Synuclein. Biochemistry (Easton). 2001;40(38):11604-13.
120. Sun Y, Hou S, Zhao K, Long H, Liu Z, Gao J, et al. Cryo-EM structure of full-length α-synuclein amyloid fibril with Parkinson's disease familial A53T mutation. Cell Res. 2020;30(4):360-2.
121. Mohite GM, Navalkar A, Kumar R, Mehra S, Das S, Gadhe LG, et al. The Familial α-Synuclein A53E Mutation Enhances Cell Death in Response to Environmental Toxins Due to a Larger Population of Oligomers. Biochemistry. 2018;57(33):5014-28.
122. Mohite GM, Kumar R, Panigrahi R, Navalkar A, Singh N, Datta D, et al. Comparison of Kinetics, Toxicity, Oligomer Formation, and Membrane Binding Capacity of α-Synuclein Familial Mutations at the A53 Site, Including the Newly Discovered A53V Mutation. Biochemistry. 2018;57(35):5183-7.
123. Conway KA, Lee SJ, Rochet JC, Ding TT, Williamson RE, Lansbury JPT. Acceleration of Oligomerization, Not Fibrillization, Is a Shared Property of Both α -

Synuclein Mutations Linked to Early-Onset Parkinson's Disease: Implications for Pathogenesis and Therapy. Proceedings of the National Academy of Sciences - PNAS. 2000;97(2):571-6.
124. Fredenburg RA, Rospigliosi C, Meray RK, Kessler JC, Lashuel HA, Eliezer D, et al. The Impact of the E46K Mutation on the Properties of α-Synuclein in Its Monomeric and Oligomeric States. Biochemistry (Easton). 2007;46(24):7107-18.
125. Khalaf O, Fauvet B, Oueslati A, Dikiy I, Mahul-Mellier A-L, Ruggeri FS, et al. The H50Q Mutation Enhances α-Synuclein Aggregation, Secretion, and Toxicity. The Journal of biological chemistry. 2014;289(32):21856-76.
126. Fares M-B, Ait-Bouziad N, Dikiy I, Mbefo MK, Jovičić A, Kiely A, et al. The novel Parkinson's disease linked mutation G51D attenuates in vitro aggregation and membrane binding of α-synuclein, and enhances its secretion and nuclear localization in cells. Human molecular genetics. 2014;23(17):4491-509.
127. Sahay S, Ghosh D, Dwivedi S, Anoop A, Mohite GM, Kombrabail M, et al. Familial Parkinson Disease-associated Mutations Alter the Site-specific Microenvironment and Dynamics of α-Synuclein. The Journal of biological chemistry. 2015;290(12):7804-22.
128. Bertoncini CW, Jung Y-S, Fernandez CO, Hoyer W, Griesinger C, Jovin TM, et al. Release of long-range tertiary interactions potentiates aggregation of natively unstructured α-synuclein. Proceedings of the National Academy of Sciences of the United States of America. 2005;102(5):1430.
129. Bertoncini CW, Fernandez CO, Griesinger C, Jovin TM, Zweckstetter M. Familial Mutants of α-Synuclein with Increased Neurotoxicity Have a Destabilized Conformation*. Journal of Biological Chemistry. 2005;280(35):30649-52.
130. Byers B, Cord B, Nguyen HN, Schüle B, Fenno L, Lee PC, et al. SNCA triplication Parkinson's patient's iPSC-derived DA neurons accumulate α-synuclein and are susceptible to oxidative stress. PloS one. 2011;6(11):e26159-e.
131. Diao X, Wang F, Becerra-Calixto A, Soto C, Mukherjee A. Induced Pluripotent Stem Cell-Derived Dopaminergic Neurons from Familial Parkinson's Disease Patients Display α-Synuclein Pathology and Abnormal Mitochondrial Morphology. Cells. 2021;10(9).
132. Nemani VM, Lu W, Berge V, Nakamura K, Onoa B, Lee MK, et al. Increased expression of alpha-synuclein reduces neurotransmitter release by inhibiting synaptic vesicle reclustering after endocytosis. Neuron. 2010;65(1):66-79.
133. Kouroupi G, Taoufik E, Vlachos IS, Tsioras K, Antoniou N, Papastefanaki F, et al. Defective synaptic connectivity and axonal neuropathology in a human iPSC-based model of familial Parkinson's disease. Proc Natl Acad Sci U S A. 2017;114(18):E3679-e88.
134. Ryan T, Bamm VV, Stykel MG, Coackley CL, Humphries KM, Jamieson-Williams R, et al. Cardiolipin exposure on the outer mitochondrial membrane modulates α-synuclein. Nat Commun. 2018;9(1):817.
135. Lee MK, Stirling W, Xu Y, Xu X, Qui D, Mandir AS, et al. Human alpha-synuclein-harboring familial Parkinson's disease-linked Ala-53 --> Thr mutation causes

neurodegenerative disease with alpha-synuclein aggregation in transgenic mice. Proc Natl Acad Sci U S A. 2002;99(13):8968-73.
136. Giasson BI, Duda JE, Quinn SM, Zhang B, Trojanowski JQ, Lee VMY. Neuronal α-Synucleinopathy with Severe Movement Disorder in Mice Expressing A53T Human α-Synuclein. Neuron. 2002;34(4):521-33.
137. Martin LJ, Pan Y, Price AC, Sterling W, Copeland NG, Jenkins NA, et al. Parkinson's disease alpha-synuclein transgenic mice develop neuronal mitochondrial degeneration and cell death. J Neurosci. 2006;26(1):41-50.
138. Ip CW, Klaus LC, Karikari AA, Visanji NP, Brotchie JM, Lang AE, et al. AAV1/2-induced overexpression of A53T-α-synuclein in the substantia nigra results in degeneration of the nigrostriatal system with Lewy-like pathology and motor impairment: a new mouse model for Parkinson's disease. Acta Neuropathol Commun. 2017;5(1):11.
139. Henrich MT, Geibl FF, Lee B, Chiu WH, Koprich JB, Brotchie JM, et al. A53T-α-synuclein overexpression in murine locus coeruleus induces Parkinson's disease-like pathology in neurons and glia. Acta Neuropathol Commun. 2018;6(1):39.
140. Okuda S, Uemura N, Sawamura M, Taguchi T, Ikuno M, Uemura MT, et al. Rapid Induction of Dopaminergic Neuron Loss Accompanied by Lewy Body-Like Inclusions in A53T BAC-SNCA Transgenic Mice. Neurotherapeutics. 2022;19(1):289-304.
141. Choi B-K, Choi M-G, Kim J-Y, Yang Y, Lai Y, Kweon D-H, et al. Large α-synuclein oligomers inhibit neuronal SNARE-mediated vesicle docking. Proceedings of the National Academy of Sciences of the United States of America. 2013;110(10):4087-92.
142. Burré J, Sharma M, Südhof TC. Systematic mutagenesis of α-synuclein reveals distinct sequence requirements for physiological and pathological activities. The Journal of neuroscience : the official journal of the Society for Neuroscience. 2012;32(43):15227-42.
143. Devi L, Raghavendran V, Prabhu BM, Avadhani NG, Anandatheerthavarada HK. Mitochondrial Import and Accumulation of α-Synuclein Impair Complex I in Human Dopaminergic Neuronal Cultures and Parkinson Disease Brain. The Journal of biological chemistry. 2008;283(14):9089-100.
144. Choi ML, Chappard A, Singh BP, Maclachlan C, Rodrigues M, Fedotova EI, et al. Pathological structural conversion of α-synuclein at the mitochondria induces neuronal toxicity. Nat Neurosci. 2022;25(9):1134-48.
145. Chinta SJ, Mallajosyula JK, Rane A, Andersen JK. Mitochondrial alpha-synuclein accumulation impairs complex I function in dopaminergic neurons and results in increased mitophagy in vivo. Neuroscience letters. 2010;486(3):235-9.
146. Choubey V, Safiulina D, Vaarmann A, Cagalinec M, Wareski P, Kuum M, et al. Mutant A53T alpha-synuclein induces neuronal death by increasing mitochondrial autophagy. J Biol Chem. 2011;286(12):10814-24.
147. Chen L, Xie Z, Turkson S, Zhuang X. A53T human α-synuclein overexpression in transgenic mice induces pervasive mitochondria macroautophagy defects preceding dopamine neuron degeneration. J Neurosci. 2015;35(3):890-905.

148. Xilouri M, Brekk OR, Stefanis L. Alpha-synuclein and Protein Degradation Systems: a Reciprocal Relationship. Molecular neurobiology. 2013;47(2):537-51.
149. Cuervo AM, Stefanis L, Fredenburg R, Lansbury PT, Sulzer D. Impaired degradation of mutant alpha-synuclein by chaperone-mediated autophagy. Science. 2004;305(5688):1292-5.
150. McKinnon C, De Snoo ML, Gondard E, Neudorfer C, Chau H, Ngana SG, et al. Early-onset impairment of the ubiquitin-proteasome system in dopaminergic neurons caused by α-synuclein. Acta Neuropathologica Communications. 2020;8(1):17.
151. Krzisch M, Yuan B, Chen W, Osaki T, Fu D, Garrett-Engele CM, et al. The A53T Mutation in α-Synuclein Enhances Proinflammatory Activation in Human Microglia Upon Inflammatory Stimulus. Biological Psychiatry. 2024.
152. Zhang W, Dallas S, Zhang D, Guo J-P, Pang H, Wilson B, et al. Microglial PHOX and Mac-1 are essential to the enhanced dopaminergic neurodegeneration elicited by A30P and A53T mutant alpha-synuclein. Glia. 2007;55(11):1178-88.
153. Hoenen C, Gustin A, Birck C, Kirchmeyer M, Beaume N, Felten P, et al. Alpha-Synuclein Proteins Promote Pro-Inflammatory Cascades in Microglia: Stronger Effects of the A53T Mutant. PLoS One. 2016;11(9):e0162717.
154. Guan Y, Zhao X, Liu F, Yan S, Wang Y, Du C, et al. Pathogenic Mutations Differentially Regulate Cell-to-Cell Transmission of α-Synuclein. Frontiers in Cellular Neuroscience. 2020;14.
155. Roodveldt C, Labrador-Garrido A, Gonzalez-Rey E, Fernandez-Montesinos R, Caro M, Lachaud CC, et al. Glial Innate Immunity Generated by Non-Aggregated Alpha-Synuclein in Mouse: Differences between Wild-type and Parkinson's Disease-Linked Mutants. PLOS ONE. 2010;5(10):e13481.
156. Martin I, Kim JW, Dawson VL, Dawson TM. LRRK2 pathobiology in Parkinson's disease. Journal of neurochemistry. 2014;131(5):554-65.
157. Myasnikov A, Zhu H, Hixson P, Xie B, Yu K, Pitre A, et al. Structural analysis of the full-length human LRRK2. Cell. 2021;184(13):3519-27.e10.
158. Biskup S, Moore DJ, Celsi F, Higashi S, West AB, Andrabi SA, et al. Localization of LRRK2 to membranous and vesicular structures in mammalian brain. Ann Neurol. 2006;60(5):557-69.
159. Miklossy J, Arai T, Guo J-P, Klegeris A, Yu S, McGeer EG, et al. LRRK2 expression in normal and pathologic human brain and in human cell lines. Journal of neuropathology and experimental neurology. 2006;65(10):953-63.
160. Tolosa E, Vila M, Klein C, Rascol O. LRRK2 in Parkinson disease: challenges of clinical trials. Nature Reviews Neurology. 2020;16(2):97-107.
161. Gotthardt K, Weyand M, Kortholt A, Van Haastert PJM, Wittinghofer A. Structure of the Roc-COR domain tandem of C. tepidum, a prokaryotic homologue of the human LRRK2 Parkinson kinase. The EMBO journal. 2008;27(16):2239-49.
162. Greggio E, Zambrano I, Kaganovich A, Beilina A, Taymans JM, Daniëls V, et al. The Parkinson disease-associated leucine-rich repeat kinase 2 (LRRK2) is a dimer that undergoes intramolecular autophosphorylation. J Biol Chem. 2008;283(24):16906-14.

163. Berger Z, Smith KA, Lavoie MJ. Membrane localization of LRRK2 is associated with increased formation of the highly active LRRK2 dimer and changes in its phosphorylation. Biochemistry. 2010;49(26):5511-23.
164. Nguyen APT, Moore DJ. Understanding the GTPase Activity of LRRK2: Regulation, Function, and Neurotoxicity. Adv Neurobiol. 2017;14:71-88.
165. Biosa A, Trancikova A, Civiero L, Glauser L, Bubacco L, Greggio E, et al. GTPase activity regulates kinase activity and cellular phenotypes of Parkinson's disease-associated LRRK2. Human molecular genetics. 2013;22(6):1140-56.
166. Greggio E, Taymans J-M, Zhen EY, Ryder J, Vancraenenbroeck R, Beilina A, et al. The Parkinson's disease kinase LRRK2 autophosphorylates its GTPase domain at multiple sites. Biochemical and biophysical research communications. 2009;389(3):449-54.
167. Webber PJ, Smith AD, Sen S, Renfrow MB, Mobley JA, West AB. Autophosphorylation in the Leucine-Rich Repeat Kinase 2 (LRRK2) GTPase Domain Modifies Kinase and GTP-Binding Activities. Journal of molecular biology. 2011;412(1):94-110.
168. Liu Z, Mobley JA, DeLucas LJ, Kahn RA, West AB. LRRK2 autophosphorylation enhances its GTPase activity. FASEB J. 2016;30(1):336-47.
169. Mills RD, Mulhern TD, Cheng HC, Culvenor JG. Analysis of LRRK2 accessory repeat domains: prediction of repeat length, number and sites of Parkinson's disease mutations. Biochem Soc Trans. 2012;40(5):1086-9.
170. Funayama M, Hasegawa K, Kowa H, Saito M, Tsuji S, Obata F. A new locus for Parkinson's disease (PARK8) maps to chromosome 12p11.2-q13.1. Ann Neurol. 2002;51(3):296-301.
171. Paisán-Ruíz C, Jain S, Evans EW, Gilks WP, Simón J, van der Brug M, et al. Cloning of the Gene Containing Mutations that Cause PARK8-Linked Parkinson's Disease. Neuron. 2004;44(4):595-600.
172. Zimprich A, Biskup S, Leitner P, Lichtner P, Farrer M, Lincoln S, et al. Mutations in LRRK2 Cause Autosomal-Dominant Parkinsonism with Pleomorphic Pathology. Neuron. 2004;44(4):601-7.
173. Ito G, Utsunomiya-Tate N. Overview of the Impact of Pathogenic LRRK2 Mutations in Parkinson's Disease. Biomolecules. 2023;13(5).
174. Healy DG, Falchi M, O'Sullivan SS, Bonifati V, Durr A, Bressman S, et al. Phenotype, genotype, and worldwide genetic penetrance of LRRK2-associated Parkinson's disease: a case-control study. The Lancet Neurology. 2008;7(7):583-90.
175. Rajput A, Dickson DW, Robinson CA, Ross OA, Dächsel JC, Lincoln SJ, et al. Parkinsonism, Lrrk2 G2019S, and tau neuropathology. Neurology. 2006;67(8):1506-8.
176. Henderson MX, Sengupta M, Trojanowski JQ, Lee VMY. Alzheimer's disease tau is a prominent pathology in LRRK2 Parkinson's disease. Acta Neuropathol Commun. 2019;7(1):183.
177. Vinagre-Aragón A, Campo-Caballero D, Mondragón-Rezola E, Pardina-Vilella L, Hernandez Eguiazu H, Gorostidi A, et al. A More Homogeneous Phenotype in

Parkinson's Disease Related to R1441G Mutation in the LRRK2 Gene. Frontiers in Neurology. 2021;12(68).
178. Martí-Massó JF, Ruiz-Martínez J, Bolaño MJ, Ruiz I, Gorostidi A, Moreno F, et al. Neuropathology of Parkinson's disease with the R1441G mutation in LRRK2. Mov Disord. 2009;24(13):1998-2001.
179. Takanashi M, Funayama M, Matsuura E, Yoshino H, Li Y, Tsuyama S, et al. Isolated nigral degeneration without pathological protein aggregation in autopsied brains with LRRK2 p.R1441H homozygous and heterozygous mutations. Acta Neuropathol Commun. 2018;6(1):105.
180. Paisán-Ruíz C, Lang AE, Kawarai T, Sato C, Salehi-Rad S, Fisman GK, et al. LRRK2 gene in Parkinson disease: mutation analysis and case control association study. Neurology. 2005;65(5):696-700.
181. Di Fonzo A, Tassorelli C, De Mari M, Chien HF, Ferreira J, Rohé CF, et al. Comprehensive analysis of the LRRK2 gene in sixty families with Parkinson's disease. Eur J Hum Genet. 2006;14(3):322-31.
182. Giordana MT, D'Agostino C, Albani G, Mauro A, Di Fonzo A, Antonini A, et al. Neuropathology of Parkinson's disease associated with the LRRK2 Ile1371Val mutation. Mov Disord. 2007;22(2):275-8.
183. Aasly JO, Vilariño-Güell C, Dachsel JC, Webber PJ, West AB, Haugarvoll K, et al. Novel pathogenic LRRK2 p.Asn1437His substitution in familial Parkinson's disease. Mov Disord. 2010;25(13):2156-63.
184. Puschmann A, Englund E, Ross OA, Vilariño-Güell C, Lincoln SJ, Kachergus JM, et al. First neuropathological description of a patient with Parkinson's disease and LRRK2 p.N1437H mutation. Parkinsonism & related disorders. 2012;18(4):332-8.
185. Wszolek ZK, Pfeiffer RF, Tsuboi Y, Uitti RJ, McComb RD, Stoessl AJ, et al. Autosomal dominant parkinsonism associated with variable synuclein and tau pathology. Neurology. 2004;62(9):1619-22.
186. Mata IF, Kachergus JM, Taylor JP, Lincoln S, Aasly J, Lynch T, et al. Lrrk2 pathogenic substitutions in Parkinson's disease. Neurogenetics. 2005;6(4):171-7.
187. Zabetian CP, Samii A, Mosley AD, Roberts JW, Leis BC, Yearout D, et al. A clinic-based study of the LRRK2 gene in Parkinson disease yields new mutations. Neurology. 2005;65(5):741-4.
188. Wszolek ZK, Vieregge P, Uitti RJ, Gasser T, Yasuhara O, McGeer P, et al. German-Canadian family (family A) with parkinsonism, amyotrophy, and dementia - Longitudinal observations. Parkinsonism Relat Disord. 1997;3(3):125-39.
189. Khan NL, Jain S, Lynch JM, Pavese N, Abou-Sleiman P, Holton JL, et al. Mutations in the gene LRRK2 encoding dardarin (PARK8) cause familial Parkinson's disease: clinical, pathological, olfactory and functional imaging and genetic data. Brain. 2005;128(Pt 12):2786-96.
190. Lesage S, Ibanez P, Lohmann E, Pollak P, Tison F, Tazir M, et al. G2019S LRRK2 mutation in French and North African families with Parkinson's disease. Annals of Neurology. 2005;58(5):784-7.

191. Gilks WP, Abou-Sleiman PM, Gandhi S, Jain S, Singleton A, Lees AJ, et al. A common LRRK2 mutation in idiopathic Parkinson's disease. Lancet. 2005;365(9457):415-6.
192. Ross OA, Toft M, Whittle AJ, Johnson JL, Papapetropoulos S, Mash DC, et al. Lrrk2 and Lewy body disease. Ann Neurol. 2006;59(2):388-93.
193. Giasson BI, Covy JP, Bonini NM, Hurtig HI, Farrer MJ, Trojanowski JQ, et al. Biochemical and pathological characterization of Lrrk2. Ann Neurol. 2006;59(2):315-22.
194. Gaig C, Martí MJ, Ezquerra M, Rey MJ, Cardozo A, Tolosa E. G2019S LRRK2 mutation causing Parkinson's disease without Lewy bodies. J Neurol Neurosurg Psychiatry. 2007;78(6):626-8.
195. Gomez A, Ferrer I. Involvement of the cerebral cortex in Parkinson disease linked with G2019S LRRK2 mutation without cognitive impairment. Acta Neuropathol. 2010;120(2):155-67.
196. Marras C, Schüle B, Schuele B, Munhoz RP, Rogaeva E, Langston JW, et al. Phenotype in parkinsonian and nonparkinsonian LRRK2 G2019S mutation carriers. Neurology. 2011;77(4):325-33.
197. Poulopoulos M, Cortes E, Vonsattel J-PG, Fahn S, Waters C, Cote LJ, et al. Clinical and pathological characteristics of LRRK2 G2019S patients with PD. Journal of molecular neuroscience : MN. 2012;47(1):139-43.
198. Ruffmann C, Giaccone G, Canesi M, Bramerio M, Goldwurm S, Gambacorta M, et al. Atypical tauopathy in a patient with LRRK2-G2019S mutation and tremor-dominant Parkinsonism. Neuropathol Appl Neurobiol. 2012;38(4):382-6.
199. Ling H, Kara E, Bandopadhyay R, Hardy J, Holton J, Xiromerisiou G, et al. TDP-43 pathology in a patient carrying G2019S LRRK2 mutation and a novel p.Q124E MAPT. Neurobiol Aging. 2013;34(12):2889.e5-9.
200. Tomiyama H, Li Y, Funayama M, Hasegawa K, Yoshino H, Kubo S, et al. Clinicogenetic study of mutations in LRRK2 exon 41 in Parkinson's disease patients from 18 countries. Mov Disord. 2006;21(8):1102-8.
201. Hasegawa K, Stoessl AJ, Yokoyama T, Kowa H, Wszolek ZK, Yagishita S. Familial parkinsonism: study of original Sagamihara PARK8 (I2020T) kindred with variable clinicopathologic outcomes. Parkinsonism & related disorders. 2009;15(4):300-6.
202. Ujiie S, Hatano T, Kubo S, Imai S, Sato S, Uchihara T, et al. LRRK2 I2020T mutation is associated with tau pathology. Parkinsonism Relat Disord. 2012;18(7):819-23.
203. Guo L, Gandhi PN, Wang W, Petersen RB, Wilson-Delfosse AL, Chen SG. The Parkinson's disease-associated protein, leucine-rich repeat kinase 2 (LRRK2), is an authentic GTPase that stimulates kinase activity. Experimental cell research. 2007;313(16):3658-70.
204. Lewis PA, Greggio E, Beilina A, Jain S, Baker A, Cookson MR. The R1441C mutation of LRRK2 disrupts GTP hydrolysis. Biochemical and Biophysical Research Communications. 2007;357(3):668-71.

205. Li X, Tan YC, Poulose S, Olanow CW, Huang XY, Yue Z. Leucine-rich repeat kinase 2 (LRRK2)/PARK8 possesses GTPase activity that is altered in familial Parkinson's disease R1441C/G mutants. Journal of neurochemistry. 2007;103(1):238-47.
206. Liao J, Wu C-X, Burlak C, Zhang S, Sahm H, Wang M, et al. Parkinson disease-associated mutation R1441H in LRRK2 prolongs the "active state" of its GTPase domain. Proceedings of the National Academy of Sciences. 2014;111(11):4055.
207. West AB, Moore DJ, Choi C, Andrabi SA, Li X, Dikeman D, et al. Parkinson's disease-associated mutations in LRRK2 link enhanced GTP-binding and kinase activities to neuronal toxicity. Hum Mol Genet. 2007;16(2):223-32.
208. Wu C-X, Liao J, Park Y, Reed X, Engel VA, Hoang NC, et al. Parkinson's disease-associated mutations in the GTPase domain of LRRK2 impair its nucleotide-dependent conformational dynamics. Journal of Biological Chemistry. 2019;294(15):5907-13.
209. Xiong Y, Coombes CE, Kilaru A, Li X, Gitler AD, Bowers WJ, et al. GTPase activity plays a key role in the pathobiology of LRRK2. PLoS Genet. 2010;6(4):e1000902.
210. Greggio E, Jain S, Kingsbury A, Bandopadhyay R, Lewis P, Kaganovich A, et al. Kinase activity is required for the toxic effects of mutant LRRK2/dardarin. Neurobiol Dis. 2006;23(2):329-41.
211. Luzón-Toro B, de la Torre ER, Delgado A, Pérez-Tur J, Hilfiker S. Mechanistic insight into the dominant mode of the Parkinson's disease-associated G2019S LRRK2 mutation. Human molecular genetics. 2007;16(17):2031-9.
212. Kalogeropulou AF, Purlyte E, Tonelli F, Lange SM, Wightman M, Prescott AR, et al. Impact of 100 LRRK2 variants linked to Parkinson's disease on kinase activity and microtubule binding. Biochem J. 2022;479(17):1759-83.
213. West AB, Moore DJ, Biskup S, Bugayenko A, Smith WW, Ross CA, et al. Parkinson's Disease-Associated Mutations in Leucine-Rich Repeat Kinase 2 Augment Kinase Activity. Proceedings of the National Academy of Sciences - PNAS. 2005;102(46):16842-7.
214. Jaleel M, Nichols RJ, Deak M, Campbell DG, Gillardon F, Knebel A, et al. LRRK2 phosphorylates moesin at threonine-558: characterization of how Parkinson's disease mutants affect kinase activity. Biochemical journal. 2007;405(2):307-17.
215. Gloeckner CJ, Kinkl N, Schumacher A, Braun RJ, O'Neill E, Meitinger T, et al. The Parkinson disease causing LRRK2 mutation I2020T is associated with increased kinase activity. Human molecular genetics. 2006;15(2):223-32.
216. Nguyen APT, Tsika E, Kelly K, Levine N, Chen X, West AB, et al. Dopaminergic neurodegeneration induced by Parkinson's disease-linked G2019S LRRK2 is dependent on kinase and GTPase activity. Proceedings of the National Academy of Sciences. 2020;117(29):17296.
217. Dusonchet J, Kochubey O, Stafa K, Young JSM, Zufferey R, Moore DJ, et al. A rat model of progressive nigral neurodegeneration induced by the Parkinson's disease-associated G2019S mutation in LRRK2. The Journal of neuroscience. 2011;31(3):907-12.

218. Bieri G, Brahic M, Bousset L, Couthouis J, Kramer NJ, Ma R, et al. LRRK2 modifies α-syn pathology and spread in mouse models and human neurons. Acta Neuropathol. 2019;137(6):961-80.
219. Lubben N, Brynildsen JK, Webb CM, Li HL, Leyns CEG, Changolkar L, et al. LRRK2 kinase inhibition reverses G2019S mutation-dependent effects on tau pathology progression. Transl Neurodegener. 2024;13(1):13.
220. Sánchez-Danés A, Richaud-Patin Y, Carballo-Carbajal I, Jiménez-Delgado S, Caig C, Mora S, et al. Disease-specific phenotypes in dopamine neurons from human iPS-based models of genetic and sporadic Parkinson's disease. EMBO Mol Med. 2012;4(5):380-95.
221. Ho PW, Leung CT, Liu H, Pang SY, Lam CS, Xian J, et al. Age-dependent accumulation of oligomeric SNCA/α-synuclein from impaired degradation in mutant LRRK2 knockin mouse model of Parkinson disease: role for therapeutic activation of chaperone-mediated autophagy (CMA). Autophagy. 2020;16(2):347-70.
222. Orenstein SJ, Kuo SH, Tasset I, Arias E, Koga H, Fernandez-Carasa I, et al. Interplay of LRRK2 with chaperone-mediated autophagy. Nat Neurosci. 2013;16(4):394-406.
223. di Domenico A, Carola G, Calatayud C, Pons-Espinal M, Muñoz JP, Richaud-Patin Y, et al. Patient-Specific iPSC-Derived Astrocytes Contribute to Non-Cell-Autonomous Neurodegeneration in Parkinson's Disease. Stem Cell Reports. 2019;12(2):213-29.
224. Fonseca-Ornelas L, Stricker JMS, Soriano-Cruz S, Weykopf B, Dettmer U, Muratore CR, et al. Parkinson-causing mutations in LRRK2 impair the physiological tetramerization of endogenous α-synuclein in human neurons. npj Parkinson's Disease. 2022;8(1):118.
225. Matta S, Van Kolen K, da Cunha R, van den Bogaart G, Mandemakers W, Miskiewicz K, et al. LRRK2 Controls an EndoA Phosphorylation Cycle in Synaptic Endocytosis. Neuron (Cambridge, Mass). 2012;75(6):1008-21.
226. MacLeod DA, Rhinn H, Kuwahara T, Zolin A, Di Paolo G, McCabe BD, et al. RAB7L1 interacts with LRRK2 to modify intraneuronal protein sorting and Parkinson's disease risk. Neuron. 2013;77(3):425-39.
227. Migheli R, Del Giudice MG, Spissu Y, Sanna G, Xiong Y, Dawson TM, et al. LRRK2 affects vesicle trafficking, neurotransmitter extracellular level and membrane receptor localization. PLoS One. 2013;8(10):e77198.
228. Dou D, Aiken J, Holzbaur ELF. RAB3 phosphorylation by pathogenic LRRK2 impairs trafficking of synaptic vesicle precursors. J Cell Biol. 2024;223(6).
229. MacLeod D, Dowman J, Hammond R, Leete T, Inoue K, Abeliovich A. The familial Parkinsonism gene LRRK2 regulates neurite process morphology. Neuron. 2006;52(4):587-93.
230. Borgs L, Peyre E, Alix P, Hanon K, Grobarczyk B, Godin JD, et al. Dopaminergic neurons differentiating from LRRK2 G2019S induced pluripotent stem cells show early neuritic branching defects. Sci Rep. 2016;6:33377.
231. Winner B, Melrose HL, Zhao C, Hinkle KM, Yue M, Kent C, et al. Adult neurogenesis and neurite outgrowth are impaired in LRRK2 G2019S mice. Neurobiology of disease. 2010;41(3):706-16.

232. Plowey ED, Cherra SJ, 3rd, Liu Y-J, Chu CT. Role of autophagy in G2019S-LRRK2-associated neurite shortening in differentiated SH-SY5Y cells. Journal of neurochemistry. 2008;105(3):1048-56.
233. Alegre-Abarrategui J, Christian H, Lufino MMP, Mutihac R, Venda LL, Ansorge O, et al. LRRK2 regulates autophagic activity and localizes to specific membrane microdomains in a novel human genomic reporter cellular model. Human molecular genetics. 2009;18(21):4022-34.
234. Kania E, Long JS, McEwan DG, Welkenhuyzen K, La Rovere R, Luyten T, et al. LRRK2 phosphorylation status and kinase activity regulate (macro)autophagy in a Rab8a/Rab10-dependent manner. Cell Death Dis. 2023;14(7):436.
235. Henry AG, Aghamohammadzadeh S, Samaroo H, Chen Y, Mou K, Needle E, et al. Pathogenic LRRK2 mutations, through increased kinase activity, produce enlarged lysosomes with reduced degradative capacity and increase ATP13A2 expression. Human Molecular Genetics. 2015;24(21):6013-28.
236. Wallings R, Connor-Robson N, Wade-Martins R. LRRK2 interacts with the vacuolar-type H+-ATPase pump a1 subunit to regulate lysosomal function. Human Molecular Genetics. 2019;28(16):2696-710.
237. Mortiboys H, Johansen KK, Aasly JO, Bandmann O. Mitochondrial impairment in patients with Parkinson disease with the G2019S mutation in LRRK2. Neurology. 2010;75(22):2017-20.
238. Wang X, Yan MH, Fujioka H, Liu J, Wilson-Delfosse A, Chen SG, et al. LRRK2 regulates mitochondrial dynamics and function through direct interaction with DLP1. Human molecular genetics. 2012;21(9):1931-44.
239. Ramonet D, Daher JPL, Lin BM, Stafa K, Kim J, Banerjee R, et al. Dopaminergic neuronal loss, reduced neurite complexity and autophagic abnormalities in transgenic mice expressing G2019S mutant LRRK2. PloS one. 2011;6(4):e18568-e.
240. Liu H, Ho PW, Leung CT, Pang SY, Chang EES, Choi ZY, et al. Aberrant mitochondrial morphology and function associated with impaired mitophagy and DNM1L-MAPK/ERK signaling are found in aged mutant Parkinsonian LRRK2(R1441G) mice. Autophagy. 2021;17(10):3196-220.
241. Williamson MG, Madureira M, McGuinness W, Heon-Roberts R, Mock ED, Naidoo K, et al. Mitochondrial dysfunction and mitophagy defects in LRRK2-R1441C Parkinson's disease models. Hum Mol Genet. 2023;32(18):2808-21.
242. Gillardon F, Schmid R, Draheim H. Parkinson's disease-linked leucine-rich repeat kinase 2(R1441G) mutation increases proinflammatory cytokine release from activated primary microglial cells and resultant neurotoxicity. Neuroscience. 2012;208:41-8.
243. Ho DH, Je AR, Lee H, Son I, Kweon HS, Kim HG, et al. LRRK2 Kinase Activity Induces Mitochondrial Fission in Microglia via Drp1 and Modulates Neuroinflammation. Exp Neurobiol. 2018;27(3):171-80.
244. Lücking CB, Dürr A, Bonifati V, Vaughan J, De Michele G, Gasser T, et al. Association between Early-Onset Parkinson's Disease and Mutations in the Parkin Gene. The New England journal of medicine. 2000;342(21):1560-7.

245. Lesage S, Lunati A, Houot M, Romdhan SB, Clot F, Tesson C, et al. Characterization of recessive Parkinson's disease in a large multicenter study. Ann Neurol. 2020.
246. Kitada T, Mizuno Y, Yamamura Y, Hattori N, Matsumine H, Yokochi M, et al. Mutations in the parkin gene cause autosomal recessive juvenile parkinsonism. Nature (London). 1998;392(6676):605-8.
247. Seirafi M, Kozlov G, Gehring K. Parkin structure and function. FEBS J. 2015;282(11):2076-88.
248. Shimura H, Hattori N, Kubo S, Yoshikawa M, Kitada T, Matsumine H, et al. Immunohistochemical and subcellular localization of Parkin protein: absence of protein in autosomal recessive juvenile parkinsonism patients. Ann Neurol. 1999;45(5):668-72.
249. Xiong H, Wang D, Chen L, Choo YS, Ma H, Tang C, et al. Parkin, PINK1, and DJ-1 form a ubiquitin E3 ligase complex promoting unfolded protein degradation. The Journal of clinical investigation. 2009;119(3):650-60.
250. Kamienieva I, Duszyński J, Szczepanowska J. Multitasking guardian of mitochondrial quality: Parkin function and Parkinson's disease. Translational Neurodegeneration. 2021;10(1):5.
251. Hristova VA, Beasley SA, Rylett RJ, Shaw GS. Identification of a novel Zn2+-binding domain in the autosomal recessive juvenile Parkinson-related E3 ligase parkin. The Journal of biological chemistry. 2009;284(22):14978-86.
252. Berndsen CE, Wolberger C. New insights into ubiquitin E3 ligase mechanism. Nat Struct Mol Biol. 2014;21(4):301-7.
253. Chaugule VK, Burchell L, Barber KR, Sidhu A, Leslie SJ, Shaw GS, et al. Autoregulation of Parkin activity through its ubiquitin-like domain. The EMBO journal. 2011;30(14):2853-67.
254. Trempe J-F, Sauvé V, Grenier K, Seirafi M, Tang MY, Ménade M, et al. Structure of Parkin Reveals Mechanisms for Ubiquitin Ligase Activation. Science. 2013;340(6139):1451-5.
255. Sakata E, Yamaguchi Y, Kurimoto E, Kikuchi J, Yokoyama S, Yamada S, et al. Parkin binds the Rpn10 subunit of 26S proteasomes through its ubiquitin-like domain. EMBO Rep. 2003;4(3):301-6.
256. Finney N, Walther F, Mantel PY, Stauffer D, Rovelli G, Dev KK. The cellular protein level of parkin is regulated by its ubiquitin-like domain. J Biol Chem. 2003;278(18):16054-8.
257. Clark IE, Dodson MW, Jiang C, Cao JH, Huh JR, Seol JH, et al. Drosophila pink1 is required for mitochondrial function and interacts genetically with parkin. Nature. 2006;441(7097):1162-6.
258. Kondapalli C, Kazlauskaite A, Zhang N, Woodroof HI, Campbell DG, Gourlay R, et al. PINK1 is activated by mitochondrial membrane potential depolarization and stimulates Parkin E3 ligase activity by phosphorylating Serine 65. Open Biol. 2012;2(5):120080-.
259. Caulfield TR, Fiesel FC, Moussaud-Lamodière EL, Dourado DFAR, Flores SC, Springer W. Phosphorylation by PINK1 releases the UBL domain and initializes the

conformational opening of the E3 ubiquitin ligase Parkin. PLoS Comput Biol. 2014;10(11):e1003935-e.
260. Kane LA, Lazarou M, Fogel AI, Li Y, Yamano K, Sarraf SA, et al. PINK1 phosphorylates ubiquitin to activate Parkin E3 ubiquitin ligase activity. J Cell Biol. 2014;205(2):143-53.
261. Sauvé V, Sung G, Soya N, Kozlov G, Blaimschein N, Miotto LS, et al. Mechanism of parkin activation by phosphorylation. Nat Struct Mol Biol. 2018;25(7):623-30.
262. Matsumine H, Saito M, Shimoda-Matsubayashi S, Tanaka H, Ishikawa A, Nakagawa-Hattori Y, et al. Localization of a gene for an autosomal recessive form of juvenile Parkinsonism to chromosome 6q25.2-27. Am J Hum Genet. 1997;60(3):588-96.
263. Kasten M, Hartmann C, Hampf J, Schaake S, Westenberger A, Vollstedt EJ, et al. Genotype-Phenotype Relations for the Parkinson's Disease Genes Parkin, PINK1, DJ1: MDSGene Systematic Review. Mov Disord. 2018;33(5):730-41.
264. Seike N, Yokoseki A, Takeuchi R, Saito K, Miyahara H, Miyashita A, et al. Genetic Variations and Neuropathologic Features of Patients with PRKN Mutations. Movement Disorders. 2021;36(7):1634-43.
265. Menon PJ, Sambin S, Criniere-Boizet B, Courtin T, Tesson C, Casse F, et al. Genotype–phenotype correlation in PRKN-associated Parkinson's disease. npj Parkinson's Disease. 2024;10(1):72.
266. Takahashi H, Ohama E, Suzuki S, Horikawa Y, Ishikawa A, Morita T, et al. Familial juvenile parkinsonism: clinical and pathologic study in a family. Neurology. 1994;44(3 Pt 1):437-41.
267. Mori H, Kondo T, Yokochi M, Matsumine H, Nakagawa-Hattori Y, Miyake T, et al. Pathologic and biochemical studies of juvenile parkinsonism linked to chromosome 6q. Neurology. 1998;51(3):890-2.
268. Ishikawa A, Takahashi H. Clinical and neuropathological aspects of autosomal recessive juvenile parkinsonism. J Neurol. 1998;245(11 Suppl 3):P4-9.
269. Hayashi S, Wakabayashi K, Ishikawa A, Nagai H, Saito M, Maruyama M, et al. An autopsy case of autosomal-recessive juvenile parkinsonism with a homozygous exon 4 deletion in the parkin gene. Mov Disord. 2000;15(5):884-8.
270. van de Warrenburg BP, Lammens M, Lücking CB, Denèfle P, Wesseling P, Booij J, et al. Clinical and pathologic abnormalities in a family with parkinsonism and parkin gene mutations. Neurology. 2001;56(4):555-7.
271. Sasaki S, Shirata A, Yamane K, Iwata M. Parkin-positive autosomal recessive juvenile Parkinsonism with alpha-synuclein-positive inclusions. Neurology. 2004;63(4):678-82.
272. Doherty KM, Silveira-Moriyama L, Parkkinen L, Healy DG, Farrell M, Mencacci NE, et al. Parkin disease: a clinicopathologic entity? JAMA Neurol. 2013;70(5):571-9.
273. Cornejo-Olivas MR, Torres L, Mata IF, Mazzetti P, Rivas D, Cosentino C, et al. A Peruvian family with a novel PARK2 mutation: Clinical and pathological characteristics. Parkinsonism Relat Disord. 2015;21(5):444-8.
274. Farrer M, Chan P, Chen R, Tan L, Lincoln S, Hernandez D, et al. Lewy bodies and parkinsonism in families with parkin mutations. Ann Neurol. 2001;50(3):293-300.

275. Pramstaller PP, Schlossmacher MG, Jacques TS, Scaravilli F, Eskelson C, Pepivani I, et al. Lewy body Parkinson's disease in a large pedigree with 77 Parkin mutation carriers. Annals of neurology. 2005;58(3):411-22.
276. Ruffmann C, Zini M, Goldwurm S, Bramerio M, Spinello S, Rusconi D, et al. Lewy body pathology and typical Parkinson disease in a patient with a heterozygous (R275W) mutation in the Parkin gene (PARK2). Acta Neuropathol. 2012;123(6):901-3.
277. Miyakawa S, Ogino M, Funabe S, Uchino A, Shimo Y, Hattori N, et al. Lewy body pathology in a patient with a homozygous parkin deletion. Mov Disord. 2013;28(3):388-91.
278. Sharp ME, Marder KS, Côté L, Clark LN, Nichols WC, Vonsattel JP, et al. Parkinson's disease with Lewy bodies associated with a heterozygous PARKIN dosage mutation. Mov Disord. 2014;29(4):566-8.
279. Shimura H, Schlossmacher MG, Hattori N, Frosch MP, Trockenbacher A, Schneider R, et al. Ubiquitination of a New Form of α-Synuclein by Parkin from Human Brain: Implications for Parkinson's Disease. Science (American Association for the Advancement of Science). 2001;293(5528):263-9.
280. Sriram SR, Li X, Ko HS, Chung KK, Wong E, Lim KL, et al. Familial-associated mutations differentially disrupt the solubility, localization, binding and ubiquitination properties of parkin. Hum Mol Genet. 2005;14(17):2571-86.
281. Hampe C, Ardila-Osorio H, Fournier M, Brice A, Corti O. Biochemical analysis of Parkinson's disease-causing variants of Parkin, an E3 ubiquitin–protein ligase with monoubiquitylation capacity. Human molecular genetics. 2006;15(13):2059-75.
282. Matsuda N, Kitami T, Suzuki T, Mizuno Y, Hattori N, Tanaka K. Diverse Effects of Pathogenic Mutations of Parkin That Catalyze Multiple Monoubiquitylation in Vitro. The Journal of biological chemistry. 2006;281(6):3204-9.
283. Van Humbeeck C, Waelkens E, Corti O, Brice A, Vandenberghe W. Parkin occurs in a stable, non-covalent, approximately 110-kDa complex in brain. The European journal of neuroscience. 2008;27(2):284-93.
284. Beasley SA, Hristova VA, Shaw GS. Structure of the Parkin in-between-ring domain provides insights for E3-ligase dysfunction in autosomal recessive Parkinson's disease. Proceedings of the National Academy of Sciences. 2007;104(9):3095.
285. Henn IH, Gostner JM, Lackner P, Tatzelt J, Winklhofer KF. Pathogenic mutations inactivate parkin by distinct mechanisms. J Neurochem. 2005;92(1):114-22.
286. Safadi SS, Barber KR, Shaw GS. Impact of autosomal recessive juvenile Parkinson's disease mutations on the structure and interactions of the parkin ubiquitin-like domain. Biochemistry. 2011;50(13):2603-10.
287. Wang C, Tan JM, Ho MW, Zaiden N, Wong SH, Chew CL, et al. Alterations in the solubility and intracellular localization of parkin by several familial Parkinson's disease-linked point mutations. J Neurochem. 2005;93(2):422-31.
288. Li W, Fu Y, Halliday GM, Sue CM. PARK Genes Link Mitochondrial Dysfunction and Alpha-Synuclein Pathology in Sporadic Parkinson’s Disease. Frontiers in Cell and Developmental Biology. 2021;9(1755).

289. Khandelwal PJ, Dumanis SB, Feng LR, Maguire-Zeiss K, Rebeck G, Lashuel HA, et al. Parkinson-related parkin reduces α-Synuclein phosphorylation in a gene transfer model. Mol Neurodegener. 2010;5:47.
290. Wilkaniec A, Lenkiewicz AM, Babiec L, Murawska E, Jęśko HM, Cieślik M, et al. Exogenous Alpha-Synuclein Evoked Parkin Downregulation Promotes Mitochondrial Dysfunction in Neuronal Cells. Implications for Parkinson's Disease Pathology. Frontiers in Aging Neuroscience. 2021;13(64).
291. Yu Z, Xu X, Xiang Z, Zhou J, Zhang Z, Hu C, et al. Nitrated alpha-synuclein induces the loss of dopaminergic neurons in the substantia nigra of rats. PloS one. 2010;5(4):e9956.
292. Danielson SR, Held JM, Schilling B, Oo M, Gibson BW, Andersen JK. Preferentially increased nitration of alpha-synuclein at tyrosine-39 in a cellular oxidative model of Parkinson's disease. Anal Chem. 2009;81(18):7823-8.
293. Jiang H, Jiang Q, Liu W, Feng J. Parkin Suppresses the Expression of Monoamine Oxidases. The Journal of biological chemistry. 2006;281(13):8591-9.
294. Jiang H, Ren Y, Yuen EY, Zhong P, Ghaedi M, Hu Z, et al. Parkin controls dopamine utilization in human midbrain dopaminergic neurons derived from induced pluripotent stem cells. Nature Communications. 2012;3(1):668.
295. Imaizumi Y, Okada Y, Akamatsu W, Koike M, Kuzumaki N, Hayakawa H, et al. Mitochondrial dysfunction associated with increased oxidative stress and α-synuclein accumulation in PARK2 iPSC-derived neurons and postmortem brain tissue. Mol Brain. 2012;5:35.
296. Shaltouki A, Sivapatham R, Pei Y, Gerencser AA, Momčilović O, Rao MS, et al. Mitochondrial alterations by PARKIN in dopaminergic neurons using PARK2 patient-specific and PARK2 knockout isogenic iPSC lines. Stem Cell Reports. 2015;4(5):847-59.
297. Chung SY, Kishinevsky S, Mazzulli JR, Graziotto J, Mrejeru A, Mosharov EV, et al. Parkin and PINK1 Patient iPSC-Derived Midbrain Dopamine Neurons Exhibit Mitochondrial Dysfunction and α-Synuclein Accumulation. Stem Cell Reports. 2016;7(4):664-77.
298. Goldberg MS, Fleming SM, Palacino JJ, Cepeda C, Lam HA, Bhatnagar A, et al. Parkin-deficient Mice Exhibit Nigrostriatal Deficits but Not Loss of Dopaminergic Neurons*. Journal of Biological Chemistry. 2003;278(44):43628-35.
299. Pickrell Alicia M, Huang C-H, Kennedy Scott R, Ordureau A, Sideris Dionisia P, Hoekstra Jake G, et al. Endogenous Parkin Preserves Dopaminergic Substantia Nigral Neurons following Mitochondrial DNA Mutagenic Stress. Neuron. 2015;87(2):371-81.
300. Noda S, Sato S, Fukuda T, Tada N, Uchiyama Y, Tanaka K, et al. Loss of Parkin contributes to mitochondrial turnover and dopaminergic neuronal loss in aged mice. Neurobiol Dis. 2020;136:104717.
301. Youle RJ, van der Bliek AM. Mitochondrial fission, fusion, and stress. Science (New York, NY). 2012;337(6098):1062-5.
302. Greene JC, Whitworth AJ, Kuo I, Andrews LA, Feany MB, Pallanck LJ. Mitochondrial pathology and apoptotic muscle degeneration in Drosophila parkin

mutants. Proceedings of the National Academy of Sciences of the United States of America. 2003;100(7):4078-83.
303. Deng H, Dodson MW, Huang H, Guo M. The Parkinson's disease genes pink1 and parkin promote mitochondrial fission and/or inhibit fusion in Drosophila. Proceedings of the National Academy of Sciences of the United States of America. 2008;105(38):14503-8.
304. Wang H, Song P, Du L, Tian W, Yue W, Liu M, et al. Parkin ubiquitinates Drp1 for proteasome-dependent degradation: implication of dysregulated mitochondrial dynamics in Parkinson disease. The Journal of biological chemistry. 2011;286(13):11649-58.
305. Lutz AK, Exner N, Fett ME, Schlehe JS, Kloos K, Lämmermann K, et al. Loss of parkin or PINK1 function increases Drp1-dependent mitochondrial fragmentation. The Journal of biological chemistry. 2009;284(34):22938-51.
306. Glauser L, Sonnay S, Stafa K, Moore DJ. Parkin promotes the ubiquitination and degradation of the mitochondrial fusion factor mitofusin 1. J Neurochem. 2011;118(4):636-45.
307. Shin J-H, Ko Han S, Kang H, Lee Y, Lee Y-I, Pletinkova O, et al. PARIS (ZNF746) Repression of PGC-1α Contributes to Neurodegeneration in Parkinson's Disease. Cell. 2011;144(5):689-702.
308. Liang H, Ward WF. PGC-1alpha: a key regulator of energy metabolism. Adv Physiol Educ. 2006;30(4):145-51.
309. Stevens DA, Lee Y, Kang HC, Lee BD, Lee Y-I, Bower A, et al. Parkin loss leads to PARIS-dependent declines in mitochondrial mass and respiration. Proceedings of the National Academy of Sciences of the United States of America. 2015;112(37):11696-701.
310. Kumar M, Acevedo-Cintrón J, Jhaldiyal A, Wang H, Andrabi SA, Eacker S, et al. Defects in Mitochondrial Biogenesis Drive Mitochondrial Alterations in PARKIN-Deficient Human Dopamine Neurons. Stem cell reports. 2020;15(3):629-45.
311. Narendra DP, Jin SM, Tanaka A, Suen D-F, Gautier CA, Shen J, et al. PINK1 is selectively stabilized on impaired mitochondria to activate Parkin. PLoS Biol. 2010;8(1):e1000298-e.
312. Geisler S, Holmström KM, Skujat D, Fiesel FC, Rothfuss OC, Kahle PJ, et al. PINK1/Parkin-mediated mitophagy is dependent on VDAC1 and p62/SQSTM1. Nature Cell Biology. 2010;12(2):119-31.
313. Cai Q, Zakaria Hesham M, Simone A, Sheng Z-H. Spatial Parkin Translocation and Degradation of Damaged Mitochondria via Mitophagy in Live Cortical Neurons. Current biology. 2012;22(6):545-52.
314. Bingol B, Tea JS, Phu L, Reichelt M, Bakalarski CE, Song Q, et al. The mitochondrial deubiquitinase USP30 opposes parkin-mediated mitophagy. Nature. 2014;510(7505):370-5.
315. Yi W, MacDougall EJ, Tang MY, Krahn AI, Gan-Or Z, Trempe J-F, et al. The landscape of Parkin variants reveals pathogenic mechanisms and therapeutic targets in Parkinson's disease. Human molecular genetics. 2019;28(17):2811-25.

316. Sliter DA, Martinez J, Hao L, Chen X, Sun N, Fischer TD, et al. Parkin and PINK1 mitigate STING-induced inflammation. Nature. 2018;561(7722):258-62.
317. Solano RM, Casarejos MJ, Menéndez-Cuervo J, Rodriguez-Navarro JA, García de Yébenes J, Mena MA. Glial dysfunction in parkin null mice: effects of aging. The Journal of neuroscience : the official journal of the Society for Neuroscience. 2008;28(3):598-611.
318. Gerasimova T, Stepanenko E, Novosadova L, Arsenyeva E, Shimchenko D, Tarantul V, et al. Glial Cultures Differentiated from iPSCs of Patients with PARK2-Associated Parkinson's Disease Demonstrate a Pro-Inflammatory Shift and Reduced Response to TNFα Stimulation. Int J Mol Sci. 2023;24(3).
319. Tran TA, Nguyen AD, Chang J, Goldberg MS, Lee J-K, Tansey MG. Lipopolysaccharide and Tumor Necrosis Factor Regulate Parkin Expression via Nuclear Factor-Kappa B. PLOS ONE. 2011;6(8):e23660.
320. Li Y, Tomiyama H, Sato K, Hatano Y, Yoshino H, Atsumi M, et al. Clinicogenetic study of PINK1 mutations in autosomal recessive early-onset parkinsonism. Neurology. 2005;64(11):1955-7.
321. Valente EM, Salvi S, Ialongo T, Marongiu R, Elia AE, Caputo V, et al. PINK1 mutations are associated with sporadic early-onset parkinsonism. Ann Neurol. 2004;56(3):336-41.
322. Valente EM, Abou-Sleiman PM, Caputo V, Muqit MM, Harvey K, Gispert S, et al. Hereditary early-onset Parkinson's disease caused by mutations in PINK1. Science. 2004;304(5674):1158-60.
323. Quinn PMJ, Moreira PI, Ambrósio AF, Alves CH. PINK1/PARKIN signalling in neurodegeneration and neuroinflammation. Acta Neuropathologica Communications. 2020;8(1):189.
324. Zhou C, Huang Y, Shao Y, May J, Prou D, Perier C, et al. The kinase domain of mitochondrial PINK1 faces the cytoplasm. Proceedings of the National Academy of Sciences. 2008;105(33):12022.
325. Okatsu K, Kimura M, Oka T, Tanaka K, Matsuda N. Unconventional PINK1 localization to the outer membrane of depolarized mitochondria drives Parkin recruitment. Journal of cell science. 2015;128(5):964-78.
326. Schubert AF, Gladkova C, Pardon E, Wagstaff JL, Freund SMV, Steyaert J, et al. Structure of PINK1 in complex with its substrate ubiquitin. Nature. 2017;552(7683):51-6.
327. Sim CH, Lio DSS, Mok SS, Masters CL, Hill AF, Culvenor JG, et al. C-terminal truncation and Parkinson's disease-associated mutations down-regulate the protein serine/threonine kinase activity of PTEN-induced kinase-1. Human molecular genetics. 2006;15(21):3251-62.
328. Trempe J-F, Fon E. Structure and Function of Parkin, PINK1, and DJ-1, the Three Musketeers of Neuroprotection. Frontiers in Neurology. 2013;4(38).
329. Valente EM, Bentivoglio AR, Dixon PH, Ferraris A, Ialongo T, Frontali M, et al. Localization of a novel locus for autosomal recessive early-onset parkinsonism, PARK6, on human chromosome 1p35-p36. Am J Hum Genet. 2001;68(4):895-900.

330. Bonifati V, Rohe CF, Breedveld GJ, Fabrizio E, Mari MD, Tassorelli C, et al. Early-onset parkinsonism associated with PINK1 mutations: frequency, genotypes, and phenotypes. Neurology. 2005;65(1):87-95.
331. Ricciardi L, Petrucci S, Guidubaldi A, Ialongo T, Serra L, Ferraris A, et al. Phenotypic variability of PINK1 expression: 12 Years' clinical follow-up of two Italian families. Movement disorders. 2014;29(12):1561-6.
332. Samaranch L, Lorenzo-Betancor O, Arbelo JM, Ferrer I, Lorenzo E, Irigoyen J, et al. PINK1-linked parkinsonism is associated with Lewy body pathology. Brain. 2010;133(Pt 4):1128-42.
333. Takanashi M, Li Y, Hattori N. Absence of Lewy pathology associated with PINK1 homozygous mutation. Neurology. 2016;86(23):2212-3.
334. Nybø CJ, Gustavsson EK, Farrer MJ, Aasly JO. Neuropathological findings in PINK1-associated Parkinson's disease. Parkinsonism Relat Disord. 2020;78:105-8.
335. Beilina A, Van Der Brug M, Ahmad R, Kesavapany S, Miller DW, Petsko GA, et al. Mutations in PTEN-induced putative kinase 1 associated with recessive parkinsonism have differential effects on protein stability. Proceedings of the National Academy of Sciences of the United States of America. 2005;102(16):5703-8.
336. Silvestri L, Caputo V, Bellacchio E, Atorino L, Dallapiccola B, Valente EM, et al. Mitochondrial import and enzymatic activity of PINK1 mutants associated to recessive parkinsonism. Hum Mol Genet. 2005;14(22):3477-92.
337. Puschmann A, Fiesel FC, Caulfield TR, Hudec R, Ando M, Truban D, et al. Heterozygous PINK1 p.G411S increases risk of Parkinson's disease via a dominant-negative mechanism. Brain. 2017;140(1):98-117.
338. Ando M, Fiesel FC, Hudec R, Caulfield TR, Ogaki K, Górka-Skoczylas P, et al. The PINK1 p.I368N mutation affects protein stability and ubiquitin kinase activity. Molecular neurodegeneration. 2017;12(1):32-.
339. Park J, Lee SB, Lee S, Kim Y, Song S, Kim S, et al. Mitochondrial dysfunction in Drosophila PINK1 mutants is complemented by parkin. Nature. 2006;441(7097):1157-61.
340. Exner N, Treske B, Paquet D, Holmström K, Schiesling C, Gispert S, et al. Loss-of-function of human PINK1 results in mitochondrial pathology and can be rescued by parkin. J Neurosci. 2007;27(45):12413-8.
341. Morais VA, Verstreken P, Roethig A, Smet J, Snellinx A, Vanbrabant M, et al. Parkinson's disease mutations in PINK1 result in decreased Complex I activity and deficient synaptic function. EMBO Mol Med. 2009;1(2):99-111.
342. Gautier CA, Kitada T, Shen J. Loss of PINK1 causes mitochondrial functional defects and increased sensitivity to oxidative stress. Proc Natl Acad Sci U S A. 2008;105(32):11364-9.
343. Gandhi S, Wood-Kaczmar A, Yao Z, Plun-Favreau H, Deas E, Klupsch K, et al. PINK1-associated Parkinson's disease is caused by neuronal vulnerability to calcium-induced cell death. Mol Cell. 2009;33(5):627-38.
344. Zhi L, Qin Q, Muqeem T, Seifert EL, Liu W, Zheng S, et al. Loss of PINK1 causes age-dependent decrease of dopamine release and mitochondrial dysfunction. Neurobiol Aging. 2019;75:1-10.

345. Matsuda N, Sato S, Shiba K, Okatsu K, Saisho K, Gautier CA, et al. PINK1 stabilized by mitochondrial depolarization recruits Parkin to damaged mitochondria and activates latent Parkin for mitophagy. J Cell Biol. 2010;189(2):211-21.
346. Seibler P, Graziotto J, Jeong H, Simunovic F, Klein C, Krainc D. Mitochondrial Parkin recruitment is impaired in neurons derived from mutant PINK1 induced pluripotent stem cells. J Neurosci. 2011;31(16):5970-6.
347. Halliday GM, McRitchie DA, Cartwright H, Pamphlett R, Hely MA, Morris JG. Midbrain neuropathology in idiopathic Parkinson's disease and diffuse Lewy body disease. J Clin Neurosci. 1996;3(1):52-60.
348. Arima K, Mizutani T, Alim MA, Tonozuka-Uehara H, Izumiyama Y, Hirai S, et al. NACP/alpha-synuclein and tau constitute two distinctive subsets of filaments in the same neuronal inclusions in brains from a family of parkinsonism and dementia with Lewy bodies: double-immunolabeling fluorescence and electron microscopic studies. Acta Neuropathol. 2000;100(2):115-21.
349. Ishizawa T, Mattila P, Davies P, Wang D, Dickson DW. Colocalization of tau and alpha-synuclein epitopes in Lewy bodies. J Neuropathol Exp Neurol. 2003;62(4):389-97.
350. Dickson DWMD, Braak HMD, Duda JEMD, Duyckaerts CMD, Gasser TMD, Halliday GMP, et al. Neuropathological assessment of Parkinson's disease: refining the diagnostic criteria. Lancet neurology. 2009;8(12):1150-7.
351. Jellinger KA. Neuropathology of sporadic Parkinson's disease: evaluation and changes of concepts. Mov Disord. 2012;27(1):8-30.
352. Swirski M, Miners JS, de Silva R, Lashley T, Ling H, Holton J, et al. Evaluating the relationship between amyloid-β and α-synuclein phosphorylated at Ser129 in dementia with Lewy bodies and Parkinson's disease. Alzheimer's research & therapy. 2014;6(5-8):77-.
353. Pagano G, Ferrara N, Brooks DJ, Pavese N. Age at onset and Parkinson disease phenotype. Neurology. 2016;86(15):1400-7.
354. Puska G, Lutz MI, Molnar K, Regelsberger G, Ricken G, Pirker W, et al. Lysosomal response in relation to α-synuclein pathology differs between Parkinson's disease and multiple system atrophy. Neurobiology of Disease. 2018;114:140-52.
355. Moors TE, Maat CA, Niedieker D, Mona D, Petersen D, Timmermans-Huisman E, et al. The subcellular arrangement of alpha-synuclein proteoforms in the Parkinson's disease brain as revealed by multicolor STED microscopy. Acta Neuropathol. 2021;142(3):423-48.
356. Wiseman JA, Murray HC, Faull R, Dragunow M, Turner CP, Dieriks BV, et al. Aggregate-prone brain regions in Parkinson's disease are rich in unique N-terminus α-synuclein conformers with high proteolysis susceptibility. NPJ Parkinsons Dis. 2024;10(1):1.
357. Liu WJ, Ye L, Huang WF, Guo LJ, Xu ZG, Wu HL, et al. p62 links the autophagy pathway and the ubiqutin–proteasome system upon ubiquitinated protein degradation. Cellular & Molecular Biology Letters. 2016;21(1):29.
358. Mori F, Nishie M, Kakita A, Yoshimoto M, Takahashi H, Wakabayashi K. Relationship Among α-Synuclein Accumulation, Dopamine Synthesis, and

Neurodegeneration in Parkinson Disease Substantia Nigra. Journal of Neuropathology & Experimental Neurology. 2006;65(8):808-15.
359. Mahul-Mellier AL, Burtscher J, Maharjan N, Weerens L, Croisier M, Kuttler F, et al. The process of Lewy body formation, rather than simply α-synuclein fibrillization, is one of the major drivers of neurodegeneration. Proc Natl Acad Sci U S A. 2020;117(9):4971-82.
360. Lam I, Ndayisaba A, Lewis AJ, Fu Y, Sagredo GT, Kuzkina A, et al. Rapid iPSC inclusionopathy models shed light on formation, consequence, and molecular subtype of α-synuclein inclusions. Neuron. 2024;112(17):2886-909.e16.
361. Sano K, Iwasaki Y, Yamashita Y, Irie K, Hosokawa M, Satoh K, et al. Tyrosine 136 phosphorylation of α-synuclein aggregates in the Lewy body dementia brain: involvement of serine 129 phosphorylation by casein kinase 2. Acta Neuropathol Commun. 2021;9(1):182.
362. Prasad K, Beach TG, Hedreen J, Richfield EK. Critical role of truncated α-synuclein and aggregates in Parkinson's disease and incidental Lewy body disease. Brain Pathol. 2012;22(6):811-25.
363. Arima K, Hirai S, Sunohara N, Aoto K, Izumiyama Y, Uéda K, et al. Cellular co-localization of phosphorylated tau- and NACP/α-synuclein-epitopes in Lewy bodies in sporadic Parkinson's disease and in dementia with Lewy bodies. Brain Research. 1999;843(1):53-61.
364. Hughes AJ, Daniel SE, Kilford L, Lees AJ. Accuracy of clinical diagnosis of idiopathic Parkinson's disease: a clinico-pathological study of 100 cases. J Neurol Neurosurg Psychiatry. 1992;55(3):181-4.
365. Hyman BT, Phelps CH, Beach TG, Bigio EH, Cairns NJ, Carrillo MC, et al. National Institute on Aging-Alzheimer's Association guidelines for the neuropathologic assessment of Alzheimer's disease. Alzheimers Dement. 2012;8(1):1-13.
366. Bankhead P, Loughrey MB, Fernández JA, Dombrowski Y, McArt DG, Dunne PD, et al. QuPath: Open source software for digital pathology image analysis. Scientific Reports. 2017;7(1):16878.
367. Schindelin J, Arganda-Carreras I, Frise E, Kaynig V, Longair M, Pietzsch T, et al. Fiji: an open-source platform for biological-image analysis. Nature Methods. 2012;9(7):676-82.
368. Schmidt SI, Blaabjerg M, Freude K, Meyer M. RhoA Signaling in Neurodegenerative Diseases. Cells. 2022;11(9).
369. Iyer M, Subramaniam MD, Venkatesan D, Cho S-G, Ryding M, Meyer M, et al. Role of RhoA-ROCK signaling in Parkinson's disease. European Journal of Pharmacology. 2021;894:173815.
370. Zerial M, McBride H. Rab proteins as membrane organizers. Nature Reviews Molecular Cell Biology. 2001;2(2):107-17.
371. Hutagalung AH, Novick PJ. Role of Rab GTPases in membrane traffic and cell physiology. Physiol Rev. 2011;91(1):119-49.
372. Gasparotto M, Lee Y-S, Palazzi A, Vacca M, Filippini F. Nuclear and Cytoplasmatic Players in Mitochondria-Related CNS Disorders: Chromatin Modifications and Subcellular Trafficking. Biomolecules [Internet]. 2022; 12(5).

373. Kon T, Lee S, Martinez-Valbuena I, Yoshida K, Tanikawa S, Lang AE, et al. Molecular Behavior of α-Synuclein Is Associated with Membrane Transport, Lipid Metabolism, and Ubiquitin-Proteasome Pathways in Lewy Body Disease. Int J Mol Sci. 2024;25(5).
374. Zenko D, Marsh J, Castle AR, Lewin R, Fischer R, Tofaris GK. Monitoring α-synuclein ubiquitination dynamics reveals key endosomal effectors mediating its trafficking and degradation. Sci Adv. 2023;9(24):eadd8910.
375. Tofaris GK, Razzaq A, Ghetti B, Lilley KS, Spillantini MG. Ubiquitination of alpha-synuclein in Lewy bodies is a pathological event not associated with impairment of proteasome function. J Biol Chem. 2003;278(45):44405-11.
376. Goralski TM, Meyerdirk L, Breton L, Brasseur L, Kurgat K, DeWeerd D, et al. Spatial transcriptomics reveals molecular dysfunction associated with cortical Lewy pathology. Nature Communications. 2024;15(1):2642.
377. Pan L, Li C, Meng L, Tian Y, He M, Yuan X, et al. Tau accelerates α-synuclein aggregation and spreading in Parkinson's disease. Brain. 2022;145(10):3454-71.
378. Vermilyea SC, Christensen A, Meints J, Singh B, Martell-Martínez H, Karim MR, et al. Loss of tau expression attenuates neurodegeneration associated with α-synucleinopathy. Transl Neurodegener. 2022;11(1):34.
379. Giasson BI, Forman MS, Higuchi M, Golbe LI, Graves CL, Kotzbauer PT, et al. Initiation and synergistic fibrillization of tau and alpha-synuclein. Science. 2003;300(5619):636-40.
380. Henderson MX, Chung CH-Y, Riddle DM, Zhang B, Gathagan RJ, Seeholzer SH, et al. Unbiased Proteomics of Early Lewy Body Formation Model Implicates Active Microtubule Affinity-Regulating Kinases (MARKs) in Synucleinopathies. The Journal of Neuroscience. 2017;37(24):5870.
381. Buée L, Bussière T, Buée-Scherrer V, Delacourte A, Hof PR. Tau protein isoforms, phosphorylation and role in neurodegenerative disorders. Brain Res Brain Res Rev. 2000;33(1):95-130.
382. Ordonez DG, Lee MK, Feany MB. α-synuclein Induces Mitochondrial Dysfunction through Spectrin and the Actin Cytoskeleton. Neuron. 2018;97(1):108-24.e6.
383. Maor G, Dubreuil RR, Feany MB. α-Synuclein Promotes Neuronal Dysfunction and Death by Disrupting the Binding of Ankyrin to β-Spectrin. The Journal of Neuroscience. 2023;43(9):1614.
384. Esposito A, Dohm CP, Kermer P, Bähr M, Wouters FS. alpha-Synuclein and its disease-related mutants interact differentially with the microtubule protein tau and associate with the actin cytoskeleton. Neurobiol Dis. 2007;26(3):521-31.
385. Uematsu M, Nakamura A, Ebashi M, Hirokawa K, Takahashi R, Uchihara T. Brainstem tau pathology in Alzheimer's disease is characterized by increase of three repeat tau and independent of amyloid β. Acta Neuropathol Commun. 2018;6(1):1.
386. Llorens-Martin M, Teixeira CM, Fuster-Matanzo A, Jurado-Arjona J, Borrell V, Soriano E, et al. Tau isoform with three microtubule binding domains is a marker of new axons generated from the subgranular zone in the hippocampal dentate gyrus: implications for Alzheimer's disease. J Alzheimers Dis. 2012;29(4):921-30.

387. Hamlin D, Ryall C, Turner C, Faull RLM, Murray HC, Curtis MA. Characterization of neurofibrillary tangle immunophenotype signatures to classify tangle maturity in Alzheimer's disease. Alzheimers Dement. 2024;20(7):4803-17.
388. Uchihara T. Neurofibrillary changes undergoing morphological and biochemical changes - How does tau with the profile shift of from four repeat to three repeat spread in Alzheimer brain? Neuropathology. 2020;40(5):450-9.
389. Chakraborty P, Rivière G, Hebestreit A, de Opakua AI, Vorberg IM, Andreas LB, et al. Acetylation discriminates disease-specific tau deposition. Nature Communications. 2023;14(1):5919.
390. Zhang S, Zhu R, Pan B, Xu H, Olufemi MF, Gathagan RJ, et al. Post-translational modifications of soluble α-synuclein regulate the amplification of pathological α-synuclein. Nat Neurosci. 2023;26(2):213-25.
391. Yan J. Interplay between HDAC6 and its interacting partners: essential roles in the aggresome-autophagy pathway and neurodegenerative diseases. DNA Cell Biol. 2014;33(9):567-80.
392. Miki Y, Mori F, Tanji K, Kakita A, Takahashi H, Wakabayashi K. Accumulation of histone deacetylase 6, an aggresome-related protein, is specific to Lewy bodies and glial cytoplasmic inclusions. Neuropathology. 2011;31(6):561-8.
393. Francelle L, Outeiro TF, Rappold GA. Inhibition of HDAC6 activity protects dopaminergic neurons from alpha-synuclein toxicity. Sci Rep. 2020;10(1):6064.
394. Uchihara T. Silver diagnosis in neuropathology: principles, practice and revised interpretation. Acta Neuropathol. 2007;113(5):483-99.
395. Narhi L, Wood SJ, Steavenson S, Jiang Y, Wu GM, Anafi D, et al. Both Familial Parkinson's Disease Mutations Accelerate α-Synuclein Aggregation*. Journal of Biological Chemistry. 1999;274(14):9843-6.
396. Conway KA, Harper JD, Lansbury PT. Accelerated in vitro fibril formation by a mutant α-synuclein linked to early-onset Parkinson disease. Nature Medicine. 1998;4(11):1318-20.
397. Greenbaum EA, Graves CL, Mishizen-Eberz AJ, Lupoli MA, Lynch DR, Englander SW, et al. The E46K Mutation in α-Synuclein Increases Amyloid Fibril Formation*. Journal of Biological Chemistry. 2005;280(9):7800-7.
398. Sampognaro PJ, Arya S, Knudsen GM, Gunderson EL, Sandoval-Perez A, Hodul M, et al. Mutations in α-synuclein, TDP-43 and tau prolong protein half-life through diminished degradation by lysosomal proteases. Molecular Neurodegeneration. 2023;18(1):29.
399. Zhou Z, Kim J, Insolera R, Peng X, Fink DJ, Mata M. Rho GTPase regulation of α-synuclein and VMAT2: implications for pathogenesis of Parkinson's disease. Mol Cell Neurosci. 2011;48(1):29-37.
400. Niu M, Xu R, Wang J, Hou B, Xie A. MiR-133b ameliorates axon degeneration induced by MPP+ via targeting RhoA. Neuroscience. 2016;325:39-49.
401. Tatenhorst L, Eckermann K, Dambeck V, Fonseca-Ornelas L, Walle H, Lopes da Fonseca T, et al. Fasudil attenuates aggregation of α-synuclein in models of Parkinson’s disease. Acta Neuropathologica Communications. 2016;4(1):39.

402. Sousa VL, Bellani S, Giannandrea M, Yousuf M, Valtorta F, Meldolesi J, et al. {alpha}-synuclein and its A30P mutant affect actin cytoskeletal structure and dynamics. Mol Biol Cell. 2009;20(16):3725-39.
403. Halliday GM, Macdonald V, Henderson JM. A comparison of degeneration in motor thalamus and cortex between progressive supranuclear palsy and Parkinson's disease. Brain. 2005;128(10):2272-80.
404. Avazzadeh S, Baena JM, Keighron C, Feller-Sanchez Y, Quinlan LR. Modelling Parkinson's Disease: iPSCs towards Better Understanding of Human Pathology. Brain Sci. 2021;11(3).
405. Bose A, Petsko GA, Studer L. Induced pluripotent stem cells: a tool for modeling Parkinson's disease. Trends Neurosci. 2022;45(8):608-20.
406. Byers B, Cord B, Nguyen HN, Schule B, Fenno L, Lee PC, et al. SNCA triplication Parkinson's patient's iPSC-derived DA neurons accumulate alpha-synuclein and are susceptible to oxidative stress. PLoS One. 2011;6(11):e26159.
407. Ludtmann MHR, Angelova PR, Horrocks MH, Choi ML, Rodrigues M, Baev AY, et al. α-synuclein oligomers interact with ATP synthase and open the permeability transition pore in Parkinson's disease. Nat Commun. 2018;9(1):2293.
408. Tagliafierro L, Zamora ME, Chiba-Falek O. Multiplication of the SNCA locus exacerbates neuronal nuclear aging. Hum Mol Genet. 2019;28(3):407-21.
409. Brazdis RM, Alecu JE, Marsch D, Dahms A, Simmnacher K, Lörentz S, et al. Demonstration of brain region-specific neuronal vulnerability in human iPSC-based model of familial Parkinson's disease. Hum Mol Genet. 2020;29(7):1180-91.
410. Hargus G, Cooper O, Deleidi M, Levy A, Lee K, Marlow E, et al. Differentiated Parkinson patient-derived induced pluripotent stem cells grow in the adult rodent brain and reduce motor asymmetry in Parkinsonian rats. Proceedings of the National Academy of Sciences. 2010;107(36):15921-6.
411. Kikuchi T, Morizane A, Doi D, Okita K, Nakagawa M, Yamakado H, et al. Idiopathic Parkinson's disease patient-derived induced pluripotent stem cells function as midbrain dopaminergic neurons in rodent brains. J Neurosci Res. 2017;95(9):1829-37.
412. Zygogianni O, Antoniou N, Kalomoiri M, Kouroupi G, Taoufik E, Matsas R. In Vivo Phenotyping of Familial Parkinson’s Disease with Human Induced Pluripotent Stem Cells: A Proof-of-Concept Study. Neurochemical Research. 2019;44(6):1475-93.
413. Hemmer K, Smits LM, Bolognin S, Schwamborn JC. In vivo phenotyping of human Parkinson’s disease-specific stem cells carrying the LRRK2-G2019S mutation reveals increased a-Synuclein levels but absence of spreading. Opera Medica et Physiologica. 2018;4(2):71-7.
414. Shrigley S, Nilsson F, Mattsson B, Fiorenzano A, Mudannayake J, Bruzelius A, et al. Grafts Derived from an α-Synuclein Triplication Patient Mediate Functional Recovery but Develop Disease-Associated Pathology in the 6-OHDA Model of Parkinson's Disease. J Parkinsons Dis. 2021;11(2):515-28.
415. Pantazis CB, Yang A, Lara E, McDonough JA, Blauwendraat C, Peng L, et al. A reference human induced pluripotent stem cell line for large-scale collaborative studies. Cell Stem Cell. 2022;29(12):1685-702 e22.

416. Pavan C, Jin J, Jong S, Strbenac D, Davis RL, Sue CM, et al. Generation of the iPSC line FINi002-A from a male Parkinson's disease patient carrying compound heterozygous mutations in the PRKN gene. Stem Cell Res. 2023;73:103211.
417. Ovchinnikov D. Reprogramming fibroblasts and mononuclear blood cells into iPSCs using Sendai virus. Protocols io: https://dx doi org/1017504/protocols io bypqpvmw https://www protocols io/view/reprogramming-fibroblasts-and-mononuclear-blood-ce-bypqpvmw html. 2021.
418. Gantner CW, Cota-Coronado A, Thompson LH, Parish CL. An Optimized Protocol for the Generation of Midbrain Dopamine Neurons under Defined Conditions. STAR Protoc. 2020;1(2):100065.
419. Thompson LH, Parish CL. Transplantation of Fetal Midbrain Dopamine Progenitors into a Rodent Model of Parkinson's Disease. In: Reynolds BA, Deleyrolle LP, editors. Neural Progenitor Cells: Methods and Protocols. Totowa, NJ: Humana Press; 2013. p. 169-80.
420. Fraser T, Thompson L. Preparation of ventral midbrain cells for transplantation. 2024.
421. Ren Y, Jiang H, Hu Z, Fan K, Wang J, Janoschka S, et al. Parkin mutations reduce the complexity of neuronal processes in iPSC-derived human neurons. Stem Cells. 2015;33(1):68-78.
422. Pu J, Gao T, Zheng R, Fang Y, Ruan Y, Jin C, et al. Parkin mutation decreases neurite complexity and maturation in neurons derived from human fibroblasts. Brain Research Bulletin. 2020;159:9-15.
423. Yokota M, Kakuta S, Shiga T, Ishikawa KI, Okano H, Hattori N, et al. Establishment of an in vitro model for analyzing mitochondrial ultrastructure in PRKN-mutated patient iPSC-derived dopaminergic neurons. Mol Brain. 2021;14(1):58.
424. Yokota M, Yoshino Y, Hosoi M, Hashimoto R, Kakuta S, Shiga T, et al. Reduced ER-mitochondrial contact sites and mitochondrial Ca(2+) flux in PRKN-mutant patient tyrosine hydroxylase reporter iPSC lines. Front Cell Dev Biol. 2023;11:1171440.
425. Kano M, Takanashi M, Oyama G, Yoritaka A, Hatano T, Shiba-Fukushima K, et al. Reduced astrocytic reactivity in human brains and midbrain organoids with PRKN mutations. NPJ Parkinsons Dis. 2020;6(1):33.
426. Bernal-Conde LD, Peña-Martínez V, Morato-Torres CA, Ramos-Acevedo R, Arias-Carrión Ó, Padilla-Godínez FJ, et al. Alpha-Synuclein Gene Alterations Modulate Tyrosine Hydroxylase in Human iPSC-Derived Neurons in a Parkinson's Disease Animal Model. Life (Basel). 2024;14(6).
427. Alerte TNM, Akinfolarin AA, Friedrich EE, Mader SA, Hong C-S, Perez RG. α-Synuclein aggregation alters tyrosine hydroxylase phosphorylation and immunoreactivity: Lessons from viral transduction of knockout mice. Neuroscience Letters. 2008;435(1):24-9.
428. Oliveira LM, Falomir-Lockhart LJ, Botelho MG, Lin KH, Wales P, Koch JC, et al. Elevated α-synuclein caused by SNCA gene triplication impairs neuronal differentiation and maturation in Parkinson's patient-derived induced pluripotent stem cells. Cell Death Dis. 2015;6(11):e1994.

429. Chu Y, Kordower JH. Age-associated increases of α-synuclein in monkeys and humans are associated with nigrostriatal dopamine depletion: Is this the target for Parkinson's disease? Neurobiology of Disease. 2007;25(1):134-49.
430. Kanazawa T, Adachi E, Orimo S, Nakamura A, Mizusawa H, Uchihara T. Pale neurites, premature α-synuclein aggregates with centripetal extension from axon collaterals. Brain Pathol. 2012;22(1):67-78.
431. Brion JP, Octave JN, Couck AM. Distribution of the phosphorylated microtubule-associated protein tau in developing cortical neurons. Neuroscience. 1994;63(3):895-909.
432. Yu Y, Run X, Liang Z, Li Y, Liu F, Liu Y, et al. Developmental regulation of tau phosphorylation, tau kinases, and tau phosphatases. J Neurochem. 2009;108(6):1480-94.
433. Yuan A, Nixon RA. Posttranscriptional regulation of neurofilament proteins and tau in health and disease. Brain Res Bull. 2023;192:115-27.
434. Kanazawa T, Uchihara T, Takahashi A, Nakamura A, Orimo S, Mizusawa H. Three-layered structure shared between Lewy bodies and lewy neurites-three-dimensional reconstruction of triple-labeled sections. Brain Pathol. 2008;18(3):415-22.
435. Awa S, Suzuki G, Masuda-Suzukake M, Nonaka T, Saito M, Hasegawa M. Phosphorylation of endogenous α-synuclein induced by extracellular seeds initiates at the pre-synaptic region and spreads to the cell body. Scientific Reports. 2022;12(1):1163.
436. Itier JM, Ibanez P, Mena MA, Abbas N, Cohen-Salmon C, Bohme GA, et al. Parkin gene inactivation alters behaviour and dopamine neurotransmission in the mouse. Hum Mol Genet. 2003;12(18):2277-91.
437. Palacino JJ, Sagi D, Goldberg MS, Krauss S, Motz C, Wacker M, et al. Mitochondrial dysfunction and oxidative damage in parkin-deficient mice. J Biol Chem. 2004;279(18):18614-22.
438. Von Coelln R, Thomas B, Savitt JM, Lim KL, Sasaki M, Hess EJ, et al. Loss of locus coeruleus neurons and reduced startle in parkin null mice. Proc Natl Acad Sci U S A. 2004;101(29):10744-9.
439. Perez Francisco A, Palmiter Richard D. Parkin-deficient mice are not a robust model of parkinsonism. Proceedings of the National Academy of Sciences. 2005;102(6):2174-9.
440. Periquet M, Corti O, Jacquier S, Brice A. Proteomic analysis of parkin knockout mice: alterations in energy metabolism, protein handling and synaptic function. J Neurochem. 2005;95(5):1259-76.
441. Sato S, Chiba T, Nishiyama S, Kakiuchi T, Tsukada H, Hatano T, et al. Decline of striatal dopamine release in parkin-deficient mice shown by ex vivo autoradiography. J Neurosci Res. 2006;84(6):1350-7.
442. Stichel CC, Zhu X-R, Bader V, Linnartz B, Schmidt S, Lübbert H. Mono- and double-mutant mouse models of Parkinson's disease display severe mitochondrial damage. Human Molecular Genetics. 2007;16(20):2377-93.

443. Schmidt S, Linnartz B, Mendritzki S, Sczepan T, Lübbert M, Stichel CC, et al. Genetic mouse models for Parkinson's disease display severe pathology in glial cell mitochondria. Hum Mol Genet. 2011;20(6):1197-211.
444. Cossu D, Yokoyama K, Sato S, Noda S, Sechi LA, Hattori N. PARKIN modifies peripheral immune response and increases neuroinflammation in active experimental autoimmune encephalomyelitis (EAE). Journal of neuroimmunology. 2021;359:577694-.
445. Ge P, Dawson VL, Dawson TM. PINK1 and Parkin mitochondrial quality control: a source of regional vulnerability in Parkinson's disease. Molecular Neurodegeneration. 2020;15(1):20.
446. Villa E, Marchetti S, Ricci J-E. No Parkin Zone: Mitophagy without Parkin. Trends in Cell Biology. 2018;28(11):882-95.
447. Onishi M, Okamoto K. Mitochondrial clearance: mechanisms and roles in cellular fitness. FEBS Lett. 2021;595(8):1239-63.
448. Ham Su J, Lee D, Yoo H, Jun K, Shin H, Chung J. Decision between mitophagy and apoptosis by Parkin via VDAC1 ubiquitination. Proceedings of the National Academy of Sciences. 2020;117(8):4281-91.
449. Gao F, Chen D, Si J, Hu Q, Qin Z, Fang M, et al. The mitochondrial protein BNIP3L is the substrate of PARK2 and mediates mitophagy in PINK1/PARK2 pathway. Hum Mol Genet. 2015;24(9):2528-38.
450. Chan NC, Salazar AM, Pham AH, Sweredoski MJ, Kolawa NJ, Graham RL, et al. Broad activation of the ubiquitin-proteasome system by Parkin is critical for mitophagy. Hum Mol Genet. 2011;20(9):1726-37.
451. Yoshii SR, Kishi C, Ishihara N, Mizushima N. Parkin mediates proteasome-dependent protein degradation and rupture of the outer mitochondrial membrane. J Biol Chem. 2011;286(22):19630-40.
452. Shoshan-Barmatz V, Maldonado EN, Krelin Y. VDAC1 at the crossroads of cell metabolism, apoptosis and cell stress. Cell Stress. 2017;1(1):11-36.
453. Schneider HC, Berthold J, Bauer MF, Dietmeier K, Guiard B, Brunner M, et al. Mitochondrial Hsp70/MIM44 complex facilitates protein import. Nature. 1994;371(6500):768-74.
454. Szabadkai G, Bianchi K, Várnai P, De Stefani D, Wieckowski MR, Cavagna D, et al. Chaperone-mediated coupling of endoplasmic reticulum and mitochondrial Ca2+ channels. J Cell Biol. 2006;175(6):901-11.
455. Honrath B, Metz I, Bendridi N, Rieusset J, Culmsee C, Dolga AM. Glucose-regulated protein 75 determines ER–mitochondrial coupling and sensitivity to oxidative stress in neuronal cells. Cell Death Discovery. 2017;3(1):17076.
456. Franco-Iborra S, Cuadros T, Parent A, Romero-Gimenez J, Vila M, Perier C. Defective mitochondrial protein import contributes to complex I-induced mitochondrial dysfunction and neurodegeneration in Parkinson's disease. Cell Death & Disease. 2018;9(11):1122.
457. Li Y, Zheng W, Lu Y, Zheng Y, Pan L, Wu X, et al. BNIP3L/NIX-mediated mitophagy: molecular mechanisms and implications for human disease. Cell Death & Disease. 2021;13(1):14.

458. Oliveira da Silva MI, Liz MA. Linking Alpha-Synuclein to the Actin Cytoskeleton: Consequences to Neuronal Function. Front Cell Dev Biol. 2020;8:787.
459. Yamada M, Mizuno Y, Mochizuki H. Parkin gene therapy for alpha-synucleinopathy: a rat model of Parkinson's disease. Hum Gene Ther. 2005;16(2):262-70.
460. Yasuda T, Miyachi S, Kitagawa R, Wada K, Nihira T, Ren YR, et al. Neuronal specificity of alpha-synuclein toxicity and effect of Parkin co-expression in primates. Neuroscience. 2007;144(2):743-53.
461. Jin J, Hulette C, Wang Y, Zhang T, Pan C, Wadhwa R, et al. Proteomic identification of a stress protein, mortalin/mthsp70/GRP75: relevance to Parkinson disease. Mol Cell Proteomics. 2006;5(7):1193-204.
462. Shi M, Jin J, Wang Y, Beyer RP, Kitsou E, Albin RL, et al. Mortalin: A Protein Associated With Progression of Parkinson Disease? Journal of Neuropathology & Experimental Neurology. 2008;67(2):117-24.
463. Chiasserini D, Tozzi A, de Iure A, Tantucci M, Susta F, Orvietani PL, et al. Mortalin inhibition in experimental Parkinson's disease. Mov Disord. 2011;26(9):1639-47.
464. Burbulla LF, Schelling C, Kato H, Rapaport D, Woitalla D, Schiesling C, et al. Dissecting the role of the mitochondrial chaperone mortalin in Parkinson's disease: functional impact of disease-related variants on mitochondrial homeostasis. Hum Mol Genet. 2010;19(22):4437-52.
465. Burbulla LF, Fitzgerald JC, Stegen K, Westermeier J, Thost AK, Kato H, et al. Mitochondrial proteolytic stress induced by loss of mortalin function is rescued by Parkin and PINK1. Cell Death Dis. 2014;5(4):e1180.
466. Yang H, Zhou X, Liu X, Yang L, Chen Q, Zhao D, et al. Mitochondrial dysfunction induced by knockdown of mortalin is rescued by Parkin. Biochem Biophys Res Commun. 2011;410(1):114-20.
467. Di Maio R, Barrett PJ, Hoffman EK, Barrett CW, Zharikov A, Borah A, et al. α-Synuclein binds to TOM20 and inhibits mitochondrial protein import in Parkinson's disease. Sci Transl Med. 2016;8(342):342ra78.
468. De Miranda BR, Rocha EM, Castro SL, Greenamyre JT. Protection from α-Synuclein induced dopaminergic neurodegeneration by overexpression of the mitochondrial import receptor TOM20. npj Parkinson's Disease. 2020;6(1):38.
469. Singh K, Han K, Tilve S, Wu K, Geller HM, Sack MN. Parkin targets NOD2 to regulate astrocyte endoplasmic reticulum stress and inflammation. Glia. 2018;66(11):2427-37.
470. Giguère N, Pacelli C, Saumure C, Bourque MJ, Matheoud D, Levesque D, et al. Comparative analysis of Parkinson's disease-associated genes in mice reveals altered survival and bioenergetics of Parkin-deficient dopamine neurons. J Biol Chem. 2018;293(25):9580-93.
471. Mouton-Liger F, Rosazza T, Sepulveda-Diaz J, Ieang A, Hassoun SM, Claire E, et al. Parkin deficiency modulates NLRP3 inflammasome activation by attenuating an A20-dependent negative feedback loop. Glia. 2018;66(8):1736-51.
472. Dulski J, Uitti RJ, Ross OA, Wszolek ZK. Genetic architecture of Parkinson's disease subtypes - Review of the literature. Front Aging Neurosci. 2022;14:1023574.

473. Boyer DR, Li B, Sun C, Fan W, Zhou K, Hughes MP, et al. The α-synuclein hereditary mutation E46K unlocks a more stable, pathogenic fibril structure. Proc Natl Acad Sci U S A. 2020;117(7):3592-602.